Development of a Tool for Determining and Evaluating the Most Optimal Reaction Pathway Systems: Converting Carbon Dioxide to Methanol and Dimethyl Ether

UNIVERSITY OF THE
WITWATERSRAND,
JOHANNESBURG

Jaimee Jugmohan

797664

797664@students.wits.ac.za **or** jaimeejugmohan@gmail.com

Supervisor: Professor Josias van der Merwe

Co-Supervisor: Professor Mulenga Bwalya

Chemical Engineering

University of the Witwatersrand

This thesis is submitted for the degree of PhD Chemical Engineering

November 2022

Dedication

This thesis is dedicated to my family for their constant support and motivation in all ventures that I have embarked on, be it in a professional or personal capacity. A special thanks to my parents, Stephen and Nadira Jugmohan, whose strong morals and ethics have shaped me into the person that I am today. I know that with each step that I take you are always there to encourage and guide me. Words can never express how grateful I am to be blessed with such incredible parents, who have equipped me with everything I need to overcome any obstacle that life may throw at me.

I am immensely grateful for my younger sister, Nikita Jugmohan, who is always there to encourage me and make me smile when my energy and motivation levels are reaching critical lows. Your work ethic and drive are inspirational, and you never cease to amaze me every day. I am truly fortunate to have a sister like you, whose intelligence is only exceeded by her own kindness and generosity.

Thank you to Professor Josias van der Merwe and Professor Mulenga Bwalya for their constant support and guidance throughout the course of my research, especially under the extenuating circumstance being faced as a result of the global pandemic. The insight that you have both provided has been invaluable in overcoming some key obstacles during this research study.

Many thanks to the Council for Scientific and Industrial Research (CSIR) for funding this research.

UNIVERSITY OF THE WITWATERSRAND, JOHANNESBURG

SCHOOL OF CHEMICAL AND METALLURGICAL ENGINEERING
Faculty of Engineering & the Built Environment

Degree	Doctor of Philosophy PhD (Chemical Engineering)
Task	PhD Thesis
Title	Development of a Tool for Determining and Evaluating the Most Optimal Reaction Pathway Systems: Converting Carbon Dioxide to Methanol and Dimethyl Ether
Year	2022
Supervisor	Prof. Josias van der Merwe
Co-Supervisor	Prof. Mulenga Bwalya

Plagiarism Declaration

- I am aware that plagiarism (the use of someone else's work without their permission and/or without acknowledging the original source) is wrong.
- I confirm that the work submitted in this dissertation is my own unaided work.
- I have followed the required conventions in referencing the thoughts and ideas of others.
- I understand that the University of the Witwatersrand may take disciplinary action against me if there is a belief that this is not my own unaided work or that I have failed to acknowledge the source of the ideas or words in my writing.

Student Number	Name	Signature
797664	Jaimee Jugmohan	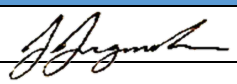

Abstract

An integral cog in the design of new chemical plants is the identification of promising, feasible reaction pathways, thereby necessitating that an extensive amount of resources be focused on this developmental stage. Despite the substantially expanded quantity of reaction pathway possibilities in the chemical and fuel industries, it is exceedingly difficult to build an economically and environmentally sound manufacturing processes. Additionally, this task has proven to be time consuming. Novel catalytic pathways that exhibit feasibilities at laboratory scale, may not hold true when scaled to an industrial level, leaving potential plant application with much uncertainty. One of the major concerns, is the cost of unit operations required to achieve the reaction and separation conditions, as well as the separation units needed in achieving a marketable purity of the desired product. To increase feasibility, products from a single reactive system can be treated as an intermediate, thereby producing a secondary product with greater economic value. Whilst this is not guaranteed, the possibility cannot be negated. This would involve employing two reactive systems consecutively, in a chemical plant, potentially optimizing the economic and environmental gains of the overall process system.

The Automated Systematic Synthesis Framework tool (ASSF tool) presented herein, is a novel, rapid screening tool which bridges the gap between the scale up of laboratory systems, process design, and economic and environmental analysis, by (1) providing generic design structures, cost and environmental implications associated with the scale up of a reactive system, (2) systematically searching for, and identifying, the possibility of pairing reactive systems as consecutive reaction mechanisms in a chemical plant, attempting to increase overall feasibility of the process structure. This, however, does not imply that the ASSF tool is able to identify new reaction pathways, but rather uses existing reaction pathways in the inputted database to look at extending the boundaries of the chemical plant to incorporate a secondary and/or tertiary reactive system. This search space reduction-based strategy aids in identifying promising reactive systems, and their likely bottlenecks, prior to the utilization of extensive time and design resources. The potential and novelty in the ASSF tool are demonstrated through its application to a case study focused on the production of methanol (MeOH) and dimethyl ether (DME) via carbon dioxide (CO_2) hydrogenation.

Existing engineering software systems require prior training, and an in depth understanding of multiple engineering concepts, including widely utilized platforms such as Aspen ® Plus. One of the novel aspects of the ASSF tool, however, lies in its generic design and level of detail

required to analyse a reactive system, only needing the balanced stoichiometric equation and its operating conditions. Once entered as a database, the ASSF tool searches for potential reaction pathway combinations. Each reactive system undergoes a basic, generic process design, costing the unit operations required in, and leading up to, the reaction and separation systems. These plant structures are then analysed using economic and environmental criteria, with the final, reduced search space being ranked in order of its expected industrial feasibility.

It is important to note, however, that the ASSF tool is not designed to replace existing engineering design and simulation software systems, such as Aspen ® Plus. Instead, the ASSF tool is a novel, precursory platform with the ability of automatically narrowing large reaction pathway search spaces in a fraction of the time than would be needed if individually simulated in the existing software platforms. Once the search space has been reduced and ranked, as per the ASSF tool, the user can focus their design resources on the intricate design of those potentially feasible reactive systems, necessitating the use of extensive engineering software. Additionally, the simple interface of the ASSF tool allows it to be utilized without prior training, providing reliable results with limited/streamlined inputs.

To ensure reliability of the results obtained from the ASSF tool, the code was validated and verified against data published when using existing simulation platforms, i.e., CHEMCAD ® and W-EcoMP, noting minor deviations (< 6%) in capital costs. This is within the ± 30% range for preliminary design procedures. Previously a reaction pathway database (RPD) developed and analysed by Jugmohan, *et al*. (2020) noted an analysis period of 10 months, owing to the manual design and transfer of data between four intricate software platforms. The use of the ASSF tool on the same RPD results in a complete analysis in under 5 hours, concluding an identical final search space of 5 potentially feasible reactive systems – using economic and environmental criteria as the crux of this feasibility. This reiterates the use and uniqueness of the ASSF tool in identifying promising reactive systems at the early onset of the design process, allowing for future design and research resources to be more focus driven.

Whilst not designed for the purpose of analysing experimental data, the ASSF tool can be expanded to provide a quick, preliminary analysis of experimental data, determining the economic practicality of attaining operating conditions in a scaled up industrial setting. When practical, the ASSF tool provides the user with an indicative range of operating conditions likely to provide the greatest chance of success in future experimental work and scale up ventures, allowing for research resources to be concentrated within this narrow scope.

Table of Contents

List of Figures

List of Tables

Acronyms

Acronym	Term Represented
ABB	Accelerated Branch and Bound
ASSF	Automated Systematic Synthesis Framework
B-RPD	Basic RPD
CEPCI	Chemical Engineering Price Cost Index
CFC	Combinatorially Feasible and Controllable
CS	Carbon Steel
CRF	Capital Recovery Factor
CZA	Copper-Zinc-Aluminium
CZZA	CuO-ZnO-ZrO_2-Al_2O_3
DME	Dimethyl Ether
EOS	Equation of State
FCCC	Fuel Cell Combine Cycle
GDP	Gross Domestic Product
GHG	Greenhouse Gas
GPSA	Gas Processors Suppliers Association
GUI	Graphical User Interface
IPCS	Integration of Process and Control Systems
MILP	Mixed Integer Linear Programming
MSG	Maximal Structure Generation
NaN	Not Applicable
NLP	Non-linear Programming
PBP	Payback Period
PEM	Proton Exchange Membrane
PNS	Process Network Synthesis
PtG	Power-to-Gas
PtL	Power-to-Liquid
PtX	Power-to-X
rGO	Reduced Graphene Oxide
ROA	Reliability of Availability

Acronym	Term Represented
ROI	Return on Investment
RPD	Reaction Pathway Database
RWGS	Reverse Water Gas Shift
SNS	Separation Network Synthesis
SS	Stainless Steel
SSG	Solution Structure Generation
W-ECoMP	Web-based Economic Co-Generative Modular Program
ZSM-5	Zeolite Socony Mobil-5

Symbols (Letters)

Symbol	Value Represented
A	Unit operation capacity (m^2, m^3, kW)
a, b	Van der Waal/Peng-Robinson constants
A_1, A_2, A_3, A_4, A_5	Specific heat capacity constants (gas)
A_c	Flash drum cross-sectional area (m^2)
ACC	Annualized capital cost ($)
Adj Profit	Adjusted annual profit ($)
ATM_{CO2}	Net atmospheric CO_2 reduction (tons/annum)
B_1, B_2	Bare module cost constants
B_1, B_2, B_3, B_4	Specific heat capacity constants (liquid)
C_1, C_2, C_3	Enthalpy of vaporization constants
C_1, C_2, C_3	Pressure factor constants
C_{BM}	Bare module cost ($)
CEPCI	Chemical Engineering Price Cost Index
$C_{i_{HX}}$	Cost of individual heat exchanger ($)
C_{j_d}	Cost of individual drivers ($)
$C_{j_{PC}}$	Cost of individual pressure-changing unit operation ($)
$C_{k_{PV}}$	Cost of individual process vessel ($)
C_{k_T}	Cost of individual tower ($)
$C_{k_{Tr}}$	Cost of trays ($)
C_{NG}	Cost of natural gas ($/annum)
$COMBUST_{CO2}$	CO_2 produced during methane combustion (tons/annum)
C_p	Specific heat capacity (J/mol.K)
C_{p_g}	Specific heat capacity of gas phase (J/mol.K)
C_{p_l}	Specific heat capacity of liquid phase (J/mol.K)
C_p^o	Purchased cost ($)
C_R	Total cost of reactants required ($/annum)
CRF	Capital recovery factor

Symbol	Value Represented
C_{Total}	Total unit operation cost ($)
CV_{NG}	Calorific value of natural gas (kJ/kg)
D	Distillation stream flow rate (kmol/hr)
D_1, D_2, D_3, D_4, D_5	Vapor pressure constants
D_c	Distillation column diameter (m)
D_f	Flash drum diameter (m)
D_p	Pipe diameter (m)
E_o	Tray efficiency
E_{Total}	Total energy required by the process (kW)
$Excess_{H2}$	Percentage excess H_2 gas fed into process (%)
F	Flash drum feed stream flow rate (kmol/hr)
F_{BM}	Bare module material factor
F_{CO2}	CO_2 feed flow rate basis (kmol/hr)
F_{H2}	H_2 feed into process (kmol/hr)
Final cost	Cost of unit operation at time of running ASSF tool ($)
F_M	Material factor
F_p	Pressure factor
$F_{p, vessel}$	Flash drum and distillation column pressure factor
F_q	Quantity factor
H	Enthalpy (kJ)
H_D	Height of distillation column (m)
h_F	Flash drum feed enthalpy (kJ/hr)
H_f	Flash drum height (m)
H_f^o	Standard enthalpy of formation (kJ/mol)
H_i	Enthalpy of each individual stream component (kJ)
HK	Heavy key component
h_L	Enthalpy of liquid stream exiting flash drum (kJ/hr)
H_{Total}	Stream enthalpy (kJ)
h_v	Enthalpy of vapor stream exiting flash drum (kJ/hr)
H_{vap}	Enthalpy of vaporization (kJ/mol)
HX_{Total}	Total cost of heat exchangers ($)

Symbol	Value Represented
IN_{CO2}	Total CO_2 taken in by the process (tons/annum)
K_1, K_2, K_3	Purchased cost constants
K_{drum}	Flash drum empirical constant
K_i	Equilibrium constant of component i
L	Liquid flow rate (kmol/hr)
l_t	Tray spacing (m)
M	Total stream mass flow rate (kg/hr)
M_{CH4}	Molar mass of methane gas (kg/kmol)
M_{CO2}	Molar mass of CO_2 (kg/kmol)
$m_{CO2,produced}$	Mas of CO_2 produced during natural gas combustion process (kg/hr)
m_{NG}	Mass of natural gas required to meet energy requirements (kg/hr)
m_P	Mass of products leaving process (kg/annum)
m_R	Mass of reactants needed (kg/annum)
MW	Molecular weight (kg/kmol)
MW_{vapor}	Average molar mass of vapor stream (kg/kmol)
N	Number of moles (moles)
N	Number of trays within distillation column
N_{Actual}	Actual number of trays within the distillation column
n_d	Total number of drivers present in chemical plant
n_{HX}	Total number of heat exchangers present in chemical plant
n_i	Molar flow rate of each individual stream component (kmol/hr)
n_l	Lifespan of chemical plant (years)
n_{PC}	Total number of pressure-changing unit operations in chemical plant
n_{PV}	Total number of process vessels present in chemical plant
n_T	Total number of towers present in chemical plant
n_{Tr}	Total number of unit operations needing trays
N_{min}	Minimum number of stages within distillation column
OC_{Annual}	Annualized operating costs ($)
P	Stream pressure (bar)
PBP	Payback period (years)
P_c	Critical pressure (bar)

Symbol	Value Represented
PC_{Total}	Total cost of pressure-changing unit operations ($)
P_i	Partial pressure of each individual stream component (bar)
$P_{i_{sat}}$	Saturation pressure of component i (mm Hg)
PI	Performance index
P_L	Pressure of liquid stream exiting flash drum (bar)
P_v	Pressure of vapor stream exiting flash drum (bar)
P_{v_i}	Vapor pressure of each individual stream component (mm Hg)
$P_v(T)$	Vapor pressure as a function of temperature (mm Hg)
$(P_v)_{Total}$	Stream vapor pressure (mm Hg)
P_{vessel}	Flash drum vessel operating pressure (Kelvin)
Q	Heat transferred into/out of system (kW)
q	Feed quality
R	Ideal gas constant (m^3.bar/K.mol)
r	Annual discount rate (%)
R_{min}	Minimum reflux ratio
R_{Theor}	Theoretical reflux ratio
SCE_{CO2}	Stoichiometric co-efficient of CO_2
SCE_{H2}	Stoichiometric co-efficient of H_2
SP_P	Total sales potential of products ($/annum)
S_{Total}	Total cost of separation unit operations ($)
T	Stream temperature (Kelvin)
T_b	Boiling temperature (Kelvin)
$T_{boiling}$	Boiling temperature (Kelvin)
T_c	Critical temperature (Kelvin)
T_{freeze}	Freezing temperature (Kelvin)
T_L	Temperature of liquid stream exiting flash drum (Kelvin)
T_{max}	Maximum temperature constraint (Kelvin)
T_{min}	Minimum temperature constraint (Kelvin)
T_r	Reduced temperature
T_{ref}	Reference temperature (Kelvin)
T_s	Stream temperature (Kelvin)

Symbol	Value Represented
T_u	Utility temperature (Kelvin)
T_v	Temperature of vapor stream exiting flash drum (Kelvin)
T_{vessel}	Flash drum vessel operating temperature (Kelvin)
U	Overall heat transfer co-efficient ($W/m^2.K$)
UC_R	Unit cost of reactants ($/kg)
U_e	Internal energy (kJ)
UNR_{CO2}	Unreacted CO_2 leaving process (tons/annum)
USP_P	Unit sales potential of products ($/annum)
u_v	Maximum allowable superficial velocity (m/s)
V	Volume (m^3)
v	Stream velocity (m/s)
$\overline{V}$	Vapor flow rate (kmol/hr)
V_c	Critical volume (cm^3/mol)
V_{final}	Final volumetric flow rate (m^3/hr)
V_i	Volumetric flow rate of each individual stream component (m^3/hr)
$V_{initial}$	Initial volumetric flow rate (m^3/hr)
V_m	Molar volume (m^3/mol)
V_{m_i}	Molar volume of each individual stream component (m^3/hr)
V_{min}	Minimum vapor flow rate (kmol/hr)
V_n	Molar vapor flow rate within flash drum (kmol/hr)
V_{Total}	Total stream volumetric flow rate (m^3/hr)
V_{vessel}	Volume of flash drum vessel (m^3)
W	Work (kW)
x_A	Molar fraction of light key component in the distillate stream
x_B	Molar fraction of heavy key component in the bottom stream
x_i	Molar fraction of each individual stream component
x_i	Liquid fraction of component i
y_i	Vapor fraction of component i
Z	Compressibility factor
z_i	Feed fraction of component i

Special Symbols (e.g. Greek Letters)

Symbol	Value Represented
α, κ	Peng-Robinson EOS factors
α_i	Relative volatility of component i
α_{LK}	Relative volatility of the light key component
ΔT_{LM}	Log mean temperature (Kelvin)
θ	Variable in the Underwood equation
ρ_L	Liquid density (kg/m^3)
ρ_{stream}	Stream density (kg/m^3)
ρ_v	Vapor density (kg/m^3)
φ	Ratio of vapor to feed flow rate of flash drum
Ω	Acentric factor
μ_{perm}	Permissible vapor velocity (m/s)

List of Appendices

Conference Presentations

The research detailed in this PhD Thesis has been presented at the following conferences:

1. International Society for Engineers and Researchers (ISER) – 878th International Conference on Chemical and Environmental Science held virtually on 10/08/2020.

Published Journal Articles

The work detailed in this PhD thesis has been published in the following journals:

1. Jugmohan, J. & Madigoe, E., 2020. The P-Graph Network: A Tool for Solving Process Network Synthesis and Similar Styled Problems through Rigorous Superstructure Development and Combinatorial Algorithms. International Journal of Advances in Science, Engineering and Technology, 8(4), pp. 37-49.
2. Jugmohan, J., Van der Merwe, J. & Bwalya, M., 2021. An Automated Systematic Synthesis Framework for Determining the Most Viable Reaction Pathway Prior to Extensive Design Procedures: The Conversion of CO_2 to Value Added Products. International Research Journal of Advanced Engineering and Science, 6(1), pp. 254-260

Chapter 1: Introduction

1.1. Background Information

There has been a growing interest in the development of tools and methodologies utilized in optimizing and reducing the search space of reaction pathways focused on the production of a single/multiple product(s). With reaction pathways serving as the core of most production facilities, this growing interest is to be expected. Ensuring that the correct reaction pathway is chosen is integral in the implementation and advancement of any potential chemical plant.

As a result of this increased interest, a substantial amount of recent research has focused on the enhancement of current chemical processes, with the primary purpose of improving their economic and environmental viability. However, it is likely that a unique chemical pathway, or a combination of them, could yield higher efficiencies or lower operating costs than can be reached by process optimization.

Unfortunately, accurately identifying this reactive system among the numerous previously explored and documented reaction pathways can prove to be a time-consuming and challenging task. Additionally, manually selecting the optimal reaction pathway increases the risk of human error. Manual procedures are inefficient when considering and comparing new reactive system developments to those already known, as this would entail re-running the entire analysis procedure to account for these additions. This endeavor is akin to 'looking for a needle in a haystack,' rendering its applicability within an industry impracticable.

The tool presented in this thesis seeks to address this issue by adopting an automated systematic synthesis framework (ASSF). This framework utilizes a reaction pathway database (RPD) to analyze the production of a single or several products, methodically planning and assessing each reaction pathway from numerous economic and environmental perspectives. This allows the user to determine the most promising reactive system prior to any extensive design procedures, allowing for subsequent design resources to be focused on pathways with the greatest chance of success.

This chapter highlights the gap in the field, that motivated the development of the ASSF tool. Additional areas covered within this introduction include the motivation behind this research,

the problem statement, the aims, and objectives, as well as an overview of the chapters within this thesis.

1.2. The Gap in the Field Addressed by the ASSF Tool

The gap in the field being addressed via the ASSF tool, and presented herein, can be distinctly categorized from two perspectives. The first perspective looks at the shortcomings of research studies focused on determining the most promising reactive system for a predefined reactant/product range. The second perspective highlights the gap in the current chemical engineering software platforms available, highlighting the placement of the ASSF tool within the vast array of existing engineering programs.

1.2.1. Basic Overview of the Shortcomings within this Research Field

Due to the fact that the reactor unit operation(s) is/are considered to be the 'heart' of any chemical process (Smith & Linnhoff, 1988), a considerable amount of design resources and research is devoted to optimizing its associated operating conditions, flow rates and catalyst composition. Therefore, when designing, examining, or optimizing on a new, or existing, chemical process, the crucial step lies in determining the reactive system to adopt within the process structure. Often the number of potential reaction pathways leading from a set of reactants to a predefined product is extremely vast, requiring extensive design resources in finding the most promising reaction route.

Whilst there have been some definitive advancements within this research area, there are also clear problem areas that have been overlooked. Previous research studies focused on reducing the potential search space of reaction pathways by considering their thermodynamic feasibility. Thus, the heat of reaction and associated Gibbs free energy were accounted for (Rotstein, *et al*., 1982), (Govind & Power, 1977). Additional research in this area attempted to create an overall thermodynamically feasible reaction pathway via the combination of multiple feasible and infeasible reactive steps (Li, *et al*., 2000). Whilst these studies did show a significant decline in the potential reaction pathway search space, a recurring issue was the extent to which

economic and environmental factors were considered when determining the reduced search space and the promising reaction pathways/system therein.

With the focus being concentrated on thermodynamic feasibility, these past research ventures did not account for the unit operations needed to achieve the desired operating conditions, the cost of these unit operations, and the expected energy costs associated with operating these systems. Whilst it is possible that some reactive systems exhibit higher conversions at increased pressures and temperatures, the cost of operating under these conditions may outweigh the economic gains of the increased conversion. This is a major factor that has been overlooked in previous research studies.

With the design and implementation of a chemical plant being largely dependent on the profitability of the venture, the economic feasibility of any future development will serve as the foundation for all investment decisions (Deddis, 2010). Previously, the consideration of economic feasibility in reducing the reaction pathway search space was limited, considering only the potential profit achieved from an input/output structure, thereby assuming complete conversion. This is evident in the research studies conducted by Buxton, *et al*., (1997) and Li, *et al*., (2000). These research studies are explicated in Section 2.1.

This assumption, however, is impractical in an industrial setting with very few catalysts being able to achieve a complete conversion, especially within continuous flow processes. Conversion is often limited by the equilibrium of the reaction (Metcalfe, *et al*., 2019). Therefore, such an assumption reduces the accuracy of the associated economic feasibility considered within previous investigations.

Furthermore, the cost of the separation system would be greatly impacted by the conversion noted within the reactive system. Assuming complete conversions would essentially nullify the costs of separating the product from the unreacted feed, thereby increasing the economic feasibility of the process structure. Therefore, the cost of the separation unit operations required in achieving a marketable, and competitive, product must be accounted for within the economic viability of the process structure.

To expand the feasibility criteria, recent research studies have attempted to incorporate economic and environmental criteria into their analysis of process structures. The environmental benefit was considered in terms of the amount of CO_2 being taken into the process (Al-Fadhli, *et al.*, 2018), not accounting for the CO_2 likely to be emitted when producing the energy required to operate the process unit operations. Additionally, the

comparisons and economic benefit considered by Al-Fadhli, *et al.* (2018) made use of data from existing chemical plants, thereby limiting the expansion of this methodology to process structures still within their design stages.

This development encompassed manual analysis procedures, necessitating that the associated plant data be analysed on a case-by-case basis. Manual frameworks make it harder to account for changes in the reactive system, as it would require the entire analysis procedure to be completed again. Another reaction pathway analysis framework, developed by Jugmohan, *et al.* (2020), required the manual analysis of each system in four different software platforms. The developed framework required that data be manually extracted and transferred between each software platform. Such frameworks are not only time-consuming with an increased chance of human error, but they also require specialized knowledge on each software system. This lowers the practicality of employing such frameworks in an industrial setting as few companies would have access to all four software platforms simultaneously – especially given the large costs associated with purchasing software such as Aspen ® Plus.

The ASSF tool developed and presented herein was developed to address these concerns and shortcomings of previous work within this research field. The key contribution of the ASSF tool is that it is able to systematically analyse an RPD, identifying the possibility of combining reaction pathway systems by extending the bounds of the associated process plant, i.e., treating the product of one reaction as an intermediate in the overall system. Each reactive system is then analysed via an economic and environmental standpoint, using a generic process flow sheet and accounting for the conversion, operating conditions, and separation systems. The final search space presented to the user as the output of the ASSF tool, is a reduced reaction pathway search space, containing only those reactive systems that are likely to show promise on an industrial scale.

It is important to note however, that the ASSF tool is a preliminary, screening platform, aimed at allowing future design resources to be focused on those pathways with the greatest likelihood for success. Therefore, the ASSF tool should be utilized as a precursor to the current existing simulation software such as Aspen and CHEMCAD. Additionally, the ASSF tool is an automated platform, thereby requiring minimum manual interactions from the user, increasing its usability within the process environment.

1.2.2. Existing Chemical Engineering Software Platforms

Currently there exists a multitude of chemical engineering software platforms focused on the simulation and optimization of process structures. Whilst it is impossible to review all chemical engineering software packages that have been developed, the most prominent software platforms are discussed to highlight the exiting gap in the software field.

One of the prominent software platforms utilized in the chemical engineering field is the range developed by Aspen Technology, including Aspen ® Plus, Aspen ® Hysys and Aspen ® Custom Modeler. These software platforms are utilized for dynamic process simulation and optimization. These developments allow users to design and build process models, simulating chemical plants without the need for extensive calculations.

Whilst extremely helpful, Aspen ® Plus does require a certain level of training and specialized skills to navigate the dashboard and user interface of this software. This training and complex user interface will result in increased periods between analysis results. Furthermore, this software platform is known to be expensive, and thereby outside the affordable limit of many smaller chemical engineering-based companies.

CHEMCAD, another prominent chemical engineering software platform, allows users to create and simulate process designs, providing equipment sizes and thermophysical property calculations. This software platform also allows for the analysis of process economics, a feature which it holds in common with Aspen ® Plus. Such simulation platforms require specialized training prior to its use, allowing the user to effectively navigate the user interface and interpret the subsequent results.

Furthermore, both CHEMCAD and Aspen ® Plus require extensive knowledge of the process structure to effectively compile and simulate the process environment. For example, the simulation of a distillation column would require extensive data relating to the distillation column design, required purities, and calculation methods. Whilst this information is readily available for process structures that are in their development process, or that have already been implemented, such information may not be at hand for new process structures.

These software platforms also require that the user manually draw the process structure into the simulation environment, a task which can be time-consuming. With the manual drawing of chemical plants and the excessive input data required, such simulation platforms are ideally

utilized for promising reactive systems. The analysis of multiple reactive systems within these software platforms would require that each reactive system be constructed and run as a separate process simulation, making the process of determining feasible reactions lengthy, expensive, and complex.

Other software platforms currently available, including DWSim, ProSimPlus, and UniSim, are also focused on process simulation. There are even software platforms that are more focused in their target audience, focusing on specific unit operations and process industries. These software platforms include ProSim HEX, REX, IDEAS, and ProMax, to name a few, with each system focusing on heat exchangers, reactor systems, hard rock mining and oil/gas refineries, respectively.

As shown here, a multitude of simulation packages are available for chemical engineering plants, however each of these software platforms require extensive time resources, detailed inputs for equipment specifications, and specialized training to effectively utilize the package. The ASSF tool, developed and presented within this thesis, aims to address these concerns. This tool aims to act as a precursor to these process simulation software packages, determining the promising reaction pathways prior to extensive design procedures.

The ASSF tool offers the user a simple, guided interface structure, providing a step-by-step walkthrough of all information required in developing the RPD and inputting the required economic data, allowing for the analysis to be relevant to the time of running the ASSF tool. This simplifies prior user training when utilizing the ASSF tool. Furthermore, the ASSF tool utilizes pre-coded generic plant structures, automating the analysis procedure and not requiring any manual intervention from the user beyond their initial input. This significantly shortens the analytical time required for reactive systems, with the user being able to analyse more reactive systems in a fraction of the time that would previously have been required. The ASSF tool does not require detailed equipment specifications, using generic equipment structures, design, and costing procedures to determine the feasibility of a chemical process. Therefore, even with the streamlined inputs required, the ASSF tool is able to achieve reliable outputs on promising reactive systems, effectively reducing the reaction pathway search space.

With the ASSF tool, a ranked list of reaction pathways/systems that are feasible on an industrial scale are obtained. Crucially, the economic and environmental implications associated with the chemical plant are considered. As a result, the design resources in the aforementioned software platforms can be more focused on detailed simulation of those reactive systems with the

greatest likelihood of success, lowering the initial time required, and aiding the engineering team, in the design of new/novel chemical plants. It is important to reiterate, however, that the ASSF tool is not a standalone application, acting as a precursory, rapid screening tool to identify feasible reaction pathways in a significantly shorter analytical time, and with limited input. Therefore, the true impact of the ASSF tool can be seen when its feasible outputs are exported and translated to existing, intricate chemical engineering platforms, such as Aspen ® Plus for detailed scale up.

1.3. Research Motivation

The motivation behind this research is to a establish a rapid screening tool that can analyse multiple reactive systems, and their potential combinations, in a fraction of the time than would be currently required, providing the user with only those reactive systems that are likely to be feasible. This would not only allow for more efficient use of design resources but would guide engineering teams in their choice of reactive systems, increasing the likelihood of economically and environmentally feasible processes being developed during the early onset design stages.

Furthermore, when developing new processes, the amount of information is often limited, with the designer and engineers being unaware of the detailed specifications of the unit operations required. Therefore, the screening tool established here conducts automated, basic designs of the unit operations required in the process, allowing reliable results to be obtained with minimal input. With effective use of design resources on only those reactions that show promise, the development of new chemical processes can be expedited. This allows for the needs of the global market to be addressed in a more timeous manner.

The reason behind this tool's development stems from the gaps in the field identified and explicated in Section 1.2. Therefore, this research motivation can be viewed from two perspectives, with the first focused on addressing the frameworks currently in place to analyse reaction pathway systems, and the second motivation being to better utilize and optimize on the process designs being simulated in existing chemical engineering software platforms.

Based on the previous frameworks developed, shown in Section 1.2.1, the common shortcoming of past research ventures is the extent to which process structures were considered and analysed when determining their feasibility in relation to alternative reaction systems. One

of the most common considerations made in past studies, is the analysis of reactive systems from an input/output perspective, thereby assuming a complete conversion of reactants. This, however, is highly inaccurate and with most chemical processes being unable to achieve a complete conversion within meaningful residence times, this will provide a false sense of feasibility.

Furthermore, a second concern with assuming complete conversion, is the subsequent downstream processing techniques, i.e., the separation system. Complete conversion would negate the need for separation systems to be focused on removing unreacted feed, thereby lowering the separation costs substantially and providing the user with an unrealistic sense of feasibility for the reactive system in question.

Finally, the use of an input/output structure in these past frameworks resulted in inaccurate consideration of the economic feasibility of the process. These frameworks did not make provisions for the amount of product being lost during the separation process, as well as the cost of energy needed for the unit operations dedicated to achieving the reaction and separation conditions.

The ASSF tool developed and presented within this thesis addresses this issue by using an RPD with provisions made for the reactant conversion, thereby allowing for an accurate profile and stream composition to be determined in the reactor outlet. This conversion noted is extracted from literature sources, providing an indication as to the reactive pathways whose conversions and operating conditions show promise, thereby allowing those to be taken and researched in more detail, using software systems such as CHEMCAD and Aspen ® Plus.

To address the lack of separation systems in previous frameworks, the ASSF tool employs a generic process flow sheet accounting for flash drum and distillation column unit operations. The flash drum system is focused on the removal of unreacted feed, with the distillation column being focused on separating and producing a product of marketable purity. This allows for potential losses in the separation system to be determined, providing a more accurate account of the process production rate and its economic feasibility.

Furthermore, the ASSF tool employs the assumption of utilizing natural gas as a means by which to produce the energy required for the process unit operations, thereby providing a more holistic view of the operational costs associated with a potential reactive system and providing increased reliability and accuracy to its economic feasibility.

In the recent research studies that focused on the development of such reaction pathway frameworks, some focus was driven to account for conversion, economic feasibility of the unit operations associated with the required operating conditions, and environmental feasibility. One such study conducted by Al-Fadhli, *et al.* (2018), looked at comparing the feasibility of multiple process structures, accounting for the criteria mentioned here. The environmental feasibility of the process plants was considered based on the amount of CO_2 being utilized in the process plant.

The concern with the work conducted by Al-Fadhli, *et al.* (2018) was that all process plants considered had already been designed and were already in operation, thereby having adequate data to apply these comparisons. This, however, would not be possible with the development of new chemical processes, as this information would not be available. Furthermore, the environmental consideration of this study only considered CO_2 being utilized in the feed, not accounting for CO_2 that is likely to be emitted when producing the energy required to run the necessary unit operations.

The ASSF tool addresses these issues by utilizing an RPD, thereby not requiring the chemical plant to be designed, or in operation, for its analysis. This would require that the ASSF tool be inputted with stoichiometric equations, conversions, and operating conditions, obtainable from literature and laboratory experimentation. In doing so, the ASSF tool can provide the user with promising reactive systems before any extensive design procedures. Additionally, the ASSF tool looks at the amount of CO_2 likely to be emitted during the combustion of natural gas (the assumed energy source for operating the necessary unit operations), thereby providing a more holistic view of the environmental benefit noted.

A research study conducted by Jugmohan, *et al.* (2020) was able to address much of these concerns, however, did so utilizing four different software platforms. This required the manual input of data into each software platform, including Aspen ® Plus, MATLAB, P-graph Studio and Microsoft ® Excel, making the framework time-consuming and increasing the risk of human error. Additionally, the use of multiple software systems would require access to all platforms and would require that the user be familiar with their interface, often necessitating specialized knowledge and training.

The ASSF tool addresses this concern by having a single, guided user interface whereby the only input required from the user is the RPD and economic data at the time of running the ASSF tool. With this being the only manual step required, the automated approach taken by

the ASSF tool increases the efficiency of the analysis framework and reduces the likelihood of human error when transferring data between the software packages.

The motivation behind this research, and the development of the ASSF tool, also stems from the current engineering software platforms available. Bulk of these software packages require extensive training in navigating the dashboard and user interface, thereby increasing the time required for them to be effectively utilized in a process environment. Furthermore, the existing software platforms focus on the simulation and optimization of chemical plants associated with a predetermined reactive system, necessitating that alternative reaction systems be simulated separately to allow for effective comparisons.

This can be extremely time consuming, and will require extensive use of design resources, with the possibility existing that the reactive system will exhibit economic and/or environmental infeasibilities. The ASSF tool acts as a precursory, screening tool, allowing the user to analyse multiple reaction pathways in a fraction of the required time, and providing the user with a reduced search space of only those promising pathways likely to exhibit feasibility on an industrial scale. These pathways can then be extracted from the ASSF tool and simulated in the existing chemical engineering software platforms, such as Aspen ® Plus, with the design resources now being focused on pathways that are likely to yield positive results.

It is these gaps in the field and shortcomings that necessitated the development of the ASSF tool. This will allow resources to be more focused, expediting the design of future chemical processes. This tool is demonstrated in this thesis, via its application to reactive systems focused on the hydrogenation of CO_2 to MeOH and DME.

1.4. Problem Statement

Given an RPD comprising of the following information:

- Stoichiometric reaction equation and sub-reactions that occur simultaneously within a single reactor unit operation
- Reaction operating conditions, with respect to temperature and pressure
- Reactant conversion, with respect to the first reactant in the stoichiometric equation
- Selectivity, in such cases where multiple products are produced simultaneously in a single reactive system

- The reference from which the reactive system was extracted, i.e., for purposes of cross-referencing during analysis

Determine, through an automated approach:

- The number of reactive system combinations possible from the RPD
- The most promising reaction pathway systems from an economic and environmental standpoint
- The reduced search space of reactive systems that exhibit characteristics of both economic and environmental feasibility
- Ranking the final reduced search space in order of viability, finding a trade-off between economic and environmental benefits of the reactive system

Alternatively, the ASSF tool can also be utilized in quick, preliminary simulations of a chemical plant, or in determining the optimal operating conditions from a practical standpoint. Whilst developed as a precursory tool for determining reaction pathways with the greatest likelihood for success when scaled up to an industrial environment, the ASSF tool can be utilized in these circumstances to obtain an indication of the range containing the optimum operating conditions. Therefore, research can be focused within this narrow operating range, refining, and validating the optimum process parameters.

1.5. Aims and Objectives

The aim of this research is to develop a single, automated systematic synthesis framework (ASSF) tool that is able to critically analyze an RPD, in terms of its possible combinations, as well as the economic and environmental benefits associated with that reactive system. This will allow for the tool to derive a list of the promising reactive systems to be analysed further within the extensive chemical engineering simulation platforms currently available, thereby acting as a precursor, reactive pathway, screening platform.

It is important to note from this aim, however, that the ASSF tool developed and presented herein does not identify new reaction pathway systems, as this would require the use of experimental data paired with regression analysis. Instead, the ASSF tool looks to explore the

possibility of expanding the process boundaries to encompass a secondary/tertiary product. This would involve treating the reactor product as an intermediate in the overall process structure, with this intermediate being fed to a subsequent reactor system.

Furthermore, the ASSF tool is not aimed at replacing existing simulation software packages, but rather is a tool that is utilized prior to these detailed design programs, allowing for design resources during these initial stages to be expedited and focused on promising reactive systems. This would aid in streamlining the design process.

The aforementioned aim is achieved through the following objectives:

1. To develop a comprehensive RPD that contains necessary reactions, conversions, and operating conditions.
2. To develop a reaction pathway combination model, that utilizes a superstructure and mapping-tool approach, similar to that of the P-graph. This was utilized in determining the number of possible combinations achievable, expanding the boundaries of the process system.
3. To develop a tool that provides basic chemical plant designs for each possible reaction pathway combination, encompassing the design of unit operations required to achieve and facilitate the reaction and its subsequent separation process. Separation systems are imperative in determining the cost required to achieve a marketable purity of the product, thereby holding a critical role in the overall feasibility of the process.
4. To develop a tool whereby a basic economic and environmental analysis can be conducted on each reaction pathway combination.
5. To develop search space reduction criteria that focuses on the comparison of each reaction pathway combination, namely their economic and environmental gains. Infeasible options are removed from the search space, whereas the remaining combinations, and reactive systems, are ranked in order of their viability.

It is important to note that the ASSF tool developed and presented within this thesis is limited to the production of methanol and dimethyl ether via the hydrogenation of CO_2. Furthermore, the ASSF tool is unable to export process flow sheets or consider alternative process designs. The reason for this, is that the ASSF tool is a screening tool that provides the user with an indication of promising reactive systems. Therefore, the use of a generic process design structure allows for the tool to determine the cost of unit operations needed to achieve the

necessary reaction and separation conditions, as well as a cost estimate of the separation system. Having a consistent generic process structure also allows for effective comparisons between case studies. The generic flow sheet, and the reasoning behind its design, is explained within Chapter 3 of this thesis.

The promising reactive systems, determined by the ASSF tool, can be further researched and designed in detail, accounting for the necessary optimization procedures such as alternate process structures, recycle loops and heat integration. This detailed design and optimization, however, is beyond the scope of this research study.

1.6. Thesis Chapter Overview

This thesis comprises seven chapters, each dealing with its own specific contribution to the ASSF tool and its development. Chapter 1, already presented here, served as an introduction to the purpose of this research, highlighting the gap in the field whilst simultaneously introducing the scope covered within this research.

Chapter 2 provides a comprehensive literature review, looking at previous work conducted within this field, as well as other theoretical areas considered and utilized throughout the course of this research. This includes areas such as process network synthesis, the process graph (P-graph), the production of MeOH and DME, equations of state and unit operations. When considering work conducted within this research field, a critical analysis is made of each investigation, identifying the shortcomings in the field. These shortcomings form the basis of the gap in the field and were mentioned in Chapter 1 above.

Chapter 3 looks at the in-depth development of the ASSF tool, accounting for the assumptions of each section, the design and construction of the reaction pathway combinations, and the analysis thereof. Furthermore, various search space reduction criteria will be presented within this chapter, focusing on economic and environmental benefits of each associated case study. The reader is referred to Appendix B for a holistic overview of the ASSF tool, along with its user interface, required inputs, default values and associated results/outputs.

The validation and verification of the ASSF tool is an integral part in ensuring that the tool is able to produce accurate results. Chapter 4 focuses on the verification of the ASSF tool, comparing the results obtained using this tool, with a reputable chemical engineering software,

such as CHEMCAD ®, based on a case study. This comparison will serve to validate the ASSF tool model, whilst simultaneously demonstrating one of the possible applications of the developed tool. This application is the quick simulation of a chemical plant focused on the production of MeOH and DME, through CO_2 hydrogenation.

Chapter 5 details two further applications of the ASSF tool, as well as its utilization within an existing RPD analyzed through the use of Aspen ® Plus, another reputable software platform. The application and demonstration of the ASSF tool to an existing RPD allows for the performance and reliability of the tool to be checked against an established software package and framework. The second application demonstrated within this chapter, involves determining optimum operating conditions for a reaction pathway, accounting for factors such as unit operation costs.

The conclusion and possible future work within this field is discussed in Chapter 6 and Chapter 7, respectively, with the final sections of this thesis containing the appendices which includes additional data that was required over the course of the model development and its application. The results obtained via the ASSF tool are also provided within these appendices.

Chapter 2: Literature Review

This chapter looks at previous work conducted within this research field, identifying, and discussing the shortcomings of each contribution. These shortcomings were utilized to identify the gap in the field addressed within this thesis. Furthermore, a review on some of the pathways utilized in producing MeOH and DME through CO_2 hydrogenation, will be highlighted within this chapter, and will be later utilized in developing an RPD. This RPD will form the basis for one case study, when demonstrating the application and usefulness of the Automated Systematic Synthesis Framework (ASSF) tool developed and detailed within this thesis.

2.1. Previous Research in this Area

The design of any chemical process can be considered through two approaches, i.e., a hierarchy approach or a superstructure approach. When considering a chemical process from a hierarchy approach, this would involve a concept that is referred to as the 'onion logic' (Smith & Linnhoff, 1988). This concept expresses the design of a process as layers, indicating the parts of the process that should be focused on in each stage.

With such an approach, the knowledge utilized in each step is dependent on the stage itself and the knowledge gained from previous stages. This approach, however, does not include forward thinking, and as such only focuses on the design at hand within that specific design-stage. Figure 2.1 details the onion model developed by Smith & Linnhoff (1988).

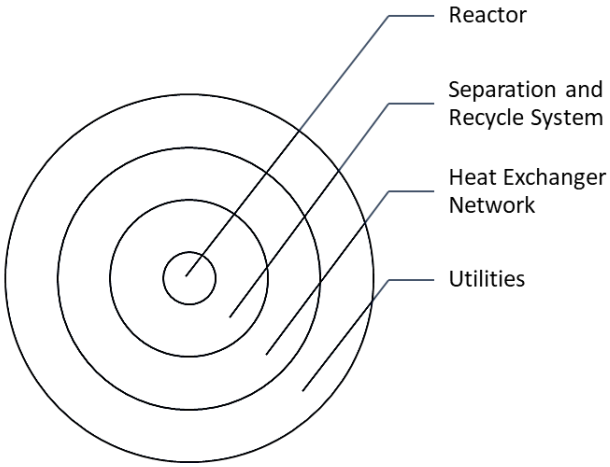

Figure 2.1: Diagrammatic representation of the 'onion logic' approach to process design (Smith & Linnhoff, 1988)

Due to the incremental approach taken in designing and solving a process problem, the onion logic follows the process of obtaining local optimums within each stage, thereby not necessarily guaranteeing a global optimum for the process structure. However, based on research conducted by Smith & Linnhoff (1988), the reactor unit operation is considered to be the most important process design, with all other unit operations and design processes, being designed around the reactor. As a result, the reactor is considered to be the 'heart' of the process.

This is expected to a large extent, as the reactor is the primary unit operation involved in the production of the desired product for the purpose of resale, and as such performs an integral role in the economic feasibility of the process. Other economic considerations that are dependent on the reactor include the unit operations surrounding the reactor, as these are required to achieve the necessary operating and separation conditions for the pre- and post-reactor processes. Furthermore, any unreacted chemical species, or by-products, affect the environmental feasibility of the process, further attesting to the importance of the reactor unit operation.

Due to the importance and central nature of a reactor unit operation, a considerable amount of research is focused on optimizing and finding the best reaction pathway possible for this unit operation. An investigation conducted in 1982, by Rotstein, *et al*., developed a framework whereby new reaction pathways were explored through the analysis of their Gibbs Free Energy, noting the importance of considering alternative reaction pathways in developing a process (Rotstein, *et al*., 1982).

The reason why much attention is spent on finding alternative reaction routes that are able to produce the same product, is that alternative systems may prove to have a greater efficiency in utilizing the reactants, or even result in the reduction of unwanted by-products. On the other hand, some by-products of potentially greater value, can be achieved by exploring alternative designs (Rotstein, *et al*., 1982). Various reaction pathways may also be of assistance in lowering the cost of subsequent separation systems (Govind & Power, 1977).

In the framework developed, three factors were considered for the analysis of the reaction pathways and their alternative routes to the desired product, namely the change in Gibbs free energy for the reaction, the heat of the reaction and the temperature (Rotstein, *et al*., 1982). Previous work in this area, conducted by Govind & Powers (1977) looked at only two variables, i.e., the Gibbs free energy and the temperature, resulting in a less holistic view when considering alternative pathways (Govind & Power, 1977).

The concern with this work, however, was the three-variable system. Such variables resulted in a large degree of freedom for the problem structure, consequently resulting in a search space containing infinite possibilities. Furthermore, the reactions are considered in terms of spontaneity, based on their Gibbs free energy, thereby not considering other important features surrounding reaction pathways, such as their economic and environmental impact.

Further research within this field, conducted in 1989 by Fornari, *et al*., aimed to contain the previous infinite reaction pathway possibilities generated from the earlier work conducted in 1982. Through the limitation of the variables, thereby decreasing the degrees of freedom, the analysis of Gibbs free energy and temperature aided in the reduction of the infinite search space to a smaller, more manageable region (Fornari, *et al*., 1989).

Whilst the newly developed search space still contained a considerable amount of reaction pathway possibilities, the remaining search space was amenable to thermodynamic feasibility analysis. This involved the consideration of the stoichiometry within the feasible $\Delta G/T$ region (Fornari, *et al*., 1989).

The concern with this work, however, is that whilst the reaction pathway search space was reduced, the process by which the thermodynamic feasibility was tested was lengthy. Furthermore, the consideration of thermodynamic feasibility, looked at energy flow with regards to stoichiometric ratios. Once again, this revised framework exhibited similar shortcomings to that which was developed in 1982, whereby the economic and environmental

feasibility of the process was not considered. These are important factors in determining the practicality of the reaction pathway being analysed.

Furthermore, changes in temperature affect the associated unit operation capital cost required to achieve these conditions, a consideration not accounted for within the course of the framework developed in 1989. This is an important consideration in factors such as payback periods and securing investments. Lastly, the consideration of stoichiometry eliminates the consideration of conversion in these reactions. Therefore, whilst the reaction pathway can be considered from a thermodynamic perspective, the implementation and practicality of the pathway is not visible.

In an effort to further reduce the search space of reaction pathways, Fornari & Stephanopoulos (1994), implemented additional screening factors, taking into account considerations such as processing, economics and process safety (Fornari & Stephanopoulos, 1994). The concern here is the extent of the economic factors considered, with the consideration not extending to current economic conditions, or the unit operations required to achieve the necessary conditions. Additionally, the environmental impact of these reaction pathways was not considered during the screening process.

Screening procedures of this nature are manual processes, which can prove to be time-consuming, and increases the likelihood of human error. These considerations and screening were considered on a case-by-case basis, thereby severely limiting its application in industry.

Further work conducted in 1997, looked at the development of a systematic procedure whereby the environmental impact of reaction pathways was considered, in order to account for possible waste reduction at an early stage in the process design. This procedure went as far as to consider the economic impacts of the reaction pathways as well, hoping to find a draw off between these two factors (Buxton, *et al*., 1997).

The environmental considerations made within this process, related to the impact of the species produced within the product, not extending beyond the wastes that are produced in an indirect manner from the process (Buxton, *et al*., 1997), such as that involved in electricity production for the running of the unit operations. This is a major shortcoming, as the energy requirements of a process contribute largely to its environmental impact and associated economic feasibility.

Furthermore, the economic feasibility considered throughout the course of this research, was done so by means of an input/output cost structure (Buxton, *et al*., 1997). However, the

economic impact does not consider the unit operations required to achieve the necessary conditions, thereby not accounting for the cost of unit operations, and the losses that may be incurred during separation. Such an assumption eliminates the possibility of considering technological developments within the framework in the future, thereby limiting its application. This does not provide an accurate representation of the economic considerations.

The reactions, within this investigation, were considered from a stoichiometric perspective, not accounting for the associated conversions (Buxton, *et al*., 1997). This assumption reduces the practicality of the proposed framework, as it is highly unlikely that an industrial process will be able to achieve complete conversion in all reactive systems.

Other assumptions made throughout the course of the investigation, include the removal of all side reactions, with no such side reactions being considered in the process, and an assumption that all reactions can proceed at 1 atm pressure (Buxton, *et al*., 1997). Given an industrial setting, these assumptions are impractical, and as such reduces the usability of the proposed framework for the development, or optimization, of new and existing plants, respectively.

In 2000, a systematic reaction pathway synthesis method, developed by Li, *et al*., looked at determining viable reaction routes, from an economic perspective. During this investigation, the economic feasibility was considered as the sales potential of the products less the cost of the reactants (Li, *et al*., 2000). However, the shortcoming here, is that this research did not account for conversion or possible losses in the product through the subsequent separation systems.

Another shortcoming, or concern, noted within this research was that one of the optimizing parameters was to minimize the number of intermediate chemicals in the overall reactions (Li, *et al*., 2000). When accounting for conversions, within a reactive system, it is likely that converting the raw material to a more reactive state, before formation of the final product, may prove to yield higher overall conversions. This, however, may not be possible with a direct reaction route. Therefore, this objective function was not fully utilized to account for the draw-offs between extra intermediary reactions, their benefits, and the associated costs.

In the year 2000, Li, *et al*. developed a hierarchy approach whereby the economic potential and thermodynamic feasibility of a reaction pathway structure was considered. In this procedure, pathways that showed promise, from an economic perspective, but were not deemed to be thermodynamically or kinetically feasible, were broken down into a series of intermediary reactions, aiming to achieve overall thermodynamic feasibility. This was accomplished by

breaking down the overall reaction into multiple thermodynamically feasible sub-reactions (Li, *et al*., 2000).

In order to demonstrate the effectiveness of this hierarchy approach, the methodology was applied to a vinyl chloride production system, finding that 17 thermodynamically feasible reactions can be developed for this reactive system, considering stoichiometry and gross profit based on the input/output of the reaction (Li, *et al*., 2000).

The shortcoming of this work, however, is that the reaction pathways are not considered in terms of their conversion, and as such the stoichiometric consideration assumes complete conversion of the reactions. Furthermore, considering only a reaction input/output flow does not account for possible losses that may occur throughout the course of the separation system. The proposed hierarchy approach was not an automated system and required manual calculations and consideration by the user. Lastly, this approach did not consider the cost of equipment required to achieve the necessary reaction conditions, and the environmental impact of the overall process.

The P-graph, explicated later in Section 2.3.5.2, was first applied to reaction pathways in 1997 (Fan & Friedler, 1997), before being utilized by Fan, *et al*. (2001) as a means by which to determine the reaction mechanism associated with catalytic reactions (Fan, *et al*., 2001). The P-graph was then further utilized by Seo, *et al*. (2001) later that same year, verifying the results obtained earlier that year (Seo, *et al*., 2001). Other reaction pathways in which the P-graph was utilized, in order to determine the pathway mechanism, was in the production of MeOH through a partial oxidation process (Tan, *et al*., 2018).

The advantage of using the P-graph in determining the associated reaction pathway mechanisms, was that the P-graph framework was able to provide a complete set of possible reaction mechanisms/routes. In order to confirm this possibility, Barany, *et al*. (2012) investigated the list of possible combinations for a set of elementary reactions through linear algebraic approaches. This was compared to the results found by the P-graph, validating the accuracy and complete search space provided by the P-Graph (Barany, *et al*., 2012).

In order to obtain the final search space of possible reaction pathway mechanisms applicable to a specific reactive system, the search space obtained from the P-graph can be compared to experimental data, noting the commonalities between intermediates. These are likely to be the reaction mechanisms. Should there be further intermediates that cannot be confirmed via the

current experimentation, more experiments will need to be conducted as a means by which to confirm these free reactions (Diaz-Alvarado, *et al*., 2018).

The concern with this work, was that the use of the P-graph focused solely on the development of reaction pathway mechanisms, and therefore was not utilized in the function of finding the optimum reaction pathway possible in producing a single product, or a desired set of products. Therefore, its use has essentially been limited to that of a single reaction pathway, eliminating the possibility of finding a pathway to develop a new chemical plant or to optimize on a reaction within an existing plant.

An investigation conducted by Lakner, *et al*. (2018), detailed extensively within Section 2.3.5.2. Reaction Pathway Synthesis and Identification, introduced the term reaction startability, in order to prevent reaction intermediates from being classified as a new pathway within the P-graph. Consequently, the term 'feasibility' in this reaction was simply a measure of the possibility of the reaction occurring (Lakner, *et al*., 2018), not accounting for the reaction conversion, production rate, economic feasibility or environmental impact. This is a major consideration when dealing with the practicality of a reaction pathway, and therefore such assumptions hinder the application of these approaches within an industrial setting.

Work conducted by Al-Fadhli, *et al*. (2018) looked at developing a multi-period symbiosis network that is capable of utilizing CO_2, H_2 and oxygen as the raw materials. The advantages of a multi-period plant are that it is able to effectively take into account seasonal variations, either in reactant availability or in the product demand (Al-Fadhli, *et al*., 2018).

The proposed approach taken by Al-Fadhli, *et al*. (2018) looked at the net benefit to atmospheric CO_2 levels, aiming to convert these emissions to value added products. Whilst this approach did consider the cases from both an economic and environmental perspective, the shortcoming noted here was that each case was based on chemical plants already in existence (Al-Fadhli, *et al*., 2018).

As a result, the information required for each plant, included their mass balances, energy balances, costs and unit operation sizes. Using this information, each case study was analysed and compared to one another on a case-by-case basis. The concern with such an approach, is that the development of a new plant is not considered, or any chemical plant that has not yet been designed, as the information required will not be available.

This reduces the usability of the approach in industry, in the finding of the optimal reaction pathway geared at producing a specific product or set of products. Furthermore, the fact that this is an analysis conducted on a case-by-case basis, results in the methodology being time consuming, and also, increases the likelihood of human error when making these comparisons.

A further concern lies in the design of the processes. Should these processes be based on existing plants, it is likely that these plants will have varying designs, either in terms of the type of unit operations used, or in the arrangement of these unit operations. Furthermore, should these designs be vastly different, comparisons between these processes may not be entirely accurate.

Work conducted by Jugmohan, *et al*. (2020) developed a systematic framework whereby the optimum reaction pathway could be determined through search space reduction. This work utilized an RPD, focused on the production of a single product, or multiple products, prior to extensive design procedures. The advantage of this work was that it was able to make provision for the economic and environmental criteria, finding a draw off between these two factors. Furthermore, factors such as conversion, payback period and unit operation costs required to achieve the operating conditions were also considered throughout the framework (Jugmohan, *et al*., 2020).

The shortcomings of this work, however, is that the framework made use of four software platforms, namely Aspen Plus ®, MATLAB ®, P-Graph Studio ® and Microsoft ® Excel. This raises two concerns with the research, based on just the software requirements alone. The first is that some of these software platforms, such as Aspen Plus ®, are not readily available, due to their high licensing cost. As a result, there are very few companies that have such platforms readily available for use, thereby limiting the application of such a framework.

Secondly, during the development and implementation of this framework, data had to be manually extracted from one software platform before being inputted into the next software. This would often involve physically drawing reaction pathways, process plants and manually inputting all data associated with the reactive system and its associated unit operations. The input style of this data, however, would be dependent on the software platform being utilized (i.e., one of the four software systems previously mentioned). This would require that the user be familiar with navigating the software interface and its functionality. Therefore, a certain level of training would be needed to meet the required competency level.

The manual extraction and input of data is a time-consuming process and increases the likelihood of human error. Furthermore, such transfers of data do not allow for changes within a process to be made, as this would result in the entire framework needing to be started from the beginning. Hence, the use of four software platforms decreases the practicality and application of the developed framework, within an industrial setting.

Another concern with this framework was that each reaction pathway, or combination thereof, had to manually be designed in Aspen ® Plus V10. This manual design process can lead to inconsistencies, such as varying plant designs, making the subsequent comparisons of their economic and environmental feasibility ineffective.

During the investigation conducted by Jugmohan, *et al*. (2020), all reactions within a reactive system were deemed as being independent, thereby not accounting for the possibility of reaction blocks. In this thesis, reaction blocks are defined as a group of reactions that occur simultaneously in a single reactor unit operation, often being divided into the main reactive pathway and the side reactions/by-products. As a result, the assumption put forward by Jugmohan, *et al*. (2020) is not considered to be practical, as it is common for multiple reactions to occur simultaneously over a single catalyst, at specified reaction conditions.

Finally, the assumption made during the investigation, regarding the design and costing of unit operations, only considered a single type of unit operation, and a single material of construction. It is likely that other types of that unit operation, or perhaps other materials, could provide the same functionality, at a reduced cost, thereby increasing the economic feasibility of the reaction pathways.

The ASSF tool developed and presented herein, provides a novel, rapid screening tool with the ability of addressing these concerns in the initial design stages, bridging the gap between the scale up of laboratory systems, process design, and economic and environmental analysis. Through use of an RPD, the ASSF tool is able to systemically search for potential reaction pathway combinations, and using a generic process structure design, analyse the reactive systems from an environmental and economic standpoint. This allows for the reaction pathway search space to be reduced and ranked in order of feasibility.

2.2. Process Network Synthesis

A process network can be characterized as an arrangement of unit operations, whose sole purpose focuses on the conversion of a set of reactants, or raw materials, to a desired product/s (Jugmohan & Madigoe, 2020). This process however focuses on conversion and does not prioritize the optimization and enhancement that is possible for that specific chemical plant.

Process network synthesis (PNS), on the other hand, is described as a methodology whereby a process network is optimized with respect to its mass and energy balances. Considerations that are accounted for within the scope of PNS, range from determining the optimum type of unit operations within the process, to determining the optimum operating conditions required for conversion of the reactants to the desired product (Maier & Narodoslawsky, 2014). This optimization procedure is conducted with respect to a predefined objective function (Cremaschi, 2015), often centering around three main aspects of a process (Jugmohan & Madigoe, 2020).

The first aspect, commonly used as an objective function during optimization, is the economic feasibility of a process. This is arguably considered to be the most important aspect in any process design (McEwan & Beveridge, 1965). The economic considerations become especially important in the development of the associated process, and in its daily operation. During the developmental stages of a process, and its associated construction thereof, companies often require funding as a means to begin the implementation of the designed process. This would involve securing investors to fund the project, with the deciding factor here being the practicality of the process and the projected economic feasibility of the plant (Pohorecki, *et al*., 2010).

The environmental impact of a process is another important consideration during the optimization process. Though many processes consider the economic impact to be their primary focus, equal attention now falls on the environmental impact of a process. This has become increasingly important based on the effects of greenhouse gas (GHG) emissions which are discussed in greater detail in Section 2.4. Additionally, in an effort to curb the negative environmental impact of many processes, emission taxes are implemented by various governments globally, aimed at compelling companies to reduce their associated emissions, thereby creating a greener and more sustainable process (Ghazouani, *et al*., 2020). Fines are imposed on companies that do not comply with the environmental guidelines and limitations

set out by the local authorities. Whilst this benefits the environment, such taxes and fines however affect the profitability of the plant (Cornelia & Lenuta, 2012).

Lastly the social aspect can be considered to be a priority in defining the objective function focused on the optimization of the chemical plant in question. Often encompassed within the economic feasibility and assessment, the social sustainability of a process factors into account the market uncertainty and the volatility in the sales price of the products, or the costs of the required reactants. This data becomes indicative of the supply and demand in the region and will in turn affect the potential sales of the process within that area (Sepiacci & Manca, 2015).

The solution for such PNS problems can be determined through two main mechanisms, namely the heuristic or computational approach, each having their own set of advantages and disadvantages (Cremaschi, 2015). The heuristic approach is defined as a solution route whereby each of the sections within the process is isolated and optimized individually before compiling a global optimum. Throughout this approach, each decision made in subsequent stages of the process, is dependent on the results and decisions made within the previous process segment, showing their interconnected nature (Yeomans & Grossmann, 1999). The disadvantage of the heuristic approach, however, lies in its hierarchy approach. Since only a single section of the process is optimized at any given point, this results in local optimum conditions that may not produce a global optimum (Blazsik, *et al*., 2001). Furthermore, the isolation of an individual section of the process does not provide adequate representation of the interaction between the variables existing within the process (Cremaschi, 2015).

Alternatively, models can be solved using a computational approach, commonly referred to as mathematical programming. The solution route involves the construction of a mathematical model aimed at optimizing the chemical process. Often this approach utilizes a superstructure, whereby all possible scenarios are accounted for within the process, with the optimal solution being a subset of the aforementioned superstructure (Yeomans & Grossmann, 1999).

The advantage of such an approach lies in the fact that a superstructure can account for multiple variables simultaneously, allowing for interactions between variables to be seen and accounted for during the optimization procedure (Yeomans & Grossmann, 1999). Furthermore, this approach is able to produce a global optimum. However, the computational approach is not without its drawbacks, and solutions generated from this method can prove to be computationally expensive. Furthermore, the development of the computational model can be quite complex, leading to the likelihood of human error being quite high (Cremaschi, 2015).

There are three common disadvantages noted between these two solution structures. The first lies in the time expense, either in the development of the computation model, or the hierarchy approach taken. Secondly, these approaches do not guarantee the consideration of all possible solution structures, resulting in the possible omission of more advantageous solutions (Varbanov, *et al*., 2017).

Lastly, when solving a problem through a computational or heuristic approach, various assumptions are made, allowing for highly complex problems to be simplified to be a more manageable problem. However, over-simplified formulations can result in an inaccurate representation of the original problem, leading to unrealistic or impractical solutions (Klemes & Varbanov, 2015).

2.3. The P-Graph

This section deals with the Process graph (P-graph), highlighting its development, solution algorithms and the associated applications of this diagrammatic representation, within and outside the engineering field.

2.3.1. Development of the P-Graph

Prior to the development of the P-graph, processes were diagrammatically represented through either a Digraph (Figure 2.2) or a Signal-flow diagram (Figure 2.3). Whilst these diagrammatic representations do appear to be very similar in nature, their key difference lies in the purpose and representing factor of its vertices. For the Digraph, each vertex characterizes a unit operation within the process, whereas in the case of a Signal-flow diagram, each vertex signifies a material flow (Palmer & Chung, 2000).

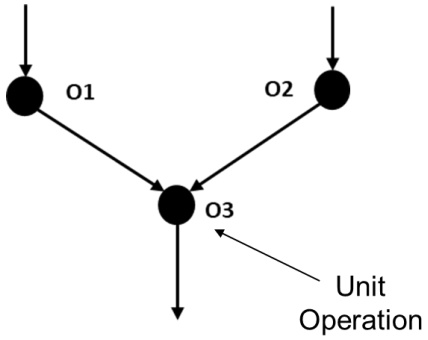

Figure 2.2: Diagrammatic representation of a Digraph

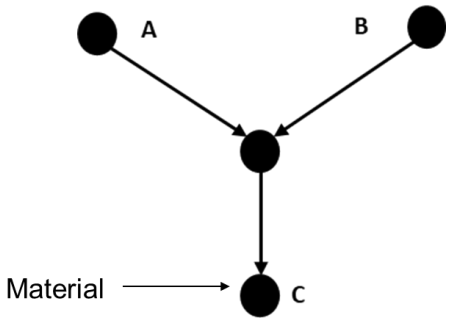

Figure 2.3: Diagrammatic representation of a Signal-Flow Structure

As seen in the diagrammatic representations given in Figure 2.2 and Figure 2.3, these process representations can often be confused, resulting in much ambiguity with processes represented using these diagrams. Furthermore, as shown in Figure 2.2, where the materials are represented as vertices, there is no distinguishing factor between the reactants and the products of the process, once again, adding to the confusion in interpreting such data (Palmer & Chung, 2000).

A typical example, where the confusion noted within these diagrammatic representations becomes especially evident, is when one considers the possibility of a reactive system against a separation system. Looking at the Digraph representation in Figure 2.2, it is unclear if unit operations O1 and O2 are producing the same product, which is then fed to unit operation O3, as a form of mixer, or if there are two separate chemical species being reacted in unit operation O3 to form a new product.

This ambiguity and confusion resulted in the Digraph and Signal-flow diagram being deemed as insufficient process flow representations, prompting the development of the P-Graph. Developed in 1992, the P-Graph aimed to provide a resolution to the concerns raised by its predecessors in the diagrammatic representations of processes (Friedler, *et al.*, 1992). This

development was able to combine the graphical theory with various combinatorial algorithms, allowing for a superstructure approach to be taken when graphically representing different chemical processes.

The distinguishing feature between the P-Graph and the aforementioned process representations, lies in its bipartite nature, implying that the P-Graph contains two vertices. This allows for easy differentiation between the materials and unit operations. Circles are used to represent materials, with the type of circle representing various types of materials, such as raw materials, intermediates and reactants. On the other hand, unit operations are represented by horizontal bars (Figure 2.4). These two vertices are joined together by means of an arc, showing the interaction of the materials with the various unit operations, as well as the direction of the associated flow (Friedler, *et al*., 1992).

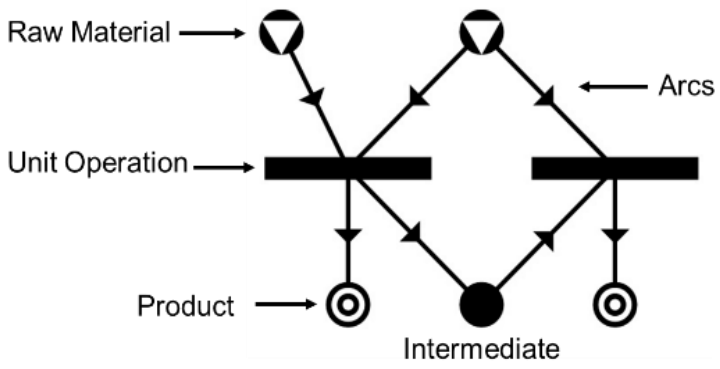

Figure 2.4: Diagrammatic representation of a P-Graph (Jugmohan & Madigoe, 2020)

As a result of the two vertices utilized in the P-Graph, along with the arcs, this diagrammatic representation is able to capture both the syntactic and the semantic contents of the process. Solution structures within such a diagram are only those that have a direct line from the reactant to the final product, with pathways that exhibit no link to the products not holding any practical value (Friedler, *et al*., 1992).

2.3.2. P-Graph Axioms

Unit operation vertices are commonly referred to as O-type vertices within the P-graph, whereas material vertices are referred to as the M-type vertices. In order for a structure to be termed as a P-Graph, there are five axioms that must be met. These axioms are as follows (Friedler, *et al*., 1992):

1. Every final product must be represented in the graph.
2. A vertex of M-type has no input if, and only if, it represents a raw material.
3. Every vertex of the O-type represents a unit operation that is defined within the synthesis problem aiming to be addressed.
4. Every vertex of the O-type has at least one pathway that leads to an M-type vertex depicting a final product.
5. If a vertex of the M-type belongs to the graph, it must be an input to or an output from at least one vertex of the O-type in the graph.

It is essential that all five of these axioms are met for any sub-structure within the P-Graph. Should a sub-structure not meet any one of these axioms, it is immediately excluded from the total P-Graph structure, as it would have no practical value to the system at hand. The resulting P-Graph is then referred to as the maximal structure.

2.3.3. P-Graph Solution Algorithms

The algorithms utilized within the P-Graph, were initially developed by Friedler, *et al*. (1979), where the algorithm was used to analyse a superstructure to determine the optimum configuration required to produce a desired product from a predefined raw material. With this algorithm, all of the possible solution structures could be systematically determined. This is based on a decision-mapping tool that involves finding the optimal solution as the minimum sum of the weights associated with each task (Friedler, *et al*., 1979). However, when this algorithm was first used, the P-Graph had not yet been developed. Therefore, the algorithm was used in conjunction with the Petri graph, represented in Figure 2.5, where a_k is used to represent the number of inlet material flows involved in the process and a'_l is used to represent the number of outlet material flows in the predefined process structure. This graphical representation bear striking resemblance to the P-Graph shown in Figure 2.4.

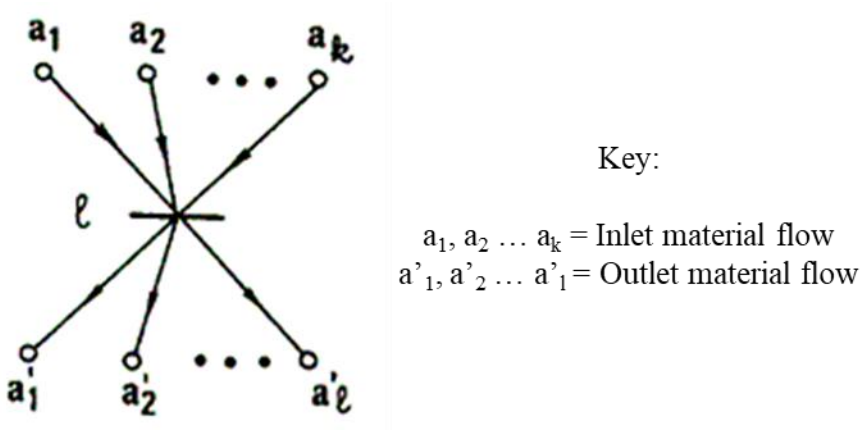

Figure 2.5: Diagrammatic representation of the Petri graph (Friedler, et al., 1979)

The disadvantage with decision mapping algorithms, is that there is no guarantee that each potential mapping, or potential route, will exist as part of the final solution space. Therefore, it is likely that decision mapping algorithms could lead to excess calculations, increasing its respective computational times, ultimately lowering the efficiency of the algorithm (Friedler, *et al*., 1979).

Friedler, *et al*. (1992) aimed to increase the efficiency of the decision mapping tool utilized in the Petri graph, through exploiting the combinatorial nature of superstructures. This algorithm is known as the Solution Structure Generation (SSG) algorithm. The advantage of this algorithm is its ability to be paired with the Accelerated Branch and Bound (ABB) algorithm, which makes use of upper and lower limits in an attempt to determine the optimum solution structure relative to an objective function (Friedler, *et al*., 1995).

With the development of the SSG algorithm being validated in 1995, these algorithms became integral in solving process network synthesis problems, as they were able to handle larger, industrial problems with greater efficiencies (Friedler, *et al*., 1995). In 1993, Friedler, *et al*. coined the term ‘maximal structure’, as was described in the P-graph axioms detailed in Section 2.3.2. P-Graph Axioms. Essentially the maximal structure aims to address two main questions within the superstructure (Friedler, *et al*., 1993). These two questions are as follows:

1. Are there any unit operations that do not serve a purpose in converting the raw material to the desired product, resulting in the model being more complex than is necessary?
2. Are there any unit operations not present within the model, thereby preventing the process from converting the raw material into its desired product?

By addressing these two questions at an early stage, the existence of a feasible solution becomes clear, allowing the possibility of a solution to be evident even before the need for mathematical modelling (Friedler, *et al*., 1993).

Later in 1993, Friedler, *et al*. moved forward in developing the Maximal Structure Generation (MSG) algorithm, whereby the aforementioned maximal structure can be generated from any P-Graph superstructure. The advantage of the MSG algorithm developed, lies in its use of combinatorial algorithms, coupled with its polynomial nature, allowing for its application in larger, more complex systems (Friedler, *et al*., 1993).

When utilizing the MSG algorithm, there are two main stages through which this algorithm operates, namely a reduction and composition stage. This involves the subsequent breakdown of the superstructure, before being reconstructed to meet the aforementioned axioms. During the reduction stage, the materials and unit operations that are unable to meet the predefined axioms are either fully, or partially excluded from the superstructure. The remaining unit operations and materials are then reconstructed, during the composition stage, forming the final maximal structure. This algorithm can even be used in the validation and verification of existing superstructures relative to the aforementioned axioms (Friedler, *et al*., 1993).

2.3.4. Software Platforms

To make use of the established frameworks, multiple software platforms have been developed. For the P-graph, explicated previously, a multitude of different software platforms have been developed, with each program having its own associated solvers and algorithms.

One of the earlier P-graph software platforms developed utilized a simple command line interface, allowing for all necessary information to be inputted by the user via a text file. However, in order for the software to adequately decipher and utilise this data, the input text must be in a predefined syntax. Any deviations from this syntax were noted to cause errors within the software, thereby making it difficult to utilize. Another concern with this software lies in its time-consuming nature, with the manual input being prone to human error (Varbanov, *et al*., 2017).

It is these shortcomings of the initial software platform, that prompted the development of the ‘PNS Editor’, which utilizes a graphical user interface (GUI) as a means by which to increase

the usability of the platform. This provided the user with a much easier, and more efficient manner, by which to input the necessary data that is to be analysed by the P-Graph (Varbanov, *et al*., 2017).

Following the development of PNS Editor, various other software platforms such as PNS Draw and PNS Studio were developed. PNS Draw provided the user with the ability to manually construct the P-Graph to be analysed, allowing for the diagrams to be formatted and edited at will. This gave the user more control over the P-Graph being drawn within the software, with this graphical approach providing ease of usability to the user. PNS Draw also contained a self-formatting feature that allowed for the P-Graph to be arranged in a clear and concise manner, through an automated process. The P-Graph developed within this software can be exported as an image file, to be further analysed within other software platforms, such as PNS Studio (Klemes & Varbanov, 2015).

An alternative software by which to construct and analyse P-Graphs is PNS Solutions. This is a pre-programmed GUI program with the capabilities of employing the aforementioned algorithms, detailed in Section 2.3.3. P-Graph Solution Algorithms (Varga, *et al*., 2010). This software platform allows the user the ability to export the associated data results to Microsoft Excel, as well as provide and generate mathematical programming model formulations (Klemes & Varbanov, 2015).

Typically, with such software platforms, the GUI and solvers, are constructed within a single program. Whilst this often allows for ease of use of the software platform, this type of software also limits the software performance to that of the user's computer system, as the solution speed and capabilities will be dependent on the processor and available memory of information technology (IT) system. Varga, *et al*. (2010) investigated a means by which to bypass this limitation, using a communication protocol, allowing the GUI and solver to exist on two separate servers. Such computational systems are referred to as having multi-tiered architecture (Varga, *et al*., 2010).

For multi-tiered architecture software, a dynamic link is developed between the client and server interfaces, whereby the client application sends problems directly to the server, in order for the relevant solver to be executed. The major advantage of such computational architecture lies in its ability to support multiple clients at any given time. Furthermore, such platforms are able to allow the user to continue to utilize their system, whilst a problem is being solved on the server, thereby accelerating the computational time required to solve the problem and

bypassing the limitations of the user's machine (Varga, *et al*., 2010). This can be represented diagrammatically by means of Figure 2.6.

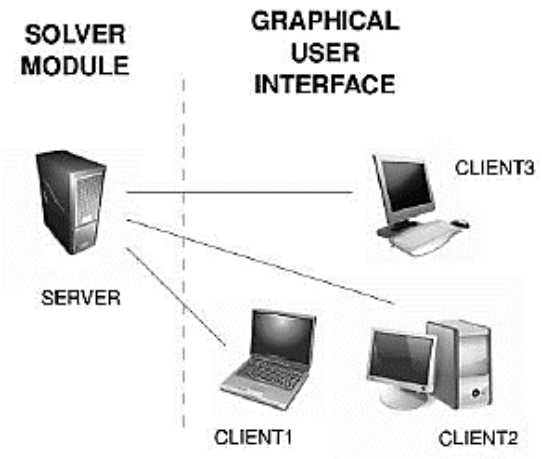

Figure 2.6: Diagrammatic representation of the link existing between a server and the clients (Varga, et al., 2010)

The latest addition in the arsenal of P-Graph related software platforms is P-Graph Studio, developed and hosted by the University of Pannonia as a freeware software (P-Graph, 2015), (Friedler, *et al*., 2019). This implies that the software is free to download and utilize globally. This software platform combines a GUI with the various computational solvers, allowing for the user to import and export data from various file formats.

2.3.5. Applications of the P-Graph within the PNS Scope

The primary aim of the P-Graph framework lies in its ability to solve PNS problems, as highlighted extensively within the founding paper (Friedler, *et al*., 1992). This section highlights some of the various methods in which the P-Graph has been utilized in solving PNS problems, including, but not limited to, separation network synthesis (SNS), reaction pathway synthesis and identification, design and ranking of various technologies, multi-period plant designs and fuel cells.

2.3.5.1. Separation Network Synthesis (SNS)

There are four main areas encompassed within the development of a chemical process, namely the reactor network, separation system, heat exchanger network and the final process flowsheet

detailing the flow of materials and the various unit operations thereof. However, bulk of the energy and water usage in a plant lies in the separation system (Cremaschi, 2015). This system is especially important in meeting the correct product purity required for the sale of the associated product. As a result, separation systems often require large capital and energy investments (Heckl, *et al*., 2010), (Cremaschi, 2015).

In 2000, Feng, *et al*. investigated the use of the P-Graph in determining the feasible combinations possible for batch and continuous azeotropic distillation systems. This approach utilized the SSG algorithm and required that all material flows and unit operations be known prior to its implementation. However, this methodology only went as far as to develop all possible separation systems, with the optimum network needing to be determined through a subsequent manual, hierarchy approach (Feng, *et al*., 2000).

Throughout the course of this investigation, over 100,000 possible solution structures were generated. This is an extremely large search space for the optimal separation system, with manual analysis of these systems being impractical and time-consuming, thereby not capitalizing on the potential for the utilization of the P-Graph within this separation system (Feng, *et al*., 2000). In order for such a system to be effectively optimized via the P-Graph framework, it is essential that the solution be coupled with process flowsheet and design algorithms.

One of the major concerns relating to separation network synthesis, however, lies in the composition of the feed and product streams. Due to infinite possibilities of stream compositions that can be achieved through separation efficiencies and mixer unit operations, there are infinitely many separation networks that can be composed. As a result, the use of heuristic and algorithmic approaches in solving SNS problems are limited. Furthermore, an infinite solution search space increases the likelihood of possible solution structures being overlooked during the analysis procedure (Feng, *et al*., 2000).

In an attempt to limit the infinite number of possible solution structures, Heckl, *et al*. (2010) coupled the P-Graph with a linear mathematical model, placing the mixer unit operations after the product streams. This resulted in a finite number of possible separation systems and stream combinations, when isolating the separation system. This approach became known as the SNS-LIN methodology (Heckl, *et al*., 2010).

The application of a linear mathematical model within this approach, also allowed for more efficient solution times (Heckl, *et al*., 2010). However, using a linear model can raise concerns

with regard to the accuracy of the model, as there are few systems that actually follow a linear formulation, with many being akin to polynomial relationships.

Through the application of this methodology, it was found that the optimal separation system was identical to that when manually solving such an SNS problem, validating and verifying the methodology proposed by the SNS-LIN approach (Heckl, *et al*., 2010).

Another concern that arises in optimizing separation systems, is the ability to determine a global optimum. Many of the systems developed throughout the optimization procedure are either incomplete or have multiple equations and mathematical models that may prove to have no practical value in solving the problem at hand. This makes the model more complex than it needs to be. The work conducted by Kovacs, *et al*. (2000) aimed to address these concerns through a model that focused on the solution of separation networks employing a linear cost function (Kovacs, *et al*., 2000).

In order to utilize this developed framework, the unit operation efficiencies and stream ratios were required as prerequisites. Through its application to four existing case studies, Kovacs, *et al*. (2000) was able to prove that the developed model yielded results with a cost of up to 30% lower than the existing solution models (Kovacs, *et al*., 2000). The concern and shortcoming, of this work, however, lies in its assumption of linear cost functions. Cost functions are often expressed as exponential relationships between the cost of the unit operation and the size/capacity required (Ong, *et al*., 2016). Thus, the simplifying assumption of linear cost equations employed within this methodology does not guarantee reliable results.

Furthermore, the developed system considers only the separation system, excluding factors such as mixers, piping, pumping energy requirements and maintenance, which decreases the practicality of the solution developed.

One manner in which the linear cost functions can be addressed is through the use of non-linear cost functions (Guillen-Gosalbez, *et al*., 2019). However, currently the P-Graph software available lacks these provisions. The work conducted by Ong, *et al*. (2016) aimed to address this concern by modelling the various non-linear cost functions as multiple linear segments, with each segment being represented by a unit operation within the P-Graph (Ong, *et al*., 2016).

Through this breakdown on non-linear cost functions, the results obtained through the P-Graph framework proved to be more accurate and practical. Furthermore, the investigation conducted by Ong, *et al*. (2016) also found that the accuracy of the cost increases when the number of

segments were increased. However, increasing the number of segments for the costing model results in drastic rises in the computational time and power required (Ong, *et al*., 2016).

2.3.5.2. Reaction Pathway Synthesis and Identification

In order to optimize a reaction pathway, with respect to its operating conditions, the reaction mechanism must be known. These operating conditions can extend from the temperature and pressure of the reactive system to its catalyst composition. Reaction mechanisms become especially important when developing or investigating the reaction kinetics behind any reactive system.

One of the concerns when determining the reaction pathway mechanism, however, is the number of possibilities that could exist from a series of elementary reactions. Each elementary reaction can proceed in one of three directions or states, including the forward reaction, the reverse reaction, or no reaction at all (Fan, *et al*., 2002). Thus, this would result in a system of just 5 elementary reactions having up to 242 possible combinations.

In 2001, an investigation conducted by Seo, *et al*. looked at the development of a rigorous methodology that can be used in determining the reaction pathway mechanism of biochemical and metabolic reactions. Through the use of the P-Graph framework, Seo, *et al*. was able to determine the number of combinatorially possible and feasible reaction pathway mechanisms, using the associated elementary reactions (Seo, *et al*., 2001).

This investigation demonstrated the effectiveness of the P-Graph in such instances, through its application to the reactive system involved in converting glucose to pyruvate. Using 14 elementary reactions, a total search space of over 4.7 million combinations can be achieved, with only 46 of these combinations being deemed to be feasible combinations (Seo, *et al*., 2001).

However, the aforementioned P-Graph axioms were specific to process networks, and therefore its application to reaction systems necessitated the need for these axioms to be revised accordingly. The follow axioms were devised to relate directly to reaction pathways within the scope of the P-Graph framework (Seo, *et al*., 2001):

1. Every final product must be represented within the network.

2. Every starting reactant must be represented within the network.
3. Every reaction step represented in the network is defined.
4. Every active species that is represented within the network has at least one pathway that leads to the final product of the overall reaction.
5. Every chemical or active species represented in the network must be a reactant for, or a product from, at least one reaction step represented in the network.
6. A reactant of any elementary reaction represented in the reaction network is a starting reactant if it is not produced by any reaction step present within the network.
7. The network includes at most either the forward or reverse step of each elementary reaction represented in the network.

Once all of the combinations have been computed, using the various elementary reactions, the proposed reaction pathway mechanisms, can be compared with experimental data, to ensure that the intermediates that are present within the reaction align with that of the reaction pathways (Seo, *et al*., 2001).

When making this comparison, however, there are two types of pathways that can be noted from the P-Graph combinations, namely the confirmed reactions and the free reactions. Confirmed reactions are those that are guaranteed to exist within the reaction pathway mechanism, as the data obtained from the P-Graph coincides with the experimental data. Free reactions, on the other hand, are those that cannot be confirmed or identified through the experimental data (Diaz-Alvarado, *et al*., 2018). Often, free reactions require more experimental data in order to be confirmed and may involve more intricate experimental procedures.

Fan, *et al*. (2002) made use of the P-graph as a means in which to determine the reaction pathway mechanism of producing ammonia from nitrogen and hydrogen gas. Once again, employing a similar methodology to that of Seo, *et al*. (2001), this model utilized 14 elementary reactions for the production of ammonia, with the final result showing that only 35 of these can be considered to be independent reaction pathways capable of being the reaction mechanism (Fan, *et al*., 2002).

Fan, *et al*. (2008) aimed to improve on this methodology in determining the reaction pathway mechanism, by also coupling a criterion that accounted for energy favourability. This considered the standard enthalpies of the elementary reactions, with a comparison being made

between the proposed reaction combination developed by the P-Graph and the overall enthalpy of the entire chemical reaction (Fan, *et al*., 2008).

Applying this approach to the water gas shift reaction, 116 combinatorially feasible reactions were found from 17 elementary reactions. Previously, investigations that looked into the reaction mechanism behind the water gas shift reaction, found 70 possible reaction pathway combinations (Fan, *et al*., 2008). This attests to the fact that the P-Graph framework was able to produce a more complex and comprehensive search space.

In 2018, Diaz-Alvarado, *et al*. investigated the possibility of utilizing reaction blocks in determining reaction pathway mechanisms. In this manner, reactions with a common intermediate, that only exist among a single pair in the elementary reactions, can be grouped together and treated as a single block, thereby lowering the complexity of the problem and reducing the associated computational time (Diaz-Alvarado, *et al*., 2018).

However, it is important to note, that in the studies mentioned above, feasibility is determined as the possibility of the reaction occurring, and the axiomatic principles of the P-Graph. As a result, factors such as conversion, unit operation cost, profitability and environmental considerations are not accounted for.

The work conducted by Lakner, *et al*. (2018), looked at determining whether a reaction is able to proceed given only the starting reactants, coining the term ‘reaction startability’. This term refers to a reaction where all starting reactants are available (Lakner, *et al*., 2018). In other words, the reaction must be able to proceed without any chemical species being produced by means of other elementary reactions.

This allowed for the P-Graph to exclude pathways that may require the use of an intermediate, thereby reducing the possible reaction pathway search space, when determining reaction pathway mechanisms. An example of a non-startable reaction can be seen in Figure 2.7.

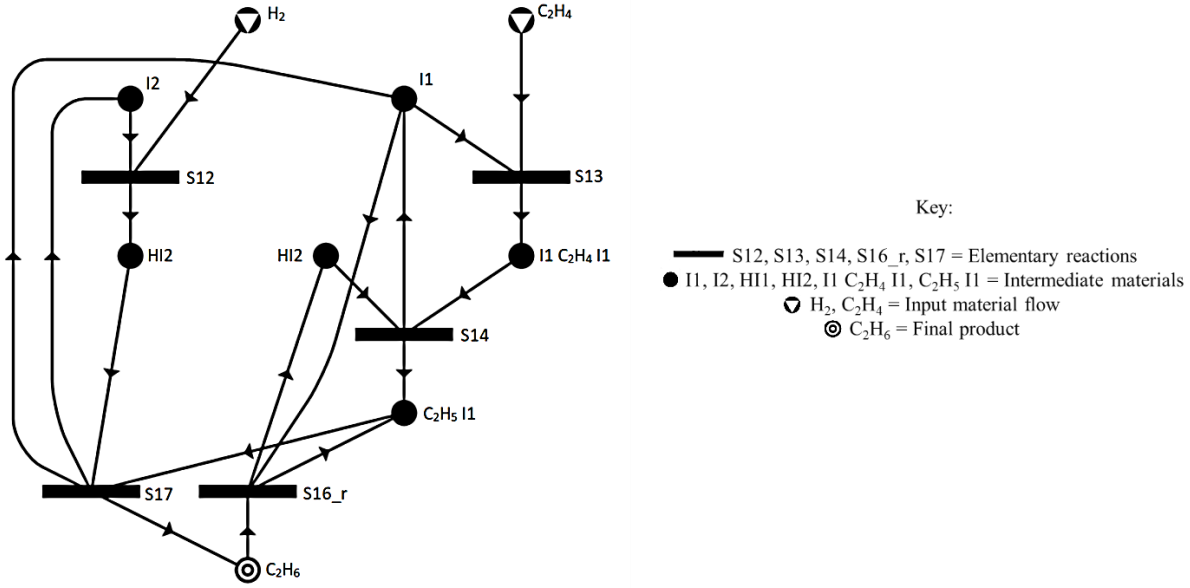

Figure 2.7: Non-startable reaction system (Lakner, et al., 2018)

Based on the P-Graph shown in Figure 2.7, it can be seen that the intermediate species I1 and I2 are required in order to proceed with the first two reactions taking place in units S13 and S12, respectively. These intermediates are not available from the start of the reaction, indicating that this reactive system cannot proceed given only the starting reactants. As a result, such a system is deemed to be non-startable.

The shortcoming of the work by Lakner, *et al*. (2018), lies in how feasibility has been defined, with a feasible reaction being described as those that are startable. The investigation conducted within this work did not account for other factors such as conversion, environmental or economic concerns, which are the crux in determining the feasibility of a process.

The advantage, however, in the use of the P-Graph in exploring the mechanism behind reaction pathways, is that this framework does not utilize a heuristic approach, thereby increasing the accuracy of the work. This allows for the user to develop a complete search space of the possible reaction mechanisms, provided that all elementary reactions are known (Fan, *et al*., 2008).

2.3.5.3. Design and Technology Rankings

During the first stage of the design process, much focus is placed on the analysis of various conceptual designs, in an attempt to find which conceptual design should be pursued further

for possible implementation. The work conducted by Bertok, *et al*. (2013) utilized the P-Graph as a means by which to rank processes on a conceptual level, with the ranking being based on the payout period of the plant and the production rate (Bertok, *et al*., 2013).

Throughout the course of this investigation, a new M-type vertex was added to the P-Graph, in order to represent the load of the unit operation. Should this added material vertex have a value of one, this indicates that the unit operation is in operation, however a material vertex value of zero indicates that the unit in not in operation or is switched off. As such, a value ranging between 0 and 1 is indicative of a partial load (Bertok, *et al*., 2013).

This work found that an increase in the payout period lowered the annualized costs, as the time frame over which the capital costs of the unit operations needed to be paid off increased. Furthermore, a lower production rate was noted to lower the annualized costs as well (Bertok, *et al*., 2013).

A recent study by Low, *et al*. (2020) utilized the P-Graph as a means by which to rank clean energy technologies. In this work, an expert ranked a small sample set of technologies, which was then used as a basis in determining the rankings and weightings of each technology, before being applied to a larger, more complex set of clean energy technologies. This makes use of the preference rule, allowing for the removal of human intervention in the decision-making process (Low, *et al*., 2020).

However, the concern with such a study, lies in the fact that discrepancies were noted between the ranked technologies determined by the P-Graph, and the manual ranking by an expert. This may be as a result of uncertainties or assumptions that were made in either instance. Another possible cause for this difference may be that the weighting obtained for a smaller set of technologies, may not hold true for the more complex systems (Low, *et al*., 2020). Therefore, more research needs to be done to validate the preference rule approach.

2.3.5.4. Multi-Period Plant Design

With the rapid increase in the global population, the rate at which energy is being consumed has increased drastically (Kettl, *et al*., 2011). Fossil fuels are utilized as the primary energy source in meeting these rising demands, resulting in increased CO_2 emissions. In fact, the transport industry alone contributes in excess of 30% to the global CO_2 emissions (Wang, *et*

al., 2020). However, it is important to note that carbon emission rates refer not only to CO_2 emissions, but also to the other GHGs, which are expressed in terms of CO_2 equivalents (Shenoy, 2010).

In light of the rise in GHGs and CO_2 emissions, a substantial amount of research is being conducted into negative emission technologies, as a solution strategy that can assist in meeting the high energy demands, whilst simultaneously reducing current atmospheric levels of these harmful gases (McLaren, 2012), (McGlashan, *et al*., 2012). Not only do these technologies provide environmental benefits, but can also provide economic benefits to the region, providing the locals with job opportunities and a marketable product (Kettl, *et al*., 2011).

There are many areas that are remote/isolated, and as such cannot be connected directly to the conventional electricity grid. As a result, these areas tend to rely on a polygeneration system. However, the challenge is to determine the optimum system configuration to meet the energy demands of the area. This challenge is further exacerbated by the volatility in raw material availability. Such systems that are able to account for these factors are referred to as multiperiod systems (Aviso, *et al*., 2016).

An investigation conducted by Aviso, *et al*. (2016) utilized the P-Graph as a means of developing a multi-period system for an isolated region. Throughout this investigation, unit operations were sub-divided into different modes using an additional unit operation in the P-Graph, labelled as ‘part load’ and ‘regulator’. These additional unit operations had the sole purpose of focusing on, and accounting for, the varying availability of the raw materials (Aviso, *et al*., 2016). This was represented in the P-Graph as shown in Figure 2.8.

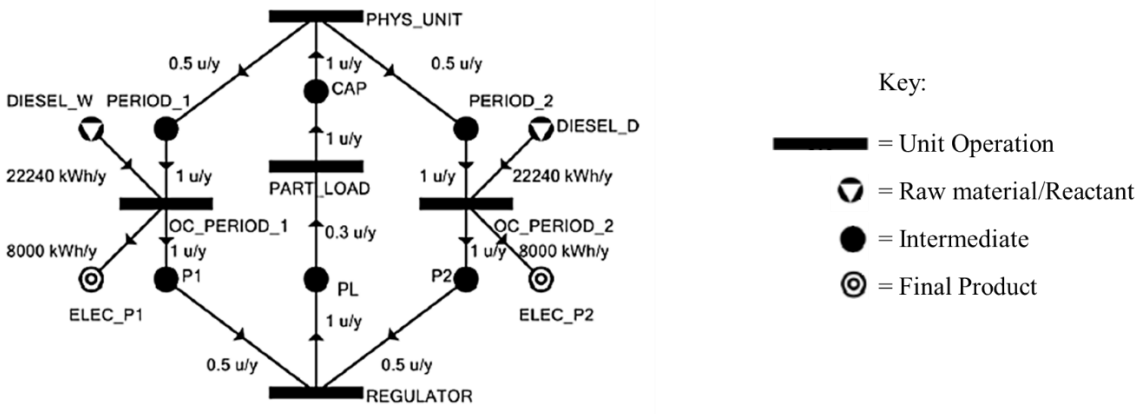

Figure 2.8: Diagrammatic representation for a multi-period diesel engine (Aviso, et al., 2016)

This approach was utilized in a hybrid renewable energy system for an isolated rural community, in order to determine the optimum configuration necessary in meeting the energy

requirements during the wet and dry seasons. The use of the P-Graph in this application, proved to be effective in accounting for the techno-economic characteristic of the unit operations, whilst simultaneously accounting for variable feeds (Aviso, *et al*., 2016).

The concern with such models, however, is their ability to adapt and be applicable at a later time period. With these models, the full nature of the problem is unable to be captured, due to simplifying assumptions, resulting in ineffective representations of the practical constraints. Furthermore, values such as energy tariffs and demand are likely to change with time, and as a result the optimal solution found now, may not hold true in the future (Voll, *et al*., 2015).

In 2017, the work conducted by Aviso, *et al*. was taken a step further by directing the focus on the importance of near optimal solutions that can be generated using the P-Graph framework. As such, one solution structure exhibits a 3% reduction in the profit, however this also lowers the biomass feed required to meet the energy requirements. Whilst this may not be considered to be the optimal solution, this shows that near optimal solutions may be acceptable in times when the reliability and supply of biomass is uncertain (Aviso, *et al*., 2017).

One of the important features of near-optimal solutions lies in the ability of the users to deduce common factors between the solution structures, as well as differences and features that are not present in any of the solution structures. These are referred to as the 'must-haves', 'real choices' and 'must avoids', respectively. By identifying these factors within solution structures, rational decision can be made as to the optimal solution structure for that specific region, or within specific conditions. This allows for practical considerations to be made that may be beyond the capabilities of the developed model (Voll, *et al*., 2015).

An investigation conducted by Tan, *et al*. (2017) looked at pairing the P-Graph framework with the Monte-Carlo simulation, attempting to determine the robustness of near optimal solutions. The approach was specifically applied to carbon management networks. The reason for pairing these two frameworks in this approach, was to consider probabilistic variations and the impact of these variations on the associated results. In this way, a sensitivity analysis could be developed in order to account for any uncertainty that may have arisen during the development of the model (Tan, *et al*., 2017).

In 2016, Tan and Aviso conducted an investigation aimed at addressing assumptions that all unit operations operate at full capacity, as well as the assumption of any partial load of the unit operation being possible (Tan & Aviso, 2016). This concern is raised as many unit operations can become unstable or inoperable if they are operated below their rated capacity, or above

their rated capacity (Aviso, *et al*., 2017), (Tan & Aviso, 2016). In order to account for this constraint, a new unit operation titled 'Limit', was introduced into the P-Graph model. This can be represented diagrammatically by means of Figure 2.9.

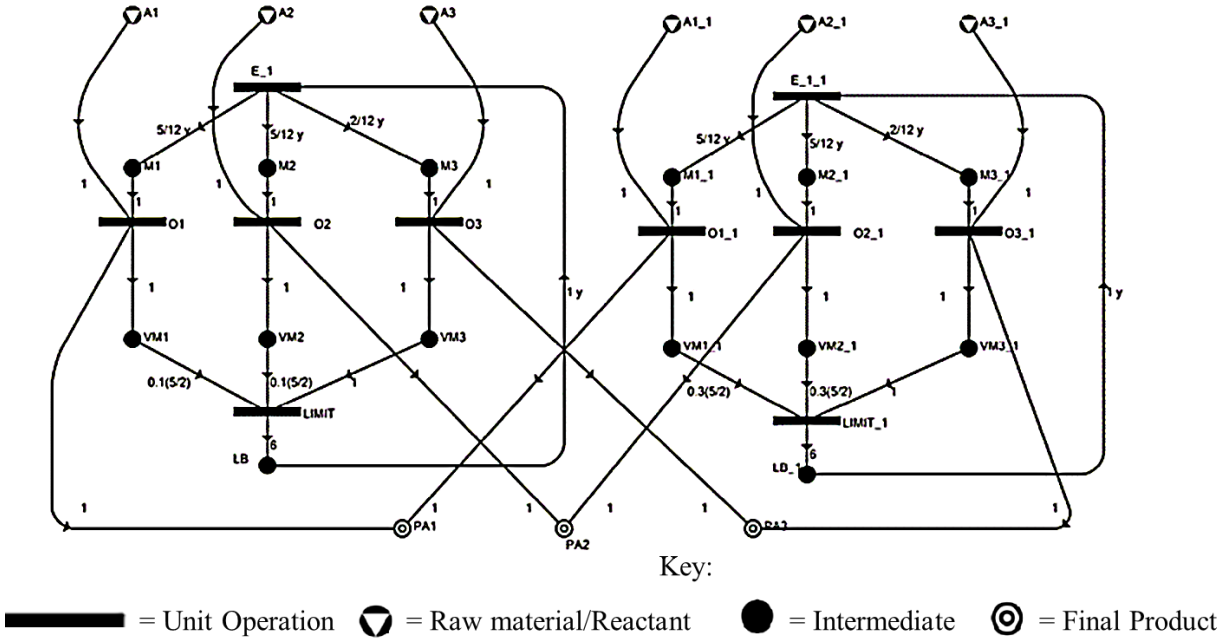

Figure 2.9: Diagrammatic representation of processes with partial limits based on their thresholds (Tan & Aviso, 2016)

The 'Limit' unit operations served the sole function of implementing the lower limit of the partial load unit operation, thereby ensuring that the unit operation remains within a range that maintains its operability. This increased the accuracy of the P-Graph and the associated unit operations (Tan & Aviso, 2016).

2.3.5.5. Fuel Cells

The application of the P-Graph framework can also be expanded to the calculations and design of fuel cells. Fuel cells have gained an increasing amount of attention in recent years, as a result of the high efficiencies noted. Varbanov and Friedler (2008) looked at the development of a procedure whereby the energy system of a fuel cell combine cycle (FCCC) can be analysed, using fossil fuels and biomass as the feed materials. Through the use of the P-Graph framework (Figure 2.10), each FCCC was analysed by means of its carbon footprint (CO_2), profit and the associated heat (Q) and power (W) produced by the biomass fuel (F), as opposed to natural gas (Varbanov & Friedler, 2008).

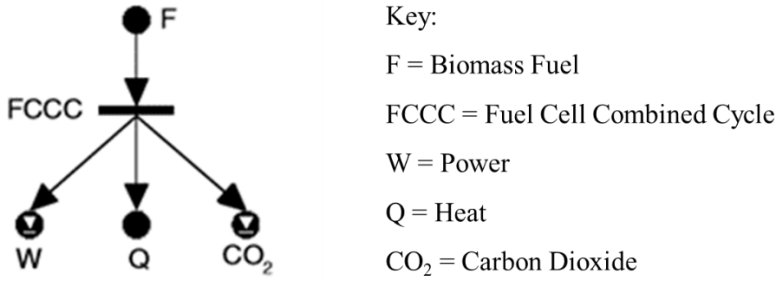

Figure 2.10: Diagrammatic representation of the P-Graph utilized in FCCC systems (Varbanov & Friedler, 2008)

The advantage of the P-Graph framework in optimizing FCCC systems, is that the P-Graph is able to provide an unambiguous representation of the network and allows for optimization of the superstructure through the ABB algorithm. This allows the fuel cell systems to be evaluated at the early stages of their development (Varbanov & Friedler, 2008). The shortcoming of this work, however, was that this work assumed a linear cost function. As mentioned in the work conducted by Ong, *et al*. (2016), this is unlikely to be the case, however this shortcoming can be addressed by the approach presented within their research (Ong, *et al*., 2016).

2.3.5.6. Fuzzy Approach

The fuzzy approach is a methodology by which inaccuracies or uncertainties, within a model can be addressed. The basis of the fuzzy method relies on probability, thereby allowing for the model to be more practical and applicable to a real-life scenario. Furthermore, this approach is able to produce a holistic view of the solution structure, taking into account the effects of possible changes on the final solution structure (Coroiu, 2015).

When determining the order by which processes should be considered for implementation, it is necessary to rank these processes/alternatives based on various criteria, including cost, safety, environmental and social standings. Unfortunately, these criteria often result in conflicts, and as a result, trade-offs are required. For example, in order to increase environmental feasibility and promote a cleaner process, the process may be subjected to added economic costs (Tan, *et al*., 2014), (Low, *et al*., 2020).

This is referred to as multiple attribute decision-making, in which each criterion is scored, or given a weighting, before being evaluated. However, in order to understand the weighting system that is utilized, a fuzzy pairwise approach is taken. The shortcoming of the fuzzy

approach, however, is that it requires a defuzzification process, whereby the fuzzy weights are required to be converted to a crisp weight (Tan, *et al*., 2014).

The work done by Tan, *et al*. (2014) looked at the use of the fuzzy approach, utilizing triangular fuzzy numbers for the comparisons. This allowed for the confidence of each weighting to also be determined and quantified, allowing for increases in the accuracy of the results presented. The drawback of this work, however, was that it was utilized on single-person decisions, and therefore cannot be utilized in group decisions, as conflicts between the data and weighting may arise. This, however, is impractical for industrial applications, where such decisions are often made by a group of people (Tan, *et al*., 2014).

One of the major uncertainties when designing or developing a chemical plant, is the demand for the associated product. In 2018, Tan and Aviso looked at the application of the Fuzzy approach, coupled with the P-Graph framework, to develop the optimal network of cogeneration and trigeneration systems. The variable factors in this study were deemed to be product demand and fuel availability (Aviso & Tan, 2018).

The advantage of utilizing the fuzzy approach, was that partial feasible solutions could also be developed and recorded. Traditionally, the application of the P-Graph could only show fully feasible solution structures, or those that are completely infeasible. The fuzzy approach, however, allows for solution structures that partially meet the requirements to be considered (Aviso & Tan, 2018). This increases the solution space and is more practical when considered from a decision-making standpoint, as it will allow the user to take into account factors that are not included within the model, before deciding on the optimal route.

To account for partial feasibility within the P-Graph, a new M-type vertex was added to the model, representing ‘Lambda’ and ‘overall’ to indicate the degree of partial feasibility of the solution structure, as shown in **Error! Reference source not found.**Figure 2.11 (Aviso & Tan, 2 018).

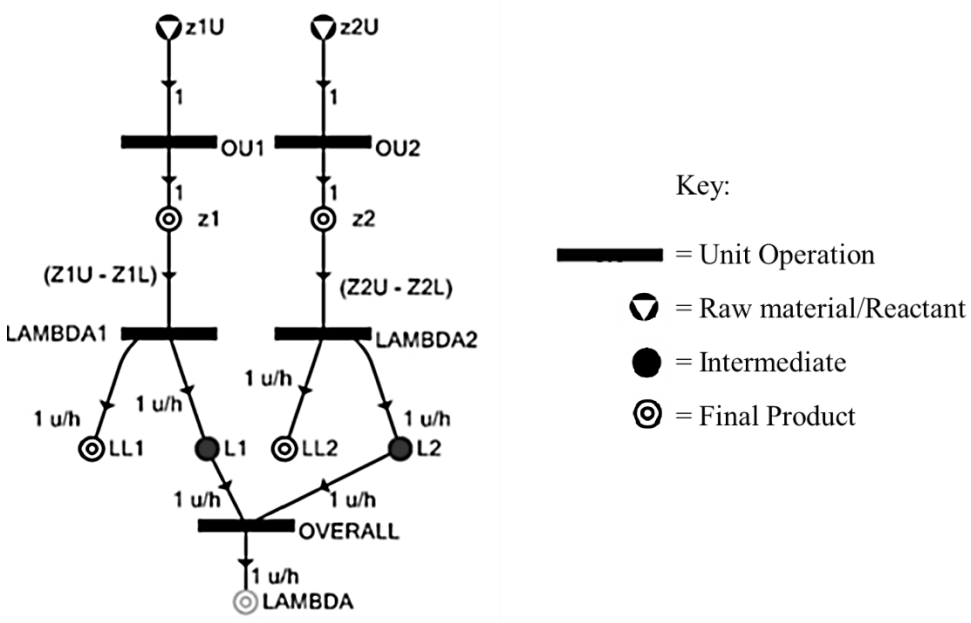

Figure 2.11: Diagrammatic representation of partial feasibility in the P-Graph via the fuzzy approach (Aviso & Tan, 2018)

2.3.6. Applications of the P-Graph beyond the PNS Scope

Whilst the P-Graph framework was initially developed to address PNS problems, its use and application extend beyond that of the process field. The uses of the P-Graph have grown to include vehicle assignment, maintenance schedules, evacuation route planning and even business models, to name a few. In order for the P-Graph framework to be utilized in such a circumstance, the only requirement is to model the problem in the style of a PNS problem. This section will detail some of the non-PNS applications of the P-Graph framework.

2.3.6.1. Resource Allocation

One of the major concerns globally, is the climate change being experienced, as it has a domino effect, affecting the environment and inadvertently the health of those within that region. Furthermore, climate change can also result in drastic changes to precipitation patterns, leading to a reduction in rainfall in certain regions. Furthermore, this can have a chain impact, affecting the production of electricity in those areas that depend on hydroelectric power (Aviso, *et al.*, 2015).

In order to try and mitigate the effects of climate change, there are multiple strategies that are being implemented globally, in an attempt to minimize the effect on the gross domestic product (GDP). Previously such strategies would be developed and implemented in an ad hoc manner, in which resources were allocated to a sector when required. However, this does not allow for future planning and optimum resource allocation (Aviso, *et al*., 2015).

Aviso, *et al*. (2015) utilized the P-Graph framework as a means by which to develop a procedure that allocate scarce resources in such crisis conditions, with the main objective function being to minimize the change to GDP. This will lower the associated economic impact. This approach was applied to three different case studies, finding the minimum possible GDP change (Aviso, *et al*., 2015). However, the shortcoming of using the P-Graph in such cases is that it is unable to account for and adjust to varying social elements. As a result, resources are allocated to businesses rather than households, as they contribute to the GDP of the area. This is not deemed to be socially acceptable.

2.3.6.2. Supply Chains

One of the concerns with the use of renewable energy sources as a means by which to power regions, lies in its intermittent and fluctuating nature. As a result, there is no constant supply of electricity that can be guaranteed from such sources, leading the primary energy source to remain as fossil fuels. An investigation conducted by Sule, *et al*. (2011) looked at utilizing the P-Graph framework in determining the optimum supply chain for renewable energy to remote areas (Sule, *et al*., 2011).

One of the major drawbacks in the P-Graph framework is its inability to account for fluctuating availability of the feed streams, i.e., the reliability of feed. Therefore Sule, *et al*. (2011) addressed this concern through the application of an additional parameter that is known as the Reliability of Availability (ROA), introduced as an M-type vertex in the P-Graph. Accompanied with the feed stream, or raw material, the ROA material vertex serves as a multiplication factor for the reactant, in order to determine the true availability of the material (Sule, *et al*., 2011).

In order to facilitate the multiplication of these two material vertices, an addition unit operation (O-type) was added to the P-Graph. The investigation was found to provide a more accurate

representation of the problem at hand. The results in this study showed that an increase in the reliability of the feed resulted in a decrease in profitability. It is likely that this scenario was caused by an increase in the raw material cost, in order to secure a higher level of availability (Sule, *et al*., 2011).

Another utilization of the P-Graph within the scope of supply chains, was demonstrated by Kalauz, *et al*. (2012) who investigated the quality of a supply chain, taking into account the cost and the time of the chain in question. Through the utilization of the ABB algorithm, the P-Graph model was able to account for upper and lower limit time constraints. The P-Graph framework does not account for time, and therefore, in order for time to be incorporated within this framework a distinction was required to differentiate the sequence of unit operations (Kalauz, *et al*., 2012).

This was achieved using intermediate streams, thereby ensuring that the supply chain follow a specific path, similar to that seen in scheduling problems. Figure 2.12 highlights a P-graph model with the associated intermediates and unit operations necessary to represent time constrained tasks. It can be noted that within this P-Graph, intermediates are treated in a similar manner to storage units, ensuring the correct order of events (Kalauz, *et al*., 2012).

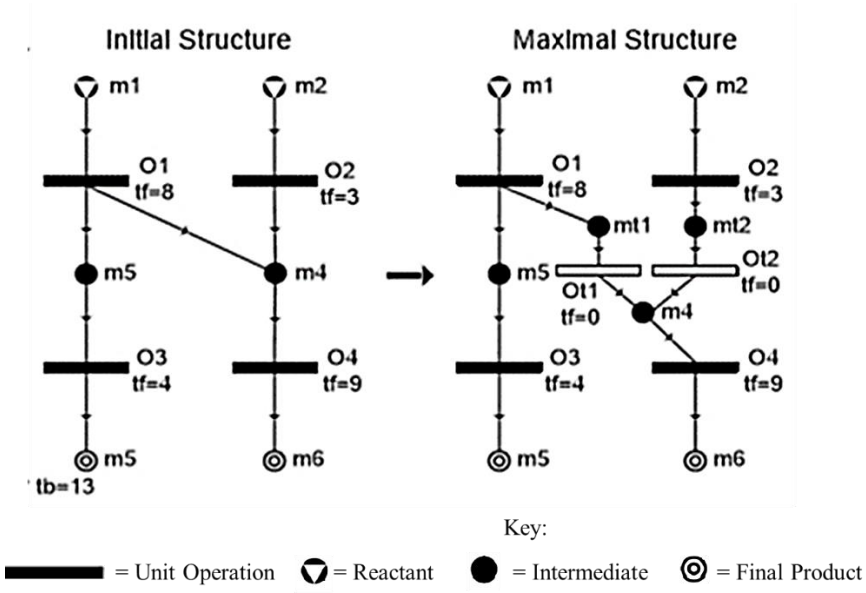

Figure 2.12: Diagrammatic representation of a time constrained P-Graph system (Kalauz, et al., 2012)

Vance, *et al*. (2013) investigated the design of a sustainable supply chain for energy systems, taking into account economic and environmental considerations, such as the cost of the supply chain and the ecological footprint associated therewith. Coupled with the P-Graph framework, this investigation was able to yield optimal and near-optimal results. The ecological footprint

of the process was handled as a separate material vertex, as shown in Figure 2.13. This allows for the ecological footprint of each feed to be taken into account (Vance, *et al*., 2013).

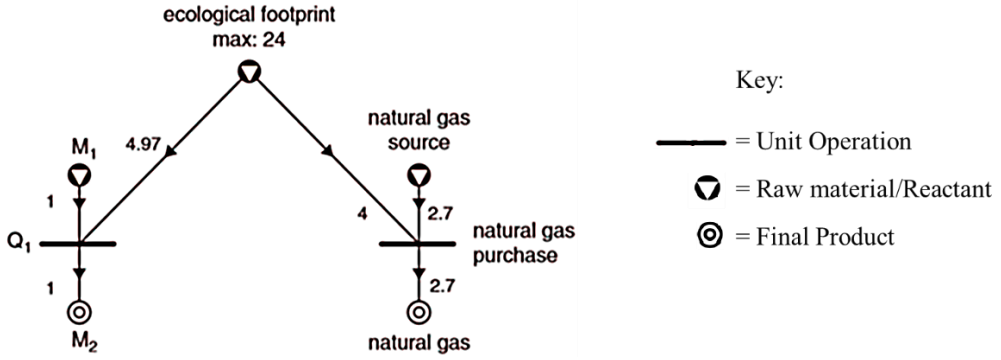

Figure 2.13: Diagrammatic representation to account for ecological footprints within the P-Graph (Vance, et al., 2013)

Two years later, a further investigation conducted by Vance, *et al*. (2015), aimed to further the above consideration through the addition of an emergy analysis, accounting for the environmental strain of the process (Vance, *et al*., 2015). Emergy involves the calculation of all of the energy required for a process, in terms of solar energy, thereby normalizing the energy requirements of a single process, and allowing for effective comparisons within the P-Graph framework.

This approach was utilized in determining the optimum supply chain for an energy system in a rural area, where cost, emergy and ecological footprint were all modelled as material units within the P-Graph, as shown in Figure 2.13 (Vance, *et al*., 2015). Emergy is defined as a unit of measurement where all energy and materials needed throughout the process, is given in terms of a single energy source, such as solar energy. The shortcoming of this work, however, was that the representation of emergy as a material node shows a once-off investment, however emergy is likely to increase with time. Therefore, as the process continues to operate, this factor may not remain the same and this could result in inaccurate results from the aforementioned application.

2.3.7. Variations of the P-Graph Framework

Whilst the P-Graph was developed for PNS problems, various adaptions of the P-graph were developed, in order for the framework to become more specialized in a specific application.

One such adaptation of the P-Graph can be seen in the schedule graph, commonly referred to as the S-Graph.

The S-Graph, shown in Figure 2.14, was first introduced in 1998, six years after the development of the P-Graph framework (Sanmarti, *et al*., 1998), and was aimed at specifically addressing scheduling problems in batch plants (Sanmarti, *et al*., 2002).

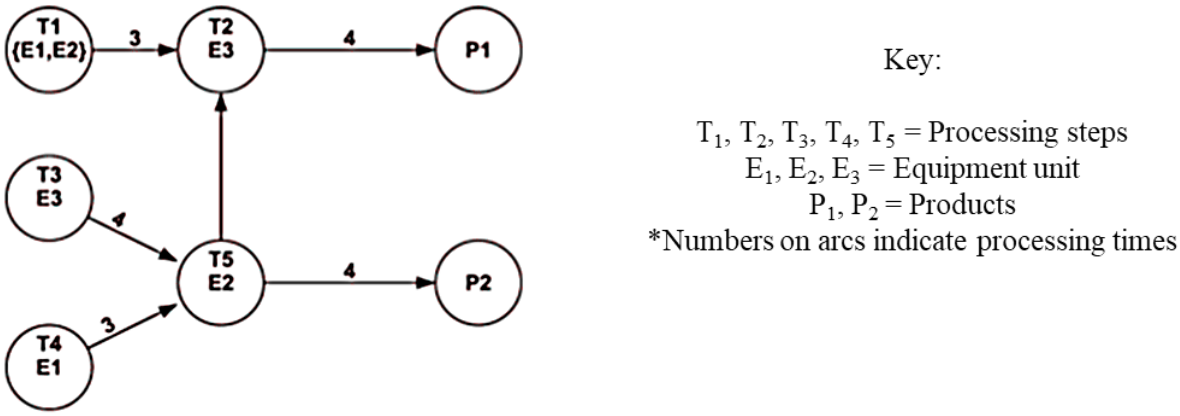

Figure 2.14: Diagrammatic representation of the schedule graph (Hegyhati & Friedler, 2011)

As seen in Figure 2.14, the S-Graph contains nodes that are used to represent tasks, with the weighting of the arcs between these tasks, representing the time taken between each task. Similar to the P-Graph, the S-Graph makes use of the combinatorial nature of the scheduling problem, thereby resulting in increased efficiencies and lowered computational times (Hegyhati & Friedler, 2011).

In 2010, Smidla and Heckl proposed the application of multiple processors to scheduling problems utilizing the S-Graph, in an effort to further reduce the computation times. This investigation was able to conclude that through the use of 'n' compressors, the computation time became an 'nth' fraction of the time required by a single processor (Smidla & Heckl, 2010).

The computational time was further decreased through overwriting the previous data at each step, thereby lowering the memory requirements in solving such a scheduling problem. These results were later confirmed by Lianez, *et al*. (2010). However, the overwriting of data did prove to have drawbacks as well. Such an approach results in the user being presented solely with the optimum solution, thereby eliminating all near-optimal solutions (Lainez, *et al*., 2010). These solutions become increasingly important in industrial applications.

Bertok, *et al*. (2011) developed an algorithm that works backwards from the solution structures, in order to develop a maximal structure. This can be utilized in conjunction with a Mixed-Integer Linear Programming (MILP) formulation, as a way to confirm the results obtained by the S-Graph (Bertok, *et al*., 2011).

Another variation of the P-Graph is the CP-Graph. This adaptation aimed to highlight the importance of safety mechanisms within a desired process. The work conducted by Hangos, *et al*. (1994) looked at a graphic method for the integration of process and control systems (IPCS). This graphic method (Figure 2.15) bears striking resemblance to the P-Graph, with the only difference being the presence of actuators and performance functions (Hangos, *et al*., 1994).

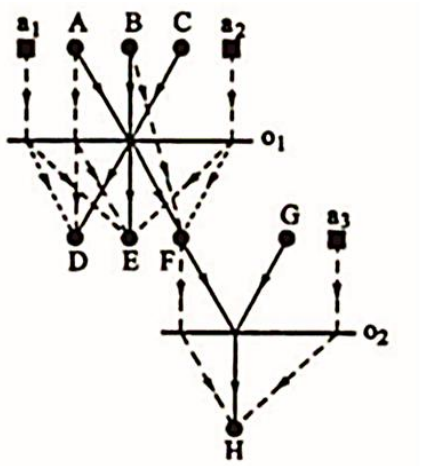

Key:

A, B, C, D, E, F, G, H = Material flows
o_1, o_2 = Unit operations
a_1, a_2, a_3 = Actuators

Figure 2.15: Diagrammatic representation of the CP-Graph (Hangos, et al., 1994)

In this investigation, it was assumed that actuators can only be implemented on the initial reactants, and therefore are not present in intermediates and products. The final maximal structure in the CP-Graph is that which is deemed to be fully controllable, referred to as the combinatorially feasible and controllable (CFC) structure (Hangos, *et al*., 1994). The shortcoming here, however, was that actuators were only used with the reactants, whereas in an industrial process, actuators are utilized along the entire course of a process, including intermediates and products.

2.3.8. Shortcomings of the P-Graph Framework

Whilst the P-Graph is able to offer many advantages within, and beyond, the PNS field, there are still shortcomings within this framework. One such shortcoming was noted in the work

conducted by Feng, Fan and Friedler (2000), where the full potential of a separation system network coupled with the P-Graph is unable to be realized without pairing the framework with an associated flowsheeting and design algorithm (Feng, *et al*., 2000). In order to address this concern, a potential dynamic link can be developed between the P-Graph software and other flowsheeting software, thereby reducing the human error associated with manually transferring the solution structures from one software platform to the next.

Dividers in separation systems are often considered to be non-linear in nature. As a means to solve this concern, Szlama, *et al*. (2012) utilized a splitting interval rather than a splitting ratio, allowing for the optimum solution to be computed in a shorter computational time, as opposed to that when utilizing non-linear algorithms. This approach was able to provide a solution which was previously not possible through the use of non-linear programming (NLP) solvers (Szlama, *et al*., 2012). It is likely that such intervals can be applied to the P-Graph, in conjunction with the existing ABB algorithm, as a means to increase the accuracy of dividers being modelled in this framework.

One of the major shortcomings of the P-Graph framework is its ability to only consider and handle a single objective function system. When considering practical problems, there are often various factors that need to be taken into account, including environmental and economic factors. In order to increase the practicality and the accuracy of the P-Graph in 'real-life' scenarios, the framework should be extended to incorporate multiple objective functions.

A recent study by Wang, *et al*. (2020) found that the use of multiple objective functions, assisted in the provision of greener solutions, as they were able to consider and optimize on multiple factors simultaneously. This allowed for the optimal solutions to be considered from a more holistic viewpoint, thereby allowing for trade-offs to also be considered (Wang, *et al*., 2020).

The current concern with multiple objective functions is the drastic rise in computational time caused by increasing the number of objective functions. In fact, this was found to exponentially increase the associated computational time. Such concerns are likely to be addressed by the use of multiple processors for a single model, such as that described by Smidla and Heckl (2010).

Other improvements to the P-graph include the addition of a lifecycle assessment to the algorithms, allowing for a more detailed environmental impact to be considered over the course of the solution structures (Santos, *et al*., 2018).

Lastly, the P-Graph should make provisions for unit operation reliability as a factor of the unit operation. Whilst it remains true that higher reliabilities in unit operations are accompanied with higher economic costs, these factors must be accounted for in determining the optimum process from an economic standpoint. For example, should unit operations in series incur a problem with a single unit operation, the entire system, and ultimately the process, will fail and be forced to shut down (Zhou, *et al*., 2020).

Parallel unit operations, on the other hand, are not limited by this concern, with the other branches remaining in operation despite a system or unit failure. This would decrease the throughput of the process but would not halt the process in its entirety. The concern with parallel systems, however, is that whilst the remaining unit operations would be able to operate, the increased flow rates through these units may result in an overload, which could cause system failure (Zhou, *et al*., 2020).

Both of these scenarios affect the reliability of the overall process and is an important consideration in determining the optimal and near-optimal solutions, and as such should be accounted for within the P-Graph framework.

2.4. The Impacts of Greenhouse Gases (GHGs)

Due to the rapid rise in global population, the need for energy to be produced has increased significantly (Darkwah, *et al*., 2018), with much of the energy being derived through fossil fuel sources. Unfortunately, throughout the production of energy via fossil fuels, there are multiple gases that are emitted from the process that have proven to be harmful (Darkwah, *et al*., 2018). These gases are GHGs and have major environmental impacts. Furthermore, such emissions can also prove to be a health challenge for those in the surrounding areas (Perera, 2017).

GHGs include various substances such as sulfur dioxide, nitrogen dioxide and CO_2, with these substances causing notable climate change, which is currently known to be one of the most prominent global concerns. Although commonly thought to impact the general temperature experienced, climate change has gained an increasing amount of attention due to the domino effect that it has. For example, climate change has been noted to have effects in areas such as ecological imbalance, economic concerns, environmental concerns and even technological

issues, as some devices are only designed to operate within specific temperature ranges (Abeydeera, *et al*., 2019).

The temperature rise caused by GHGs can be seen in factors such as precipitation patterns, sea level rise and the melting of ice caps (Darkwah, *et al*., 2018). Based on the current rate at which these gases are being emitted, the temperature rise of the earth is expected to be between 2 and 6 degrees Celsius by 2100 (Singh & Singh, 2012).

Whilst this may appear to be a small temperature change globally, such a temperature rise could result in sea levels rising by as much as two meters by 2100, ultimately causing the displacement of up to 187 million people and 1.79 million square kilometers of land (Bamber, *et al*., 2019).

Another concern with climate change is the effect that it has on biodiversity of the planet, including plant life, animals, and their associated ecosystems. There are many species that are only able to survive within specific climate conditions and are unable to adapt to the changes in weather patterns or increases in temperature. As a result of impacts such as climate change, there are currently over 40% of insects that are threatened with extinction. Another concern becomes especially prominent with plant species, defined as the primary producers in an ecosystem. Such alterations to ecosystems can have drastic effects on all subsequent organisms, resulting in the extinction of many species (Sanchez-Bayo & Wyckhuys, 2019).

Based on a study conducted in 2015, approximately 9.5% of all species on Earth will become extinct within the next 100 years. However, if considered with other effects that result from climate changes, this prediction increases to 21% of species (Javeline, *et al*., 2015).

In order to address the concerns of GHGs, it is necessary to target various emission sources. One of the major concerns is the large amount of CO_2 that is emitted during many chemical processes, and as a result there is a substantial amount of research that focuses on possible methods that could aid in either reducing or utilizing CO_2 emissions.

In order to address the CO_2 levels in the atmosphere, through utilization, the following possible utilization routes were noted by Arthur Vanhove (Vanhove, 2015):

1. The utilization of CO_2 as an inert in application, including the food industry, i.e., carbonated drinks.
2. CO_2 can be utilized as a heat transfer fluid under supercritical conditions.

3. CO_2 can be utilized in the recovery of hydrocarbons through its ability to act as a solvent.
4. CO_2 can be chemically converted into value added products.

2.5. The Production of Methanol

With the effect of rising GHG emissions, much attention has been focused on the utilization of CO_2 as a possible reactant, either in reacting the gas so that it may be stored safely, or in converting it to value-added products. One such manner in which this has been explored, centers around the power-to-liquid (PtL) mechanism, whereby excess power is stored in value added products, preventing power wastage (Meunier, *et al*., 2020).

One such promising PtL system is the production of MeOH from CO_2 hydrogenation, especially with the production of MeOH becoming vast within chemical and energy processes. In fact, many consider MeOH to be an imperative part of many processes, either acting as the final product, energy source, or even as a feedstock for other products, such as acetic acid (Meunier, *et al*., 2020).

In the MeOH economy proposed by Olah (2005), MeOH can be used as a cleaner substitute for oil and can be utilized as a fuel in heat engines and fuel cells, with minimal change to their current infrastructure and operation mechanisms. This allows for easy integration of this fuel source (Olah, 2005). Furthermore, MeOH was deemed to have greater efficiencies than the current fuel sources, as it was found to have a higher-octane ratio. This allows for greater compression ratios (Bellotti, *et al*., 2017). In fact, with such major advantages associated with MeOH, it is expected that the market for this compound will exceed 48 billion Euros by the end of 2021 (Meunier, *et al*., 2020).

Additional uses of MeOH can be seen in household products, such as paints and household cleaning products, attesting to their usefulness and the diverse nature of their application (Borisut & Nuchitprasittichai, 2019).

In 1998, Cabrera, *et al*. investigated the production of MeOH using a syngas feed stream, comprising of CO_2, CO and H_2. This investigation was conducted over a zinc oxide (ZnO)-supported copper catalyst, and in order to increase the conversion and selectivity of the reaction to favor the production of MeOH, the reaction was further promoted with the presence of

aluminum oxide (Al_2O_3). Equation 2.1 to Equation 2.3 details the production of MeOH via the syngas route (Cabrera, *et al*., 1998).

$$CO_2 + 3H_2 \leftrightarrow CH_3OH + H_2O \quad \text{(Equation 2.1)}$$

$$CO_2 + H_2 \leftrightarrow CO + H_2O \quad \text{(Equation 2.2)}$$

$$CO + 2H_2 \leftrightarrow CH_3OH \quad \text{(Equation 2.3)}$$

The investigation conducted also included the effect of palladium on the performance of the copper-zinc-aluminum (CZA) catalyst, finding that when preparing the catalyst in 55:30:15 atomic ratio, the presence of palladium increased the conversion of CO_2 at all given operating temperatures. The temperature range utilized within this investigation was between 433 K and 473 K, at a constant pressure of 40 bar (Cabrera, *et al*., 1998).

The shortcoming of this research, however, was that the effect of pressure changes on the performance of the catalyst was not considered. This is an important parameter, as certain catalysts tend to become denatured at higher pressures. Furthermore, the temperature range considered was rather limited, thereby not providing a holistic view on the advantage of palladium in the CZA catalyst. Also, the concern with utilizing palladium to increase catalyst efficiency lies in the high price of palladium, which may affect the overall economic feasibility of the process.

Van der Ham, *et al*. (2012) noted that the production of MeOH via CO_2 hydrogenation, occurs by means of two routes, i.e., the direct and indirect synthesis route. During the direct synthesis route, all reactions occur simultaneously in a single reactor, however, in the indirect route two reaction steps are used, generally first focusing on the production of syngas before converting that to MeOH (Van der Ham, *et al*., 2012). The production of MeOH via the reverse water gas shift reaction can be termed as the CAMERE process. CAMERE is an acronym that is used to represent ‘carbon dioxide hydrogenation to form methanol via a reverse-water-gas-shift reaction’ (Joo, *et al*., 1999).

During the research conducted by Van der Ham, *et al*. (2012) the production of MeOH via the reverse water gas shift reaction was investigated. This reactive system is a combination of Equation 2.2 and Equation 2.3. Through the use of a fluidized bed membrane reactor, and a CZA catalyst, this research generated mass and energy balances through the UniSim® process simulator (Van der Ham, *et al*., 2012).

The advantage of the process detailed here, lies in the zeolite membrane that was within the reactor system, allowing for MeOH to be constantly removed from the process as it was being produced. This resulted in constant shifts of the reaction equilibrium, promoting the production of the final MeOH product (Van der Ham, *et al*., 2012).

However, the concern associated with such a process lies in the production of water over the course of the reaction, as water is known to result in deactivation of the CZA catalyst. A basic plant simulation to produce 10 kilotons of MeOH on an annual basis, utilized a feed of 15.4 kilotons of CO_2, and whilst this was considered an environmental benefit, the investigation conducted by Van der Ham, *et al*. (2012) showed that the process was not economically feasible.

As mentioned previously, however, the demand for MeOH has grown significantly recently, resulting in the subsequent sale prices of this product increasing as well (Meunier, *et al*., 2020). It is likely that this factor, paired with the current technological developments in this area, could improve the economic feasibility of the process.

In order to overcome the high activation energy required to utilize CO_2 as a feed reactant, in the production of MeOH, a catalyst can be used. This lowers the required activation energy, allowing for the reaction to proceed under less strenuous, or extreme operating conditions. The addition of ruthenium (Ru) enabled the lowering of the activation energy; however, this is a rare transition metal, and as such increases the cost of the process (Hong, 2013).

A review on the hydrogenation of CO_2 to MeOH, conducted in 2014, highlighted that at this point, the commercial production of MeOH was achieved using natural gas. Natural gas was first converted to syngas before performing the aforementioned reactive system to convert the syngas to MeOH over a CZA catalyst. The production of MeOH occurs at temperatures of between 250^{o}C and 300^{o}C, and pressures ranging from 5 to 10 MPa (Jadhav, *et al*., 2014).

Based on thermodynamics of the system, the review conducted by Jadhav, *et al*. (2014) noted that the conversion of CO_2 to MeOH at equilibrium conditions is slightly lower than 40%, due to the stable nature of CO_2. However, converting CO to MeOH is known to be much more efficient, with CO conversions in excess of 80% being achieved (Jadhav, *et al*., 2014).

In order to increase the conversion of CO_2, the temperature can be increased, however it was noted that at temperatures exceeding 250^{o}C, the reverse water gas shift reaction becomes more favorable over MeOH production, resulting in excess byproducts. As a result, the first pilot

plant for CO_2 hydrogenation to MeOH, based in Japan, utilized operating conditions of 250^oC and 5 MPa, over a SiO_2-modified Cu/ZnO catalyst (Jadhav, *et al*., 2014), (Tursunov, *et al*., 2017). With 8000 hours of operation, a 99.9% selectivity towards MeOH was achieved. The concern, however, is the time required for operation, which could lead to infeasible processes, as this process was deemed to only produce MeOH at 50 kilograms per hour.

Based on research conducted in 2003, by Mahajan and Goland, in order to promote CO_2 conversion, without promoting the reverse water gas shift reaction, operating pressures would have to be raised to around 30 MPa (Jadhav, *et al*., 2014).

Later in 2014, Maria and her colleagues looked into the improvement of the catalyst associated with this reactive system, furthering the palladium promoter investigation conducted by Cabrera, *et al*. (1998). This investigation considered the possibility of adding chromium and gallium to a Cu/Zn/Zr catalyst, finding that whilst palladium is considered to be the best promoter at lower temperatures, from a selectivity standpoint, gallium is the preferred promoter at a larger operating temperature range (CHEMIK, 2014).

This research however, was conducted under constant pressure, therefore the effect of varying pressures on catalyst performance was not taken into account. Gallium, is however, cheaper than palladium, thereby addressing the cost concern, which was previously raised in this literature review, regarding the work conducted by Cabrera, *et al*. (1998).

In 2015, an investigation that was conducted by Miguel and his colleagues in Portugal looked at the effect of the CO_2/H_2 feed ratio, operating conditions, and the presence of other chemical species in the inlet stream on the yield of MeOH produced, and its associate selectivity. This research was evaluated from a simulation standpoint, utilizing the Gibbs Free reactor unit operation in Aspen ® Plus, and along with the Soave-Redlich-Kwong equation of state (Miguel, *et al*., 2015).

This investigation accounted for the possibility of methane production via the feed stream, finding that whereas a high pressure resulted in an overall increase in CO_2, the pressure needed to promote the production of MeOH over methane, was considerably high. Methane production from this feed stream was noted to be possible at atmospheric conditions (Miguel, *et al*., 2015).

Vanhove (2015) investigated the possibility of improving the design of existing MeOH production plants, finding that in order to meet the high-pressure requirements needed to promote MeOH production, compressors can be broken up into multiple unit operations in

series. This approach was noted to decrease the electricity consumption of the process by approximately 36%, improving the feasibility of achieving such extreme operating conditions (Vanhove, 2015).

In 2016, an investigation conducted in Barcelona looked at the effect of various operational parameters, on the production of MeOH, utilizing an 8% feed composition of Argon (Ar). This investigation confirmed the previous relationships reported within this literature review, finding that increased pressures resulted in an increase in CO_2 conversion and MeOH selectivity, however increasing the temperature decreased the MeOH selectivity (Gaikwad, *et al*., 2016).

Further investigation found that increasing the flow rate through the reactor, decreased the conversion and selectivity, due to the lowered contact time between the reactants and the catalyst. Therefore, should processes require increased flow rate, catalyst particles should be decreased in diameter, in order to increase the exposed surface area, facilitating the reaction process (Gaikwad, *et al*., 2016).

The main concern within this investigation, however, was that whilst argon was present within the feed stream, this was considered to be inert, with there being no other impurities. In efforts targeting atmospheric CO_2 reduction, or the utilization of CO_2 from industrial processes, in the form of flue gas, contaminants may be present, and this may deter the production of the desired product. Such considerations are imperative in achieving a holistic view of this reaction and gauging its practicality with known feed streams.

In 2016, an investigation conducted by Fan and Wu, found that the utilization of reduced graphene oxide (rGO), as a support for copper-based catalysts, increased the dispersion of copper, assisting in maximizing the exposed surface area of the catalyst. Paired with a CuO-ZnO-ZrO_2-Al_2O_3 (CZZA) catalyst, this support increased the conversion of CO_2 by 11.7% (Fan & Wu, 2016).

The concern with this investigation was the weight composition of catalyst which was chosen to be 80% rGO and 20% CZZA, with no indication being made to the reasoning behind the chosen ratio. Therefore, further investigations in this field should consider the possibility of altering this composition, in order to determine the possible impact on conversion and cost of the reactive system.

Bellotti, *et al*. (2017) looked at the feasibility of direct MeOH production via a CZA catalyst at temperatures of between 250ºC and 300ºC, and a pressure range of between 50 and 100 bar. The conditions were chosen as it was the then-current operating conditions of a German MeOH production plant. This study found that should H_2 be produced via a proton-exchange membrane (PEM) electrolyzer, the cost of H_2 would be too expensive, causing the plant to become economically infeasible (Bellotti, *et al*., 2017).

However, in order to offset the cost of the PEM electrolyzer, deemed as the most expensive unit operation within the plant, the selling of the oxygen produced during the electrolysis of water, would be mandatory (Bellotti, *et al*., 2017).

The shortcoming of this feasibility study, however, was that the CO_2 was considered to be pure, and therefore did not account for the purification process, as was done so with the H_2 feed. Furthermore, the cost of electricity, inflations rates and income tax were constant over a 15-year period, which is highly unlikely to occur in a practical scenario.

Hus, *et al*. (2017) identified the possibility of producing MeOH via the production of formate, rather than the reverse water gas shift reaction. This reaction, however, would need to occur at low temperatures, in order to prevent the occurrence of the reverse water gas shift reaction. Unfortunately, the production of MeOH and the CO_2 conversion rates are hindered at lower operating temperatures (Hus, *et al*., 2017). Therefore, the investigation was able to show the thermodynamic possibility of utilizing the formate route, however at this point the practicality of such a route did not appear to be viable.

In 2018, an investigation conducted by Kar, *et al*. found that in order to promote the conversion of CO_2, it is advantageous to either utilize a catalyst that is promoted with ruthenium, which is extremely expensive as a it is considered to be a rare transition metal, or to increase the feed ratio of H_2 to CO_2. Increasing this ratio beyond the stoichiometric ratio of 3:1, resulted in the reactive system containing excess H_2, increasing the likelihood of CO_2 reacting (Kar, *et al*., 2018).

An investigation conducted by Rui, *et al*. (2020) looked at improving gold catalysts for MeOH production, through the addition of indium oxide (In_2O_3) to the gold catalyst, achieving the highest MeOH selectivity, over a gold catalyst, when produced through CO_2 hydrogenation. The selectivity achieved was 100% favoring MeOH, with the operating temperature being below 225ºC. This is advantageous as it lowers the cost needed to achieve this reaction

temperature. An increase above 275^{o}C showed that the selectivity dropped, however MeOH selectivity maintained a value above 70% (Rui, *et al*., 2020).

A recent study conducted by Hu, *et al*. (2021) found that the use of sulfur in the form of Molybdenum disulfide (MoS_2) helps in breaking the bond between the carbon and oxygen molecules within CO_2, forming CO and O at room temperature. This is highly advantageous in hydrogenating the subsequent CO, in order to achieve more efficient conversion to MeOH, at lowering operating conditions. At 180^{o}C this catalyst achieved a selectivity of 94.3%, however the conversion of CO_2 achieved was 12.5% over the MoS_2 plane alone (Hu, *et al*., 2021).

2.6. The Production of Dimethyl Ether

As with the PtL system described in Section 2.5. The Production of Methanol, another system whereby power can be stored is within a gas state, known as the Power-to-Gas (PtG) system. PtG involves the use of conversion technologies as a means by which to convert excess electricity within the energy sector into a product that can be used to store this energy and allow it to be utilized in future applications (Eveloy & Gebreegziabher, 2018). Such a system is seen in the production of DME. PtG systems are especially important in the development of renewable energy systems, with an integral part of the system being an electrolysis unit operation. During the process of electrolysis, H_2 is produced, and subsequently converted into an energy-gas, thereby preserving excess electricity through its conversion to value added products (Gotz, *et al*., 2016).

From a safety perspective, the production of value-added products via the PtL and PtG systems, is imperative as H_2 gas is much more volatile and explosive, and therefore storing the energy in the form of liquid MeOH, or DME, has proved to be a safer option (Olah, *et al*., 2009).

Other advantages of a PtG system include its ability for the value-added product to be utilized within seasonal changes, allowing for a more consistent supply of energy to isolated areas. When stored within a gas form, as with these PtG system, they are able to be stored for long periods of time, ensuring minimal wastage of excess electricity. Furthermore, these systems have been noted for being extremely portable and cost effective, providing a major economic benefit in the transfer of energy (Eveloy & Gebreegziabher, 2018).

DME has gained a lot of attention over the years, with one of its major applications being as an alternative fuel for transportation vehicles. As a result of the lower boiling point that is experienced with DME, the fuel is able to vaporize at a faster rate, improving the combustion process within the engine, and in turn resulting in a more efficient transportation system. Furthermore, the lower ignition temperature of DME, allows for a higher cetane number to be achieved, in comparison to traditional diesel fuels. This results in easier ignition, with cleaner exhaust gases, providing an environmental benefit (Arcoumanis, *et al*., 2008), (Cho, *et al*., 2017).

With the structure and requirements for DME being quite similar to the currently used liquefied petroleum gas (LPG), it is possible to use existing infrastructure for the utilization of the fuel, as well as its associate transportation. This allows for the fuel to be easily integrated into the present fuel-systems (Arcoumanis, *et al*., 2008).

Commercialized applications of DME can also be seen in recent developments, whereby DME and CO_2 mixtures are being integrated into air-conditioning systems, acting as a refrigerant (Zharov, *et al*., 2019).

The production of DME through the hydrogenation of CO_2 can occur by one of two main routes, i.e., a direct and indirect synthesis route. During the direct synthesis of DME, CO_2 is directly hydrogenated to DME, as shown in Equation 2.4 (Catizzone, *et al*., 2017).

$$2CO_2 + 6H_2 \leftrightarrow CH_3OCH_3 + 3H_2O \qquad \text{(Equation 2.4)}$$

The second route that can be used in the production of DME, is the indirect route. This would first involve the production of MeOH, as per the reactive systems detailed in Equation 2.1 to Equation 2.3 in Section 2.5, before further dehydrating the MeOH to DME by means of Equation 2.5 (Catizzone, *et al*., 2017).

$$2CH_3OH \leftrightarrow CH_3OCH_3 + H_2O \qquad \text{(Equation 2.5)}$$

Alternatively, the CO in syngas can be converted directly to DME via Equation 2.6, however this reaction is typically not preferred due to the production of CO_2 within this process, negatively affecting the environment and adding to the current concerns experienced with GHGs. This reaction, however, only occurs in cases where CO_2 is not present within the syngas stream. Should CO_2 be present in the system, then the conversion of CO to DME can be noted by Equation 2.7 (Hankin & Shah, 2017).

$$3CO + 3H_2 \leftrightarrow CH_3OCH_3 + CO_2 \quad \text{(Equation 2.6)}$$

$$2CO + 4H_2 \leftrightarrow CH_3OCH_3 + H_2O \quad \text{(Equation 2.7)}$$

In 1992, an investigation conducted by Jean-Luc, Kazuhiro and Hironori looked at converting CO_2 to MeOH and DME, over the utilization of a hybrid catalyst. This hybrid catalyst was composed of a traditional CZA catalyst, which proved highly efficient for MeOH synthesis in past investigations, as well as a solid acid catalyst. The solid acid was primarily introduced into the catalyst system, in order to increase the conversion to DME that takes place within this reactive system. The investigation conducted, was done so at a temperature of 240^{o}C and 3 MPa (Jean-Luc, *et al*., 1992).

The addition of solid acid to the CZA catalyst was able to increase the yield of products from this reactive system, resulting in a 24.3% yield in MeOH and DME. This was considerably higher than the previous yields noted with a traditional CZA catalyst, of 11.6% (Jean-Luc, *et al*., 1992).

Another addition to the CZA catalyst, in the form of zeolites was also found to be quite effective, also producing higher yields than the traditional CZA catalyst. With the addition of a zeolite, which is a crystalline solid that is made from silicon, aluminum and oxygen, the yield of MeOH and DME was recorded at being 17%. This yield is greater than the 11.7% noted with the MeOH synthesis catalyst utilized at 240^{o}C and 3 MPa. Furthermore, this highlights the effectiveness of adding these zeolite species to the catalyst in the production of MeOH and DME (Jean-Luc, *et al*., 1992).

Hirano & Yasutake (2002) investigated the direct synthesis of DME using the traditional CZA catalyst, with additions of gallium oxide (Ga_2O_3) and magnesium oxide (MgO). The purpose of adding these components to the CZA catalyst was an attempt at combining the catalyst required for MeOH formation and its subsequent dehydration to DME, into a single catalyst (Hirano & Yasutake, 2002).

During the investigation various oxides were added to the CZA catalyst, as well as a zeolite for the promotion of DME production. This investigation found that an increase in the surface area of the catalyst resulted in a subsequent increase in the production of DME. The addition of oxides was found to increase the catalyst's activity in the synthesis of DME, with ZrO_2 providing the best results from the investigated compound oxides (Hirano & Yasutake, 2002).

The addition of a Zeolite Socony Mobil–5 (ZSM-5) was introduced with the hope of increasing the synthesis of DME from MeOH dehydration, however the results were the opposite of what was expected. The presence of this specific zeolite, resulted in a decrease in the synthesis of DME, with the reaction being steered towards the production of olefins, i.e., alkenes (Hirano & Yasutake, 2002).

This investigation was taken a step further in 2004, utilizing the same hybrid catalysts previously utilized by Hirano & Yasutake (2002), with the focus on how the composition ratios of these catalysts affected yield of MeOH and DME. Additionally, the parameters of DME selectivity and the durability of the catalyst were also considered throughout the course of this investigation (Hirano, *et al*., 2004).

Based on this investigation, it was found that in order to achieve the highest yield for direct DME synthesis, the MeOH catalyst and DME catalyst should be combined in a 50/50 ratio. Furthermore, this investigation showed that an increase in the temperature of the reactive system provided subsequent increases in the yield of MeOH and DME (Hirano, *et al*., 2004).

When the focus is specifically on the dehydration of MeOH to DME, the compound oxides, specifically $ZrO_2.Al_2O_3$, were more effective in producing DME than the γ-Al_2O_3 catalyst. The most effective catalyst structure was found to be a complete MeOH synthesis catalyst at the top, with a second, bottom layer containing the aforementioned composition of a mixture of the two catalyst compounds, i.e that for MeOH synthesis and that for DME production (Hirano, *et al*., 2004).

In 2013, an investigation conducted by Liu, *et al*. aimed to move away from the traditional CZA catalyst and investigated the synthesis of producing DME over a CuO/Fe_2O_3 catalyst. This catalyst was doped with traces of ZrO_2 finding that this was able to assist in increasing the surface area of the catalyst. This increase in surface area affected the selectivity of the CO_2 to hydrocarbons, thereby providing a benefit in the production of DME (Liu, *et al*., 2013).

An additional consideration within this investigation looked at the addition of HZSM-5 (the protonic type of ZSM-5) to the aforementioned doped catalyst. This refers to an aluminosilicate zeolite that has a monoclinic framework (Van Koningsveld, *et al*., 1990). The addition of this zeolite to the catalyst, resulted in a bifunctional catalyst, yielding higher CO_2 conversions and selectivities towards DME, than those experiments conducted without the presence of the ZrO_2 compound oxide. Using just a 1% mass percentage of ZrO_2, at 260^{o}C and 3 MPa, this catalyst

achieved a CO_2 conversion rate of approximately 28.4%, with a high DME selectivity of 64.5% (Liu, *et al*., 2013).

In 2016, an Aspen ® based life cycle assessment of MeOH and DME was conducted by Matzen & Demirel. This assessment utilized the traditional CZA catalyst for the MeOH production plant, with an aluminum-based catalyst being used for the dehydration of MeOH to DME. Through the use of a fixed bed reactor operating between 250^{o}C and 400^{o}C, with a pressure of 25 bar, the investigation showed that whilst high MeOH to DME conversion yields were achieved in excess of 80%, small amounts of formaldehyde were also being formed (Matzen & Demirel, 2016).

This raises a concern with the DME production plant, as formaldehyde is deemed to be carcinogenic. Thus, raising the need for implementing waste treatment to minimize the quantity and concentration of formaldehyde formed throughout the course of this process. The quantity would still be quite substantial, and sufficient enough to raise safety concerns (Matzen & Demirel, 2016).

Furthermore, this lifecycle assessment found that whilst the production of DME was deemed to be less environmentally friendly than the production of MeOH, its combustion was cleaner than that of MeOH. The use of this system within the current petroleum system, is predicted to have a reduction of up to 86% in GHGs. Additionally, such fuels would be able to reduce the depletion of current fossil fuel reserves by up to 91%, attesting to the importance of such fuel systems (Matzen & Demirel, 2016).

Ateka, *et al*. (2018) investigated the effect of various operating conditions on the conversion of syngas to DME, focusing specifically on factors such as pressure, temperature, space time and the composition of the syngas developed. Using a CuO-ZnO-MnO/SAPO-18 (small pore silicoaluminophosphate) catalyst, this work showed that one of the factors of extreme importance is the ratio of CO_2 to CO in the feed stream. Having a ratio that is below 1:3, i.e., implying that for every one part of CO_2 in the feed stream there are three parts of CO, was advantageous to the production of DME, resulting in higher production rates (Ateka, *et al*., 2018).

However, in order to increase the conversion of CO_2 within the reactive system, it is important that the ratio be maintained above one, ensuring that there are more CO_2 molecules within the feed than CO molecules. Based on this finding, it can be noted that the possibility of producing

DME via the reverse water gas shift reaction, may actually prove to be valuable in increasing yields, as CO has proven to be much more reactive than CO_2 (Ateka, *et al*., 2018).

Maintaining a pressure of 30 bar, the highest conversions of CO_2 recorded were at approximately 250^oC, with conversions being approximately 8%. The selectivity to DME at these conditions was approximately 7%. Increasing the temperature above this proved to be highly disadvantageous to CO_2 conversion, as the reported values for conversion became negative. This implies that more CO_2 was being produced within the system, than was being utilized, thus resulting in a negative environmental impact (Ateka, *et al*., 2018).

An investigation conducted by Nakyai & Saebea (2019) looked at the thermodynamic feasibility of varying the feed stream compositions over a zeolite catalyst, considering both the direct and indirect synthesis of DME. Throughout the course of this investigation, it was found that the optimal levels of DME synthesis can be achieved through a feed ratio of 4:1, in respect to H_2 and CO, respectively. This system yielded energy efficiencies of up to 46% (Nakyai & Saebea, 2019).

In order to focus on the utilization of CO_2, the H_2 to CO_2 ratio would need to be increased to 5 to 1, however this still proved to be less efficient than the use of carbon monoxide. In fact, much of the results, indicated that an increase in the CO_2 composition within the feed flow rate, resulted in decreased yield of DME (Nakyai & Saebea, 2019).

This trend shows that DME production is promoted when considered via the reverse water gas shift reaction, increasing the presence of carbon monoxide (CO) within the feed to the DME reactor. This concurs with the work presented by Ateka, *et al*. (2018).

The concern with the reverse water gas shift reaction, however, is that it is promoted at higher temperatures, which can result in or promote, the formation of hydrocarbons and coke. When coke is formed however, it forms deposits on the catalyst surface leading to deactivation. Therefore, the catalyst choice in following this route is extremely important, to ensure that the catalyst is not replaced on a regular basis and is able to suppress the formation of these unwanted byproducts (Catizzone, *et al*., 2019).

With regards to operating conditions of the process, the generalized trend of converting syngas to DME found that a decrease in temperature, along with a simultaneous increase in pressure, results in an increased DME yield (Nakyai & Saebea, 2019).

As with the work conducted by Hirano, *et al*. (2004), Ardy, *et al*. (2019) also investigated the functionality of a dual catalyst in producing DME, with the catalyst containing components that are involved in the formation of MeOH, and those involved in the dehydration of MeOH to DME. However, the difference with this research, was that the feed stream considered in the production of DME, was CO and H_2, as opposed to the presence of CO_2 previously studied (Ardy, *et al*., 2019).

In the presence of CO, a copper-based catalyst was utilized for the production of MeOH, and an γ-Al_2O_3 catalyst was utilized for its subsequent dehydration (Ardy, *et al*., 2019). Due to the fact that CO is considered to be much more reactive than CO_2, the need for the MeOH producing catalyst was reduced.

This resulted in only 20% of the total catalyst structure being that of the MeOH catalyst, with the remaining 80% focusing on the production of DME via the aluminum oxide catalyst. With this catalyst structure, the CO conversion achieved was 62%, with a DME/MeOH ratio of 40% within the product stream (Ardy, *et al*., 2019).

In 2021, Giuliano, *et al*. looked at the conversion of syngas to DME, via the CHEMCAD ® simulation software. The results obtained from this research aligned with that of Nakyai & Saebea (2019), showing that the presence of CO_2 in the feed stream, decreased the yield of DME. However, the results also showed that with an 85% efficient carbon capture process, the environmental impact of producing DME via the use of CO_2 is substantial. In fact, the environmental impact was shown to produce a 113-kilogram decrease in the CO_2 levels, per gigajoule of energy produced via DME (Giuliano, *et al*., 2021). This highlights the effectiveness and sustainability of such a route moving forward.

2.7. Equations of State

Equations of state (EOS) mathematically define the thermodynamic relationship that exists between the pressure, temperature and volume of a species or mixture thereof (Ramdharee, *et al*., 2013). The type of equation of state is categorized by its class as follows (Mansour, 2020):

- First class EOS: These relationships exhibit a cubic function, and include thermodynamic models such as the Van der Waals, Redlich-Kwong, Soave-Redlich-Kwong and the Peng-Robinson equations.

- Second class EOS: These are non-cubic equations, which are able to provide a single answer or solution under specific operating conditions. An example of such a thermodynamic model is the Benedict equation.
- Third class EOS: These equations are limited in terms of their application and can only be utilized for certain fluids. However, when utilized within their predefined constraints, these equations have been known to provide accurate and precise thermodynamic models.

The selection of the appropriate EOS is imperative in any chemical process model, as it is this thermodynamic data, such as enthalpy and equilibrium data, and equation that will form the basis along which the stream data is calculated and utilized. Choosing the incorrect thermodynamic model is likely to cause convergence problems and possibly even inaccurate model results, resulting in the model not being representative of the 'real problem' being addressed (Edwards, 2000).

Furthermore, the EOS is the thermodynamic model that determines the relevant vapor-liquid equilibrium, which is essential in designing and determining the type of separation systems needed (Hill & Justice, 2011).

Typically, the ideal gas EOS is utilized in order to describe the relationships that occur at low pressures, or to provide initial estimates of these thermodynamic properties. However, these ideal EOS do not yield accurate results at high pressures and cannot be used to model real gas scenarios (Stewart, 2014).

Unfortunately, there is no single factor that can be employed to all chemical species to modify this EOS, and as a result there are many different equations that relate these thermodynamic factors, as seen by some of the models mentioned within the three-class category detailed previously. The first equation of state, known as the ideal gas EOS, utilized two main assumptions in its development (Ahmed, 2019):

1. The volume of the gas is considered to be negligible in relation to the volume of the container into which the gas is placed.
2. There are no forces between the molecules of the gas within the container, i.e., there are neither attractive nor repulsive forces between the various molecules.

In order to correct these assumptions, a compressibility factor was initially introduced to the ideal gas equation (as seen in Equation 2.8), with Z representing the ratio of the actual/real gas

volume to that of the ideal gas (Stewart, 2014). This shows the relationship that exists between pressure (P), volume (V), number of moles (n), the ideal gas constant (R), and temperature (T).

$$PV = ZnRT \qquad \text{(Equation 2.8)}$$

This, approach, however, was ineffective to various fluids, and was considered to be too generalized to address the aforementioned concerns. Therefore, in 1873, Van der Waal completed his thesis in this field, aiming to address the two assumptions made by the ideal gas equation. The first assumption of the volume of the gas being negligible in relation to the volume of the container, was addressed by introducing a factor 'b' into the ideal gas equation, accounting for the repulsive forces of the molecules within the gas volume. It is as a result of these repulsive forces that the volume is often larger than that of the gas. This correction factor resulted in the development of Equation 2.9 (Berberan-Santos, *et al*., 2007).

$$P = \frac{RT}{V - b} \qquad \text{(Equation 2.9)}$$

This, however, only considered the repulsive forces and its impact on the volume of the gas, and therefore a second additional term was added to Equation 2.9, to allow for the attractive forces within the gas to also be accounted for. This resulted in the Van der Waal equation denoted by Equation 2.10 (Ahmed, 2019), where $\frac{a}{V^2}$ accounts for the attractive forces between molecules.

$$P = \frac{RT}{V - b} - \frac{a}{V^2} \qquad \text{(Equation 2.10)}$$

This EOS became the basis on which future thermodynamic models were constructed and developed. One of the major shortcomings of the Van der Waal EOS, was the lack of consideration for the liquid-gas critical points. In fact, one of the assumptions utilized in the development of this EOS, was the lack of a phase change between gas and liquids, resulting in continuity of their phase state (Woodcock, 2018).

In an attempt to rectify the limitations of the Van der Waal EOS, many thermodynamic models have been developed, with two of the major models being that of the Peng-Robinson EOS and the Soave-Redlich-Kwong EOS, developed in 1976 and 1972 respectively (Bell & Lemmon, 2017).

The Redlich-Kwong EOS was initially applied to mixtures, building on the attraction term found in the Van der Waal EOS, adding an additional term to the pressure parameter. This

modification to the Van der Waal EOS can be seen in Equation 2.11, with V_m representing the molar volume. The shortcoming of this EOS, however, was that it was unable to be applied to liquid-liquid and vapor-liquid equilibrium situations and was limited to only gases during its application. This made the use of this EOS impractical to chemical process systems, as most systems often contain a degree of vapor-liquid equilibrium, especially within the separation processes (Ramdharee, *et al*., 2013).

$$P = \frac{RT}{(V_m - b)} - \frac{a}{\left(\sqrt{T}\, V_m(V_m + b)\right)} \qquad \text{(Equation 2.11)}$$

The constants a and b, in Equation 2.11, were calculated by means of the following equations, utilizing the critical temperature (T_c) and the critical pressure (P_c):

$$a = \frac{0.42748(R^2 \times T_c^{2.5})}{P_c} \qquad \text{(Equation 2.12)}$$

$$b = 0.08664 \times \frac{RT_c}{P_c} \qquad \text{(Equation 2.13)}$$

In 1972, Soave aimed to build on this EOS formulation and address the aforementioned limitations, by fitting in experimental vapor-liquid equilibrium data to the thermodynamic model. Prior to this development, the attraction between molecules was considered solely from a temperature standpoint, however Soave proposed the addition of the acentric factor, accounting for the shape of the molecules as well. The revised EOS can be represented by means of Equation 2.14 to Equation 2.16 (Ramdharee, *et al*., 2013), where T_r represents the reduced temperature and ω represents the acentric factor.

$$P = \frac{RT}{V_m - b} - \frac{a\alpha}{V_m(V_m + b)} \qquad \text{(Equation 2.14)}$$

Where:

$$\alpha = \left(1 + S(1 - T_r)\right)^2 \qquad \text{(Equation 2.15)}$$

$$S = 0.48 + 1.574\omega - 0.176\omega^2 \qquad \text{(Equation 2.16)}$$

The concern with the Soave-Redlich-Kwong EOS is that the critical compressibility factor becomes unrealistic and registers a value of 0.333 for all chemical species. Furthermore, this EOS demonstrated poor accuracies when calculating liquid densities (Ramdharee, *et al*., 2013).

The Peng-Robinson EOS aimed to address these issues and was found to have higher accuracies for predicting liquid densities. Equation 2.17 to Equation 2.22 detail the formulations associated with the Peng-Robinson EOS (Jugmohan, *et al*., 2021).

$$P = \frac{RT}{V_m - b} - \frac{a\alpha}{V_m^2 + 2bV_m - b^2} \quad \text{(Equation 2.17)}$$

Where:

$$a = 0.45723553\ \frac{R^2 T_c^2}{P_c} \quad \text{(Equation 2.18)}$$

$$b = 0.07779607\ \frac{RT_c}{P_c} \quad \text{(Equation 2.19)}$$

$$\alpha = \left(1 + \kappa\left(1 - \sqrt{T_r}\right)\right)^2 \quad \text{(Equation 2.20)}$$

$$\kappa = 0.37464 + 1.54226\omega - 0.26992\omega^2 \quad \text{(Equation 2.21)}$$

$$T_r = \frac{T}{T_c} \quad \text{(Equation 2.22)}$$

The accuracies noted within the Soave-Redlich-Kwong and Peng-Robinson EOS are the reason that these two thermodynamic models are utilized extensively with the process industry field for vapour and vapour-liquid mixtures, respectively. (Ramdharee, *et al*., 2013).

The correct EOS is imperative when designing and determining the efficiency of various process unit operations needed throughout the course of the chemical plant. These unit operations include heat exchangers, pressure-changing unit operations such as compressors and turbines, and separation systems, including flash drums and distillation columns. Appendix A provides a brief overview of these unit operations, highlighting the different types of each unit operation, and providing diagrammatic representations of the various process units.

Chapter 3: Methodology – ASSF Tool Development

The primary purpose of developing the ASSF tool, is to provide the user with an automated, precursory, screening tool that utilizes an RPD in determining the most promising reactive systems/combinations thereof. The advantage of such a tool is that it can be utilized prior to any extensive design procedures, thereby maximizing on the efficiency with which subsequent design resources are allocated and utilized. Figure 3.1 provides a summary of the problem statement addressed within this thesis, and the solutions offered by the ASSF tool.

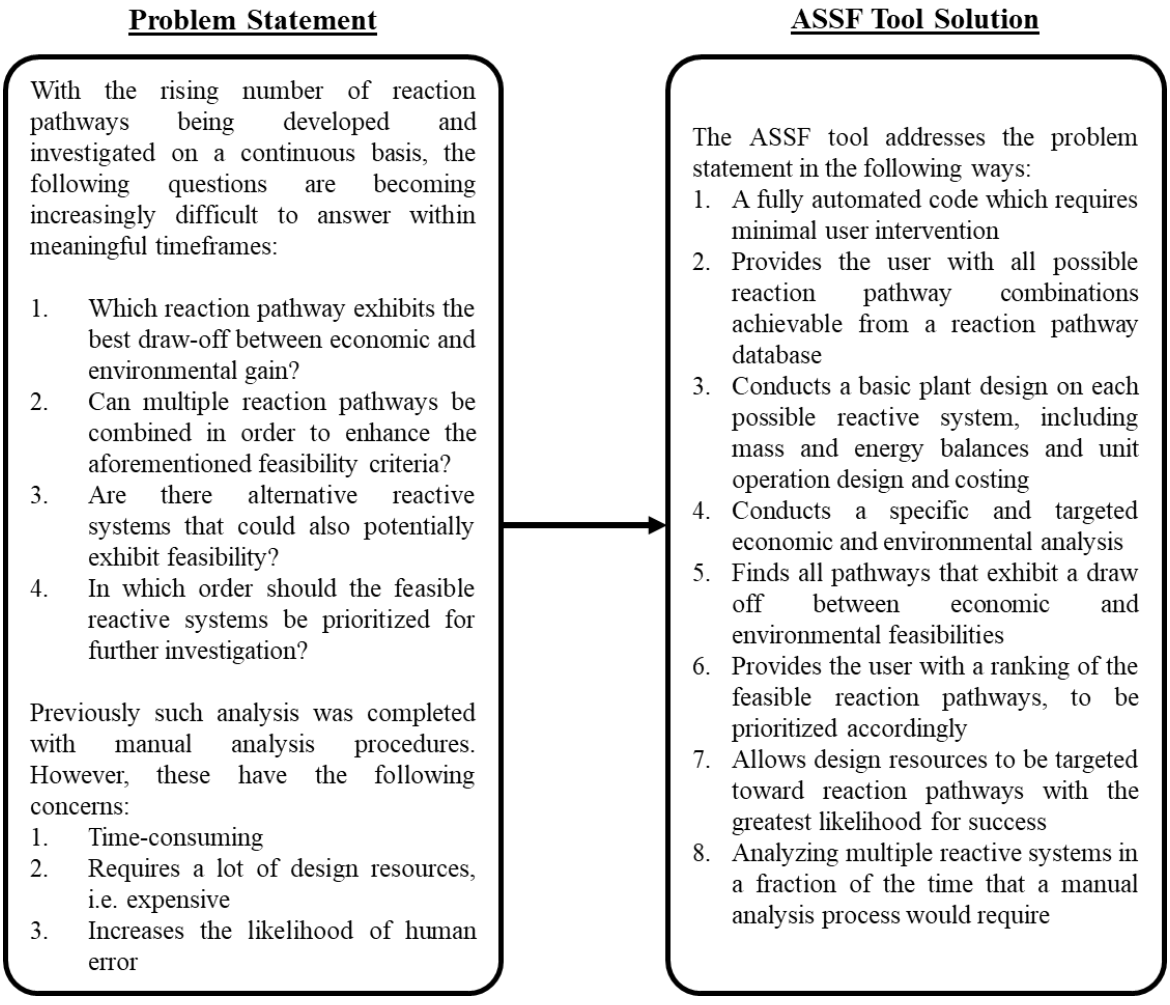

Figure 3.1: Summary of the problem statement addressed by the ASSF tool and the solution structure offered

In addition to this purpose, the ASSF tool has been successfully applied to other applications, including quick chemical plant simulations, and determining the expected optimum operating conditions for a reactive system using experimental data. These applications are discussed and demonstrated in Chapters 4 and 5, respectively. Chapter 4 looks at validating the ASSF tool,

ensuring that the trends, results, and coding of the tool are reliable and accurate for its application and analysis of the RPDs denoted in Chapter 5. Whilst a precursory screening tool, the ASSF tool can be employed for basic, preliminary simulations, providing the user with an indication of the practicality of a reactive system. This would be in terms of the cost to achieve the necessary operating conditions and a marketable purity. Design resources can then be focused within a narrow range, during the subsequent detailed design and experimentation.

When creating the ASSF tool, various factors were considered, ranging from the development of the RPD to the combinations possible from this database, and their associated design and analysis thereof. This chapter focuses on the development of the ASSF tool, highlighting the associated assumptions and formulae utilized in each code segment of this tool.

A generalized overview of the ASSF tool is given in Appendix B, detailing the inputs required from the user, default data encoded within the ASSF tool, decisions to be made by the user and the associated outputs. It is important to note, however, that these default values can be adjusted should the user have more specific information related to their process environment.

Additionally, Appendix B also shows the user interface of the ASSF tool, showcasing the step-by-step guide provided to the user when building the RPD and its subsequent analysis. A brief technical analysis, relating to the tool's operation, and the loops that exist within the framework of the ASSF tool, is detailed in Appendix C. Appendix D contains flowcharts representing the code associated with each segment of the ASSF tool, allowing the chronological sequence, and loops within these segments, to be clearly perceived.

3.1. Physical and Chemical Properties

There are a total of 8 chemical species utilized within the ASSF tool, with each chemical species containing its own associated identification number. These identification numbers allow each substance to be treated as a numeric value, thereby allowing all subsequent calculations to be completed via numeric matrices. In so doing, the number of decimal points retained throughout the course of the tool, is much higher than the use of a string array, with up to 15 digits being retained. This increased the accuracy of the associated calculations. The following list details the eight chemical species and their associated identification numbers:

1. Carbon dioxide (CO_2)
2. Hydrogen gas (H_2)
3. Carbon monoxide (CO)
4. Water (H_2O)
5. Methanol (CH_3OH)
6. Dimethyl ether (CH_3OCH_3)
7. Calcium oxide (CaO)
8. Calcium carbonate ($CaCO_3$)

Chemical species 7 and 8 were utilized in the separation of CO_2 from DME. This process is explained in Section 3.11. Due to the fact that the calcium-based chemical species were only required in separation processes containing DME, and were not utilized in any other stream, the only chemical and physical data required throughout the course of the ASSF tool relates to chemical species 1 through to 6. Table 3.1 details the properties of the first six chemical species, where MW = molecular weight (g/mol), T_{freeze} = freezing temperature (Kelvin), $T_{boiling}$ = boiling temperature (Kelvin), T_c = critical temperature (Kelvin), P_c = critical pressure (bar), V_c = critical volume (cm^3/mol) and ω = acentric factor.

Table 3.1: Properties of chemical species utilized in the ASSF tool (Yaws, 1999)

Species	**MW (g/mol)**	**T_{freeze} (K)**	**$T_{boiling}$ (K)**	**T_c (K)**	**P_c (bar)**	**V_c (cm^3/mol)**	**ω**
CO_2	44.010	216.58	194.67	304.19	73.82	94.0	0.228
H_2	2.016	13.95	20.39	33.18	13.13	64.2	-0.220
CO	28.010	68.15	81.70	132.92	34.99	93.1	0.066
H_2O	18.016	273.15	373.15	647.13	220.55	56.0	0.345
CH_3OH	32.042	175.47	337.85	512.58	80.96	117.8	0.566
CH_3OCH_3	46.068	131.66	248.31	400.10	53.70	170.0	0.204

The standard enthalpy of formation (H_f^o) is defined as the enthalpy change that is associated with the formation of one mole of the chemical compound. This value is typically noted at a pressure of 1 bar and a reference temperature that allows the element to exist in a stable state (Honig, 2007). The enthalpy of formation given in Table 3.2, utilizes ambient conditions of 298 K temperature and 1 atm pressure as its reference state, with all enthalpy values being given in unit of kJ/mol.

Table 3.2: Enthalpy of formation for chemical species utilized in ASSF tool (Yaws, 1999)

Chemical Species	H_f^o @ 298 K (kJ/mol)
CO_2	-393.51
H_2	0
CO	-110.54
H_2O	-241.80
CH_3OH	-201.17
CH_3OCH_3	-184.05

The specific heat capacity (C_p) function is divided into two segments, i.e., that which deals with the species gas phase, and another that deals with the liquid phase. For each specific heat capacity, the chemical species have their own associated constants and equations. The specific heat capacity of a gas was calculated by means of Equation 3.1, where specific heat is given in J/mol.K and the temperature (T) is given in Kelvin (Yaws, 1999).

$$C_p(T) = A_1 + A_2T + A_3T^2 + A_4T^3 + A_5T^4 \qquad \text{(Equation 3.1)}$$

Table 3.3 details the constants (A_1, A_2, A_3, A_4 and A_5) associated with Equation 3.1, as well as the temperature range for which Equation 3.1 is applicable, denoted by T_{min} and T_{max}, respectively.

Table 3.3: Specific heat capacity constants for gases (Yaws, 1999)

Species	**A_1**	**A_2**	**A_3**	**A_4**	**A_5**	**T_{min} (K)**	**T_{max} (K)**
CO_2	27.437	4.2315×10^{-2}	-1.9555×10^{-5}	3.9968×10^{-9}	-2.9872×10^{-13}	50	5000
H_2	25.399	2.0178×10^{-2}	-3.8549×10^{-5}	3.1880×10^{-8}	-8.7585×10^{-12}	250	1500
CO	29.556	-6.5807×10^{-3}	2.0130×10^{-5}	-1.2227×10^{-8}	2.2617×10^{-12}	60	1500
H_2O	33.933	-8.4186×10^{-3}	2.9906×10^{-5}	-1.7825×10^{-8}	3.6934×10^{-12}	100	1500
CH_3OH	40.046	-3.8287×10^{-2}	2.4529×10^{-4}	-2.1679×10^{-7}	5.9909×10^{-11}	100	1500
CH_3OCH_3	34.668	7.0293×10^{-2}	1.6530×10^{-4}	-1.7675×10^{-7}	4.9313×10^{-11}	100	1500

The specific heat capacity of a liquid was calculated using Equation 3.2, where C_p is given in J/mol.K and T is given in Kelvin (Yaws, 1999).

$$C_p(T) = B_1 + B_2T + B_3T^2 + B_4T^3 \qquad \text{(Equation 3.2)}$$

The associated constants (B_1, B_2, B_3 and B_4) and temperature ranges are highlighted in Table 3.4.

Table 3.4: Specific heat capacity constants for liquids (Yaws, 1999)

Species	B_1	B_2	B_3	B_4	T_{min} (K)	T_{max} (K)
CO_2	-338.956	5.2796	-2.3279×10^{-2}	3.5980×10^{-5}	218	274
H_2	50.607	-6.1136	3.0930×10^{-1}	-4.1480×10^{-3}	14	32
CO	-19.312	2.5072	-2.8970×10^{-2}	1.2745×10^{-4}	69	120
H_2O	92.053	-3.9953×10^{-2}	-2.1103×10^{-4}	5.3469×10^{-7}	273	615
CH_3OH	40.152	3.1046×10^{-1}	-1.0291×10^{-3}	1.4598×10^{-6}	176	461
CH_3OCH_3	48.074	5.6225×10^{-1}	-2.3915×10^{-3}	4.4614×10^{-6}	133	360

The latent heat of vaporization, also referred to as the enthalpy of vaporization, is required during a phase change, where the change from liquid to gas occurs at constant temperature (Smith, *et al*., 2018). This is referred to as latent heat of vaporization, or enthalpy of vaporization, and is calculated using Equation 3.3. The constants (C_1 and C_2) and temperature range associated with this equation are highlighted in Table 3.5 (Yaws, 1999).

$$H_{vap}(T) = C_1 \times \left(1 - \frac{T}{C_2}\right)^{C_3} \qquad \text{(Equation 3.3)}$$

Table 3.5: Enthalpy of vaporization constants (Yaws, 1999)

Species	C_1	C_2	C_3	T_{min} (K)	T_{max} (K)
CO_2	15.326	304.19	0.227	216.58	304.19
H_2	0.659	33.18	0.380	13.95	33.18
CO	8.003	132.92	0.318	68.15	132.92
H_2O	52.053	647.13	0.321	273.16	647.13
CH_3OH	52.723	512.58	0.377	175.47	512.58
CH_3OCH_3	27.769	400.10	0.261	131.65	400.10

Vapor pressure (P_v) is an indication of the pressure exerted by the vapor stream when it is in thermodynamic equilibrium and is dependent on the temperature of the system (Stauffer, *et al*., 2008). P_v can be calculated by means of Equation 3.4, with P_v being represented in units of mmHg (Yaws, 1999).

$$P_v(T) = 10^{D_1+\frac{D_2}{T}+D_3\log_{10}(T)+D_4T+D_5T^2} \quad \text{(Equation 3.4)}$$

The regression co-efficients (D_1, D_2, D_3, D_4 and D_5) utilized in Equation 3.4 are highlighted in Table 3.6, with the respective temperature range associated with these constants.

Table 3.6: Vapor pressure constants (Yaws, 1999)

Species	D_1	D_2	D_3	D_4	D_5	T_{min} (K)	T_{max} (K)
CO_2	35.0169	-1.5119×10^{3}	-1.1334×10^{1}	9.3368×10^{-3}	1.7136×10^{-9}	216.58	304.19
H_2	3.4132	-4.1316×10^{1}	1.0947×10^{0}	-6.6896×10^{-10}	1.4589×10^{-4}	13.95	33.18
CO	51.8145	-7.8824×10^{2}	-2.2734×10^{1}	5.1225×10^{-2}	6.1896×10^{-11}	68.15	132.92
H_2O	29.8605	-3.1522×10^{3}	-7.3037×10^{0}	2.4247×10^{-9}	1.8090×10^{-6}	273.16	647.13
CH_3OH	45.6171	-3.2447×10^{3}	-1.3988×10^{1}	6.6365×10^{-3}	-1.0507×10^{-13}	175.47	512.58
CH_3OCH_3	20.2699	-1.5914×10^{3}	-4.6530×10^{0}	-1.3178×10^{-10}	2.5623×10^{-6}	131.65	400.10

This concludes the chemical and physical property data needed for the operation of the ASSF tool. All information mentioned within this section was programmed directly into the ASSF tool, and using the component's associated identification number, was extracted and utilized when the species was present within any given stream. It is important that this data only be extracted when necessary, as this avoids unnecessary calculations, thereby reducing the memory usage of the ASSF tool, and its associated computational times.

3.2. Generic Plant Design

To allow for effective comparisons between the various case studies, it is imperative that a generic design be employed for each reactive system. In doing so, all case studies are evaluated from an equivalent standpoint, increasing the accuracy of subsequent comparisons. Figure 3.2 below details the generic flowsheet employed for each reaction pathway.

It is important to note, however, that this generic flow sheet was followed for each reaction pathway within a reactive system. In other words, should a reactive system contain three sub-reactions/reaction blocks, occurring in three separate reactor unit operations, this generic flow sheet was employed three times.

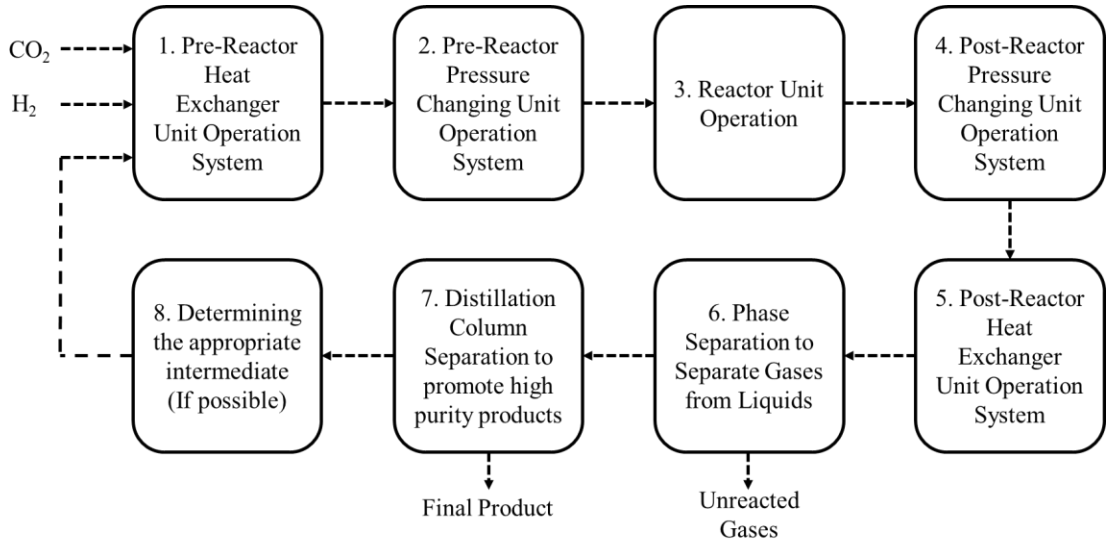

Figure 3.2: Generic flowsheet structure for process designs

Additionally, it may not be necessary that all sub-reactions contain a phase separator and distillation column. Distillation columns were only utilized in achieving streams of high purity and separation, thereby allowing for the subsequent sale or reaction of that chemical species. Should that species not be required to be utilized at a further point in the process or was considered to be a 'waste' stream, phase separators would suffice, as the purity of the chemical species was not deemed to be a concern.

This 'decision-making' procedure is encompassed within the ASSF tool. The ASSF tool is able to deduce the species required in further reactive systems within the reaction combination, selecting the appropriate separation system accordingly. There was a total of four separation

systems possible within the ASSF tool, depending on the chemical species present within the process being analyzed.

The first possible combination involved the reverse water gas shift reaction (RWGS), where CO and H_2O were produced. In such a scenario, the absence of MeOH and DME eliminated the need for a distillation column, as there were no products that could be commercialized. The species present in such a reactive system included the feed CO_2 and H_2, as well as the CO and H_2O produced.

With CO_2, H_2 and CO remaining in a vapor state, liquid H_2O was separated through the utilization of a flash drum unit operation, utilizing the vapor/liquid equilibrium of the mixture. The separation system required for such a scenario can be represented using the process flowsheet in Figure 3.3. The red box is used to distinguish the post-reactor separation system.

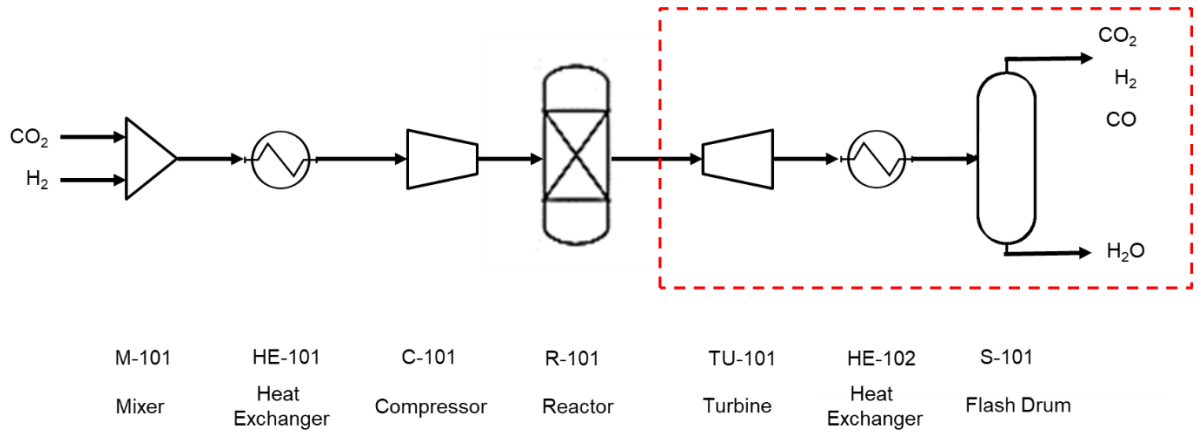

Figure 3.3: Process flow sheet for the separation system utilized in the RWGS reaction

In cases where MeOH is produced, the need for a distillation column is essential. MeOH is one of the main products considered in the ASSF tool, therefore it was imperative that MeOH exit the process at a purity sufficient to promote commercialization. This purity also needs to be sufficiently high, so as to be competitive within the current market.

In order to account for different economic conditions, depending on the region or year in which this tool is utilized, the user is required to enter the desired product purity that would be competitive under current market conditions, with distillation columns being redesigned to meet this specification. This further improves, and extends, the application of the ASSF tool.

During the direct production of MeOH, the unreacted gases (CO_2 and H_2) were first separated from the MeOH/H_2O mixture using a flash drum unit operation. It is important to note however,

that small amounts of CO_2 are likely to escape through the bottom of the flash drum, after being partially dissolved within the MeOH/H_2O mixture. In order to minimize the CO_2 dissolution within the bottom liquid stream of the flash drum, the ASSF tool actively performs iterations, finding the optimum operating conditions. The objective function of this optimization focused on the flash drum recovering, at minimum, 95% of the CO_2 to the vapor stream. This minimizes the impact on the product purity and reduces the need for subsequent separation systems focused on CO_2.

The MeOH/H_2O mixture was then separated using a distillation column. These two chemical species have similar boiling points, as seen in Table 3.1. As such, separation of this mixture through a flash drum unit operation proved to be inefficient. A distillation column promotes the separation of these two chemical species, with the trays, reflux ratio, and reboiler ratio enhancing the separation process. With this unit operation, a product purity of more than 99.9% is targeted as the default setting within the ASSF tool. Figure 3.4 presents the flow sheet utilized in the separation of direct MeOH synthesis reactions.

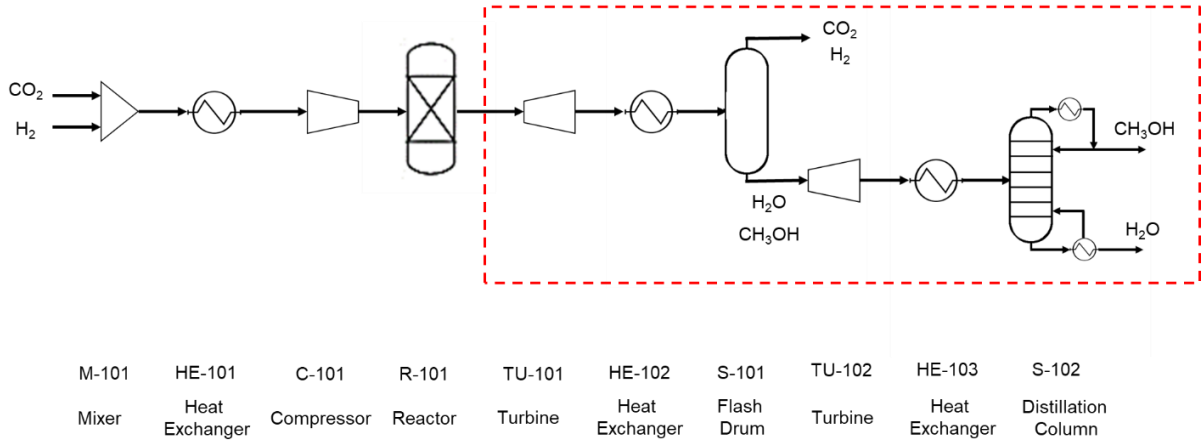

Figure 3.4: Process flow sheet for the separation system utilized in direct MeOH synthesis

In cases where DME was produced through direct CO_2 hydrogenation, an initial flash drum was utilized as a means by which to separate H_2 and bulk of the CO_2 from the DME/H_2O mixture. However, due to the soluble nature of CO_2 in the DME/H_2O mixture, there was still a considerable portion of CO_2 that exited the flash drum unit operation through the bottom stream. Failure to remove this CO_2 would result in major hindrances to the purity of the product stream. As a result, a secondary separation system was required to remove the remaining CO_2.

This carbon capture process involved the use of a secondary reactor, whereby CaO was introduced into the system. This reactor focused on the carbonation of CaO, forming $CaCO_3$, a

solid which can easily be removed from the reaction vessel. The resulting stream exiting the carbonation reactor was lowered considerably in its CO_2 content, with the carbonation process being able to react and remove as much as 90% of the CO_2 content (Geimer, 2014). This is explained extensively in Section 3.11.

The remaining DME/H_2O mixture was then separated through the use of a distillation column. Whilst a flash drum would be able to achieve separation of these two components, due to the fact that DME exists as a vapor at ambient conditions, the dissolution of DME within H_2O severely hinders product recovery and purity. This results in significant product losses, and a final product stream with a purity that cannot be commercialized. The use of a distillation column allowed for a product purity in excess of 99.9% to be achieved with a DME recovery rate above 99.9%. Figure 3.5 highlights the process flow sheet associated with direct DME production, and the associated separation system employed in such scenarios.

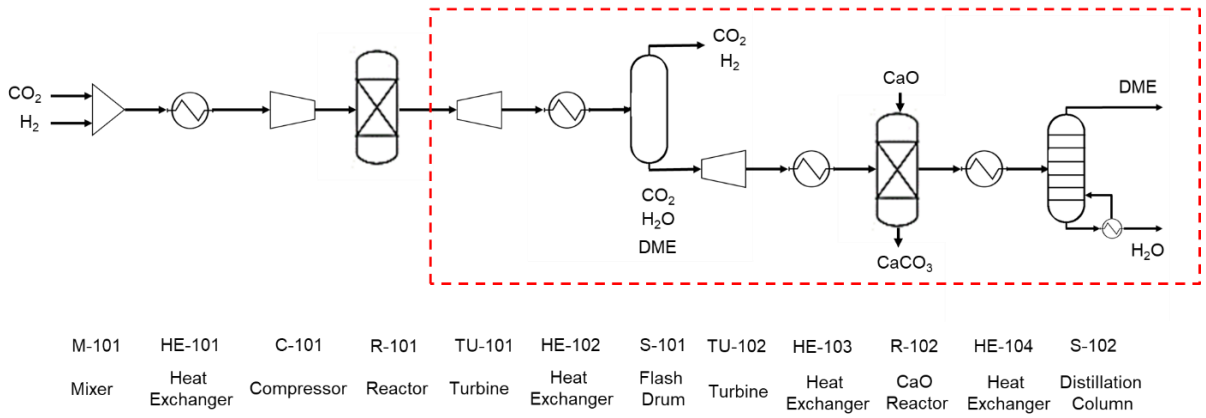

Figure 3.5: Process flow sheet for the separation system utilized in direct DME synthesis

The final scenario possible, and considered within the ASSF tool, was the presence of all chemical species within the process. In such a scenario, an initial flash drum unit operation was first utilized to separate the unreacted gases (CO_2, H_2 and CO) from the liquid mixture containing MeOH, DME and H_2O. Due to the dissolution of CO_2 within the liquid mixture, a portion of CO_2 escapes the flash drum through the bottom stream. In order to remove the CO_2 from this stream, and increase the associated product purity, a CaO carbonation reaction was utilized, as per that detailed within the direct DME synthesis reaction.

With the CO_2 being removed from the liquid stream, a distillation column was utilized to separate DME from the MeOH/H_2O mixture. The use of a distillation column allowed for purities greater than 99.9% to be achieved in the DME product stream, also maximizing the

recovery of DME. This allowed for a product stream capable of commercialization, within the current competitive market.

The MeOH/H_2O mixture exiting the bottom of the distillation column can further be separated into its components. The reason why this separation was deemed necessary, is that the MeOH which is unreacted during the production of DME, can be sold as an additional product stream, thereby increasing the economic feasibility of the process under analysis. In order to allow for such commercialization of the MeOH produced, however, a sufficient and marketable purity must be achieved. The purity is largely dependent on the end application use. This separation was achieved through a subsequent distillation column, allowing for a MeOH purity and recovery in excess of 99.9% to be achieved. Figure 3.6 depicts the flow sheet associated with the separation of a system containing all chemical species considered within the ASSF tool.

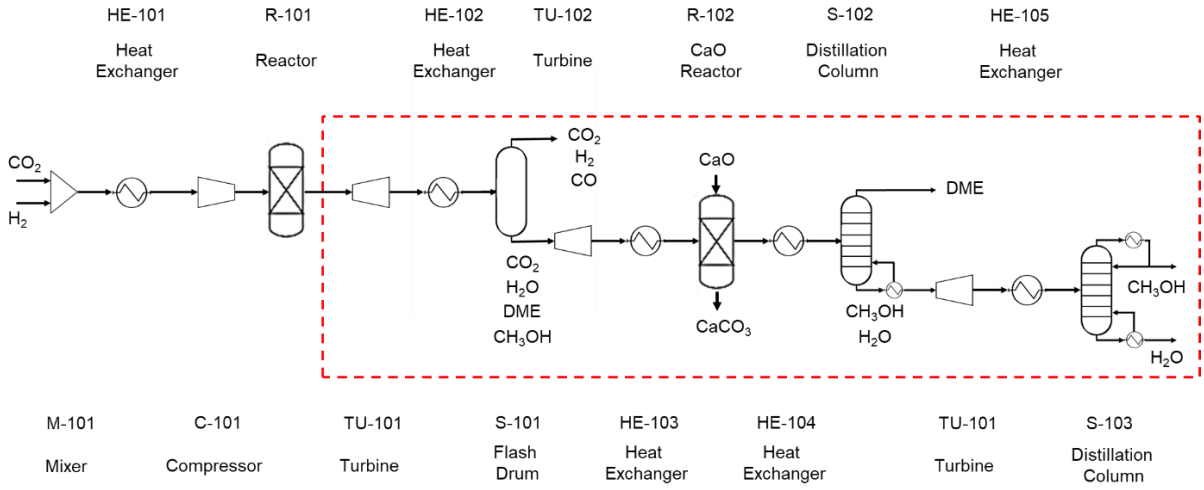

Figure 3.6: Process flow sheet for the separation system utilized when all chemical species are present

With the exception of the reactor unit operation, each section within this generic process was coded to account for and record the change in operating conditions in the associated stream tables, as well as sizing and costing of unit operation/s involved in the system. The reactor is not considered within the ASSF tool, as this tool makes use of an RPD containing the conversions noted in previous experimentation, thereby not accounting for reaction kinetics.

The exclusion of the reactor design from the ASSF tool was an intentional decision, as it allows for the feasibility of a case study to be determined prior to the intricate design of the reactor unit operation. Should a process be deemed infeasible, either through the economic or environmental criteria considered within this thesis, this conclusion is guaranteed to hold true after considering the reactor unit operation. Therefore, the consideration of the reactor can be completed by the user upon obtaining the reduced search space pertinent to the production of

the desired final product. This allows for design resources to be focused on those pathways with a greater likelihood of implementation.

3.3. Development of the Reaction Pathway Database

This section contains the explanation of the ASSF tool involved with the development of the RPD. Appendix D1 contains a diagrammatic flow chart representation of this segment in the ASSF tool. The flow chart highlights the inputs and loops present within the ASSF tool, providing a comprehensive overview of the code associated with each section.

3.3.1. Reaction Pathway Database Explanation

During this stage of the ASSF tool, the user is prompted to enter the necessary reactions that are to be analyzed. This database comprises of the reaction pathways, their associated operating conditions, conversions and selectivity to the product in question. An important aspect required in the database, is the reference from which the pathway was extracted, as this allows for cross-referencing case studies in the reduced search space, i.e., the output of the automated tool developed.

It was not deemed necessary to encompass reaction kinetics within the RPD. As mentioned in Section 3.2, the ASSF tool analyzes reaction pathways using the specified conversion noted in previous experimentation. Once the final search space has been presented to the user, the user can then progress the analysis by incorporating the reaction kinetics, focusing their design resources on the newly reduced search space.

When developing the RPD within the ASSF tool, there are two provisionary checks that are made on each reaction entered:

- Checking the chemical species entered within the reaction, to ensure that each species lies within the limitations of the ASSF tool
- Verifying if the chemical reaction is balanced

Should either of these two provisionary checks not be met, the user is requested to revise the equation input, until both of these conditions are satisfied. Upon satisfying these two

conditions, the user is prompted to input the necessary operating conditions of the reaction, including temperature, pressure, conversion, and a reference marker.

This input can be accomplished through one of two methods. The first involves using the command prompts and directions provided by the ASSF tool, where the user is guided in a stepwise manner to input the reaction and its associated data. This is ideal for first time users of the software platform.

Alternatively, the user is able to input the conditions into a predefined format, in a Microsoft ® Excel spreadsheet, whereby the ASSF tool extracts and utilizes the reaction pathways accordingly. The advantage of this input procedure lies in its ability to add multiple reactions and their conditions simultaneously.

In both of these input methods, the user is required to follow a specific syntax when entering the chemical reaction. For example, the production of MeOH via the hydrogenation of CO_2 (represented by Equation 3.5 below) is required to be inputted as Equation 3.6 within the ASSF tool.

$$CO_2 + 3H_2 \leftrightarrow CH_3OH + H_2O \qquad \text{(Equation 3.5)}$$

$$1.\,co2 + 3.\,h2 = 1.\,ch3oh + 1.\,h2o \qquad \text{(Equation 3.6)}$$

It is essential that reactions inputted into the ASSF tool contain the associated stoichiometric co-efficient with each chemical species, as per Equation 3.6, with these two entities being separated by means of a period symbol/full stop. Furthermore, it is important to note that as opposed to other software platforms in the engineering space, the ASSF tool does not require that reactants be differentiated from products using a negative sign. Instead, as seen in Equation 3.6, the reactants are separated from the products by means of an equal (‘=’) symbol, with all chemical species on the left of this symbol denoting a reactant, and those on the right of the symbol denoting a product.

Additionally, upon entering the reaction pathway and its associated data, the user is prompted to indicate whether the reaction is part of a reaction block. Should a reaction be part of a reaction block, the sub-reaction is deemed to be one of multiple reaction pathways that occur simultaneously within a single reactor system. This is common in catalytic reactions, where there is often a main reaction followed by one, or multiple, side reactions.

This ensures that the ASSF tool is able to account for all the reactions that are occurring in a single reactor unit operation resulting from the catalyst involved. Furthermore, this allows the ASSF tool to group these reaction pathways together when considering possible reaction pathway combinations. This is accomplished through the development of an overall reaction within the ASSF tool, which is subsequently utilized in determining the number of possible reaction pathway combinations. Upon finding the associated combinations, the reaction block is once again split apart, allowing each reaction and its respective conversion to be computed within the design stages.

If a reaction is not part of a reaction block, the reaction is considered to be an independent reaction. These are the reactions that occur solely within a single reactor unit operation. Appendix D1 contains a diagrammatic representation of the code responsible for the development of the RPD.

3.4. Determining the Number of Reaction Pathway Combinations

As with Section 3.3, this section deals with the explanation of this portion of the ASSF tool, which is focused on determining the number of reaction pathway combinations achievable from the previously developed RPD.

3.4.1. Reaction Pathway Combinations – Explanation

An investigation into a reaction pathway or reaction block, is the primary means by which to determine the feasibility of a process. However, the possibility remains that reaction pathways previously deemed to be unfavorable, can be combined with other reactive systems, in an attempt to increase their feasibility.

In such cases, the product of a single reaction becomes the reactant to the second reaction, thereby acting in the role of an intermediate for the overall reactive system. In this way, reaction pathway combinations are also considered. It is important to reiterate, however, that these reaction pathway combinations are not considered as novel reactive systems. Rather the pairing

of reaction pathways looks to extend the boundaries of the process plant, employing a secondary/tertiary reactor unit operation.

The ASSF tool considers a total of four sub-reactions/reaction blocks within a process plant system. The reason why 4 sub-reactions were chosen, was that MeOH and DME production via CO_2 hydrogenation often occurs by means of three main reactions. Therefore, a fourth sub-reaction system was included to ensure that any outliers in this norm was still considered, accounting for a worst-case scenario event.

During this section of the ASSF tool, the individual reactions/reaction blocks, are treated as a superstructure, with all possible reaction pathway combinations being a subset of the superstructure. The final reactive system must show a clear link between the starting reactants (CO_2 and H_2) and the desired products (MeOH and DME), as per the scope of the developed ASSF tool.

An example of these reaction pathway combinations can be clearly illustrated through the reactions shown in Equation 3.7 to Equation 3.10. Suppose the following four reactions are considered, with each reaction being considered to be independent, i.e., not part of a reaction block:

$$CO_2 + H_2 \leftrightarrow CO + H_2O \quad \text{(Equation 3.7)}$$

$$CO_2 + 3H_2 \leftrightarrow CH_3OH + H_2O \quad \text{(Equation 3.8)}$$

$$CO + 2H_2 \leftrightarrow CH_3OH \quad \text{(Equation 3.9)}$$

$$2CH_3OH \leftrightarrow CH_3OCH_3 + H_2O \quad \text{(Equation 3.10)}$$

Based on the reactions in Equation 3.7 to Equation 3.10, there are only two reactions that are able to proceed utilizing a CO_2/H_2 feed stream, namely Equation 3.7 and Equation 3.8. These reaction pathways focus on the production of CO and MeOH, with only one of these products having the possibility of being commercialized. Equation 3.9 and Equation 3.10 however do not hold any practical value considering the feed stream at hand.

By combining the aforementioned reactions, the number of possible reactive systems is able to extend to five possible combinations, focusing on the production of both of the desired products, namely MeOH and DME. This can be achieved through the following five reaction pathway combinations:

1. Equation 3.7

2. Equation 3.7 → Equation 3.9
3. Equation 3.7 → Equation 3.9 → Equation 3.10
4. Equation 3.8
5. Equation 3.8 → Equation 3.10

Based on these combinations, options 1 and 4 would occur in a single reactor process plant. Options 2 and 5 on the other hand, involves the use of two reactor unit operations, with the product of the first reactor acting as an intermediary in the overall process, and being fed into the secondary reactor unit operation. Option 3 employs three reactor unit operations, with the products of the first and second reactor acting as intermediates in the overall process. This highlights how the boundaries of the process plants are extended within the ASSF tool upon identifying possible reaction pathway combinations.

These combinations allow for alternative production pathways to be considered within the ASSF tool. Appendix D2 provides a diagrammatic representation of the code focused on the development of the associated reaction pathway combinations, utilizing the RPD previously developed.

3.5. Feed Streams

There are two feeds streams considered as part of the scope of the ASSF tool, and are the primary focus in its demonstration. These feed streams are CO_2 and H_2. As part of the ASSF tool, there are two inputs required from the user relating to the feed streams, namely:

- The CO_2 feed flow rate basis in kmol/hr (F_{CO2})
- The percentage excess H_2 gas fed into the process ($Excess_{H2}$)

The advantage of having the user input the desired CO_2 flow rate basis, is that all subsequent process designs will be based on this input, scaling the process and the size of the required unit operations as per the desired flow rate. Furthermore, this allows for the user to have more control over the ASSF tool designs allowing the analysis process to be more accurate and relative to the task at hand, based on user requirements.

The amount of excess H_2 that is fed into the system (F_{H2}) is calculated using Equation 3.11, whereby the minimum H_2 requirements, as per the stoichiometric co-efficient ratio (SCE_{H2}/SCE_{CO2}), is multiplied by the excess H_2 input.

$$F_{H2} = \left(F_{CO2} \times \frac{SCE_{H2}}{SCE_{CO2}}\right) \times \left(1 + \frac{Excess_{H2}}{100}\right) \quad \text{(Equation 3.11)}$$

The assumptions related to the feed streams entering the process are as follows:

- Both feed streams have 100% purity.
- Feed streams enter the process at ambient conditions of 25^{o}C and 1.01325 bar.

It is important to note that these feed conditions assume a worst case-scenario. It is often the case that H_2 gas purchased/produced via electrolysis units, enters the subsequent processes at elevated pressures. This has proven especially useful in transportation of H_2 gas from the source to the point of utilization. One such technology by the Linde group, found that pressurizing H_2 to the pressures exceeding 500 bar resulted in liquid H_2, allowing a single truck trailer to house and deliver 1100 kilograms of H_2, which would have previously taken up 13000 cubic meters as a gas (Dagdougui, *et al*., 2018). This allows for more efficient transport systems.

An input of pressurized H_2 would reduce the work and energy needed by the compressor unit operation, to achieve the reaction pressure, thereby alleviating some of the energy and unit operation costs. The utilization of ambient conditions for the feed stream ensures a worst-case scenario consideration, with changes in the feed stream being to the economic benefit of the processes.

In order to prevent multiple duplicate unit operations, the feed streams are mixed together, to form a single stream which is passed through the pre-reactor compressor and heat exchanger unit operations. The data calculated for these feed streams, as well as all other streams in the process, is given Section 3.6.

3.6. Stream Data

There are various stream data components calculated within the ASSF tool, with each data value being utilized in subsequent calculations. For each process designed within the ASSF tool, the following data is calculated for each stream within the process:

- Mass and molar flow rates
- Mass and molar compositions
- Temperature
- Pressure
- Volumetric flow rate (species-wise and overall stream value)
- Density
- Enthalpy (species-wise and overall stream value)
- Vapor Pressure (species-wise and overall stream value)
- Pipe Diameter
- Phase (specie-wise and overall stream value)

This section details the calculations associated with each of these parameters.

3.6.1. Equation of State

The Equation of State (EOS) highlights the relationship that exists between pressure, volume and temperature of the components within a stream, as well as the relationships that exists within the stream as a whole. Essentially the EOS is able to provide a thermodynamic description of the state of matter present within the stream, when exposed to specific conditions (Ramdharee, *et al*., 2013).

Throughout the course of the ASSF tool, the Peng-Robinson EOS was utilized. This EOS is commonly utilized in the petroleum industry. Furthermore, this EOS has been utilized extensively within reactive systems focusing on the production of MeOH and DME, as is the case with the products considered within the ASSF tool. The Peng-Robinson EOS is able to handle both liquid and vapor properties (Ramdharee, *et al*., 2013), making it perfectly suited for these reactive systems, where vapor-liquid equilibrium is often present. Equations 2.17 to 2.22, presented in Section 2.7, details the equations associated with the Peng-Robinson EOS.

The Peng-Robinson EOS was utilized in calculating the volumetric flow rate of the stream and its associated components. This allowed for the subsequent calculation of the stream density, utilized in sizing separation vessels, and the sizing of pipe diameters required for the associated flow.

3.6.2. Vapor Pressure

Vapor pressure is an indication of the pressure exerted by the vapor stream when it is in thermodynamic equilibrium and is dependent on the temperature of the system. The vapor pressure of a stream ($(P_v)_{Total}$) can be defined as the sum of the vapor pressures of each individual chemical species within the stream (P_{v_i}), relative to its molar fraction (x_i) (Stauffer, *et al*., 2008). This relationship is represented by Equation 3.12.

$$(P_v)_{Total} = \sum x_i P_{v_i} \qquad \text{(Equation 3.12)}$$

The partial vapor pressure of each component within any given stream, was calculated using Equation 3.4, along with the constants provided in Table 3.6. However, the vapor pressure constants provided in Table 3.6, are only applicable within a certain temperature range, outside of which the constants are not able to accurately calculate the vapor pressure of the chemical species.

With vapor pressures being indicative of the vapor/liquid equilibrium pressure, this entity was utilized in determining the phase of the species within the stream as well. This was especially important in determining their volumetric flow rate, as per the Peng-Robinson equation detailed in Section 3.6.1, as well as the possibility of phase separation.

The phase was determined through the comparison of stream pressure (P) and temperature (T) to that of the chemical species vapor pressure (P_v), and its respective temperature constraints associated thereof (T_{min} and T_{max}). Four possible scenarios arise from this comparison, namely:

- $P < P_v$ = Gas
- $P > P_v$ = Liquid
- $T < T_{min}$ = Liquid
- $T > T_{max}$ = Gas

In order to ensure that the calculation of the vapor pressure within the ASSF tool was computed with minimal memory usage and computational time, the first check related to the chemical species present within the stream. Should a chemical species not be present, there is no practical value in calculating its vapor pressure, thereby reducing the computational calculations required.

The second check made by the ASSF tool was to compare the stream's operating temperature (T) with the temperature range of the chemical species within Table 3.6. Should the stream temperature lie outside of the vapor pressure range, the chemical species vapor pressure cannot be accurately calculated. Therefore, the species recorded vapor pressure would be listed as "NaN" (in MATLAB ® terms NaN is used to denoted not applicable), indicating that the vapor pressure is not applicable at the predefined stream temperature.

The diagrammatic representation of the code associated with these vapor pressure calculations is given in Appendix D3. Appendix D6 contains an overall diagrammatic representation of the ASSF tool section employed, which consolidates all of the stream data within the ASSF tool into a single flow chart representation.

3.6.3. Enthalpy

The enthalpy (H) of a system can be defined as the summation of the internal energy (U_e), with the pressure-volume product (PV). This can be represented by means of Equation 3.13, where all of the necessary values in the equation must be uniform in terms of their relative units, i.e., related to mass or molar flows (Smith, *et al*., 2018).

$$H = U_e + PV \qquad \text{(Equation 3.13)}$$

The enthalpy of a multi-component stream, on the other hand, can be calculated relative to the molar flow rate of the individual species within the stream. Therefore, as opposed to the vapor pressure which required the molar fraction of the chemical species to be taken into account, the total enthalpy of the stream (H_{Total}) is defined as the sum of the enthalpy of each individual species (H_i) within the stream, as shown in Equation 3.14. This is only true, however, when the same reference state is chosen for all the species within the stream (Jones, 1997).

$$H_{Total} = \sum x_i H_i \qquad \text{(Equation 3.14)}$$

When calculating the enthalpy of a stream, a reference temperature of 298.15 K was utilized. This required the calculation of the change in enthalpy from the reference state to the actual temperature of the stream, assuming that the enthalpy change due to pressure change is negligible. As a result, the enthalpy of any species can be calculated by means of Equation 3.15.

$$\Delta H_i = H_f^o + \int_{Tref}^{Tb} C_{p_l}\, dT + H_{vap} + \int_{Tb}^{T} C_{p_g}\, dT \qquad \text{(Equation 3.15)}$$

As per Equation 3.15, the change in the enthalpy of a chemical species is dependent on the enthalpy of formation (H_f^o), the specific heat of the liquid and vapor phases (C_{p_l} and C_{p_g}) and the heat of vaporization (H_{vap}). It is important to note, however, that these specific heat values are given with respect to temperature (T), and therefore it is important that the specific heat function be integrated over predefined temperature range.

When there was a phase change, the liquid specific heat was integrated from the reference temperature (T_{ref}) to the boiling temperature (T_b) of the specie in question. However, the boiling point of any chemical species changes with the pressure it is exposed to, thereby necessitating the need to calculate this new boiling point.

The ASSF tool looks at the pressure of the stream, utilizing this pressure as the 'vapor pressure', and iteratively calculating the temperature at which the stream pressure would equate to that of the vapor pressure of the component, as per Equation 3.4. This calculates the temperature at which vapor-liquid equilibrium exists under the stream conditions, thereby indicating the new boiling point at the predefined stream pressure.

This 'new boiling point' for each species is accounted for within the ASSF tool, thereby ensuring that pressure changes to the physical properties of chemical species was considered.

After calculating the new boiling point and integrating the liquid's specific heat capacity within this temperature range, the heat of vaporization was calculated for the species flow. As can be seen by Equation 3.15, this does not require any integration with respect to temperature, as temperature remains constant during a phase change. Finally, the vapor specific capacity is integrated from the newly calculated boiling point to the final temperature of the stream.

The ASSF tool is able to decisively choose the extent to which Equation 3.15 is followed, depending on whether or not the species experiences a phase change from the reference temperature. Chemical species such as H_2, CO_2 and CO do not experience these phase changes as they exist as vapors at the predefined reference conditions. Appendix D4 diagrammatically represents this section of the ASSF tool.

3.6.4. Volumetric Flow Rate

The volumetric flow rate of the stream was calculated using the Peng-Robinson EOS defined in Equation 2.17 to Equation 2.22. It is important to note however, that the volume term given in the Peng-Robinson EOS (V_m) is defined as the molar volume, and therefore is the volume per mole of species within the specified stream. Therefore, the total volumetric flow rate of the stream (V_{Total}) is the summation of the individual volumetric flow rates of each component within the stream (V_i), as represented by Equation 3.16.

$$V_{Total} = \sum V_i \qquad \text{(Equation 3.16)}$$

The ASSF tool computes and solves for the molar volume of each chemical species present in the stream, utilizing Equation 2.17. In order to adjust the Peng-Robinson EOS to individual components within the stream, the equation was modified to allow for the partial pressure (P_i) of each chemical species to be considered, as per Equation 3.17.

$$P_i = \frac{RT}{V_{m_i} - b} - \frac{a\alpha}{V_{m_i}^2 + 2bV_{m_i} - b^2} \qquad \text{(Equation 3.17)}$$

The partial pressure of each chemical species was calculated as the product of the species molar composition (x_i) and total stream pressure (P), as represented by Equation 3.18.

$$P_i = x_i P \qquad \text{(Equation 3.18)}$$

The species volumetric flow rate (V_i) was then calculated as the product of the species molar flow rate (n_i) and the molar volume (V_{m_i}), previously calculated in Equation 3.17. This relationship is represented by means of Equation 3.19.

$$V_i = n_i V_{m_i} \qquad \text{(Equation 3.19)}$$

The need for a species physical phase (liquid or vapor) becomes especially important when determining its volumetric flow rate. As seen by Equation 3.17, the Peng-Robinson EOS is a cubic equation of state, resulting in three possible solutions for the molar volume of a stream/chemical species. It is the phase of a chemical species that ultimately determines the molar volume chosen within the ASSF tool, with the ASSF tool being able to systematically and automatically choose the molar volume aligning with the associated phase.

The lowest value noted for the molar volume represents that of a liquid phase, whereas the largest molar volume represents that of a vapor phase. The third molar volume value, on the other hand, holds no practical importance (Lin, 1994). It is for this reason that the vapor pressure and associated chemical species phases was coded into the ASSF tool and calculated prior to the calculations surrounding the volumetric flow rates.

As with the vapor pressure and enthalpy calculations, this procedure was only followed for the chemical species present within the stream, ensuring that the ASSF tool was not involved with unnecessary calculations. This ultimately reduces the memory requirements of the ASSF tool, and its computational time, allowing for the analysis and results to be obtained in a shorter period of time. Appendix D5 presents a diagrammatic flow chart representation of the ASSF tool section responsible for the calculation of a stream's volumetric flow rate.

3.6.5. Other Stream Data

Using the data previously calculated, additional stream data was computed for each flow within the process. Assuming a velocity (v) of 1.5 m/s flow throughout the entire process, the pipe diameter (D_p) required was calculated by means of Equation 3.20. The assumed velocity chosen here however, is a baseline value on which the ASSF tool was developed and can be altered within the ASSF tool depending on user requirements.

$$D_p = 2 \times \sqrt{\frac{V_{Total}}{3600} \times \frac{1}{v\pi}} \qquad \text{(Equation 3.20)}$$

The total volumetric flow rate (V_{Total}) was divided by a factor of 3600, allowing for the conversion of an hourly volumetric flow rate to the flow per second, aligning with the units of the velocity. The ASSF tool, however, does provide the user with the opportunity to adjust the assumed velocity throughout the process, thereby providing the user with more control over the process design.

Additionally, utilizing the mass flow rate of a stream (M), and its associated volumetric flow rate (V_{Total}), the stream density (ρ_{stream}) was calculated using Equation 3.21.

$$\rho_{stream} = \frac{M}{V_{Total}} \qquad \text{(Equation 3.21)}$$

The stream density is especially important when designing and sizing the necessary separation vessels required throughout the process.

3.7. Heat exchangers

Heat exchangers are unit operations that are focused on transferring thermal energy between two or more substances within the process. These fluids exhibit a temperature gradient, promoting and allowing for the necessary heat transfer to take place, and allowing for the stream to be heated or cooled accordingly (Edreis & Petrov, 2020). Heat exchangers are an integral part of any process, allowing for reaction and separation operating conditions to be achieved, as well as the recovery of heat energy utilized throughout the course of the process (Chaudhari & Adroja, 2014).

This section focuses on the assumptions, design and costing of the heat exchangers utilized throughout the ASSF tool, during its associated case study analysis. A flow chart is presented within Appendix D7, highlighting the chronological structure of this segment of the ASSF tool, and its associated loops.

3.7.1. Heat Exchanger Assumptions

Due to the lack of information available at the preliminary design stage, there exists a degree of uncertainty, as not all information covering sizing, costing, etc. is available. In order to bridge this gap in information, assumptions were made during this design stage. The ASSF tool employed the following assumptions related to heat exchanger unit operations:

- All heat exchanger unit operations were considered to be isobaric, implying that there was no pressure change across these unit operations.
- Heat exchangers that were below the lower limits associated with their costing equations, were costed using the lower cost/size limit, accounting for a worst-case costing scenario.

- Heat exchangers that were above the upper limits associated with their costing equations, were broken up into a series of heat exchanger unit operations with incremental temperature changes.

The first assumption made, in relation to heat exchangers, requires no pressure change within these unit operations. Based on the Peng-Robinson EOS presented in Section 3.6.1, a direct proportionality relationship exists between temperature and pressure. Therefore, with constant volume and molar flow rate, an increase in temperature would result in an increase in the pressure of the stream exiting the heat exchanger. Conversely, a decrease in temperature would result in a decrease in pressure of the stream exiting the heat exchanger.

In order to allow for the heat exchanger to be assumed to operate under isobaric conditions, the pipe diameter exiting the heat exchanger is varied. Therefore, the change in pressure is offset by the change in volumetric flow rate, allowing the heat exchanger to operate at constant pressure.

The final assumption made regarding heat exchangers was that all of the heat exchangers that were larger than the size constraint denoted by the costing equation, were broken up into multiple heat exchangers in series. Consider a heat exchanger required to increase the temperature of a stream from ambient conditions of 25^{o}C to a temperature of 800^{o}C, as per Figure 3.7. This heat exchanger is likely to have a large area, beyond that which can be utilized within the constraints of the costing equations.

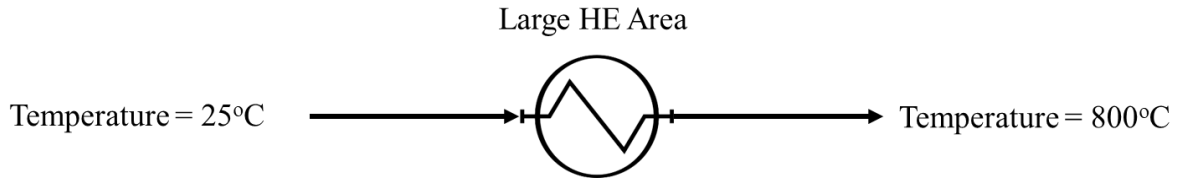

Figure 3.7: Diagrammatic representation of a heat exchanger unit operation with a large temperature change

By breaking up this heat exchanger into multiple unit operations in series, with incremental temperature increases, the individual heat exchanger areas are reduced, thereby allowing for the costing equations to be utilized accurately, as shown in Figure 3.8.

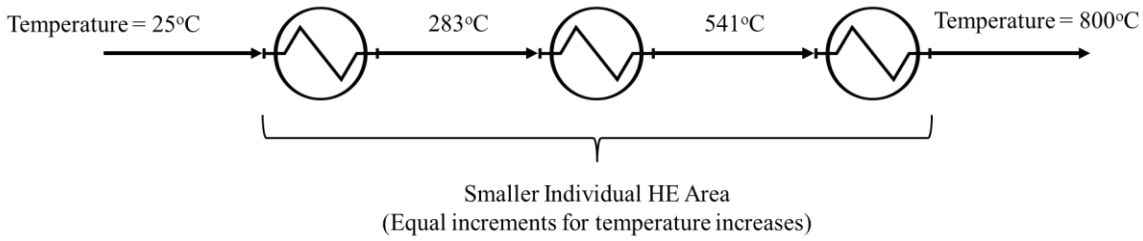

Figure 3.8: Diagrammatic representation of the series heat exchanger system utilized in the ASSF tool

3.7.2. Sizing of Heat Exchanger Unit Operations

In order to cost the heat exchangers (detailed in Section 3.7.3), the size of the unit operation was required. With heat exchanger unit operations, this size is expressed in terms of heat transfer area, calculated by means of Equation 3.22 (Dubey, *et al*., 2014).

$$Q = UA\Delta T_{LM} \qquad \text{(Equation 3.22)}$$

Equation 3.22 shows that the heat transferred between the two working fluids with a heat exchanger (Q), is dependent on the area of the heat exchanger (A), the overall heat transfer co-efficient (U), and the log-mean temperature (ΔT_{LM}). The log mean temperature utilizes the desired temperature change of the process stream, as well as that of the utility used in promoting the transfer of thermal energy.

Figure 3.9 shows a schematic representation of the flow within a countercurrent heat exchanger configuration, where T_s denotes the stream temperature entering and exiting the heat exchanger, and T_u denotes the temperature of the utility stream. Figure 3.10 shows the associated temperature profile graph associated within this configuration.

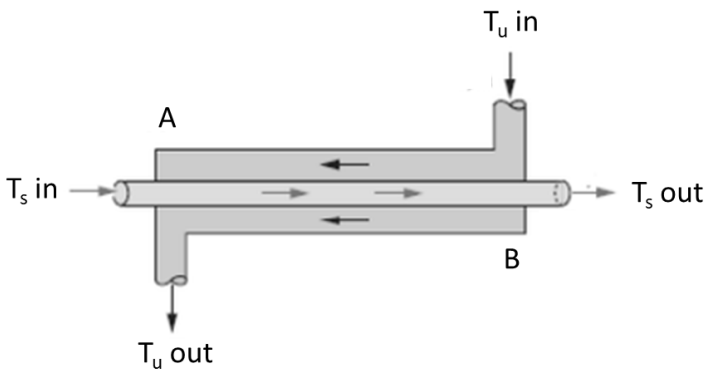

Figure 3.9: Diagrammatic representation of the flow of fluids in a counter-current heat exchanger configuration

It is important to note that the temperature profile given in Figure 3.10 is relevant to a heat exchanger focused on the heating of a process stream. Cooling heat exchangers will show a decrease in the stream temperature and an increase in the utility temperature.

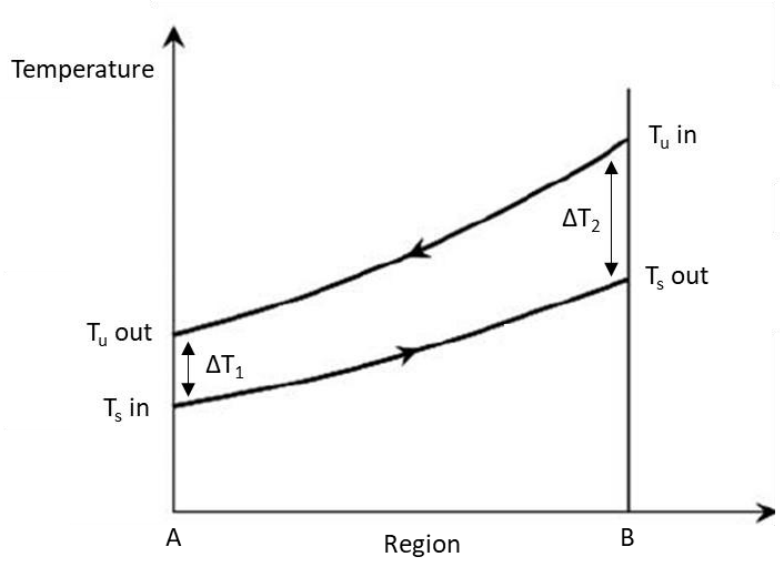

Figure 3.10: Graphical representation of the temperature profile that exists within a counter current heat exchanger

Counter current heat exchangers were chosen for the ASSF tool, as these unit operations are noted to have greater thermal transfer efficiencies. This is likely exacerbated by the increased contact time between the stream and its associated utility, as these two fluids flow in opposite directions to one another (Sridhar & Bicha , 2017). As a result of this increased efficiency, counter current flow heat exchangers are noted to require smaller heat transfer areas, thereby lowering the cost of the unit operation in question.

The log mean temperature was calculated using Equation 3.23 (Dubey, *et al*., 2014), with the temperature changes denoted in the equation being indicative of that shown in Figure 3.10.

$$\Delta T_{LM} = \frac{\Delta T_1 - \Delta T_2}{\ln\left(\frac{\Delta T_1}{\Delta T_2}\right)} \qquad \text{(Equation 3.23)}$$

The overall heat transfer co-efficient (U), denoted in Equation 3.22, is dependent on the fluid present within the stream, as well as the utility being utilized to promote the heat transfer. Table 3.7 details the ranges utilized for the overall heat transfer co-efficient values when sizing the heat exchanger unit operations.

Table 3.7: Overall heat transfer co-efficient utilized for heat exchanger design (Kakac & Liu, 2002)

Fluids	U ($W/m^2.K$)
Water to Water	1300 – 2500
Gas to Water	10 – 250
Light Organics to Water	370 – 750
Medium Organics to Water	240 – 650
Heavy Organics to Water	25 – 400
Water to Steam	2200 – 3500
Gas to Steam	25 – 240
Light Organics to Steam	490 – 1000
Medium Organics to Steam	250 – 500
Heavy Organics to Steam	30 – 300

The ASSF tool is able to systematically analyze the chemical species within a stream, making the appropriate choice for the overall heat transfer co-efficient. This allows for the ASSF tool to present heat transfer areas that are more accurate and relative to the stream's constituents. As seen in Table 3.7, however, these values are presented within a range, and therefore when extracted into the ASSF tool, the mid-point of this range was utilized.

3.7.3. Costing of Heat Exchanger Unit Operations

The procedure that was utilized in the costing of all unit operations within the ASSF tool, including heat exchangers, was developed by Turton, *et al*. (2009). This section deals with the costing procedure developed by Turton, *et al*. (2009) and the constants associated with heat exchanger unit operations.

The first step in costing any unit operation involves the calculation of the purchased cost (C_p^o) value, accomplished by means of Equation 3.24, where K_1, K_2 and K_3 are constants, and A represented the area of the heat exchanger in square meters (m^2).

$$\log_{10} C_p^o = K_1 + K_2 \log_{10}(A) + K_3 [\log_{10}(A)]^2 \qquad \text{(Equation 3.24)}$$

The constants and constraints associated with Equation 3.24 are given in Table 3.8.

Table 3.8: Heat exchanger constants associated with Equation 3.24 (Turton, et al., 2009)

Type	K_1	K_2	K_3	Min Area (m^2)	Max Area (m^2)
Scraped Wall	3.7803	0.8569	0.0349	2	20
Teflon Tube	3.8062	0.8924	-0.1671	1	10
Bayonet	4.2768	-0.0495	0.1431	10	1000
Floating Head	4.8306	-0.8509	0.3187	10	1000
Fixed Tube	4.3247	-0.3030	0.1634	10	1000
U-Tube	4.1884	-0.2503	0.1974	10	1000
Kettle Reboiler	4.4646	-0.5277	0.3955	10	100
Double Pipe	3.3444	0.2745	-0.0472	1	10
Multiple Pipe	2.7652	0.7282	0.0783	10	100
Flat Plate	4.6656	-0.1557	0.1547	10	1000
Spiral Plate	4.6561	-0.2947	0.2207	1	100
Air Cooler	4.0336	0.2341	0.0497	10	10000
Spiral Tube	3.9912	0.0668	0.2430	1	100

Once the C_p^o value was calculated, the focus was shifted to the pressure factor (F_p) that is associated with the heat exchanger. This was calculated by means of Equation 3.25, where C_1, C_2 and C_3 are constants, and P is used to denote the operating gauge pressure of the heat exchanger in units of barg (bar gauge).

$$\log_{10} F_p = C_1 + C_2 \log_{10}(P) + C_3 [\log_{10}(P)]^2 \qquad \text{(Equation 3.25)}$$

Table 3.9 details the constants associated with calculating the pressure factors.

Table 3.9: Heat exchanger pressure factor constants associated with Equation 3.25 (Turton, et al., 2009)

Type	C_1	C_2	C_3	Min Pressure (barg)	Max Pressure (barg)
Scraped Wall	0	0	0	0	40
	0.6072	-0.9120	0.3327	40	100
	13.1467	-12.6574	3.0705	100	300
Teflon Tube	0	0	0	0	15

Bayonet, Fixed Tube Sheet, Floating Head, Kettle Reboiler, U-Tube (both shell and tube)	0	0	0	0	5
	0.03881	-0.11272	0.08183	5	140
Bayonet, Fixed Tube Sheet, Floating Head, Kettle Reboiler, U-Tube (tube only)	0	0	0	0	5
	-0.00164	-0.00627	0.0123	5	140
Double Pipe and Multiple Pipe	0	0	0	0	40
	0.6072	-0.9120	0.3327	40	100
	13.1467	-12.6574	3.0705	100	300
Flat Plate and Spiral Plate	0	0	0	0	19
Air Cooler	0	0	0	0	10
	-0.1250	0.15361	-0.02861	10	100
Spiral Tube (both shell and tube)	0	0	0	0	150
	-0.4045	0.1859	0	150	400
Spiral Tube (tube only)	0	0	0	0	150
	-0.2115	0.09717	0	150	400

The next step involved the consideration of the material of construction when costing the heat exchangers. This was done through the use of a material factor (F_M). Table 3.10 details the material factors that are associated with heat exchangers, with CS representing carbon steel, Cu representing copper, SS representing stainless steel, Ni Alloy representing nickel alloy, Ti representing titanium, and Al representing aluminum.

Table 3.10: Material factors associated with heat exchangers (Turton, et al., 2009)

Heat Exchanger Type	Material	Material Factor (F_M)
Double pipe, multiple pipe, fixed tube sheet, floating head, U-tube, bayonet, kettle reboiler, scraped wall, spiral tube	CS-Shell/CS-Tube	1
	CS-Shell/Cu-Tube	1.4
	Cu-Shell/Cu-Tube	1.7
	CS-Shell/SS-Tube	1.8
	SS-Shell/SS-Tube	2.7
	CS-Shell/Ni Alloy Tube	2.7
	Ni Alloy Shell/Ni Alloy Tube	3.7
	CS-Shell/Ti-Tube	4.6
	Ti-Shell/Ti-Tube	11.4
Air cooler	CS Tube	1
	Al Tube	1.4
	SS Tube	2.9
Flat plate and Spiral plate	CS (in contact with fluid)	1
	Cu (in contact with fluid)	1.4
	SS (in contact with fluid)	2.4
	Ni Alloy (in contact with fluid)	2.7
	Ti (in contact with fluid)	4.6

The costing equations developed by Turton, *et al*. (2009) costs all of these unit operations as per 2001. As a result, this cost is termed as being a bare module cost and was used as a basis for the costing procedure when taking into account inflation through the chemical engineering price cost index (CEPCI) value. The bare module cost (C_{BM}) was calculated by means of Equation 3.26, where B_1 and B_2 represent the constants associated with this equation.

$$C_{BM} = C_p^o(B_1 + B_2 F_M F_P) \qquad \text{(Equation 3.26)}$$

Table 3.11 provides the constants associated with Equation 3.26.

Table 3.11: Bare module cost constants for costing heat exchangers (Turton, et al., 2009)

Type	B_1	B_2
Double pipe, multiple pipe, scraped wall, spiral tube	1.74	1.55
Fixed tube sheet, floating head, U-tube, bayonet, kettle reboiler, Teflon tube	1.63	1.66
Air cooler, spiral plate and flat plate	0.96	1.21

Having calculated the bare module cost as per 2001, the cost was then corrected to account for inflation at the time at which the ASSF tool was run. This is accomplished through the use of the ratio between the CEPCI value at the time of operating the ASSF tool, and the CEPCI as per 2001 (recorded as 397). The user is requested for this CEPCI value in the ASSF tool, allowing for the costs to be relative to the time at which the ASSF tool is being utilized. This adjustment of the unit operation cost can be represented by means of Equation 3.27.

$$\text{Final Cost} = \frac{\text{CEPCI}}{397} * C_{BM} \qquad \text{(Equation 3.27)}$$

During the costing process within the ASSF tool, all possible heat exchanger types are considered, with the optimal choice being selected as the cheapest unit operation which can achieve the desired temperature change.

3.8. Compressors & Turbines

Compressor and turbine unit operations are those which are primarily focused on changing the pressure of a stream, either by increasing or lowering the pressure, respectively. This section deals with the assumptions, design and costing of the compressors and turbines within the ASSF tool. Appendix D8 provides a diagrammatic flow chart representation of the ASSF tool segment associated with pressure changing unit operations.

3.8.1. Compressor & Turbine Assumptions

As with the heat exchanger unit operations, assumptions were required at this stage of the preliminary design process, bridging the gap between the known data and that which is required but not yet available. The assumptions made during these design stages, must be realistic and have a degree of practical weighting, thereby increasing the accuracy of the preliminary design.

The assumptions made during the design of the compressor, compressor driver and turbine were as follows:

- All pressure changing unit operations operate under isothermal conditions, implying that there was no temperature change across the unit operation. In this case, the temperature at which the stream enters the unit operation was the same as the temperature that the stream exits the unit operation.
- The only work that was associated with the compressor and turbine was that of pressure-volume work, due to the constant temperature around this unit operation.
- Unit operations that were below the costing size constraints were costed as the minimum size constraint, accounting for a worst-case scenario cost.
- Unit operations that were above the costing size constraints were broken up into multiple pressure-changing unit operations, connected in a parallel configuration.

The assumption of isothermal operation can be considered to be counter-intuitive to the thermodynamic relationships that exist between pressure, temperature and volume. As seen by the Peng-Robinson EOS, an increase in pressure results in an increase in temperature, thereby exhibiting a direct proportionality relationship between these two factors.

In order to maintain the temperature across the pressure-changing unit operation, the volume of the stream entering and leaving the compressor was be adjusted, thereby achieving the desired pressure through pressure-volume work, as per the second assumption. This change in volume was achieved by varying the diameter of the pipe entering and leaving the unit operation, thereby still accounting for physical changes to the stream brought about by the change in pressure.

As per the last assumption highlighted within this section, pressure-changing unit operations that require a large pressure change, are likely be associated with a high fluid power, as per Figure 3.11.

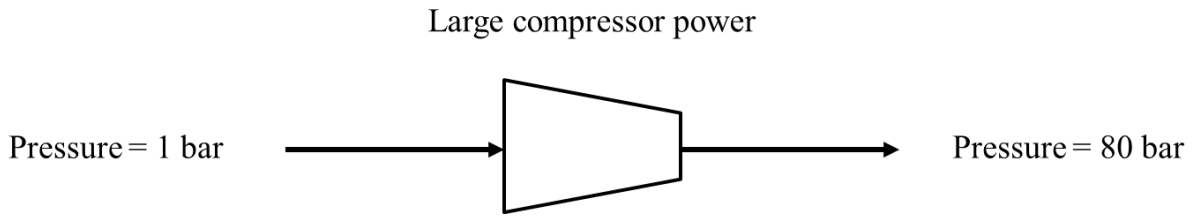

Figure 3.11: Diagrammatic representation of a compressor unit operation with a large pressure change

In order to reduce the individual fluid power of each compressor unit operation, the compressor was broken down into multiple compressor unit operations in parallel. Unlike the heat exchanger unit operations, pressure-changing unit operations proved to be unable to be connected in a series configuration, as the high flow rate through these unit operations is what leads to the elevated fluid power values noted. Therefore, by breaking down the pressure-changing unit operation in a parallel configuration, the flow rate moving through each individual unit operation is drastically reduced, thereby reducing the associated fluid power of each unit operation. This can be diagrammatically represented by means of Figure 3.12.

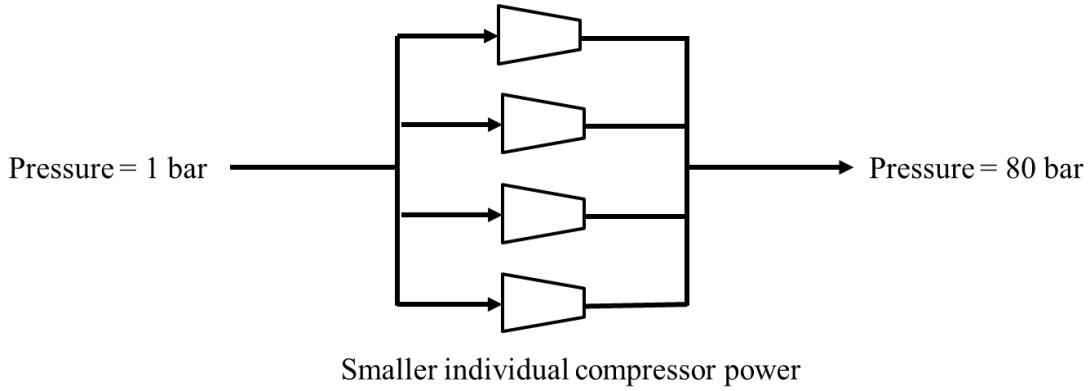

Figure 3.12: Diagrammatic representation of the parallel configuration pressure-changing unit operation system utilized in the ASSF tool

3.8.2. Sizing of Compressor & Turbine Unit Operations

The size of pressure changing unit operations is expressed in terms of the unit's energy rating or work done, often denoted in terms of kilowatts (kW) or megawatts (MW), depending on the size of the chemical plant in operation. As mentioned in Section 3.8.1, one of the main assumptions of these pressure-changing unit operations, was that these unit operations functioned under isothermal conditions, thereby creating a scenario where only pressure-volume work is required.

Due to there being no temperature change across these unit operations, the energy rating of each pressure-changing unit operation was calculated using the first law of thermodynamics. This law is demonstrated by Equation 3.28, whereby the work (W) is calculated by integrating the streams pressure function (P), with respect to volume (V), from the initial to final volumetric flow rate of the stream.

$$\delta W = \int_{V_{initial}}^{V_{final}} P \, dV \qquad \text{(Equation 3.28)}$$

The pressure function required in Equation 3.28 is given in the Peng-Robinson EOS noted in Equation 2.17. Therefore, substituting this equation into the first law of thermodynamics, results in Equation 3.29, whereby the molar volume term (V_m) is expressed as V/n.

$$\delta W = \int_{V_{initial}}^{V_{final}} \left(\frac{RT}{\frac{V}{n} - b} - \frac{a\alpha}{\left(\frac{V}{n}\right)^2 + 2b\left(\frac{V}{n}\right) - b^2} \right) dV \qquad \text{(Equation 3.29)}$$

When calculating the initial and final volume of the stream, i.e., the integration limits of Equation 3.29, the volumetric flow rate of the stream entering and leaving the process was utilized. This volumetric flow rate (m^3/hr) was first converted to a per second flow, aligning with the units of work, where kilowatts can be expanded to kilojoules per second.

3.8.3. Costing of Compressor Unit Operations

The costing procedure for compressor unit operations employed a similar structure to that presented in Section 3.7.3 relating to heat exchangers. The C_p^o value was calculated as per Equation 3.24, with A being used to represent the fluid power of the compressor in kilowatts (kW). The constants related to compressors are given in Table 3.12.

Table 3.12: Constants associated with compressors for Equation 3.24 (Turton, et al., 2009)

Type	K_1	K_2	K_3	Min Power (kW)	Max Power (kW)
Centrifugal	2.2897	1.3604	-0.1027	450	3000
Axial	2.2897	1.3604	-0.1027	450	3000
Reciprocating	2.2897	1.3604	-0.1027	450	3000
Rotary	5.0355	-1.8002	0.8253	18	950

Due to the inert nature of a compressor unit operation, there is no pressure factor that needs to be considered in its costing. It is likely that the pressure factor is either incorporated directly into Equation 3.24, or that it is an implied inclusion within the fluid power that was calculated as per the energy balance.

Due to the absence of a pressure factor and bare module cost constants for compressor unit operations, the material factor considered was deemed as the bare module material factor (F_{BM}). Table 3.13 details the bare module material factors associated with compressor unit operations.

Table 3.13: Material factors associated with the costing of compressor unit operations (Turton, et al., 2009)

Unit Operation	Material of Construction	Material Factor (F_{BM})
Centrifugal	Carbon Steel	2.7
	Stainless Steel	5.7
	Nickel Alloy	11.5
Axial	Carbon Steel	3.8
	Stainless Steel	8.0
	Nickel Alloy	15.9
Rotary	Carbon Steel	2.4
	Stainless Steel	5.0
	Nickel Alloy	9.8
Reciprocating	Carbon Steel	3.3
	Stainless Steel	7.0
	Nickel Alloy	13.9

Accounting for only the C_p^o and bare module material factors, the bare module cost (C_{BM}) for the compressor unit operation was calculated by means of Equation 3.30.

$$C_{BM} = C_p^o F_{BM} \qquad \text{(Equation 3.30)}$$

As with the costing procedure detailed for heat exchangers, the bare module cost provided in Equation 3.30 is the cost of the unit operation as per September 2001, and therefore when accounting for inflation to the time at which the ASSF tool is run, the current CEPCI value is utilized in conjunction with Equation 3.27.

3.8.4. Costing of Compressor Drivers

Compressor drivers are an integral part of the compressor system and are focused on the production of the rotational shaft work required to operate the compressor unit operation. Furthermore, compressor drivers are able to vary the speed of rotation of these unit operations, thereby controlling the power output achievable and its associated performance (Mohitpour, *et al*., 2008).

Due to the importance that compressor drivers play, these unit operations are purchased in a pair-wise manner, with each purchase containing a coupling of a compressor and its associated driver. The C_p^o value was calculated as per Equation 3.24, with A being used to represent the shaft power of the compressor in kilowatts (kW). The constants and constraints related to compressor drivers are given in Table 3.14.

Table 3.14: Constants associated with compressor drivers for Equation 3.24 (Turton, et al., 2009)

Type	K_1	K_2	K_3	Min Power (kW)	Max Power (kW)
Gas Turbine	-21.7702	13.2175	-1.5279	7500	23000
Internal Combustion Engine	2.7635	0.8574	-0.0098	10	10000
Steam Turbine	2.6259	1.4398	-0.1776	70	7500
Electric – Explosion Proof	2.4604	1.4191	-0.1798	75	2600
Electric – Totally Enclosed	1.9560	1.7142	-0.2282	75	2600
Electric – Open/Drip Proof	2.9508	1.0688	-0.1315	75	2600

As with the costing of compressor unit operations, a bare module material factor is utilized in the costing of compressor drivers, as per Equation 3.30. Table 3.15 details the bare module material factors associated with compressor driver unit operations.

Table 3.15: Bare module material factors associated with the costing of compressor drivers (Turton, et al., 2009)

Unit Operation	Material Factor (F_{BM})
Gas Turbine	3.5
Internal Combustion Engine	2.0
Steam Turbine	3.5
Electric – Explosion Proof	1.5
Electric – Totally Enclosed	1.5
Electric – Open/Drip Proof	1.5

Inflation was then factored into the compressor driver cost using Equation 3.27, and the appropriate CEPCI value at the time of running the ASSF tool.

3.8.5. Costing of Turbine Unit Operations

The procedure involved in costing turbine unit operations is identical to that of costing the compressor unit operations, with the only difference being the constants associated when calculating the C_p^o value, and the bare module material factors. Table 3.16 details the constants for turbines, utilized in conjunction with Equation 3.24.

Table 3.16: Constants associated with turbines for Equation 3.24 (Turton, et al., 2009)

Type	K_1	K_2	K_3	Min Power (kW)	Max Power (kW)
Axial Gas Turbines	2.7051	1.4398	-0.1776	100	4000
Radial Gas/ Liquid Expanders	2.2476	1.4965	-0.1618	100	1500

Table 3.17 details the bare module material factors associated with turbine unit operations.

Table 3.17: Material factors that are associated with the costing of turbine unit operations (Turton, et al., 2009)

Material of Construction	Material Factor (F_{BM})
Carbon Steel	3.5
Stainless Steel	6.1
Nickel Alloy	11.6

Inflation was then factored into the cost of the turbine unit operation, through the use of Equation 3.27, and the CEPCI value noted at the time the ASSF tool was being utilized.

The costing of the pressure-changing unit operations was considered utilizing the same objective function as with the heat exchanger costing, with all possible types being considered and the cheapest unit operation selected.

3.9. Flash Drums

Flash drums are considered to be one of the simplest, and cheapest separation systems, relying on vapor/liquid equilibrium in order to achieve phase separation. During this process, the feed stream is subjected to the operating conditions of the flash drum, in terms of temperature and pressure, creating a partially vaporized stream. Components with lower boiling points are vaporized whereas those with higher boiling points are maintained in the liquid phase. As a result, the liquid is drained through the bottom of the vessel, whereas the gas escapes through the top of the vessel (Iggland & Mazzotti, 2015).

3.9.1. Flash Drum Assumptions

As with previous unit operations described within this chapter, the following assumptions were made in relation to the flash drum unit operation, when developing the ASSF tool:

- The pressure drop across the flash drum unit operation was deemed to be negligible, as is the case of the assumptions employed within the Rachford-Rice methodology. This methodology is utilized in determining the stream compositions exiting the flash drum and is discussed later in this section. As a result, the pressure of the vapor and liquid stream were both equal to that of the operating pressure of flash drum.
- The chemical species H_2 and CO were not included in the Rachford-Rice calculations as their critical temperatures are extremely low (below freezing point). As a result, it was assumed that during the phase separation, these two species go directly into the vapor stream of the flash drum.

- A change in pressure was utilized to create vapor/liquid equilibrium within the feed stream. The optimum pressure was calculated in an iterative manner, finding conditions that yielded the highest recovery rate of the desired product. Test runs of the ASSF tool found that the temperature drop needed to promote separation is too high in certain case studies, thereby resulting in impractical final temperatures. Therefore, pressure was chosen as the operating variable to promote the separation of components within the flash drum.
- All flash drums operated at a temperature of 298 Kelvin (ambient temperature). This reduces the safety risks associated with the final products exiting the process, whilst simultaneously preparing the product for its subsequent storage and transport to its end facilities. This storage and transport system, however, is beyond the scope of this research study.
- Should the flash drum unit operation volume be lower than the lower limit constraint of the costing equations, the lower limit was used to cost the flash drum, accounting for a worst-case scenario. Therefore, should pathways exhibit feasibility via the ASSF tool, accurate design of these reactive system would only serve to enhance the feasibility noted by the ASSF tool.
- The flash drum was set to achieve a 95% recovery of unreacted CO_2 in the vapor stream. When simulated using the ASSF tool, a portion of CO_2 was found to dissolve within the liquid stream, resulting in the flash drum being unable to achieve complete phase separation. Therefore, a 95% recovery constraint was selected for the ASSF tool to ensure a recovery with minimal impact on the subsequent product streams. This recovery rate also aids in producing a product stream of marketable purity, that is likely to be competitive within the current market environment.
- Should the size of the flash drum unit operation exceed that of the size constraints related to the costing equations, the flash drum is broken down into multiple flash drum unit operations in parallel, whereby the flow rate through each individual unit operation is lowered. This employs a similar concept to that noted for the pressure-changing unit operations in Section 3.8.1.

3.9.2. Determining Vapor & Liquid Stream Compositions

The design of a flash drum is comprised of two parts, namely determining the separation achievable from the flash drum, and the physical sizing of the unit operation. The separation achieved within the flash drum unit operation, was determined through use of the Rachford-Rice method. This method allows for the stream compositions leaving the flash drum to be determined, allowing for the efficiency of separation to also be calculated. The Rachford-Rice method is explicated in Appendix E.

For the purpose of the ASSF tool, the operating pressure of the vessel was iterated until 95% of the unreacted CO_2 gas was recovered via the vapor stream. This was set as a constraint of the flash drum to ensure that the product purity exiting in the liquid stream, be it MeOH, water or DME, is not contaminated by the unreacted CO_2.

With the stream data entering and leaving the flash drum unit operation now known, the focus was shifted to the physical sizing of the flash drum unit operation, in terms of its diameter and height. These are necessary parameters in determining the volume of the process vessel, and its subsequent cost.

3.9.3. Sizing of the Flash Drum Unit Operation

With the vapor and liquid stream compositions now known, the focus was shifted to the sizing of the flash drum unit operations. One of the most important values required in sizing the flash drum unit operation, is the empirical constant K_{drum}, which typically ranges between a value of 0.1 and 0.35. This value is dependent on the type of flash drum employed, as well as the mechanisms utilized within the flash drum unit operation to promote separation and reduce entrainment (Wankat, 2012).

According to the GPSA Engineering Data Book, vertical flash drum unit operations with a horizontal mesh pad, such as the ones designed and utilized throughout the course of the ASSF tool, have empirical constant values that are dependent on the pressure of the unit operation. Table 3.18 details the pressure ranges and associated K_{drum} values necessary in sizing flash drum unit operations.

Table 3.18: Empirical constants associated with various flash drum operating pressures (Gas Processors Suppliers Association, 2004)

Pressure of vessel	Empirical Constant (K_{drum})
0 psig	0.35
300 psig	0.33
600 psig	0.30
900 psig	0.27
1500 psig	0.21

The ASSF tool is able to systematically decide the appropriate K_{drum} value, based on the operating conditions of the flash drum being analyzed, thereby increasing the accuracy of the ASSF tool.

With this empirical constant being known, the permissible vapor velocity (μ_{perm}) was calculated by means of Equation 3.31, where ρ_L represents the density of the liquid exiting the bottom of the flash drum unit operation and ρ_v represents the density of the vapor stream exiting the top of the flash drum unit operation (Wankat, 2012).

$$\mu_{perm} = K_{drum}\sqrt{\frac{\rho_L - \rho_v}{\rho_v}} \qquad \text{(Equation 3.31)}$$

Utilizing the permissible vapor velocity, as well as the associated molar vapor flow rate (V_n), average molar mass of the vapor stream (MW_{vapor}) and vapor density (ρ_v), the cross-sectional area of the flash drum unit operation was calculated. This relationship is denoted by Equation 3.32 (Wankat, 2012).

$$A_c = \frac{V_n MW_{vapor}}{3600(\mu_{perm}\rho_v)} \qquad \text{(Equation 3.32)}$$

With the cross-sectional area of the flash drum known, the diameter of the vessel (D_f) was calculated by means of Equation 3.33 (Wankat, 2012).

$$D_f = \sqrt{\frac{4A_c}{\pi}} \qquad \text{(Equation 3.33)}$$

As a rule of thumb, the ratio of the height to the diameter of a flash drum typically lies between the ranges of 3 to 5. Therefore, the ASSF tool employs the midpoint of this typical range,

whereby a height (H_f) to diameter ratio of 4 was assumed for further design. The height of the vessel was calculated by means of Equation 3.34 (Wankat, 2012).

$$H_f = 4 \times D_f \qquad \text{(Equation 3.34)}$$

When costing flash drum unit operations, however, the vessel size required is in terms of the volume capacity of the flash drum. The volume of the flash drum unit operation was calculated by means of Equation 3.35.

$$V_{vessel} = \pi H \left(\frac{D}{2}\right)^2 \qquad \text{(Equation 3.35)}$$

3.9.4. Costing of the Flash Drum

The costing of flash drum unit operations differs slightly from the previous costing procedure reported for heat exchangers and pressure-changing unit operations. Initially, the C_p^o value was calculated by means of Equation 3.24, with A being used to represent the capacity of the process vessel in units of cubic meters (m^3). Table 3.19 details the constants and capacity range employed for Equation 3.24.

Table 3.19: Constants associated with process vessels for Equation 3.24 (Turton, et al., 2009)

Orientation	K_1	K_2	K_3	Min Volume (m^3)	Max Volume (m^3)
Horizontal	3.5565	0.3776	0.0903	0.1	628
Vertical	3.4974	0.4485	0.1074	0.3	520

Once the C_p^o value has been calculated the focus can then be shifted to the pressure factor (F_p) that is associated with the process vessel. This was calculated using Equation 3.36, utilizing the diameter of the vessel (D_f) and its operating pressure (P_{vessel}).

$$F_{p,vessel} = \frac{\frac{(P_{vessel} + 1)D_f}{2[850 - 0.6(P_{vessel} + 1)]} + 0.00315}{0.0063} \qquad \text{(Equation 3.36)}$$

It is important to note, however, that Equation 3.36 only holds true when the thickness of the vessel is greater than 0.0063 meters (developed by Turton, *et al*. (2009)), as noted in the

denominator of the aforementioned equation. Furthermore, Equation 3.36 was derived with the following considerations (Turton, *et al*., 2009):

- A maximum stress of carbon steel of 944 bar.
- A weld efficiency of 0.9.
- The corrosion allowance of 0.00315 meters or 1/8 inch.

Should the pressure factor of the vessel be less than one, this would imply that the thickness of the vessel is less than the aforementioned thickness constraint of 0.0063 meters. As a result, a default value of $F_{p,vessel}$ equal to 1 was utilized during the costing of these process vessels. Additionally, for an operating pressure less than 0.5 barg, $F_{p,vessel}$ was noted as 1.25 (Turton, *et al*., 2009).

Equation 3.36 is additionally constrained with the diameter of the vessel, with this equation only being applicable to process vessels whose diameter ranges between 0.3 meters and 4 meters, with a maximum operating pressure of 320 barg (Turton, *et al*., 2009).

Having calculated the pressure factor associated with the process vessel, the material factor was then extracted from Table 3.20, accounting for the material of construction within the cost of the flash drum unit operation.

Table 3.20: Material factors associated with the costing of process vessels (Turton, et al., 2009)

Unit Operation	Material of Construction	Material Factor (F_M)
Process Vessel (Horizontal & Vertical)	Carbon Steel	1
	Stainless Steel Clad	1.7
	Stainless Steel	3.1
	Nickel Alloy Clad	3.6
	Nickel Alloy	7.1
	Titanium Clad	5.7
	Titanium	9.4

In order to calculate the bare module cost of the process vessel, the associated bare module cost constants are required. These constants are highlighted in Table 3.21 and utilized in conjunction with Equation 3.26.

Table 3.21: Bare module cost constants for costing process vessels (Turton, et al., 2009)

Orientation	B_1	B_2
Horizontal	1.49	1.52
Vertical	2.25	1.82

As with the previous costing procedures explicated, this bare module cost relates the process vessel cost to that of September 2001. Therefore, through the use of the appropriate CEPCI value, inflation can be taken into account, providing an estimated cost of the unit operation at the time the ASSF tool is being utilized. Both horizontal and vertical flash drums were considered within the ASSF tool, with the cheapest unit operation being selected for the process design. Appendix D9 contains a diagrammatic representation of the ASSF tool segment focused on the sizing and costing of flash drum unit operations.

3.10. Distillation Columns

Distillation columns are separation unit operations that are able to achieve greater recovery rates than that which is possible through the use of a flash drum unit operation. As a result, these unit operations are especially integral in developing high purity product streams capable of commercialization (Bamatov & Bamatov, 2020). The internal trays within a distillation column, coupled with the reboiler and condenser heat exchangers, promotes the separation process (Spreight, 2020). Distillation columns are commonly utilized in separating mixtures that have close boiling points.

This section deals with the assumptions, design and costing of the distillation columns utilized throughout the course of the ASSF tool. Appendix D10 provides a flow chart representation of the segment within the ASSF tool that deals with these unit operations.

3.10.1. Distillation Column Assumptions

In bridging the gap between the known and unknown data required for the design and costing of distillation columns at a preliminary design level, the following assumptions were made during the development of the ASSF tool:

- The pressure drop across the length of the distillation column is negligible.
- The pressure of the streams exiting the distillation column do so at the operating pressure of the distillation column.
- The size of the trays utilized in the costing of the unit operations is equal to that of the tower cross sectional area, thereby providing a worst case-scenario costing for the trays.
- Should the tower capacity or tray area be below the lower costing constraint, the lower limit is utilized in the costing procedure, once again accounting for a worst-case scenario option.

The advantage of considering a worst-case scenario when costing unit operations, is that should a case study be deemed to be feasible under these conditions, the practical application of the scenario would be subject to additional economic benefits/merits.

3.10.2. Design & Sizing of Distillation Column Unit Operation

During the operation of a distillation column, the light key chemical species exits the unit operation via the top of the tower, becoming known as the distillate stream. The heavy key chemical species, that which exhibits a higher density, exits the distillation column via the bottom stream.

The distillate stream contains a condenser unit operation, whereby a portion of the vapor stream is partially condensed and fed back into the distillation column via a reflux stream. This aids in promoting the separation within the distillation column. In order to facilitate this partial condensation, the distillate stream is cooled to the dew point temperature. This is the point at which the vapor stream begins to condense, forming a saturated vapor. The dew point temperature was calculated by means of Equation 3.37, where y_i denotes the composition of component i in the vapor phase, x_i denotes the composition of component i in the liquid stream, and K_i denotes the equilibrium constant (Towler & Sinnott, 2008).

$$\sum x_i = \sum \frac{y_i}{K_i} = 1 \qquad \text{(Equation 3.37)}$$

The reboiler unit operation partially vaporizes the bottom liquid stream, bringing the temperature to the bubble point, i.e., the temperature at which the first vapor bubble of vapor begins to form. The bubble point temperature was calculated by means of Equation 3.38.

$$\sum y_i = \sum K_i x_i = 1 \qquad \text{(Equation 3.38)}$$

The design of a distillation column can be completed through one of two approaches, namely a graphical approach or an analytical approach. Due to the nature of the ASSF tool being computational, the analytical approach was chosen as the preferred design route.

The quality of the feed to the distillation column (q) is defined as the fraction of the feed that is liquid. In order to create an appropriate feed quality, whilst calculating the feed quality to the column, the iterative Rachford-Rice procedure employed within the design of the flash drum unit operation, was utilized. The feed quality was then calculated using Equation 3.39 (Douglas, 1988).

$$q = 1 - \varphi \qquad \text{(Equation 3.39)}$$

The relative volatility of the chemical species within the feed stream, and involved in the separation, is an important constituent in the Underwood and Fenske equations, utilized in the analytical design of distillation columns. The relative volatility of any chemical species (α_i) is calculated as the ratio of the saturated vapor pressures of the constituents ($\left(P_{sat}(T)\right)_i$), relative to the heavy key component ($\left(P_{sat}(T)\right)_{HK}$). This relationship is noted in Equation 3.40 (Douglas, 1988).

$$\alpha_i = \frac{\left(P_{sat}(T)\right)_i}{\left(P_{sat}(T)\right)_{HK}} \qquad \text{(Equation 3.40)}$$

With the quality of the feed and relative volatility known, the Underwood equation was utilized to calculate for the value of θ, as per Equation 3.41 (Douglas, 1988), where z_i denotes the composition of component i in the feed stream to the distillation column and F represents the feed flow rate.

$$F(1-q) = \sum \left(\frac{\alpha_i z_i}{\alpha_i - \theta}\right) \qquad \text{(Equation 3.41)}$$

Upon iteratively solving for the value of θ, the minimum vapor flow rate (V_{min}) was calculated by means of Equation 3.42 (Douglas, 1988), where D is used to denote the flow rate of the distillate stream, and x_i denotes the composition of component i in the distillation stream.

$$V_{min} = \sum \left(\frac{\alpha_i x_i D}{\alpha_i - \theta} \right) \quad \text{(Equation 3.42)}$$

The reflux ratio is defined as the ratio of vapor flow that is returned to the distillation column, promoting the separation system (Douglas, 1988). The minimum possible reflux ratio was calculated by means of Equation 3.43, where R_{min} is used to denote the minimum reflux ratio.

$$R_{min} = \frac{V_{min}}{D} \quad \text{(Equation 3.43)}$$

A study performed in 1988 noted that an increase in reflux ratio promotes the separation process, however this also increases the number of trays required within the distillation column, and the associated capital cost thereof. Therefore, a trade-off between these two values, found that as a rule of thumb, the theoretical reflux ratio (R_{Theor}) lies between 1.2 and 1.5 times the minimum reflux ratio, as shown in Equation 3.44 (Douglas, 1988).

$$R_{Theor} = 1.2 \times R_{min} \quad \text{(Equation 3.44)}$$

The theoretical boil up ratio, i.e the portion of the bottom stream that is fed back to the distillation column, was calculated in the same manner as the theoretical reflux ratio. The only difference between these calculations lies in the utilization of the bottoms stream and its associated compositions, as opposed to the use of the distillate stream, as seen in the Underwood equation.

With the theoretical reflux and boil up ratio now known; the focus was shifted to calculating the number of stages/trays within the distillation column. The minimum number of stages within the distillation column (N_{min}) followed the Fenske equation, represented by Equation 3.45 (Wankat, 2011). This equation utilizes the molar compositions of components A and B in the distillate and bottom stream (x_A and x_B), as well as their relative volatilities (α_{AB}).

$$N_{min} = \frac{\ln\left(\frac{\left(\frac{x_A}{x_B}\right)_{Dist}}{\left(\frac{x_A}{x_B}\right)_{Bottom}} \right)}{\ln(\alpha_{AB})} \quad \text{(Equation 3.45)}$$

The actual number of trays (N_{Actual}) required in the distillation column is dependent on the efficiency of each tray, calculated by means of Equation 3.46 and Equation 3.47 (Douglas, 1988), where the tray efficiency (E_o) is dependent on the relative volatility of the light key component (α_{LK}).

$$E_o = \frac{0.5}{(0.3\alpha_{LK})^{0.25}} \qquad \text{(Equation 3.46)}$$

$$N_{Actual} = \frac{N_{min}}{E_o} \qquad \text{(Equation 3.47)}$$

When calculating the height of the distillation column, the tray spacing was required. As a rule of thumb, the spacing between distillation column trays is approximately 2 ft, equating to 0.6096 meters. In addition to this height, common practice employs a spacing above and below the trays. This allows for vapor-liquid disengaging space to be created at the top of the unit operation, and a liquid slump to be created at the bottom. Typically, this excess space accounts for roughly 15% of the minimum required height on either side, as shown by Equation 3.48 (Douglas, 1988).

$$H_D = \frac{2.3N_{Actual}}{E_o} \qquad \text{(Equation 3.48)}$$

With the height of the distillation column known, the only outstanding parameter required in calculating the tower volume capacity is the diameter of the vessel. The maximum allowable superficial vapor velocity (u_v) was calculated by means of the Souders and Brown equation, represented by Equation 3.49 (Towler & Sinnott, 2008). This equation makes use of the plate spacing (l_t), as well as the liquid and vapor density (ρ_L and ρ_v, respectively).

$$u_v = (-0.171l_t^2 + 0.27l_t - 0.047)\left(\frac{\rho_L - \rho_v}{\rho_v}\right)^{0.5} \qquad \text{(Equation 3.49)}$$

The diameter of the column and its associated trays can then be calculated by means of Equation 3.50 (Towler & Sinnott, 2008), D_c denotes the diameter of the column in meters, and V_w denotes the maximum vapor flow rate in units of kilograms per second.

$$D_c = \sqrt{\frac{4V_w}{\pi\rho_v u_v}} \qquad \text{(Equation 3.50)}$$

The design of the condenser and reboiler heat exchanger unit operations were sized and costed utilizing the same procedure as that demonstrated in Section 3.7.

3.10.3. Costing of Distillation Column Unit Operation (Tower)

The costing of the tower required for distillation columns follows an identical costing procedure to that noted in Section 3.9.4, with the only difference being the constants and size range associated with Equation 3.24, and the constants associated with the bare module cost. The constants necessary with Equation 3.24 are denoted in Table 3.22.

Table 3.22: Constants associated with distillation column towers for Equation 3.24 (Turton, et al., 2009)

Orientation	K_1	K_2	K_3	Min Volume (m^3)	Max Volume (m^3)
Tray and packed	3.4974	0.4485	0.1074	0.3	520

The constants necessary to calculate the bare module costs of the tower required for a distillation column is given in Table 3.23.

Table 3.23: Bare module cost constants for costing towers (Turton, et al., 2009)

Orientation	B_1	B_2
Tray and packed	2.25	1.82

3.10.4. Costing of Distillation Column Trays

The internal configuration of a distillation column is made up of trays. The costing of these trays follows a marginally different costing procedure as that detailed for the previous unit operations. The C_p^o is calculated by means of Equation 3.24, where A is used to represent the size of the trays in square meters (m^2). The constants and ranges utilized in this equation are detailed in Table 3.24.

Table 3.24: Constants associated with costing trays for Equation 3.24 (Turton, et al., 2009)

Type	K_1	K_2	K_3	Min Area (m^2)	Max Area (m^2)
Sieve	2.9949	0.4465	0.3961	0.07	12.30
Valve	3.3322	0.4838	0.3434	0.70	10.50
Demisters	3.2353	0.4838	0.3434	0.70	10.50

After calculating the C_p^o value, the quantity factor (F_q) was calculated. This factor is dependent on the number of trays within the distillation column (N) and is denoted by Equation 3.51.

$$\log_{10}F_q = 0.4771 + 0.08516\log_{10}(N) - 0.3473[\log_{10}(N)]^2 \qquad \text{(Equaiton 3.51)}$$

This equation, however, is limited to cases where the number of trays is less than 20 (N < 20). For cases where the number of trays is equal to or greater than 20, the quantity factor is set at a value of 1.

Now that the quantity factor has been calculated, the bare module material factors (F_{BM}) can be considered. Table 3.25 details the possible materials of construction for the trays, as well as their respective bare module material factors.

Table 3.25: Bare module material factors for trays based on the material of construction (Turton, et al., 2009)

Type of Tray	Material of Construction	Bare Module Material Factor
Sieve and Valve	Carbon Steel	1
Sieve and Valve	Stainless Steel	1.8
Sieve and Valve	Nickel Alloy	5.6
Demister Pad	Stainless Steel	1
Demister Pad	Fluorocarbon	1.8
Demister Pad	Nickel Alloy	5.6

The bare module cost of the trays within the distillation column, was then calculated by means of Equation 3.52.

$$C_{BM} = C_p^o N F_{BM} F_q \qquad \text{(Equation 3.52)}$$

As with all other unit operations costed over the course of the ASSF tool and its respective case study analysis, the bare module cost of the trays was calculated as per September 2001, and therefore, through the use of the CEPCI value at the time of operating the ASSF tool, inflation in the unit operation cost can be accounted for.

Appendix D10 provides a flow chart representation of the code associated with the design and costing of the distillation columns required within the chemical plant.

3.11. The Separation of CO_2/DME

One of the major concerns noted over the course of developing the ASSF tool was the dissolution of CO_2 in the DME/MeOH streams, thereby reducing product purity and recovery. Repeated separation systems, including flash drums and distillation columns, were noted to increase the cost substantially, with minimal gain to the product recovery. Much of the product was noted to be removed from the process via a waste purge stream, thereby necessitating a separate system focusing primarily on the separation of CO_2 from DME/MeOH.

In order to address this issue, CaO was introduced into the plant system, providing a CO_2 capturing mechanism. By feeding the CO_2 laden stream to a reactor, in the presence of CaO, the CO_2 undergoes a reaction process, producing $CaCO_3$. This chemical reaction is denoted by means of Equation 3.53.

$$CaO + CO_2 \leftrightarrow CaCO_3 \qquad \text{(Equation 3.53)}$$

Previous experimentation into the utilization of CaO as a carbon capture mechanism has noted removal rates as high as 90% (Geimer, 2014). Furthermore, the $CaCO_3$ being formed within this process provides an additional product stream for the chemical plant in question, allowing for an additional commercial benefit. As a result, this can drastically improve the economic feasibility of processes focused on the production of DME.

Through the carbonation of CaO, the $CaCO_3$ product being formed exists in the solid phase, thereby facilitating simple separation, with the exit stream to the process being severely decreased in its CO_2 composition. For this reaction to proceed, the reactor experiences an operating temperature of 650^{o}C, with the partial pressure of CO_2 being approximately 0.15 bar (Oritz, *et al*., 2018).

Based on these operating conditions, the carbonation reactor was placed before the separation of water, lowering the partial pressure of CO_2 to within the range necessary for the aforementioned carbon capture process to be facilitated.

3.12. Reactor Unit Operations

As mentioned previously, the ASSF tool did not focus on the design of the reactor unit operation, as the RPD does not have a provision for reaction kinetics. Instead, the ASSF tool utilizes the conversion and selectivity of the reactions noted within previous experimental work.

However, when determining the molar and mass flow exiting the reactor unit operation, the possibility of a limiting reagent must be taken into account, as this would affect the potential conversion of the reactants within the predefined reactive system. Appendix D11 provides a diagrammatic flow chart representation of the ASSF tool segment dealing with the reactor unit operations.

3.13. Case Study Calculations

Based on all of the data calculated over the course of the designed process within the ASSF tool, additional equations were required in order to complete the analysis of the case study and its subsequent comparison with the other potential reaction pathway combinations. One of the most important factors considered when constructing any chemical plant, is the capital investment required. Therefore, the total capital cost required for each chemical plant is denoted as the summation of the cost of all unit operations previously calculated. This is represented by Equation 3.54 through to Equation 3.57.

$$HX_{Total} = \sum_{i_{HX}=1}^{n_{HX}} C_{i_{HX}} \quad \text{(Equation 3.54)}$$

$$PC_{Total} = \sum_{j_{PC}=1}^{n_{PC}} C_{j_{PC}} + \sum_{j_d=1}^{n_d} C_{j_d} \quad \text{(Equation 3.55)}$$

$$S_{Total} = \sum_{k_{PV}=1}^{n_{PV}} C_{k_{PV}} + \sum_{k_T=1}^{n_T} C_{k_T} + \sum_{k_{Tr}=1}^{n_{Tr}} C_{k_{Tr}} \quad \text{(Equation 3.56)}$$

$$C_{Total} = HX_{Total} + PC_{Total} + S_{Total} \quad \text{(Equation 3.57)}$$

Equation 3.54 shows that the total cost of the heat exchangers (HX_{Total}) utilized in any chemical plant as the sum of the cost of each individual heat exchanger ($C_{i_{HX}}$). Equation 3.85 shows that the total cost of pressure changing unit operations (PC_{Total}) is comprised of the cost of all the pressure changing unit operations throughout the process ($C_{j_{PC}}$), as well as the associated drivers required for each unit operation (C_{j_d}).

Equation 3.56 employs the same principle with separation systems, with the total cost of the separation system (S_{Total}) being calculated as the summation of the cost of process vessels ($C_{k_{PV}}$), the cost of distillation towers (C_{k_T}) and the cost of trays required within the distillation columns ($C_{k_{Tr}}$). Equation 3.57 states the total capital investment required at this preliminary stage, is calculated by summing all of the unit operation costs calculated by means of the previous three equations.

The total energy required by the process (E_{Total}) was determined through the summation of its constituents, namely the heat energy (Q) and the work done by/on the process (W), as denoted by Equation 3.58. This equation highlights that the total work and heat required or released from the process, is calculated as a summation of the energy requirements of all unit operations throughout the process.

$$E_{Total} = \sum_{a=1}^{n} Q_a + \sum_{b=1}^{m} W_b \qquad \text{(Equation 3.58)}$$

The total cost of reactants required in the process (C_R) was calculated as the summation of the mass flow of the feed stream (m_R) and its associated unit cost (UC_R), as denoted by Equation 3.59. The sales potential of the products within the process (SP_P), was also calculated in a similar manner, accounting for the mass flow rate of the product streams (m_P) and the potential selling price of the product (USP_P). This relationship is denoted by Equation 3.60. It is important to note that the sales potential of the product must align with and be competitive with current market values of the product, thereby promoting its sale.

$$C_R = \sum_{c=1}^{r} m_R UC_R \qquad \text{(Equation 3.59)}$$

$$SP_P = \sum_{d=1}^{s} m_P USP_P \qquad \text{(Equation 3.60)}$$

3.14. Search Space Reduction Criteria

Upon analyzing and designing all possible case studies/reaction pathway combinations, the process data is tabulated for subsequent comparisons. These comparisons look at each of the case studies from an economic and environmental standpoint, eliminating those deemed to be infeasible from the search space. The purpose of this reduction criteria is that it allows the ASSF tool to reduce the search space to an extent that is manageable for further consideration, with the final search space only containing those pathways deemed to have both economic and environmental merit.

This section highlights three search space reduction criteria utilized within the ASSF tool. A fourth criterion was used as a ranking system, allowing the final search space to be ranked in order of feasibility, guiding the user as to which pathways are likely to exhibit the greatest chance for success and implementation.

3.14.1. Criteria #1 – Economic Feasibility

The first criterion looks at each process from an economic standpoint, considering the input/output structure of the case studies. This criterion is placed first in the search space reduction, as process profitability is arguably the most important factor in any plant development. Inevitably, the design of any process is a business venture, and in order to promote investment, the venture must exhibit a profitable status.

For this criterion, the basic annual profit of the chemical plant is calculated, taking into account the cost of the reactants (C_R) and the sales potential of the products being produced within the plant (SP_P). This relationship is denoted by Equation 3.61.

$$\text{Profit} = SP_P - C_R \qquad \text{(Equation 3.61)}$$

At first, this profit consideration appears to be a simple criterion, however the complexity of this profit calculation becomes evident when dissecting each of the associated terms. The sales potential of the product accounts for the purity of the stream, with varying purities affecting the sales potential of the product within an already competitive market. Furthermore, this sales potential value encompasses possible product losses within the product, during the various

separation stages. As a result, this criterion ensures that the efficacy of the separation systems is also considered within the ASSF tool. Therefore, the sales potential value, within the profit calculation, considers only the marketable product stream.

The cost of the reactants necessary, namely CO_2 and H_2, can be used as a means by which to incorporate CO_2 scrubbing to obtain a pure CO_2 feed stream, or even the cost of producing H_2 gas, potentially using electrolysis unit operations.

It is important to note however, that this criterion considered annual potential profit, before accounting for other operational costs that may be incurred, such as labor and plant maintenance.

Based on this criterion, any case study that exhibits a negative profit value, i.e., a loss, is excluded from the search space. The resulting search space then contains only those reactive systems that exhibit a degree of financial feasibility.

3.14.2. Criterion #2 – Environmental Benefit

The second search space reduction criterion looks at the remaining case studies from an environmental perspective, specifically focusing on the effect that the process has on atmospheric CO_2 levels. Whilst economic gains are often considered to be the driving force of any business venture, equal attention should be paid to the environmental impact thereof, as this determines the potential of the business to promote sustainable development.

Rising atmospheric CO_2 levels is a major concern that has led to increased environmental concerns, including climate change. There are numerous green sources of energy that can be utilized in meeting the energy requirements of a chemical plant, however the concern with these sources lies in their intermittent and fluctuating nature (Azarpour, *et al*., 2013). For example, wind turbines require constant wind energy, and energy supply can be decreased substantially with varying weather conditions. This is not ideal for stable operation of a chemical plant.

As a result, the ASSF tool utilized natural gas as the primary means by which the energy requirements of the process are met. The provision of this energy source within the ASSF tool, allows for the chemical plant's energy costs to be taken into account, whilst reducing the strain

placed on the current electricity grid. Assuming that natural gas is comprised primarily of methane gas, the combustion of natural gas can be represented by Equation 3.62.

$$CH_4 + 2O_2 \leftrightarrow CO_2 + 2H_2O \qquad \text{(Equation 3.62)}$$

Unfortunately, this combustion shows that CO_2 is produced during this process, whereas the purpose of the ASSF tool is to utilize and reduce current atmospheric CO_2 levels. Therefore, in order for a case study to remain environmentally viable, the process has to take in more CO_2 than it emits, thereby still posing an overall environmental benefit. The net atmospheric CO_2 reduction (ATM_{CO2}) was calculated by means of Equation 3.63, taking into account unreacted CO_2 (UNR_{CO2}), the CO_2 produced during the combustion of methane ($COMBUST_{CO2}$) and the CO_2 taken in by the process (IN_{CO2}).

$$ATM_{CO2} = UNR_{CO2} + COMBUST_{CO2} - IN_{CO2} \qquad \text{(Equation 3.63)}$$

Based on Equation 3.63, in order for a case study to be considered environmentally beneficial, the net atmospheric CO_2 should be negative, implying that the process is taking in more CO_2 than it is emitting. Therefore, any case study exhibiting a positive value as per Equation 3.63, is immediately removed from the search space as being environmentally infeasible.

Not only can this be considered an environmental benefit, but the utilization of natural gas can also be viewed as an economic benefit. At steady state operation of the chemical process, the CO_2 produced via the aforementioned combustion process, can be recycled to the feed stream. This would reduce atmospheric emissions, whilst simultaneously reducing the amount of fresh CO_2 feed required for the process, ultimately reducing the cost of reactants. A reduction in reactant cost increases the annual profit associated with the case study.

The amount of natural gas required to meet the energy requirements of the process (m_{NG}), was calculated via Equation 3.64, taking into account the total energy of the process (E_{Total}) and the calorific value of natural gas (CV_{NG}).

$$m_{NG} = \frac{E_{Total}}{CV_{NG}} \qquad \text{(Equation 3.64)}$$

The amount of CO_2 produced through this combustion process ($m_{CO2,produced}$), was calculated by Equation 3.65, taking into account the molecular weights of methane (M_{CH4}) and CO_2 (M_{CO2}).

$$m_{CO2,produced} = \frac{m_{NG}}{M_{CH4}} \times M_{CO2} \quad \text{(Equation 3.65)}$$

As natural gas is constantly required to keep the plant operational, this was accounted for within the annual profit calculation by means of Equation 3.66, where the adjusted annual profit (Adj Profit) considers the annual cost of natural gas denoted by C_{NG}.

$$\text{Adj Profit} = SP_P - C_R - C_{NG} \quad \text{(Equation 3.66)}$$

3.14.3. Criterion #3 – Payback period

The final search space reduction criterion considers a simplified version of the payback period of the plant. In developing a chemical plant, capital investment is required. This capital is often obtained via potential investors, however, in order for an investor to show interest in a chemical plant, the economic benefit to them must be clearly highlighted. This benefit is presented to investors as the return on investment (ROI) indicator, indicating the time period and percentage profit they are expected to see on their investment.

The chemical plants considered throughout the course of the ASSF tool can be considered within the region of medium to large scale production plants, and ideally should be paid off within 2 to 10 years (Lean Manufacturing & Operations Management, 2019). Therefore, the third criterion reduces the search space, by employing this payback period constraint to each of the case studies. The payback period (PBP) calculated was achieved by means of Equation 3.67, whereby total unit operation cost (Equation 3.83) is divided by the adjusted annual profit (Equation 3.66).

$$PBP = \frac{C_{Total}}{\text{Adj Profit}} \quad \text{(Equation 3.67)}$$

It is important to note, that this payback period calculation is a simplified version, not accounting for labor costs, maintenance, land expenditure and so forth. This calculation simply provides a preliminary payback period, ensuring that case studies exhibiting exorbitant payback periods are eliminated from the search space.

3.14.4. Criterion #4 – Ranking the Final Reduced Search Space

After employing the previous three search space reduction criteria, the final reduced search space contains only those reaction pathways that exhibit both economic and environmental merit. At this stage, it is necessary that the user of the ASSF tool be guided as to the pathways that have the greatest likelihood for success and implementation, allowing design resources to be prioritized accordingly.

Therefore, a performance index (PI) was utilized to rank the remaining case studies in order of feasibility. Unfortunately, an increase in environmental benefit is met with increased capital costs, thereby reducing the economic feasibility of the process. As a result, it is imperative that a compromise, or draw-off, be found between these two parameters. Equation 3.68 shows a ratio between these factors, with OC_{Annual} being used to represent the annualized operating costs of the process. This annualized operating cost was denoted by the annualized capital cost (ACC), and the annual feed cost to the process, including the cost of the reactants and natural gas utility. This relationship is denoted by means of Equation 3.69.

$$PI = \frac{|ATM_{CO2}|}{OC_{Annual}} \qquad \text{(Equation 3.68)}$$

$$OC_{Annual} = C_R + C_{NG} + ACC \qquad \text{(Equation 3.69)}$$

As per Equation 3.68, a higher performance index is indicative of a greater environmental benefit (where ATM_{CO2} is an indication of the net atmospheric CO_2 reduction), or lower operating costs. This objective function was utilized within the ASSF tool as the search function in MATLAB ®, ranking the final search space from the highest performance index to the lowest potential performance index.

In order to calculate the annualized capital costs, a capital budgeting tool was utilized and coded within the ASSF tool. This added tool normalized the cost of the unit operations required, considering a duration of 1 year, and account for potential interest rates during the payback period.

Equation 3.70 calculates the capital recovery factor (CRF) necessary in determining the annualized capital costs, utilizing the annual discount rate (r) and the lifespan of the chemical plant (n_l). The annualized capital cost was then calculated by means of Equation 3.71.

$$\mathrm{CRF} = \frac{\mathrm{r}}{1 - (1 + \mathrm{r})^{-\mathrm{n_l}}} \qquad \text{(Equation 3.70)}$$

$$\mathrm{ACC} = \mathrm{CRF} \times \mathrm{C_{Total}} \qquad \text{(Equation 3.71)}$$

The ASSF tool requests the annual discount rate and lifespan of the plant from the user, as these values tend to fluctuate depending on the country's economic standing and the desired lifespan of the plant, respectively.

Chapter 4: Results and Discussion - Validation and Verification of the ASSF Tool

An integral component in the development and implementation of any tool, relates to both its accuracy and efficacy. The integrity of the ASSF tool was validated using two existing case studies. This also highlights the accuracy of the results obtained using the ASSF tool, with limited information being available at the onset. This process allows for the model to be verified, whilst simultaneously determining its associated limitations.

Additionally, the validation process highlights one of the applications of the ASSF tool, which encompasses quick simulations of chemical plants prior to its construction or any design procedures.

The third validation of the ASSF tool is provided in Chapter 5 (Section 5.2.2), where the ASSF tool was utilized in conjunction with an already developed RPD. This database was developed and reduced by Jugmohan, *et al*. (2020), using a manual procedure coupled with various software platforms, including P-Graph Studio ® and Aspen Plus ®. This application served to verify and validate the ASSF tool model in relation to an established framework making use of reputable chemical engineering software platforms, as well as demonstrate the usefulness of the ASSF tool in reaction pathway search space reduction, resulting in a smaller final reaction pathway search space in a fraction of the time previously required. This is a major development in enhancing the productivity and allocation of design resources during the initial design stages.

4.1. Case Study 1 – Methanol Production Plant (W-EcoMP tool)

An investigation conducted by Bellotti, *et al*. (2019) focused on the techno-economic assessment of a MeOH production plant, centered on the direct hydrogenation of CO_2. This reactive system is represented by Equation 4.1.

$$CO_2 + 3H_2 \leftrightarrow CH_3OH + H_2O \qquad \text{(Equation 4.1)}$$

The feed streams to this system were CO_2, obtained as the waste stream of a fossil-fuel power station, and H_2 gas, produced via a proton exchange membrane (PEM) electrolyzer (Bellotti,

et al., 2019). Electrolysis is the process whereby water molecules are separated into its oxygen and H_2 constituents, via an electric current.

The aforementioned investigation looked at the possibility of constructing a MeOH-producing chemical plant in different geographical regions, namely China, Germany and Italy. Each assessment accounted for varying economic conditions within each proposed region. Figure 4.1 provides a diagrammatic representation of the proposed chemical plant evaluated within the aforementioned techno-economic assessment.

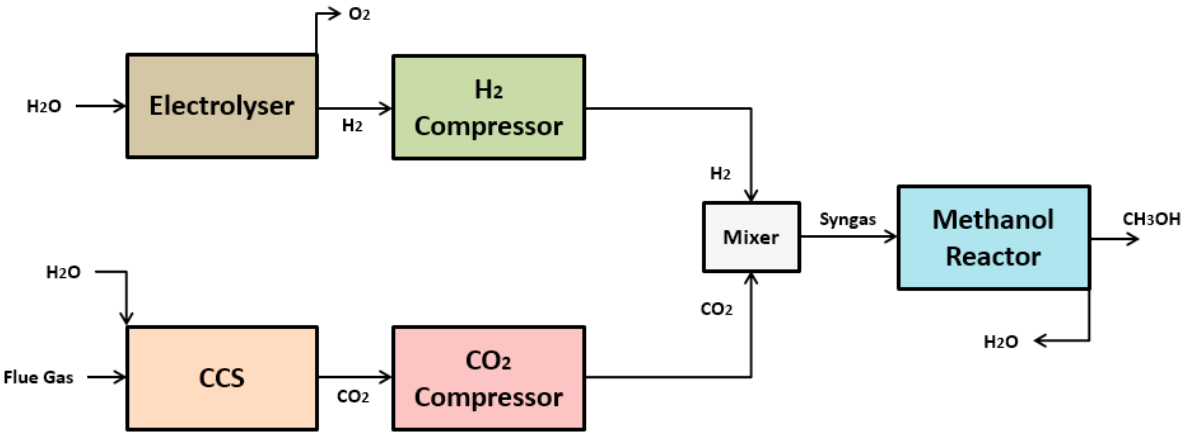

Figure 4.1: Process diagram of the chemical plant utilized by Bellotti, et al. (2019)

Figure 4.1 highlights the boundary of the chemical plant utilized by Bellotti, *et al*. (2019). This plant structure encompasses the unit operations that are responsible in producing the relevant feed streams, namely the electrolyzer for H_2 production and the carbon capture system (CCS) for CO_2 feed. However, this representation does not encompass the separation system required after the reactor. Separation systems are often considered to be an integral part of any chemical process, with the focus of these systems being to remove unreacted gases, and potential byproducts, from the desired product stream.

Table 4.1 highlights the MeOH production operating conditions utilized within this investigation, as was determined by Bellotti, *et al*. (2017).

Table 4.1: Operating conditions associated with the MeOH plant (Bellotti, et al., 2017)

Specification	Value
H_2 : CO_2 Feed Ratio	3 : 1
Operating Pressure	80 bar
Operating Temperature	240^oC
Conversion of CO_2	95.31%
Pressure-Changing Unit Operation Efficiency	86%

The 'Germany scenario' was utilized within the ASSF tool, where the energy cost was recorded as being €33.31/MWh. The choice of the region for this comparison was based on utilizing a region with intermediary energy costs. China was noted to have the cheapest energy costs in the investigation conducted by Bellotti, *et al*. (2019), with energy costing €10/MWh. Italy, on the other hand, noted excessively high energy costs, amounting to €53.95/MWh. Therefore, with Germany exhibiting an energy cost between these two extremes, this was chosen as the scenario to utilize within the ASSF tool when validating the model.

In addition to the reactive system and its associated operating conditions presented in Equation 4.1 and Table 4.1, respectively, Table 4.2 details the input data required for the operation of the ASSF tool.

Table 4.2: Input data required for the operation of the ASSF tool

Factor Input	Value	Units	Reference
Excess H_2 Feed	0	%	(Bellotti, *et al*., 2019)
Pressure-Changing Efficiency	86	%	(Bellotti, *et al*., 2019)
CEPCI (2018)	603.1	n/a	(Viswanathan, *et al*., 2020)
Pressure of HE Utility	3	bar	n/a (User input)
Steam Temp Change	50	Kelvin	n/a (User input)
Cooling Water Temp Change	20	Kelvin	n/a (User input)
Cost of CO_2	0.06	$/kg	(Schmelz, *et al*., 2020)
Cost of H_2	1.25	$/kg	(Dagdougui, *et al*., 2018)
Cost of Electricity	40.56	$/MWh	(Bellotti, *et al*., 2019)
Sales Potential of MeOH	0.53	$/kg	(Bellotti, *et al*., 2019)
Distillation Recovery	99.99	%	n/a (User input)

Table 4.3 provides a summarized list of the data obtained when analysing this reactive system within the ASSF tool. In addition to the ASSF tool results, this table also contains the data determined by Bellotti, *et al*. (2019) as per their techno-economic assessment.

Table 4.3: Data comparison between Bellotti, et al. (2019) and ASSF tool

Quantity	Bellotti, *et al*. (2019)	ASSF Tool
MeOH Production Cost	$ 515.27/ton *	$ 168.95/ton
Feed Compression Energy Requirement	1.44 MW	1.52 MW
Capital Cost (MeOH production only)	$ 3.601 million	$ 4.075 million
Payback Period	6 years *	1.57 years

* Including electrolyzer unit operation

Upon initial inspection, the difference in data between that obtained by Bellotti, *et al*. (2019) and the ASSF tool appears to be quite substantial. This is seen when considering the MeOH production cost and payback period. However, the differences between these two analyses must be taken into account in order to adjust the necessary values and make comparisons based on equal footing. The paragraphs to follow will detail the differences noted within the research study conducted by Bellotti, *et al.* (2019) and that of the ASSF tool, providing changes that can be employed to compare these two scenarios on equal footing. The accurate comparison of these two systems is then provided in Table 4.4, having taken into account these necessary adjustments.

The first major difference between the work conducted by Bellotti, *et al*. (2019) and the ASSF tool, is the production of H_2 gas. Bellotti, *et al*. (2019) conduced the techno-economic assessment, whereby the production of H_2 via a PEM electrolyzer, was considered within the analysis scope of the chemical plant. The capital cost necessary to produce this H_2 accounted for approximately 76% of the total capital cost. The PEM electrolyzer was the most expensive unit operation within the aforementioned assessment.

However, the ASSF tool does not consider the cost of the electrolyzer within its analysis scope, with the only consideration made being the cost of raw materials needed. The scope of the ASSF tool looks at the design and analysis of a chemical plant under the assumptions that the feed streams are readily available and are of sufficient purity to not affect subsequent process stages.

The addition of the electrolyzer unit operation had a major impact on the MeOH production cost per tonnage, as well as the associated payback period, increasing the capital cost of the plant in its entirety. It is important to note, however, that the capital cost reported in Table 4.3, for the investigation conducted by Bellotti, *et al*. (2019), encompasses only the unit operations responsible for the production of MeOH, and excludes the CCS and electrolyzer unit operation.

Another difference in the work conducted by Bellotti, *et al*. (2019) and the ASSF tool, is seen in the feed conditions. As mentioned previously, the techno-economic assessment made use of H_2 produced from an electrolyzer unit operation, which resulted in elevated feed pressures to the process. Bellotti, *et al*. (2019) noted an input H_2 pressure of 30 bar. This resulted in a reduction to the amount of work required for subsequent compressor systems, which was focused on achieving the desired reaction pressure, i.e., 80 bar.

The ASSF tool, on the other hand, assumes that all feed streams enter the process at ambient conditions of 1 atm (1.01325 bar) and 25^{o}C. Subsequent stages in the ASSF tool encompasses a heat exchanger and pressure changing unit operation system that is focused on achieving desired reaction conditions. This was chosen as the basis feed conditions for the ASSF tool as it allows for subsequent analyses to be conducted using a worst-case scenario perspective. This ensures that should a case study exhibit feasibility under these conditions, elevated feed stream conditions would only enhance this feasibility.

One of the prominent differences between the previously mentioned investigation and the ASSF tool, lies in the extent or boundaries of the chemical plant developed. The investigation conducted by Bellotti, *et al*. (2019) considers the process until the reactor unit operation, using the effluent of the reactor as the product stream. This, however, is not accurate as the reactor effluent contains unreacted gases and a water by-product that must be separated before achieving a commercial product.

The ASSF tool, however, does account for a separation system, factoring in the necessary post reactor unit operations required in achieving a marketable product. Therefore, with regards to the end usability of the product, the ASSF tool does go further than the techno-economic assessment considered by Bellotti, *et al*. (2019).

By making necessary adjustments, the aforementioned investigation and the ASSF tool can be brought to the same foundation, promoting effective comparisons. This involved two reductions, with the first being in the investigation conducted by Bellotti, *et al*. (2019) and the second being in the ASSF tool. These adjustments were as follows:

- The removal of the electrolyzer unit operation from the techno-economic assessment results, which accounted for 76% of the total capital cost of the plant.
- The removal of the separation system from the ASSF tool.

Table 4.4 presents the comparison of the adjusted results.

Table 4.4: Adjusted data comparison between Bellotti, et al. (2019) and ASSF tool

Quantity	Bellotti, *et al*. (2019)	ASSF Tool
MeOH Production Cost	$ 123.66/ton	$ 141.85
Feed Compression Energy Requirement	1.44 MW	1.52 MW
Capital Cost (MeOH production only)	$ 3.601 million	$ 3.424 million
Payback Period	1.44 years	1.31 years

After adjusting these analyses through the removal of the electrolyzer and the separation system, from the techno-economic assessment by Bellotti, *et al*. (2019) and the ASSF tool, respectively, the results show many similarities. Table 4.5 details the percentage deviations noted between the ASSF tool, and the case study analysis conducted by Bellotti, *et al*. (2019).

Table 4.5: Percentage deviations noted between the results of Bellotti, et al. (2019) and ASSF tool

Factor	Deviation
Capital Cost (MeOH production only)	4.8 %
Feed Compression Energy Requirement	5.5 %

As seen in Table 4.5, by utilizing the same basic process structure, the difference in capital cost between the scenarios is just 4.8%. Furthermore, a 5.5% difference in the compression requirements were noted between the techno-economic assessment and the ASSF tool. This difference, however, has been explicated previously, with the change in compression requirements being attributed to varying feed conditions.

It is important to note that in designing these chemical plants, with their subsequent analyses, the ASSF tool utilizes a preliminary design procedure. Preliminary designs have an accuracy level of -25% to +30% of the actual cost involved (Van Amsterdam, *et al*., 2018), (Towler & Sinnott, 2012). As seen by the previous financial indicators reported, both exhibit an economic discrepancy below 6%, falling well within the desired accuracy range of preliminary designs. This attests to the high accuracy level of the ASSF tool.

Bellotti, *et al*. (2019) made use of the W-ECoMP tool. This is a reputable software tool, utilized in optimizing energy systems, and thermo-economic analyses that are time dependent. The ASSF tool is able to show its usefulness and effectiveness, with results that are verified as per the aforementioned online software platform.

The ASSF tool was able to compute all data related to this chemical reactive system within 34 seconds, attesting to its efficacy. This tool was run on a Dell Intel ® Core™ i5-2520M CPU @ 2.50 GHz with 8.00 GB Installed RAM (7.88 GB usable).

4.2. Case Study 2 – Methanol Production Plant (CHEMCAD ® Software)

An investigation conducted in 2016, by Perez-Fortes, *et al*. looked at the techno-economic assessment of a MeOH production plant using the CHEMCAD ® software. CHEMCAD ® is a reputable, intuitive chemical process simulation software that is designed to optimize on efficiency.

This investigation looked at reducing environmental CO_2 levels, through the use of captured CO_2 as the feed stream of the MeOH-producing chemical plant. The reaction utilized in this techno-economic assessment varied slightly from the previous investigation explicated in Case Study 1, with a side reaction involving the production of CO also being present. This side reaction is represented by means of Equation 4.2.

$$CO_2 + H_2 \leftrightarrow CO + H_2O \qquad \text{(Equation 4.2)}$$

The total reactive system is a combination of the reactions given in Equation 4.1 and Equation 4.2. Table 4.6 details the operating conditions of this reactive system.

Table 4.6: Operating conditions associated with the investigation conducted by Perez-Fortes, et al. (2016)

Factor	Value
CO_2 : H_2 Feed Ratio	3 : 1
Operating Temperature (^oC)	210
Operating Pressure (bar)	76
Catalyst	$Cu/ZnO/Al_2O_3$
CO_2 Process Conversion (%)	93.85%

With the accuracy of the data in the ASSF tool being validated within the first case study (Section 4.1), this section focuses on the validation of trends determined by the ASSF tool. Table 4.7 provides a summary of the data obtained for this system using the ASSF tool.

Table 4.7: Case Study data obtained via the ASSF tool for the research study conducted by Perez-Fortes, et al. (2016)

Case Study Data	Value
CO_2 Feed (tons/annum)	34,855.92
H_2 Feed (tons/annum)	4,790.02
MeOH Produced (tons/annum)	23,778.02
MeOH Purity (mass %)	96.15
MeOH Sales Potential ($/annum)	11,889,012.15
Total Reactant Cost ($/annum)	8,078,875.20
Total Product revenue ($/annum)	11,889,012.15
Cost of Heat Exchanger System ($)	780,543.05
Cost of Pressure-Changing System ($)	9,980,258.57
Cost of Separation System ($)	704,177.83
Annual Profit before Natural Gas ($/annum)	3,810,136.95
Net CO_2 Environmental Impact (tons/annum)	-8,643.76
Payback Period (years)	-19.90

As seen in Table 4.7, a basic input/output economic analysis (as per search space reduction criterion 1) yields a positive profit (approximately $3.81 million). This is indicative of a sufficient conversion being achieved within the process, allowing for the sales potential of the product to outweigh that of the reactant cost. Search space reduction criterion 2, focused on the environmental impact of the process design, noted a CO_2 benefit of 8643.76 tons per annum. The negative value indicated in Table 4.7 is representative of the process system taking in more CO_2 than is being emitted, considering both the unreacted CO_2 and that which is produced via the combustion of natural gas, i.e., the chosen energy source for the process.

The concern, however, is noted in search space reduction criteria 3, focused on the payback period of the potential plant structure. As seen in Table 4.7, the payback period for this scenario is -19.90 years. The negative payment period is indicative of an annual loss being noted after incorporating the cost of natural gas needed to meet the energy requirements associated with the reaction and separation operating conditions.

Therefore, this production facility is deemed to be infeasible, as per the outcome of the ASSF tool. This outcome aligns with that determined by Perez-Fortez, *et al.* (2016), who also deemed the MeOH production plant to be economically infeasible.

In addition to the commonality demonstrated in the end result of the analysis conducted using CHEMCAD ® software and the ASSF tool, several trend commonalities were also noted. The first commonality was the dominating factor in raw material costs. H_2 was found to dominate the cost of reactants required within the process. The ASSF tool showed that H_2 gas accounted for 74.11% of the total reactant cost of the system. The elevated cost of H_2 is due to this reactant being sold at high prices when produced via an electrolysis unit operation – a costly process.

The pressure-changing unit operations, i.e., compressors and turbines, were found to dominate the capital cost required for purchasing unit operations, with these unit operations found to be more expensive than the required heat exchangers. This reinforces the decisions made when developing the ASSF tool, to attempt creating separation conditions by adjusting the temperature of a stream, as opposed to the pressure. In doing so, heat exchangers are utilized, as opposed to pressure-changing unit operations, resulting in an overall reduction of the capital cost associated with the potential chemical plant.

It is important to note that this case study was primarily run within the ASSF tool, to validate the trends noted by the automated preliminary processes designed within the developed tool. Whilst the commonality in the trends noted were clear, a direct comparison between the unit operation costs was not possible within this case study as the configuration of these chemical plants were vastly different. This provided an ineffective foundation for comparison.

The novelty of the ASSF tool is also demonstrated through this validation procedure, as it shows that the input data required to achieve these results, is simply the chemical reaction and its operating conditions. With this data, the ASSF tool is able to compute and provide the user with the likely economic and environmental feasibility under the aforementioned operating conditions. All precursory design procedures are automated, thereby minimizing the likelihood of human error in transferring data between different software platforms.

Furthermore, the advantage of a fully automated system, such as the ASSF tool, is that the total analysis time is reduced, bypassing the action of extensive human data inputs. The total time required to run this case study within the ASSF tool was approximately 31 seconds, with the tool being run on a Dell Intel ® Core™ i5-2520M CPU @ 2.50 GHz with 8.00 GB Installed RAM (7.88 GB usable).

Chapter 5: Results and Discussion – Applications of the ASSF Tool

This section deals with two types of applications associated with the ASSF tool, namely its use in determining the likely optimum operating conditions, and its use in reducing a reaction pathway search space.

5.1. Determining the Optimum Reaction Conditions

One of the major factors in optimizing a reaction pathway, is the conversion of reactants, and the selectivity of these reactants to the desired product. Optimizing reaction pathways aims to maximize conversion, whilst simultaneously reducing the production of by-products.

There are multiple optimization techniques that can be utilized in reaction pathways, ranging from varying reaction conditions to changing the catalyst in its entirety, or its composition thereof. The main goal in maximizing conversion to the desired product, is to increase the amount of commercially available product being sold, thereby maximizing the profitability of the potential venture. Furthermore, an increase in conversion decreases associated waste streams, thereby reducing the need for subsequent waste processing systems, or environmental taxes. This serves as both an economic benefit and an environmental benefit for the potential chemical plant.

However, when determining optimum operating conditions of a reaction, including operating temperature and pressure, it is important to consider the cost of achieving these optimized conditions. Elevated pressures and temperatures may aid in achieving higher conversions in certain reactive systems, but the increased sales potential could also be offset by the heightened unit operation costs.

This section deals with two case study applications of the ASSF tool, focusing on the determination of optimum operating conditions. Through the use of the ASSF tool, these applications consider the cost of unit operations involved in achieving the aforementioned conditions and separating the product in anticipation of its subsequent sale. The advantage and novelty in the ASSF tool being utilized in these applications, lies in its automated nature, thereby allowing multiple operating conditions to be analyzed simultaneously, and providing

the user with not only the optimal operating conditions, but also a ranking of other conditions that exhibit both economic and environmental feasibilities. Once the likely optimum range has been determined via the ASSF tool, experimentation and research can be concentrated within this narrow scope, thereby improving on the efficacy of future research studies and the subsequent process developments.

5.1.1. Application #1 – Producing Methanol at Elevated Pressures

Research conducted by Gaikwad, *et al*. (2016), investigated the effect of high operating pressures on the conversion of CO_2 and MeOH selectivity. The main reactive system employed within this investigation involved the hydrogenation of CO_2 to MeOH, with the side reaction being the reverse water gas shift (RWGS) reaction. Using the commercial catalyst $Cu/ZnO/Al_2O_3$, there were three main chemical reactions involved in this reactive system, represented by Equation 5.1 to Equation 5.3.

$$CO_2 + 3H_2 \leftrightarrow CH_3OH + H_2O \quad \text{(Equation 5.1)}$$

$$CO_2 + H_2 \leftrightarrow CO + H_2O \quad \text{(Equation 5.2)}$$

$$CO + 2H_2 \leftrightarrow CH_3OH \quad \text{(Equation 5.3)}$$

This research was conducted over five operating pressures, ranging from a minimum pressure of 46 bar, to a maximum of 442 bar. At each pressure the temperature was varied, with five operating temperatures being investigated. These temperatures ranged from 220°C to 300°C, in increments of 20°C. Table 5.1 details the operating conditions tested within the aforementioned investigation, along with their associated conversion and selectivity towards MeOH. The case study number displayed in Table 5.1 refers to the scenario number utilized during the analysis of these operating conditions via the ASSF tool.

It is important to note that the data provided within Table 5.1, was extracted from the graphical representations presented by Gaikwad, *et al*. (2016). Thus, a 2% deviation in the conversion of CO_2, and MeOH selectivity, may be present within this data. This deviation, however, is relatively small, and therefore does not have any impact on the overall results.

Table 5.1: Conversion and selectivity noted in the direct hydrogenation of CO2 under varying pressures and temperatures (Gaikwad, et al., 2016)

Case Study	Pressure (bar)	Temperature (°C)	CO_2 Conversion (%)	MeOH Selectivity (%)
1	442	220	52	82
2		240	85	90
3		260	86	95
4		280	90	96
5		300	80	93
6	331	220	40	80
7		240	57	88
8		260	73	90
9		280	70	88
10		300	65	90
11	184	220	35	76
12		240	38	81
13		260	40	82
14		280	40	85
15		300	39	75
16	92	220	23	31
17		240	25	51
18		260	29	54
19		280	30	55
20		300	29	21
21	46	220	18	33
22		240	22	37
23		260	22	26
24		280	22	18
25		300	21	15

As per the data presented in Table 5.1, an increase in the operating pressure of the reactor allowed for an increase in CO_2 conversion and MeOH selectivity. At 442 bar, conversions of up to 90% where noted, with the selectivity towards MeOH being 96%. This shows minimal

byproduct production as well as minimal waste streams of unreacted CO_2. The investigation conducted by Gaikwad, et al. (2016) noted that optimum reaction conditions were achieved at 442 bar, where a CO_2 conversion rate of 87.7% was achieved with a 97.7% selectivity towards MeOH (Gaikwad, *et al*., 2016). Based on the data presented in Table 5.1, this was achieved within the temperature range of 260^{o}C and 280^{o}C.

Through inspection, this appears to be the optimum operating conditions, with the associated objective function focused on maximizing conversion and selectivity. However, when analyzing this data within the ASSF tool, the practicality of these operating conditions was taken into account.

As mentioned in Chapter 3, the input of reaction pathways within the ASSF tool is completed through a sequential process, with the ASSF tool prompting the user for each reaction pathway and its associated conditions. Alternatively, the reaction pathways and their associated conditions can be inputted into a predefined Microsoft ® Excel spreadsheet, which is imported directly into the ASSF tool. In situations involving the same reactive system under multiple conditions, the use of a Microsoft ® Excel spreadsheet proved to be much simpler, and therefore this approach was utilized when applying the ASSF tool to this case study.

By inputting the reactions presented in Equation 5.1 to Equation 5.3, as well as the associated conditions highlighted in Table 5.1, the ASSF tool was able to systematically analyze and design each of these associated reactive systems. This analysis not only considered the cost of the unit operations necessary to meet the reaction conditions, but also the cost of the unit operations required to separate the desired product from the reactor output. By encompassing the separation system within this analysis, possible losses incurred during this separation process was accounted for. This provided a more holistic and accurate representation of potential chemical plants under the specified operating conditions.

Furthermore, accounting for the separation system, allowed for the post-reactor unit operations to also be sized and costed. Apart from the actual separation vessel, be that a flash drum and/or a distillation column, a post-reactor pressure-changing and heat exchanger system is required to meet the separation conditions. The ASSF tool makes provision for this consideration, ensuring that the cost of this separation system is considered in its entirety.

Table 5.2 details the additional input data required for operation of the ASSF tool.

Table 5.2: Input data required for operation of the ASSF tool

Data Required	Value	Units	Reference
CO_2 Basis Flow Rate	100	kmol/hr	n/a (User input)
H_2 Excess	0	%	(Gaikwad, *et al*., 2016)
Pressure-Changing Efficiency	74	%	(U.S. Department of Energy, 2006)
CEPCI	603.1	dimensionless	(Viswanathan, *et al*., 2020)
Pressure of Heat Exchanger Utility	3	bar	n/a (User input)
Steam Temperature Change	50	Kelvin	n/a (User input)
Cooling Water Temperature Change	20	Kelvin	n/a (User input)
Cost of CO_2	0.06	$/kg	(Schmelz, *et al*., 2020)
Cost of H_2	1.25	$/kg	(Dagdougui, *et al*., 2018)
Sales Potential of MeOH	0.50	$/kg	(Kajaste, *et al*., 2018)
Distillation Recovery	99.99	%	n/a (User input)

It is important to note that all values reported within this thesis, and within the ASSF tool, are given in dollars as this tends to be a universal currency. After obtaining the necessary results required from the ASSF tool, the user can then proceed with the necessary financial conversion, converting the dollar results to the local currency, using the most recent rate of exchange.

Based on Table 5.2, it can be seen that during this application of the ASSF tool, a distillation recovery factor of 99.99% was utilized. This allowed for maximum product recovery, thereby maximizing the potential revenue from the commercial product, i.e., MeOH. It is important to note however, that this distillation recovery factor refers to the recovery of product within the top/bottom stream of the distillation column, based on the feed composition being fed to the column. Thus, this recovery factor provides no indication of product purity, with product purity noting a minor difference from the defined recovery rate.

The ASSF tool systematically designs the distillation column to meet this recovery factor. Should the user require a change in the purity however, this recovery factor can be adjusted,

which will consequentially change the associated product purity. All ASSF tool data associated with this application is tabulated in Appendix F.

The first search space reduction criteria employed within the ASSF tool, considered the gross profit of each scenario, accounting for the reactant cost and the sales potential of the associated products. Through the application of this criteria, the search space of 25 possible scenarios (Table 5.1) was lowered to only 5 economically feasible scenarios, showing an 80% reduction in the search space. These five scenarios were case studies 2, 3, 4, 5 and 8.

As seen from Table 5.1, the economically feasible case studies were those which occurred at elevated pressures of 331 bar and 442 bar. The other 20 case studies were deemed to be economically infeasible due to their insufficient conversion of CO_2, or low methanol selectivity. Thus, these conditions resulted in low product flow rates, thereby reducing potential revenue from these potential chemical plants. Table 5.3 on the next page contains a summarized version of the results extracted from the ASSF tool, relating to these five case studies.

The second search space reduction criterion employed within the ASSF tool, analyzed each of these five case studies from an environmental perspective. This criterion looked at comparing the amount of CO_2 entering the process to the CO_2 being emitted through natural gas combustion. As seen by Table 5.3, all net CO_2 emissions of these five case studies are negative values, indicating that more CO_2 is being taken into the process than is being emitted. This shows an environmental benefit, leaving all five case studies in the potentially feasible search space.

The third search space reduction criterion considered a simplified version of the payback period, in order to ensure that potential investments into the chemical plant are able to be ascertained. Using this criterion, all unit operation capital costs were divided by the gross profit. This revised gross profit accounted for the annual cost of natural gas needed to meet the energy requirements of the chemical plant.

Table 5.3: Summarized results of the case studies exhibiting economic feasibility when analysed within the ASSF tool

Quantity/Value	2	3	4	5	8
Heat Exchanger Cost ($)	490,010.01	625,601.13	643,483.47	494,498.40	472,385.01
Separation System Cost ($)	551,486.74	657,909.53	676,391.67	544,275.33	514,190.54
Pressure-Changing System Cost ($)	12,522,769.41	10,517,772.94	11,057,324.03	6,756,897.38	6,521,881.14
Total Reactant Cost ($/annum)	8,078,875.20	8,078,875.20	8,078,875.20	8,078,875.20	8,078,875.20
MeOH Production (tons/annum)	19,222.05	20,391.16	21,684.63	18,657.29	16,360.91
Total Product Sales Potential ($/annum)	9,611,024.03	10,195,580.13	10,842,312.60	9,328,644.12	8,180,453.05
Yearly profit (before natural gas cost) ($)	1,532,148.83	2,116,704.93	2,763,437.40	1,249,768.92	101,577.85
Natural gas required (tons/annum)	9,116.00	7,966.23	7,138.09	4,936.71	3,773.90
Net CO_2 released (tons/annum)	-3,915.05	-7,719.19	-11,574.37	-14,403.44	-14,757.26
Payback period (years)	-4.77	-6.91	-18.67	-6.96	-4.39

As seen by Table 5.3, all payback periods, for these five case studies, were negative. This is not a realistic payback period. Through operation of the ASSF tool, a negative payback period is an indication that the revised gross profit is exhibiting a loss. This shows that the profit generated from the product sales is not sufficient to offset the cost of utility required to operate the unit operations, thereby resulting in a negative payback period. As a result, all five case studies, in the reduced search space, were found to be infeasible.

The final conclusion of the ASSF tool was that, whilst some of these case studies did initially exhibit economic and environmental benefits, none of the 25 case studies were able to be practically implemented industrially. Thus, even though the operating conditions at 442 bar, and within the temperature range of 260°C and 280°C, were deemed to be the optimal operating conditions, this optimum was simply based on an objective function that maximizes conversion and selectivity. However, these conversions are unable to be achieved within meaningful time frames, i.e., the payback period. Therefore, design resources should rather be allocated to another reactive system.

Table 5.4 provides a summary of the sequential process conducted using the ASSF tool when determining the feasibility of the aforementioned operating conditions.

Table 5.4: Summarized results of the search space reduction results within the ASSF tool

Factor	Value
Total number of operating condition scenarios investigated	25
Number of economically feasible scenarios (excluding utility cost)	5
Number of environmentally feasible scenarios	5
Number of economically feasible scenarios (incorporating utility cost to power unit operations)	0

The time taken to run this reactive system within the ASSF tool, designing and analyzing the chemical plants associated with each operating condition pair, was 1341.1 seconds, approximating to 22.36 minutes. This tool was run on a Dell Intel ® Core™ i5-2520M CPU @ 2.50 GHz with 8.00 GB Installed RAM (7.88 GB usable).

5.1.2. Application #2 – Producing Methanol at Lower Pressures

An investigation conducted by Leonzio, *et al*. (2019), also looked into the production of MeOH via CO_2 hydrogenation. This research was conducted using the same reaction system as the investigation conducted by Gaikwad, *et al*. (2016), with the only difference lying in the operating conditions being investigated.

Leonzio, *et al*. (2019) investigated the production of MeOH over a pressure range of 15 to 55 bar, in increments of 10 bar. At each operating pressure, five different operating temperatures

were investigated, ranging from 200°C to 280°C, in increments of 20°C. As opposed to the experimental results obtained by Gaikwad, *et al*. (2016), this work modelled the reactive system using CHEMCAD ® software, a reputable chemical engineering tool.

Utilizing a single pass reactor system, this investigation noted a maximum CO_2 conversion of 38% to MeOH. Table 5.5 (presented on the next page) details the temperature and pressure points investigated, as well as the associated CO_2 conversion and the conversion to MeOH at each operating condition pair. As with the application of the ASSF tool in Section 5.1.1, the data presented in Table 5.5 was extracted from a graph, utilized to report the results obtained by a single pass reactor. Therefore, an error threshold of ±2% is expected to exist on conversion readings. This, however, is a small value, and has no impact on the overall results obtained by the ASSF tool.

As seen by Table 5.5, an increase in reaction pressure was accompanied by an increase in both the global CO_2 conversion rates, as well as the conversion of CO_2 to MeOH. An increase in temperature, on the other hand, was found to have adverse effects on the conversion, decreasing both of these associated conversion rates. The reason for the decrease in MeOH production, however, is due to the presence of the RWGS reaction, which is promoted at elevated temperatures due to its exothermic nature.

The investigation conducted by Leonzio, *et al*. (2019) also looked at possible recycle streams within the reactor configuration, thereby resulting in a multiple pass reactor system. This did result in an increase in CO_2 conversion and the conversion to MeOH. However, these results were not utilized within the application of the ASSF tool, as the ASSF tool currently does not account for the presence of recycle streams. Therefore, only the single pass reactor results were analyzed.

The ASSF tool input data required for this case study, remained consistent with the data represented in Table 5.2 of the first application. The ASSF tool deduced that all operating conditions were economically infeasible and were therefore excluded from the search space following search space reduction criterion #1. This shows that the conversions noted within this data was deemed to be insufficient, thereby not producing sufficient product to overcome the required cost of the reactants. Furthermore, these low conversions are likely to cause reduced efficiencies in separating the product from the unreacted feed, further impacting on the economic feasibility of the process structure via search space reduction criterion #1. The complete ASSF tool data associated with each case study is tabulated in Appendix G.

Therefore, further research into this reactive system would be ill-advised as the likelihood of success, i.e., the potential for scale up, is low.

Table 5.5: Conversions noted in the production of MeOH under varying pressures and temperatures (Leonzio, et al., 2019)

Case Study	Pressure (bar)	Temperature (°C)	CO_2 Conversion (%)	Conversion to MeOH (%)
1	15	200	18	13
2		220	16	8
3		240	17	5
4		260	19	3
5		280	21	2
6	25	200	24	21
7		220	21	15
8		240	20	10
9		260	20	7
10		280	21	3
11	35	200	30	28
12		220	26	21
13		240	23	15
14		260	22	10
15		280	23	7
16	45	200	35	34
17		220	30	26
18		240	26	20
19		260	25	14
20		280	24	9
21	55	200	40	38
22		220	34	31
23		240	30	24
24		260	27	18
25		280	26	12

The total run time of the ASSF tool in designing and analyzing all 25 operating condition scenarios was 1374.39 seconds, equating to approximately 22.91 minutes. This tool was run on a Dell Intel ® Core™ i5-2520M CPU @ 2.50 GHz with 8.00 GB Installed RAM (7.88 GB usable).

5.2. Reducing a Reaction Pathway Search Space

When developing a new chemical plant, or optimizing an existing chemical plant, the chosen reactive system is integral in determining economic and environmental feasibility. It is possible that a novel reaction pathway, or combination thereof, could potentially allow for greater efficiencies to be achieved, either in terms of conversion, operating costs, or environmental benefit. Ideally, an optimum process should possess a balance of these characteristics.

There are currently many documented pathways, with each having a wide range of catalysts that can be used to promote the reaction at various operating conditions. The manual analysis of each pathway is impractical and can be likened to the common phrase of “looking for a needle in a haystack”. This is not only time consuming but can also be an inefficient use of design resources.

The ASSF tool was developed to be utilized in conjunction with an RPD. With this tool, the associated database can be utilized to narrow down the potential workspace of reaction pathways, to only those reactive systems that are likely to exhibit a balance of economic and environmental benefits. The advantage of such a development lies in the ability to analyze and consider reaction pathways prior to any extensive design procedures. This enhances not only efficiency, but the allocation of design resources for future projects within this area. Furthermore, this precursory, screening tool is able to complete this analysis within hours, as opposed to the months or years needed for manual analysis procedures, allowing for only the promising reactive systems to be investigated in more detail. This section focuses on the application of the ASSF tool to the reduction of two RPDs.

5.2.1. Application #3 – Initial Demonstration of the ASSF Tool

As an initial demonstration of the ASSF tool, the tool was utilized in conjunction with a small RPD containing six independent reactions. All these reactive systems focused on the production of MeOH and DME. Table 5.6 highlights the basic RPD utilized in demonstrating the application and usefulness of the ASSF tool, where T represents the reaction temperature in degrees Celsius, P represents reaction pressure in bar, and X represents the conversion of the reactant as a percentage. It is important to note, that the conversion value given in this table is relative to the first reactant displayed within the chemical reaction equation.

Table 5.6: Basic RPD to demonstrate the application of the ASSF tool

No.	Reaction	T (°C)	P (bar)	X (%)	Reference
1	$CO_2 + 3H_2 \leftrightarrow CH_3OH + H_2O$	240	80	96	(Bellotti, *et al*., 2017)
2	$2CH_3OH \leftrightarrow CH_3OCH_3 + H_2O$	400	25	87.2	(Matzen & Demirel, 2016)
3	$CO_2 + 3H_2 \leftrightarrow CH_3OH + H_2O$	400	20	10	(Hus, *et al*., 2017)
4	$CO_2 + 3H_2 \leftrightarrow CH_3OH + H_2O$	280	20	20.7	(Fan & Wu, 2016)
5	$CO_2 + H_2 \leftrightarrow CO + H_2O$	360	1	58.2	(Zhu, *et al*., 2020)
6	$CO + 2H_2 \leftrightarrow CH_3OH$	290	14.5	1.35	(Agny & Takoudis, 2002)

As mentioned previously, there are specifications that need to be inputted into the ASSF tool before analysing the case studies. These include possible design specifications, and economic data, allowing for the analysis to be more accurate to the desired specifications, and relevant at the time of operation. Table 5.7 details the input data that was associated with this application.

Table 5.7: Input data required from the user in the ASSF tool

Factor Input	Value	Units	Reference
CO_2 Feed basis	100	kmol/hr	n/a (User input)
Excess H_2 Feed	50	%	n/a (User input)
Pressure-changing Efficiency	74	%	(U.S. Department of Energy, 2006)
CEPCI (2018)	603.1	n/a	(Viswanathan, *et al*., 2020)
Pressure of HE Utility	3	bar	n/a (User input)
Steam Temp Change	50	Kelvin	n/a (User input)
Cooling Water Temp Change	20	Kelvin	n/a (User input)
Cost of CO_2	0.1	$/kg	(Keith, *et al*., 2018)
Cost of H_2	1	$/kg	(Kayfeci, *et al*., 2019)
Cost of CaO	0.12	$/kg	(Gebremariam & Marchetti, 2019)
Cost of NG Utility	0.48	$/kg	(Department of Energy, 2018)
Sales Potential of MeOH	0.47	$/kg	(Jasper & El-Halwagi, 2015)
Sales Potential of DME	0.99	$/kg	(Otaraku & Onyekaonwu, 2018)
Sales Potential of $CaCO_3$	0.26	$/kg	*
Distillation Recovery	99.99	%	n/a (User input)

*Based on the average market price as per 10 February 2021

Utilizing the RPD established in Table 5.6, in conjunction with a CO_2/H_2 feed stream, four out of the six reaction pathways are startable. The startable reactions are reactions 1, 3, 4 and 5. However, these reactions focused solely on the production of syngas and MeOH, with none of the four startable reactions focusing on the production of DME.

When this RPD was utilized within the ASSF tool, a total of 9 possible reaction pathway combinations were derived, extending the potential products to encompass both MeOH and DME. It is important to note, that these reaction pathway combinations indicate that the boundaries for the chemical plant have been extended to incorporate a secondary/tertiary production route, with each reaction taking place in its own reactor unit operation. The product of the previous reaction is treated as an intermediate. This shows that with the same feed stream of CO_2 and H_2, certain products can be utilized as intermediates, to expand the potential product search space. Table 5.8 details the reaction pathway combinations achieved, through application of the ASSF tool.

Table 5.8: Case studies derived from the basic RPD

Case Study	Reaction	T (ºC)	P (bar)	X (%)	Reference
1	$CO_2 + 3H_2 \leftrightarrow CH_3OH + H_2O$	240	80	96	(Bellotti, *et al*., 2017)
2	$CO_2 + 3H_2 \leftrightarrow CH_3OH + H_2O$	400	20	10	(Hus, *et al*., 2017)
3	$CO_2 + 3H_2 \leftrightarrow CH_3OH + H_2O$	280	20	20.7	(Fan & Wu, 2016)
4	$CO_2 + H_2 \leftrightarrow CO + H_2O$	360	1	58.2	(Zhu, *et al*., 2020)
5	$CO_2 + 3H_2 \leftrightarrow CH_3OH + H_2O$	240	80	96	(Bellotti, *et al*., 2017)
	$2CH_3OH \leftrightarrow CH_3OCH_3 + H_2O$	400	25	87.2	(Matzen & Demirel, 2016)
6	$CO_2 + 3H_2 \leftrightarrow CH_3OH + H_2O$	400	20	10	(Hus, *et al*., 2017)
	$2CH_3OH \leftrightarrow CH_3OCH_3 + H_2O$	400	25	87.2	(Matzen & Demirel, 2016)
7	$CO_2 + 3H_2 \leftrightarrow CH_3OH + H_2O$	280	20	20.7	(Fan & Wu, 2016)
	$2CH_3OH \leftrightarrow CH_3OCH_3 + H_2O$	400	25	87.2	(Matzen & Demirel, 2016)
8	$CO_2 + H_2 \leftrightarrow CO + H_2O$	360	1	58.2	(Zhu, *et al*., 2020)
	$CO + 2H_2 \leftrightarrow CH_3OH$	290	14.5	1.35	(Agny & Takoudis, 2002)
9	$CO_2 + H_2 \leftrightarrow CO + H_2O$	360	1	58.2	(Zhu, *et al*., 2020)
	$CO + 2H_2 \leftrightarrow CH_3OH$	290	14.5	1.35	(Agny & Takoudis, 2002)
	$2CH_3OH \leftrightarrow CH_3OCH_3 + H_2O$	400	25	87.2	(Matzen & Demirel, 2016)

Through use of the ASSF tool, the 9 possible reaction pathway combinations shown in Table 5.8 can be reduced to a single pathway exhibiting both economic and environmental feasibility within a meaningful time frame. This reactive system is represented by Case Study 5 and involves the production of DME as the primary product, with unreacted MeOH being sold as a secondary product to increase economic feasibility of the chemical plant. The complete data associated with these nine case studies is tabulated in Appendix H.

The data provided in Appendix H shows that out of the 9 case studies analysed in this initial demonstration of the ASSF tool, 7 of these case studies yielded negative annual profits (losses) before incorporating the cost of natural gas needed to meet the energy requirements of the process. This is indicative of a loss being noted in search space reduction criteria #1 – dealing with the economic feasibility from an input/output perspective. When a loss is experienced at this stage in the ASSF tool, this is indicative of one of two potential reasons, namely:

- The conversions noted within the reactive systems are too low, thereby not producing sufficient marketable product.
- The product being produced cannot be sufficiently separated from the unreacted feed, or byproducts, thereby not producing a marketable purity that is likely to generate sufficient revenue for the process structure.

Whilst the remaining two case studies (case study 1 and 5) both exhibit economic feasibility from an initial input/output standpoint, the concern with case study 1 lies in its economic feasibility after accounting for the cost of natural gas needed to meet the energy requirements of the process. Incorporating this cost into economic analysis (as per search space reduction criterion 3) is indicative of a negative payback period, implying a loss in the annual profit/loss calculation of the chemical plant. Case study 5, on the other hand, exhibits feasibility on all three search space reduction criteria, indicating that this case study is a promising reactive system that can be paid off within meaningful time frames.

As Case Study 5 is a two-reaction system, utilizing the generic plant structures provided in Section 3.2, the process structure employed by the ASSF tool would be a combination of the process flow sheet involved with direct methanol synthesis, and that involved with all chemical species being present. Whilst the ASSF tool is not able to export process flow sheets, and variations thereof, only using the generic process structure previously explicated, the analysed process flow sheet can be drawn as a combination of these two generic structures. The expected process flow sheet analysed is given in Figure 5.1.

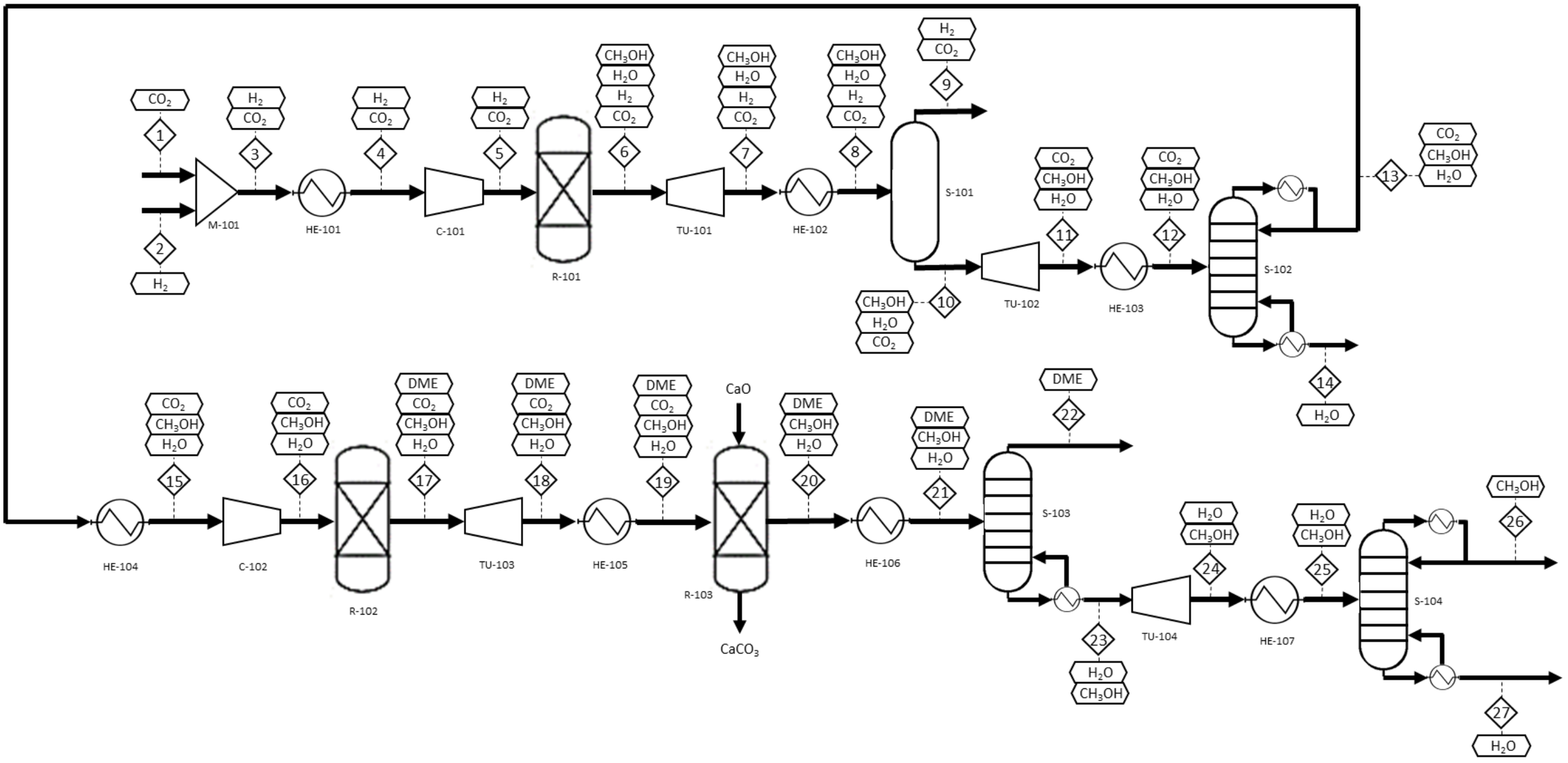

Figure 5.1: Process flow diagram of Case Study 5, i.e., the promising reactive system determined during the initial demonstration of the ASSF tool

As noted in Figure 5.1, the production of methanol aligns directly with that presented in the generic process structure highlighted in Figure 3.4. However, the production and separation of DME does note a deviation from Figure 3.6. The flash drum unit operation noted in Figure 3.6, along with its preceding heat exchanger and turbine, have been removed. This is due to the nature of the design system, with the ASSF tool noting that the unreacted hydrogen gas would have been removed during the methanol separation system. Therefore, the need for the flash drum separation system within the DME section of the process structure is negated. The remaining CO_2 that may be present in the methanol/DME stream is removed via its reaction with calcium oxide (CaO), forming calcium carbonate ($CaCO_3$), as shown in reactor R-103.

Table 5.9 provides a summarized list of the data associated with the feasible case study, i.e., Case Study 5. This data shows that the economic feasibility of this reactive system is enhanced by the sale of three potential products, namely DME, MeOH and $CaCO_3$, which is formed during the separation of CO_2 from the DME product stream.

The negative net CO_2 environmental impact is an indication of the amount of overall CO_2 taken into the reactive system. This shows that this potential chemical plant is expected to take in more CO_2 than the summation of the CO_2 being emitted as an unreacted waste stream and being formed during the combustion of natural gas utility. A positive payback period was an indication that an annual profit was still achievable after accounting for the yearly cost of natural gas utility required to meet the energy requirements of all unit operations. Furthermore, this payback period of 1.25 years is within the range allotted by search space reduction criterion #3, thereby promoting potential investments into this potential venture.

Table 5.9: Properties of Case Study 5

Case Study Data	Value
CO_2 Feed (tons/annum)	34 855.92
MeOH Produced (tons/annum)	3 113.91
MeOH Purity (mass %)	99.93
DME Produced (tons/annum)	15 251.25
DME Purity (mass %)	99.36
CaO Needed (tons/annum)	1 115.72
$CaCO_3$ Produced (tons/annum)	1 991.34
Total Reactant Cost ($/annum)	10 804 502.58
Total Product revenue ($/annum)	17 080 027.62
Cost of Heat Exchanger System ($)	1 264 117.63
Cost of Pressure-Changing System ($)	4 247 435.68
Cost of Separation System ($)	1 271 266.16
Annual Profit ($/annum)	6 275 525.03
New CO_2 Environmental Impact (tons/annum)	-2 9530.44
Payback Period (years)	1.25

This application shows the potential of the ASSF tool to find nine reaction combinations among six independent reactions, with only one of these possible combinations exhibiting both

economic and environmental feasibility. This was achieved prior to any extensive design procedures. The promising reactive system (case study 5) can now be investigated in more detail, necessitating the need for intricate simulation and optimization software packages, such as Aspen ® Plus.

The total time required to run the ASSF tool for this RPD was 1024.50 seconds, approximating to 17.07 minutes. This tool was developed and run on a Dell Intel ® Core™ i5-2520M CPU @ 2.50 GHz with 8.00 GB Installed RAM (7.88 GB usable).

5.2.2. Application #4 – Comparison with an Existing Reaction Pathway Database Analysis

With the application and efficacy of the ASSF tool being demonstrated in relation to a small RPD (Section 5.2.1), the ASSF tool was then applied to an existing RPD developed by Jugmohan, *et al*. (2020). The investigation conducted by Jugmohan, *et al*. (2020) developed a screening framework, aimed at determining the promising reaction pathways prior to extensive design resources being expended. This framework utilized a manual analysis procedure, whereby the following software platforms were utilized to determine the number of reaction combinations possible and analyze these associated combinations:

- P-Graph Studio ®
- Aspen Plus ®
- MATLAB ®
- Microsoft ® Excel

As mentioned in Chapter 1, this work required the manual input and extraction of data from each software platform, resulting in the developed procedure being time consuming and increasing the likelihood of human error. Table 5.10 details the RPD developed by Jugmohan, *et al*. (2020), consisting of 22 reactions.

Table 5.10: RPD utilized in the investigation conducted by Jugmohan, et al. (2020)

No.	Reaction	Temp (K)	Pressure (bar)	Catalyst	X_{CO2}	CO_2 : H_2 Ratio
1	$CO_2 + 3H_2 \rightarrow CH_3OH + H_2O$	513	20	CZZA/rGO	11.6%	1:3
2	$CO_2 + 3H_2 \rightarrow CH_3OH + H_2O$	553.15	442	$Cu/ZnO/Al_2O_3$	85.5%	1:3
3	$CO_2 + 3H_2 \rightarrow CH_3OH + H_2O$	474	40	CZA – Pd modified	61.54%	1:3
4	$CO_2 + 3H_2 \rightarrow CH_3OH + H_2O$	533.15	330	Fe-Cu	93.5846%	1:3
5	$CO_2 + 3H_2 \rightarrow CH_3OH + H_2O$	513.15	80	$Cu/ZnO/Al_2O_3$	96%	1:3
6	$CO_2 + 3H_2 \rightarrow CH_3OH + H_2O$	493.15	18.9	1% Na/20% Co-SiO_2	17.202%	1:3
7	$CO_2 + 3H_2 \rightarrow CH_3OH + H_2O$	523-543	20	Cu-Ga/ZnO	5%	1:3
8	$CO_2 + 3H_2 \rightarrow CH_3OH + H_2O$	493	80	Cu/Zn/Zr/Cr	18%	1:3
9	$2CH_3OH \rightarrow CH_3OCH_3 + H_2O$	673.15	25	Alumina Based	86.764%	n/a
10	$CO_2 + H_2 \rightarrow CO + H_2O$	613	20	Li, Na, K, Rb, Cs (Fe based)	2.774%	1:1
11	$CO + 2H_2 \rightarrow CH_3OH$	553.15	442	$Cu/ZnO/Al_2O_3$	1.67%	n/a
12	$CO + 2H_2 \rightarrow CH_3OH$	533.15	330	Fe-Cu	90.53%	n/a
13	$CO + 2H_2 \rightarrow CH_3OH$	523-543	20	Cu-Ga/ZnO	7.04%	n/a
14	$CO_2 + H_2 \rightarrow CO + H_2O$	533.15-553.15	442	$Cu/ZnO/Al_2O_3$	4.5%	1:1
15	$CO_2 + H_2 \rightarrow CO + H_2O$	474	40	CZA-Pd Modified	34.375%	1:1
16	$CO_2 + H_2 \rightarrow CO + H_2O$	533.15	330	Fe-Cu	13.5%	1:1
17	$CO_2 + H_2 \rightarrow CO + H_2O$	623	15	Fe-ZrO_2	9.423%	1:2
18	$CO_2 + H_2 \rightarrow CO + H_2O$	623	15	Fe-TiO_2	4.7941%	1:2

19	$CO_2 + H_2 \rightarrow CO + H_2O$	498-548	50	$Cu/ZnO/Al_2O_3$	2.7025%	1:1
20	$CO_2 + H_2 \rightarrow CO + H_2O$	523-543	20	Cu-Ga/ZnO	0.75%	1:1
21	$CO_2 + H_2 \rightarrow CO + H_2O$	298-363	70	Pt-Cu	15.13%	1:1
22	$CO_2 + H_2 \rightarrow CO + H_2O$	433-513	80	Cu/Zn/Zr/Cr	5.76%	1:1

Table 5.11 highlights the references associated with each of the reaction pathways provided in the above RPD.

Table 5.11: References associated with the RPD developed by Jugmohan, et al. (2020)

Reaction No.	Reference	Reaction No.	Reference
1	(Fan & Wu, 2016)	12	(Vanhove, 2015)
2	(Gaikwad, *et al*., 2016)	13	(Van der Ham, *et al*., 2012)
3	(Cabrera, *et al*., 1998)	14	(Gaikwad, *et al*., 2016)
4	(Vanhove, 2015)	15	(Cabrera, *et al*., 1998)
5	(Bellotti, *et al*., 2017)	16	(Vanhove, 2015)
6	(Gnanamani, *et al*., 2015)	17	(Zhanghuai & Yuan, 2000)
7	(Van der Ham, *et al*., 2012)	18	(Zhanghuai & Yuan, 2000)
8	(CHEMIK, 2014)	19	(Van der Ham, *et al*., 2012)
9	(Matzen & Demirel, 2016)	20	(Van der Ham, *et al*., 2012)
10	(You, *et al*., 2013)	21	(Chan, *et al*., 2018)
11	(Gaikwad, *et al*., 2016)	22	(CHEMIK, 2014)

Utilizing the 22 reactions presented in Table 5.10, within the ASSF tool, the number of startable reaction combinations were determined to be 86 possible reactive systems, focusing on the production of syngas, MeOH and DME. The complete table of reaction pathway combinations is tabulated in Appendix I, with all analysis data for these reactive systems being tabulated in Appendix J. As with the demonstration given in Section 5.2.1, these reaction system combinations involve extending the boundaries of the process plant, i.e., including secondary and tertiary reactor unit operations that utilize previous product streams as intermediates in the overall process structure.

Based on the ASSF tool analysis of the RPD given in Table 5.10, there were 32 case studies that were deemed to be economically feasible, when considered by means of search space reduction criterion #1. This criterion resulted in a 62.79% reduction in the reaction pathway search space. The second criteria, focusing on the environmental feasibility of the pathways utilizing the net CO_2 benefit to the environment, did not reduce the search space any further, with all reactive systems in the reduced search space exhibiting environmental benefits.

The third search space reduction criterion employed within the ASSF tool, analyzed the payback period of each case study. This ensured that the capital cost is able to be paid off in a meaningful time frame as discussed in Chapter 3 (Section 3.14.3), thereby promoting investment into the chemical plant. Furthermore, this criterion took into account the annual cost of natural gas utility necessary to meet the energy requirements of all the unit operations, encompassing this value within the annual gross profit calculation.

This search space reduction criterion resulted in five reactive systems exhibiting both economic and environmental benefits within meaningful time frames, thereby resulting in a total reduction of 94.19% from the initial search space. The excluded pathways within this criterion were those that were either outside of the bounds for a meaningful payback period, thus not promoting investment into the chemical plant, or those that exhibited negative payback periods. These negative payback periods were indicative of a gross loss, after factoring in the annual cost of natural gas required.

The final search space criterion utilized a ratio, finding a trade-off between economic and environmental benefits. This criterion ranked the remaining reactive systems in order of their viability, with the aforementioned ratio being deemed as a performance index. Table 5.12 and Table 5.13 summarizes the data associated with these five remaining reactive systems.

As seen in Table 5.12, Case study 5 exhibits the highest performance index, and is therefore considered to be the most feasible option within the remaining search space, showing economic and environmental gains within a short payback period of just under three and a half years.

Table 5.12: Summarized results of the reduced search space based on the RPD by Jugmohan, et al. (2020)

Case Study Number	**5**	**23**	**21**
Heat Exchanger Cost ($)	638,766.03	1,087,342.27	768,908.29
Separation System Cost ($)	713,200.06	1,272,513.91	965,705.32
Pressure-Changing System Cost ($)	2,913,976.02	4,479,774.52	3,028,395.43
MeOH Production (tons/annum)	24,332.28	3,219.98	2,014.90
MeOH Purity (mass %)	96.15	99.93	99.93
MeOH Sales Potential ($/annum)	12,166,139.29	1,609,988.15	1,007,452.14
DME Production (tons/annum)	0.00	15,175.00	9,495.77
DME Purity (mass %)	0.00	99.36	98.71
DME Sales Potential ($/annum)	0.00	15,023,248.65	9,400,817.04
CaO Needed (tons/annum)	0.00	1,115.72	1,420.76
CaO Cost ($/annum)	0.00	133,886.59	170,491.58
$CaCO_3$ Produced	0.00	1,991.34	2,535.78
$CaCO_3$ Sales Potential ($/annum)	0.00	517,748.13	659,302.03
Total Reactant Cost ($/annum)	8,078,875.20	8,212,761.79	8,249,366.78
Total Product Sales Potential ($/annum)	12,166,139.29	17,150,984.93	11,067,571.20
Yearly profit (before natural gas cost) ($)	4,087,264.09	8,938,223.14	2,818,204.42
Natural gas required (tons/annum)	1,501.29	1,785.56	818.85
Net CO_2 released (tons/annum)	-30,315.43	-29,535.45	-20,442.51
Payback period (years)	1.27	0.85	1.96
Performance index ($\times 10^3$)	3.45	3.26	2.37

Table 5.13: Summarized results of the reduced search space based on the RPD by Jugmohan, et al. (2020)

Case Study Number	22	20
Heat Exchanger Cost ($)	1,081,795.47	1,055,469.99
Separation System Cost ($)	1,255,714.87	1,202,398.32
Pressure-Changing System Cost ($)	12,180,390.58	12,477,623.51
MeOH Production (tons/annum)	3,131.40	2,835.04
MeOH Purity (mass %)	99.93	99.93
MeOH Sales Potential ($/annum)	1,565,698.61	1,417,521.85
DME Production (tons/annum)	14,757.55	13,360.90
DME Purity (mass %)	99.36	99.36
DME Sales Potential ($/annum)	14,609,970.59	13,227,291.92
CaO Needed (tons/annum)	1,086.17	987.28
CaO Cost ($/annum)	130,340.43	118,473.11
$CaCO_3$ Produced	1,938.60	1,762.09
$CaCO_3$ Sales Potential ($/annum)	504,034.92	458,143.20
Total Reactant Cost ($/annum)	8,209,215.63	8,197,348.31
Total Product Sales Potential ($/annum)	16,679,704.12	15,102,956.98
Yearly profit (before natural gas cost) ($)	8,470,488.49	6,905,608.67
Natural gas required (tons/annum)	8,122.06	7,238.31
Net CO_2 released (tons/annum)	-11,281.88	-10,802.50
Payback period (years)	3.18	4.29
Performance index ($\times 10^3$)	0.93	0.92

Based on Table 5.12, it is likely that this increased feasibility of MeOH production could be as a result of the lower unit operation cost noted in this case study, when compared to that of the DME production system in Case Study 23. Based on the analysis conducted by the ASSF tool, the capital cost for unit operations involved in the production of MeOH, proved to be 62.37% of that required in the production of DME.

Whilst the production of DME does show a shorter payback period, which is likely due to the production of a higher-valued product and the addition of the $CaCO_3$ product, the environmental feasibility of Case Study 5 was noted to be higher. Furthermore, the smaller unit

operations required in the production of MeOH, resulted in reduced energy requirements of the chemical plant, subsequently reducing the amount and cost of natural gas utility required.

The results obtained via the ASSF tool, coincides with the final results determined by Jugmohan, *et al*. (2020), where the same reactive system was deemed as the most feasible option given this RPD. This attests to the reliability of the results obtained via the ASSF tool. Additionally, the ASSF tool was able to further reduce the search space analyzed from this RPD, noting only 5 feasible reactive systems, as opposed to the 6 noted within the manual procedure conducted by Jugmohan, *et al*. (2020). This shows that the ASSF tool is able to provide a more targeted search space in a fraction of the time previously required.

Furthermore, the work conducted by Jugmohan, *et al*. (2020) took approximately 10 months to analyze all these reaction pathway systems manually, with each system being inputted and extracted manually from each software platform. The ASSF tool on the other hand, was able to compute these results in just under 5 hours, with the only major input required from the user being the RPD and the economic data at the time of running this tool. This tool was developed and run on a Dell Intel ® Core™ i5-2520M CPU @ 2.50 GHz with 8.00 GB Installed RAM (7.88 GB usable). Table 5.14 details the comparison of the final data obtained using the manual analysis procedure developed by Jugmohan, *et al*. (2020) and the ASSF tool.

Table 5.14: Final data obtained from Jugmohan, et al. (2020) vs ASSF tool

Factor	**Jugmohan, *et al*. (2020)**	**ASSF Tool**
Number of possible reaction pathway combinations	86	86
Reactive systems exhibiting economic and environmental feasibility	6	5
Time taken	~10 months	~5 hours

The results obtained via this application of the ASSF tool proved that the production of MeOH is more feasible than the production of DME, with a slight difference in their performance indices. It is important to reiterate that this tool is not designed to replace any existing chemical engineering software platforms, but rather acts as a precursory, screening tool to identify and focus design resources on those promising reactive systems with the greatest likelihood for success.

Chapter 6: Conclusion

Explicated in this thesis is an automated, precursory, screening tool for reaction pathway search space reduction. This novel tool, referred to as the ASSF tool, was verified over a wide range of applications, namely:

- The basic design of a chemical plant, utilizing only the reaction pathway and its associated operating conditions.
- Determining the expected trends within a potential chemical plant, prior to the use of extensive design resources.
- Determining the likely range of optimum operating conditions of a reactor, accounting for the cost of unit operations required to achieve the necessary reaction conditions and subsequent separation conditions.
- Determining and recording the number of possible reaction pathway combinations achievable, based on a predefined RPD, extending the boundaries of a process structure.
- The design and analysis of potential chemical plants associated with an RPD, and its achievable combinations. This analysis is conducted from an economic and environmental standpoint, reducing the potential search space to only those pathways exhibiting feasibility in both of the aforementioned criteria.

With the aforementioned applications of the ASSF tool, this tool is able to analyze and detect the most promising reaction pathway/combination, finding a draw-off between the economic and environmental benefits of the potential chemical plant. As a result, this allows for subsequent design resources to be focused on reactions pathways with the greatest likelihood for success and implementation.

The verification procedure and applications of the ASSF tool show the alignment of this novel tool with the results of work previously conducted within this field, thereby attesting to the efficacy and accuracy of the ASSF tool. The application of the ASSF tool to an existing RPD containing 22 reaction pathways, yielded 86 possible reaction pathway combinations. These combinations were possible under the assumption that CO_2 and H_2 are the only available feed streams. These 86 case studies were reduced to just 5 reactive systems in the automated process of the ASSF tool, resulting in a search space reduction of 94.19%. Furthermore, the final search

space noted, aligned with previous research conducted in this area, where reputable chemical engineering software, such as Aspen ® Plus, P-Graph Studio and MATLAB were utilized.

The alignment of this tool with the results of research studies previously conducted in this field, attests to its efficacy and accuracy, proving that this tool can be a great asset to the chemical industry, and play an integral role in the future of process synthesis. Furthermore, with the screening mechanism provided by the ASSF tool, design resources can be more focused, expediting the process of translating laboratory reactive systems to a pilot/manufacturing process scale.

The novel tool developed within this thesis can be a great asset to the chemical industry, and based on the research presented within this this, could potentially play an integral role in the future of process synthesis and optimization.

Chapter 7: Limitations & Future Work

The ASSF tool does have its own associated limitations, with the most prominent limitation being the scope of chemical species encompassed within the coding framework. The ASSF tool was developed to target reactive systems surrounding the hydrogenation of CO_2 to MeOH and DME, with CO and water being potentially produced as byproducts. This limits the use of the ASSF tool in terms of the reactive systems to which it can be applied. Therefore, future developments would involve expanding the chemical specie database of the ASSF tool, to encompass other chemical species, thereby increasing the potential use of this novel tool developed.

Furthermore, the ASSF tool is based on existing equipment designs and formulae. Adapting this tool to other reactive systems or plant designs would require the changes to be incorporated directly into its coding mechanism, requiring the user to have the necessary programming skills. Future innovations could potentially involve the development of a user-friendly graphic user interface (GUI) allowing the user to easily make changes to the design system.

Additionally, future improvements to the ASSF tool could potentially involve being paired with an artificial intelligence (AI) system, allowing for new developments within the process equipment field, to be extracted in real time and implemented within the ASSF tool. This would allow for the resulting data to be coherent with the latest technological developments.

Another limitation of the ASSF tool is that it currently operates on a single pass reactive system, thereby not accounting for the possibility of recycle streams. Recycle streams could potentially increase the feasibility of a chemical plant, reducing the amount of waste leaving the process, and the amount of feed reactant needing to be purchased. This provides the potential chemical plant with both an environmental and economic benefit, respectively. Future developments to the ASSF tool should encompass a potential recycle system into the automated plant design.

For the purposes of this thesis, i.e., the reduction of a reaction pathway search space, a single pass reactive system sufficed, as it narrows down the list of feasible reactive systems by employing a worst-case scenario perspective. Therefore, should a reactive system be deemed to be feasible with the current ASSF tool, it is likely that the addition of a recycle stream will only serve to enhance this feasibility.

References

Abeydeera, L. H. U. W., Mesthrige, J. W. & Samarasinghalage, T. I., 2019. Global Research on Carbon Emissions: A Scientometric Review. MDPI: Sustainability, Volume 11, pp. 1-24.

Agny, R. M. & Takoudis, C. G., 2002. Catalytic Synthesis of Methanol from Hydrogen and Carbon Monoxide on a Copper-Zinc Oxide Supported Catalyst. Industrial & Engineering Chemistry Product Research and Development, 24(1), pp. 50-55.

Ahmed, T., 2019. Chapter 15 - Vapor-Liquid Phase Equilibria. In: Reservoir Engineering Handbook (Fifth Edition). s.l.: Gulf Professional Publishing, pp. 1109-1225.

Al-Fadhli, F. M., Mukherjee, R., Wang, W. & El-Halwagi, M. M., 2018. Design of Multiperiod C-H-O Symbiosis Networks. ACS Sustainable Chemistry and Engineering, 6(7), pp. 9130-9136.

Alhelal, A. & Sultan, I., 2015. Improving the performance of reciprocating compressors, Australia: School of Engineering and Information Technology, Federation University.

Al-Mhanna, N. M., 2018. Simulation of High-Pressure Separator Used in Crude Oil Processing. MDPI: Processes, 6(219), pp. 1-14.

Alone, D. B., Kumar, S. S., Thimmaiah, S. M., Mudipalli, J. R. R., Pradeep, A. M., Ramamurthy, S. & Iyengar, V. S., 2014. Improvement of Moderately Loaded Transonic Axial Compressor Performance Using Low Porosity Bend Skewed Casing Treatment. International Journal of Rotating Machinery.

Arcoumanis, C., Bae, C., Crookes, R. & Kinoshita, E., 2008. The potential of di-methyl ether (DME) as an alternative fuel for compresion-ignition engines: A review. Fuel, Volume 87, pp. 1014-1030.

Ardy, A., Rizkiana, J., Laniwati, M. & Susanto, H., 2019. Synthesis of dimethyl ether using a fixed bed of dual catalyst for methanol synthesis and its dehydration. MATEC Web of Conferences, Volume 268, pp. 1-5.

Ateka, A., Erena, J., Sanchez-Contador, M., Perez-Uriarte, P., Bilbao, J. & Aguayo, A. T., 2018. Capability of the Direct Dimethyl Ether Synthesis Process for the Conversion of Carbon Dioxide. MDPI: Applied Sciences, 8(5), p. 677.

Aviso, K. B. & Tan, R. R., 2018. Fuzzy P-graph for optimal synthesis of cogeneration and trigeneration systems. Energy, Volume 154, pp. 258-268.

Aviso, K. B., Cayamanda, C. D., Solis, F. D. B., Danga, A. M. R., Promentilla, M. A. B., Yu, K. D. S., Santos, J. R. & Tan, R. R., 2015. P-graph approach for GDP-optimal allocation of resources, commodities and capital economic systems under climate change-induced crisis conditions. Journal of Cleaner Production, Volume 92, pp. 308-317.

Aviso, K. B., Lee, J. Y., Dulatre, J. C., Madria, V. R., Okusa, J. & Tan, R. R., 2017. A P-graph model for multi-period optimization of sustainable energy systems. Journal of Cleaner Production, Volume 161, pp. 1338-1351.

Aviso, K. B., Lee, J. Y. & Tan, R. R., 2016. A P-Graph Model for Multi-period Optimization of Isolated Energy Systems. Chemical Engineering Transactions, Volume 52, pp. 865-870.

Azarpour, A., Suhaimi, S., Zahedi, G. & Bahadori, A., 2013. A Review of the Drawbacks of Renewable Energy as a Promising Energy Source of the Future. Arabian Journal for Science and Engineering, 38(2), pp. 317-328.

Bamatov, I. M. & Bamatov, D. M., 2020. Engineering design of second distillation column of IPA. Orlando, IOP Conference Series: Materials Science and Engineering.

Bamber, J. L., Oppenheimer, M., Kopp, R. E., Aspinall, W. P. & Cooke, R. M., 2019. Ice sheet contributions to future sea-level rise from structured expert judgment. Proceedings of the National Academy of Sciences of the United States of America, 116(23), pp. 11195-11200.

Bandarkar, A. W., Sozer, Y. & De Abreu-Garcia, J. A., 2019. CFD Based Design of an Impeller for a Novel Integrated Motor-Compressor System. Maryland, United States of America, 2019 IEEE Energy Conversion Congress and Exposition (ECCE).

Barany, M., Bertok, B., Imreh, C., Fan, L. T. & Friedler, F., 2012. On the equivalence of direct mechanisms and structurally minimal pathways. Journal of Mathematical Chemistry, Volume 50, pp. 1347-1361.

Bell, I. H. & Lemmon, E. W., 2017. 4 - Organic fluids for Organic Rankine Cycle systems: Classification and calculation of thermodynamic and transport properties. In: Organic Rankine Cycle (ORC) Power Systems: Technologies and Applications. s.l.:Woodhead Publishing, pp. 91-119.

Bellotti, D., Rivarolo, M. & Magistri, L., 2019. Economic feasibility of methanol synthesis as a method for CO2 reduction and energy storage. Energy Procedia, Volume 158, pp. 4721-4728.

Bellotti, D., Rivarolo, M., Magistri, L. & Massardo, A. F., 2017. Feasibility study of methanol production plant from hydrogen and captured carbon dioxide. Journal of CO2 Utilization, Volume 21, pp. 132-138.

Berberan-Santos, M. N., Bodunov, E. N. & Pogliani, L., 2007. The van der Waals equation: analytical and approximate solutions. Journal of Mathematical Chemistry, 43(4), pp. 1437-1457.

Bertok, B., Adonyi, R., Friedler, F. & Fan, L. T., 2011. Superstructure Approach to Batch Process Scheduling by S-graph Representation. Computer Aided Chemical Engineering, Volume 29, pp. 1105-1109.

Bertok, B., Barany, M. & Friedler, F., 2013. Generating and Analyzing Mathematical Programming Models of Conceptual Process Design by P-graph Software. Industrial and Engineering Chemical Research, Volume 52, pp. 166-171.

Bhavsar, J. J., Matawala, V. K. & Dixit, S., 2013. Design and Experimental Analysis of Spiral Tube Heat Exchanger. International Journal of Mechanical and Production Engineering, 1(1), pp. 37-42.

Blazsik, Z., Hollo, C., Imreh, C. & Kovacs, Z., 2001. Heuristics for the Process Network Synthesis Problem. Optimization Theory, pp. 1-17.

Bloch, H. P., 2006. A Practical Guide to Compressor Technology. 2nd ed. New Jersey: John Wiley & Sons, Inc.

Boes, S., 2017. Improve Air-Cooled Heat Exchanger Performance, s.l.: CEP American Institute of Chemical Engineers (AIChE).

Borisut, P. & Nuchitprasittichai, A., 2019. Methanol Production via CO_2 Hydrogenation: Sensitivity Analysis and Simulation-Based Optimization. Frontiers in Energy Research, 7(81).

Boyce, M. P., 2012. Axial-Flow Compressors. In: Gas Turbine Engineering Handbook. United Kingdom: Butterworth-Heinemann, pp. 303-355.

Brown, R. N., 1997. 6 - Axial Compressors. In: Compressors: Selection and Sizing. Texas: Gulf Professional Publishing, pp. 515-544.

Buxton, A., Livingston, A. G. & Pistikopoulos, E. N., 1997. Reaction Path Synthesis for Environmental Impact Minimization. Computers & Chemical Engineering, Volume 21, pp. S959-S964.

Cabrera, I. M., Granados, M. L., Terreros, P. & Fierro, J. L. G., 1998. CO_2 Hydrogenation over Pd-Modified Methanol Synthesis Catalysts. Catalysis Today, Issue 45, pp. 251-256.

Catizzone, E., Bonura, G., Migliori, M., Frusteri, F. & Giordano, G., 2017. CO2 Recycling to Dimethyl Ether: State-of-the-Art and Perspectives. MDPI: Molecules, Volume 23, pp. 1-28.

Catizzone, E., Bonura, G., Migliori, M., Braccio, G., Frusteri, F. & Giordano, G., 2019. Direct CO2-to-dimethyl Ether Hydrogenation over CuZnZr/zeolite Hybrid Catalyst: New Evidences on the Interaction Between Acid and Metal Sites. Annales de Chimie - Science des Matériaux, 43(3), pp. 141-149.

Chan, F. L., Altinkaya, G., Fung, N. & Tanksale, A., 2018. Low temperature hydrogenation of carbon dioxide into formaldehyde in liquid media. Catalysis Today, Volume 309, pp. 242-247.

Chaudhari, N. R. & Adroja, F. N., 2014. A Review on Design & Analysis of Double Pipe Heat Exchanger. International Journal of Engineering Research & Technology (IJERT), 3(2), pp. 2502-2505.

CHEMIK, 2014. Methanol Synthesis from Carbon Dioxide and Hydrogen over CuO/ZnO/ZrO2 promoted catalysts. 1(68), pp. 61-68.

Cho, W., Yu, H. & Mo, Y., 2017. CO_2 Conversion to Chemicals and Fuel for Carbon Utilization. In: Recent Advances in Carbon Capture and Storage. s.l.:IntechOpen.

Cornelia, P. G. & Lenuta, T. C., 2012. Assessing the Impact and Effectiveness of Environmental Taxes. Procedia Economics and Finance, Volume 3, pp. 728-733.

Coroiu, A. M., 2015. Fuzzy methods in decision making process - A particular approach in manufacturing systems. IOP Conf. Series: Materials Science and Engineering, Volume 95, pp. 1-6.

Cremaschi, S., 2015. A perspective on process synthesis: Challenges and prospects. Computers and Chemical Engineering, Volume 81, pp. 130-137.

Dagdougui, H., Sacile, R., Bersani, C. & Ouammi, A., 2018. Chapter 4 - Hydrogen Storage and Distribution: Implementation Scenarios. In: Hydrogen Infrastructure for Energy Applications: Production, Storage, Distribution and Safety. s.l.:Academic Press, pp. 37-52.

Dagdougui, H., Sacile, R., Bersani, C. & Ouammi, A., 2018. Chapter 2 - Hydrogen Production and Current Technologies. In: Hydrogen Infrastructure for Energy Applications. s.l.:Academic Press, pp. 7-21.

Darkwah, W. K., Odum, B., Addae, M. & Koomson, D., 2018. Greenhouse Effect: Greenhouse Gases and Their Impact on Global Warming. Journal of Scientific Research and Reports, 17(6), pp. 1-9.

Deddis, C. R., 2010. Process Economics. In: J. B. M. M. R. G. a. C. G. Ryzhard Pohorecki, ed. Chemical Engineering and Chemical Process Technology Vol IV. s.l.:EOLSS Publications, pp. 311-337.

Department of Energy, 2018. 2018 Energy Price Report. Pretoria, South Africa: Department of Energy.

Deshpande, G. N., 2020. Designing of a Proficient Heat Exchanger by Using Spiral Tube for Augmentation of Heat Transfer. Multidisciplinary International Research Journal of Gujarat Technological University, 2(2), pp. 17-26.

Diaz-Alvarado, F. A., Miranda-Perez, J. & Grossmann, I. E., 2018. Search for reaction pathways with P-graphs and reaction blocks: methanation of carbon dioxide with hydrogen. Journal of Mathematical Chemistry, Volume 56, pp. 1011-1102.

Diniz, M. C. & Deschamps, C. J., 2016. Comparative Analysis of Two Types of Positive Displacement Compressors for Air Conditioning Applications. s.l., International Compressor Engineering Conference.

Douglas, J. M., 1988. Shortcut Procedures for Equipment Design. In: B. J. Clark & J. W. Bradley, eds. Conceptual Design of Chemical Processes. Singapore: McGraw-Hill Book Co., pp. 425-507.

Dubey, V. V. P., Verma, R. R., Verma, P. S. & Srivastava, A. K., 2014. Steady State Thermal Analysis of Shell and Tube Type Heat Exchanger to Demonstrate the Heat Transfer Capabilities of Various Thermal Materials using Ansys. Global Journal of Researches in Engineering: A Mechanical and Mechanics Engineering, 14(4), pp. 25-30.

Edreis, E. & Petrov, A., 2020. Types of heat exchangers in industry, their advantages and disadvantages, and the study of their parameters. IOP Conference Series: Materials Science and Engineering, Volume 963.

Edwards, J. E., 2000. Process Modelling Selection of Thermodynamic Methods, s.l.: UK CHEMCAD Seminar.

Eveloy, V. & Gebreegziabher, T., 2018. A Review of Projected Power-to-Gas Deployment Scenarios. MDPI:Energies, Volume 11, pp. 1-52.

Fan, L. T. & Friedler, F., 1997. Reaction Pathway Analysis by a Network Synthesis Technique. Los Angeles, USA, s.n.

Fan, L. T., Lin, Y. C., Shafie, S., Hohn, K. L., Bertok, B. & Friedler, F., 2008. Graph-theoretic and energetic exploration of catalytic pathways of the water-gas shift reaction. Journal of the Chinese Institute of Chemical Engineers, Volume 39, pp. 467-473.

Fan, L. T., Bertok, B. & Friedler, F., 2002. A graph-theoretic method to identify candidate mechanisms for deriving the rate law of a catalytic reaction. Computers and Chemistry, Volume 26, pp. 265-292.

Fan, L. T., Bertok, B., Friedler, F. & Shafie, S., 2001. Mechanisms of ammonia-synthesis reaction revisited with the aid of a novel graph-theoretic method for determining candidate mechanisms in deriving the rate law of a catalytic reaction. Hungarian Journal of Industrial Chemistry, 29(1), pp. 71-80.

Fan, Y. J. & Wu, S. F., 2016. A graphene-supported copper-based catalyst for the hydrogenation of carbon dioxide to form methanol. Journal of CO_2 Utilization, Volume 16, pp. 150-156.

Feng, G., Fan, L. T. & Friedler, F., 2000. Synthesizing alternative sequences via a P-graph-based approach in azeotropic distillation systems. Waste Management, Volume 20, pp. 639-643.

Florez, A. A. G., 2018. Spiral Tube Heat Exchangers, Variables that Affect its Normal Behavior, Colombia: Industrial University of Santander.

Fornari, T. & Stephanopoulos, G., 1994. Synthesis of Chemical Reaction Paths: Economic and Specification Constraints. Chemical Engineering Communications, 129(1), pp. 159-182.

Fornari, T., Rotstein, E. & Stephanopolous, G., 1989. Studies on the synthesis of chemical reaction paths—II. reaction schemes with two degrees of freedom. Chemical Engineering Science, 44(7), pp. 1569-1579.

Friedler, F., Aviso, K. B., Bertok, B., Foo, D. C. Y. & Tan, R. R., 2019. Prospects and challenges for chemical process synthesis with the P-Graph. Current Opinion in Chemical Engineering, Volume 26, pp. 58-64.

Friedler, F., Blicklet, T., Gyenis, J. & Tarjan, K., 1979. Computerized Generation of Technological Structures. Computers & Chemical Engineering, Volume 3, pp. 241-249.

Friedler, F., Tarjan, K., Huang, Y. W. & Fan, L. T., 1992. Combinatorial Algorithms for Process Synthesis. Computers and Chemical Engineering, 16(1), pp. S313-S320.

Friedler, F., Tarjan, K., Huang, Y. W. & Fan, L. T., 1992. Graph-theoretic approach to process synthesis: Axioms and Theorems. Chemical Engineering Science, 47(8), pp. 1973-1988.

Friedler, F., Tarjan, K., Huang, Y. W. & Fan, L. T., 1993. Graph-theoretic Approach to Process Synthesis: Polynomial Algorithm for Maximal Structure Generation. Computers & Chemical Engineering, 17(9), pp. 929-942.

Friedler, F., Verga, J. B. & Fan, L. T., 1995. Decision-mapping: A tool for consistent and complete decisions in process synthesis. Chemical Engineering Science, 50(11), pp. 1755-1768.

Gaikwad, R., Bansode, A. & Urakawa, A., 2016. High-pressure advantages in stoichiometric hydrogenation of carbon dioxide to methanol. Journal of Catalysis, Volume 343, pp. 127-132.

Gas Processors Suppliers Association, 2004. Engineering Data Book. 12th ed. Oklahoma: Gas Processors Suppliers Association.

Gebremariam, S. N. & Marchetti, J. M., 2019. The effect of economic variables on a bio-refinery for biodiesel production using calcium oxide catalyst. Biofuels Bioproducts and Biorefining , 13(5), pp. 1-14.

Geimer, C., 2014. CO_2 Capturing using Lime, Germany: FIZ Karlsruhe - Leibniz Institute for Information Infrastructure.

Ghazouani, A., Xia, W., Jebli, M. B. & Shahzad, U., 2020. Exploring the Role of Carbon Taxation Policies on CO2 Emissions: Contextual Evidence from Tax Implementation and Non-Implementation European Countries. Sustainability (MDPI), Volume 12, pp. 1-16.

Giuliano, A., Catizzone, E. & Freda, C., 2021. Process Simulation and Environmental Aspects of Dimethyl Ether Production from Digestate-Derived Syngas. International Journal of Environmental Research and Public Health, Volume 18, pp. 1-21.

Gnanamani, M. K., Jacobs, G., Keogh, R. A., Shafer, W. D., Sparks, D. E., Hopps, S. D., Thomas, G. A. & Davis, B. H., 2015. Fischer-Tropsch synthesis: Effect of pretreatment conditions of cobalt on activity and selectivity for hydrogenation of carbon dioxide. Applied Catalysis A: General, Volume 499, pp. 39-45.

Golder, A. K. & Goud, V. V., 2018. Module #1: Process Design of Heat Exchanger. In: NPTEL - Chemical Engineering Design - II. s.l.:Joint initiative of IITs and IISc – Funded by MHRD, pp. 1-41.

Gotz, M., Lefebvre, J., Mors, F., Koch, A. M., Graf, F., Bajohr, S., Reimert, R. & Kolb, T., 2016. Renewable Power-to-Gas: A technological and economic review. Renewable Energy, Volume 85, pp. 1371-1390.

Govind, R. & Power, G. J., 1977. A Chemical Engineering View of Reaction Pathway Synthesis. ACS Symposium Series, Volume 61.

Gresh, M. T., 2018. Chapter 1 - Introduction to Aerodynamics. In: Compressor Performance Aerodynamics for the User (Third Edition). s.l.:Butterworth-Heinemann, pp. 3-11.

Guillen-Gosalbez, G., You, F., Galan-Martin, A., Pozo, C. & Grossmann, I. E., 2019. Process systems engineering thinking and tools applied to sustainability problems: current landscape and future opportunities. Current Opinion in Chemical Engineering, Volume 26, pp. 170-179.

Guzda, A. & Szmolke, N., 2015. Compressors in Heat Pumps. Machine Dynamics Research, 39(2), pp. 71-83.

Hangos, K. M., Friedler, F., Varga, J. B. & Fan, L. T., 1994. A graph-theoretic approach to integrated process and control system synthesis. IFAC Proceedings Volumes, 27(7), pp. 61-66.

Hankin, A. & Shah, N., 2017. Process exploration and assessment for the production of methanol and dimethyl ether from carbon dioxide and water. Sustainable Energy & Fuels, Volume 1, pp. 1541-1556.

Heaslip, B., 2008. Heat Exchangers, Canada: Queens University.

Heckl, I., Friedler, F. & Fan, L. T., 2010. Solution of separation-network synthesis problems by the P-graph methodology. Computers and Chemical Engineering, Volume 34, pp. 700-706.

Hegyhati, M. & Friedler, F., 2011. Combinatorial Algorithms of the S-Graph Framework for Batch Scheduling. Industrial and Engineering Chemistry Research, Volume 50, pp. 5169-5174.

Hill, D. & Justice, F. C., 2011. Understand Thermodynamics to Improve Process Simulations, Unite States of America: American Institute of Chemical Engineers (AIChE) CEP Magazine.

Hirano, M. & Yasutake, T., 2002. Dimethyl ether synthesis from carbon dioxide by catalytic hydrogenation (Part 1) Activities of methanol dehydration catalysts. Journal of the Japan Petroleum Institute, 45(3), pp. 169-174.

Hirano, M., Imai, T., Yasutake, T. & Kuroda, K., 2004. Dimethyl Ether Synthesis from Carbon Dioxide by Catalytic Hydrogenation (Part 2) Hybrid Catalyst Consisting of Methanol Synthesis and Methanol Dehydration Catalysts. Journal of the Japan Petroleum Institute, 47(1), pp. 11-18.

Hong, S. H., 2013. Catalytic Hydrogenation of Carbon Dioxide. Organic Chemistry Current Research, 2(2).

Honig, J. M., 2007. Chapter 3 - Characterization of Nonideal Solutions. In: Thermodynamics: Principles Characterizing Physical and Chemical Processes (Third Edition). Indiana: Academic Press, pp. 159-247.

Hu, J., Yu, L., Deng, J., Wang, Y., Cheng, K., Ma, C., Zhang, Q., Wen, W., Yu, S., Pan, Y., Yang, J., Ma, H., Qi, F., Wang, Y., Zheng, Y., Chen, M., Huang, R., Zhang, S., Zhao, Z., Mao, J., Meng, X., Ji, Q., Hou, G., Han, X., Bao, X., Wang, Y. & Deng, D., 2021. Sulfur vacancy-rich MoS_2 as a catalyst for the hydrogenation of CO_2 to methanol. Nature Catalysis, Volume 4, pp. 242-250.

Hus, M., Dasireddy, V. D., Stefancic, N. S. & Likozar, B., 2017. Mechanism, kinetics and thermodynamics of carbon dioxide hydrogenation to methanol on $Cu/ZnAl_2O_4$ spinel-type heterogeneous catalysts. Applied Catalysis B: Environmental, Issue 207, pp. 267-278.

Iggland , M. & Mazzotti, M., 2015. Introduction to Chemical Engineering for Lecture 7: Flash Distillation, Zurich, Switzerland: ETH Zurich, Institute of Process Engineering.

Jacimovic, B., Genic, S., Budimir, N. & Jaric, M., 2008. Criteria for the vapor space design in kettle reboilers. Scientific Bulletin of Transaction on Mechanics, 53(67), pp. 297-300.

Jadhav, S. G., Vaidya, P. D., Bhanage, B. M. & Joshi, J. B., 2014. Catalytic carbon dioxide hydrogenation to methanol A review of recent studies. Chemical Engineering Research and Design, Issue 92, pp. 2557-2567.

Jasper, S. & El-Halwagi, M. M., 2015. A Techno-Economic Comparison between Two Methanol-to-Propylene Processes. MDPI: Processes, 3(3), pp. 684-698.

Jassim, E., 2016. Spiral Coil Heat Exchanger - Experimental Study. Ottawa, Canada, Proceedings of the 3rd International Conference on Fluid Flow, Heat and Mass Transfer.

Javeline, D., Hellmann, J., McLachlan, J., Sax, D., Schwartz, M. & Cornejo, R., 2015. Expert opinion on extinction risk and climate change adaptation for biodiversity. Elementa Science of the Anthropocene, Volume 3, pp. 1-11.

Jean-Luc, D., Kazuhiro, S. & Hironori, A., 1992. Conversion of CO_2 to Dimethyl ether and Methanol over Hybrid Catalysts. CSJ Journals: Chemistry Letters, 21(7), pp. 1115-1118.

Jones, R. T., 1997. Thermodynamics and its applications – an overview. Randburg, SAIMM Pyrometallurgy School.

Joo, O. S., Jung, K. D., Moon, I., Rozovskii, A. Y., Lin, G. I., Han, S. H. & Uhm, S. J., 1999. Carbon Dioxide Hydrogenation to Form Methanol via a Reverse-Water-Gas-Shift Reaction (the CAMERE Process). Industrial & Engineering Chemistry Research, 38(5), pp. 1808-1812.

Jugmohan, J. & Madigoe, E., 2020. The P-Graph Network: A Tool for Solving Process Network Synthesis and Similar Styled Problems through Rigorous Superstructure Development and Combinatorial Algorithms. International Journal of Advances in Science, Engineering and Technology, 8(4), pp. 37-49.

Jugmohan, J., Majozi, T., North, B. & Mukoma, P., 2020. Systematic Synthesis Framework for the Generation of CO_2 and H_2 Sinks: The P-Graph Approach, Johannesburg: University of the Witwatersrand [MSc Thesis].

Jugmohan, J., Van der Merwe, J. & Bwalya, M., 2021. An Automated Systematic Synthesis Framework for Determining the Most Viable Reaction Pathway Prior to Extensive Design Procedures: The Conversion of CO2 to Value Added Products. International Research Journal of Advanced Engineering and Science, 6(1), pp. 254-260.

Kabeel, A. E. & Abdullah, A. S., 2016. Experimental Study of the New Bayonet Heat Exchanger. Journal of Energy Engineering, 142(1), p. 04015015.

Kajaste, R., Hurme, M. & Oinas, P., 2018. Methanol-Managing greenhouse gas emissions in the production chain by optimizing the resource base. AIMS Energy, 6(6), pp. 1074-1102.

Kakac, S. & Liu, H., 2002. Heat Exchangers: Selection, Rating and Thermal Design (Second Edition). In: Florida: CRC Press LLC, pp. 283-348.

Kalauz, K., Sule, Z., Bertok, B., Friedler, F. & Fan, L. T., 2012. Extending Process-Network Synthesis Algorithms with Time Bounds for Supply Network Design. Chemical Engineering Transactions, Volume 29, pp. 259-264.

Kar, S., Kothandaraman, J., Goeppert, A. & Prakash, S., 2018. Advances in catalytic homogeneous hydrogenation of carbon dioxide to methanol. Journal of CO2 Utilization, Volume 23, pp. 212-218.

Kayansayan, N., 1996. Thermal design method of bayonet-tube evaporators and condensers. International Journal of Refrigeration, 19(3), pp. 197-207.

Kayfeci, M., Kecebas, A. & Bayat, M., 2019. Solar Hydrogen Production. In: Processes, Systems and Technologies. s.l.:Academic Press, pp. 45-83.

Keith, D. W., Holmes, G., Angelo, D. S. & Heidel, K., 2018. A Process for Capturing CO_2 from the Atmosphere. Joule, 2(8), pp. 1573-1594.

Kettl, K. H., Niemetz, N., Sandor, N., Eder, M., Heckl, I. & Narodoslawsky, M., 2011. Regional Optimizer (RegiOpt) - Sustainable energy technology network solutions for regions. Computer aided chemical engineering, Volume 29, pp. 1959-1963.

Khorshidi, J. & Heidari, S., 2016. Design and Construction of a Spiral Heat Exchanger. Advances in Chemical Engineering and Science, Volume 6, pp. 201-208.

Klemes, J. J. & Varbanov, P. S., 2015. Spreading the Message: P-graph Enhancements: Implementations and Applications. Chemical Engineering Transactions, Volume 45, pp. 1333-1338.

Kolmetz, K. & Dwijayanti, A., 2013. Distillation Column Reboiler Selection, Sizing and Troubleshooting: Engineering Design Guidelines, Johor, West Malaysia: KLM Technology Group.

Kovacs, Z., Ercsey, Z., Friedler, F. & Fan, L. T., 2000. Separation-network synthesis: global optimum through rigorous super-structure. Computers and Chemical Engineering, Volume 24, pp. 1881-1900.

Lainez, J. M., Hegyhati, M., Friedler, F. & Puigjaner, L., 2010. Using S-graph to address uncertainty in batch plants. Clean Technologies and Environmental Policy, Volume 12, pp. 105-115.

Lakner, R., Bertok, B. & Friedler, F., 2018. Synthesis of startable reaction pathways. Chemical Engineering Transactions, Volume 70, pp. 1129-1134.

Larowski, A. & Taylor, M. A., 1983. Systematic procedure for selection of heat exchangers. Process Industries Division, Volume 197A, pp. 51-69.

Lean Manufacturing & Operations Management, 2019. Payback Period. [Online] Available at: http://www.leanmanufacture.net/kpi/paybackperiod.aspx [Accessed 18 January 2021].

Lees, F., 2012. Chapter 11 - Process Design. In: S. Mannan, ed. Lees' Loss Prevention in the Process Industries. Texas: Butterworth-Heinemann, pp. 443-508.

Leonzio, G., Zondervan, E. & Foscolo, P. U., 2019. Methanol production by CO_2 hydrogenation: Analysis and simulation of reactor performance. International Journal of Hydrogen Energy, Volume 44, pp. 7915-7933.

Li, M., Hu, S., Li, Y. & Shen, J., 2000. A Hierarchical Optimization Method for Reaction Path Synthesis. Industrial & Engineering Chemistry Research, Volume 39, pp. 4315-4319.

Li, M., Hu, S., Li, Y. & Shen, J., 2000. Reaction path synthesis for a mass closed-cycle system. Computers and Chemical Engineering, Volume 24, pp. 1215-1221.

Li, S. & Zhou, C., 2017. Heat transfer analysis of scraped surface heat exchanger. Advances in Engineering Research, Volume 125, pp. 84-88.

Lin, Y. L., 1994. Application of a Generalized Quartic Equation of State to Pure Polar Fluids, Knoxville: University of Tennessee.

Liu, R. W., Qin, Z. Z., Ji, H. B. & Su, T. M., 2013. Synthesis of Dimethyl Ether from CO_2 and H2 Using a Cu–Fe–Zr/HZSM-5 Catalyst System. Industrial & Engineering Chemistry Research, 52(47), pp. 16648-16655.

Lock, G. S. & Minhas, H., 1997. Bayonet Tube Heat Exchanger. Applied Mechanics Reviews, 50(8), pp. 445-473.

Lopez-Echeverry, J. S., Reif-Acherman, S. & Araujo-Lopez, E., 2017. Peng-Robinson equation of state: 40 years through cubics. Fluid Phase Equilibria, Volume 447, pp. 39-71.

Low, C. X., Ng, W. Y., Putra, Z. A., Aviso, K. B., Promentilla, M. A. B. & Tan, R. R., 2020. Induction approach via P-Graph to rank clean technologies. Heliyon, Volume 6, p. e03083.

Maheshwari, D. & Trivedi, K., 2016. Experimental Investigation of U-tube heat exchanger using Plain tube and Corrugated tube. International Research Journal of Engineering and Technology (IRJET), 3(5), pp. 1931-1936.

Maier, S. & Narodoslawsky, M., 2014. Optimal Renewable Energy Systems for Smart Cities. Computer Aided Chemical Engineering, Volume 33, pp. 1849-1854.

Mansour, E. M., 2020. Equation of State, Cairo, Egypt: IntechOpen.

Matzen, M. & Demirel, Y., 2016. Methanol and dimethyl ether from renewable hydrogen and carbon dioxide: Alternative fuels production and life-cycle assessment. Journal of Cleaner Production, Volume 139, pp. 1068-1077.

McEwan, M. W. & Beveridge, G. S., 1965. Process optimization at the design stage with objective function linear in profit and investment. Chemical Engineering Science, Volume 20, pp. 987-995.

McGlashan, N., Shah, N., Caldecott, B. & Workman, M., 2012. High-level techno-economic assessment of negative emissions technologies. Process Safety and Environmental Protection, Volume 90, pp. 501-510.

McLaren, D., 2012. A comparative global assessment of potential negative emissions technologies. Process Safety and Environmental Protection, Volume 90, pp. 489-500.

Metcalfe, I. S., Ray, B., Dejoie, C., Hu, W., De Leeuwe, C., Dueso, C., Garcia-Garcia, F. R., Mak, C. M., Papaioannou, E. I., Thompson, C. R. & Evans, J. S. O., 2019. Overcoming chemical equilibrium limitations using a thermodynamically reversible chemical reactor. Nature Chemistry, Volume 11, p. 638–643.

Meunier, N., Chauvy, R., Mouhoubi, S., Thomas, D. & De Weireld, G., 2020. Alternative production of methanol from industrial CO_2. Renewable Energy, Volume 146, pp. 1192-1203.

Miguel, C. V., Soria, M. A., Mendes, A. & Madeira, L. M., 2015. Direct CO2 hydrogenation to methane or methanol from post-combustion exhaust streams - A thermodynamic study. Journal of Natural Gas Science and Engineering, Issue 22, pp. 1-8.

Mohitpour, M., Botros, K. K. & Van Hardeveld, T., 2008. Pipeline Pumping and Compression Systems: A Practical Approach. 3rd ed. s.l.:ASME Press.

Mukherjee, R., 1998. Effectively Design Shell-and-Tube Heat Exchangers. Chemical Engineering Progress.

Nakyai, T. & Saebea, D., 2019. Energy and exergy analyses of dimethyl ether production using CO and CO2 hydrogenation. International Journal of Smart Grid and Clean Energy, pp. 544-549.

Olah, G. A., 2005. Beyond Oil and Gas: The Methanol Economy. Angewandte Chemie International Edition, Volume 44, pp. 2636-2539.

Olah, G. A., Goeppert, A. & Surya Prakash, G. K., 2009. Chemical Recycling of Carbon Dioxide to Methanol and Dimethyl Ether: From Greenhouse Gas to Renewable, Environmentally Carbon Neutral Fuels and Synthetic Hydrocarbons. The Journal of Organic Chemistry Perspectives, 74(2), pp. 487-498.

Ong, B. H. Y., Walmsley, T. G., Atkins, M. J., Walmsley, M. R. W. & Neale, J. R., 2016. Approximation of Non-linear Cost Functions in P-graph Structures. Chemical Engineering Transactions, Volume 52, pp. 1093-1098.

Oritz, C., Valverde, J. M., Chacartegui, R. & Perez-Maqueda, L. A., 2018. Carbonation of Limestone Derived CaO for Thermochemical Energy Storage: From Kinetics to Process Integration in Concentrating Solar Plants. ACS Sustainable Chemistry & Engineering, Volume 6, pp. 6404-6417.

Otaraku, I. & Onyekaonwu, C., 2018. Process Design of Associated Natural Gas to Dimethyl Ether Production Via Direct Synthesis. International Journal of Chemical and Process Engineering, 5(1), pp. 1-7.

Ozkul, F. B. & Kayabasi, E., 2018. A general overview on distillation columns and column circuits. Karabuk, Turkey, 14th International Combustion Symposium (INCOS2018).

Palmer, C. & Chung, P. W., 2000. Creating Signed Directed Graph Models for Process Plants. Industrial & Engineering Chemistry Research, 39(7), p. 2548–2558.

Perera, F., 2017. Pollution from Fossil-Fuel Combustion is the Leading Environmental Threat to Global Pediatric Health and Equity: Solutions Exist. International Journal of Environmental Research and Public Health, 15(16), pp. 1-17.

Perez-Fortes, M., Schoneberger, J. C., Boulamanti, A. & Tzimas, E., 2016. Methanol synthesis using captured CO2 as raw material: Techno-economic and environmental assessment. Applied Energy, Volume 161, pp. 718-732.

P-Graph, 2015. P-Graph Studio. [Online] Available at: http://p-graph.com/ [Accessed 27 May 2020].

Pohorecki, R., Bridgwater, J., Molzahn, M., Gani, R. & Gallegos, C., 2010. Process Economics. In: Chemical Engineering and Chemical Process Technology - Volume IV: Process Development, Modeling, Optimization, Control and Process. EOLSS Publications: s.n., pp. 311-337.

Rabah, A. A., 2014. Heat Exchangers: Design, Operation, Maintenance and Enhancement, Khartoum, Sudan: University of Khartoum.

Ramachandran, S., Kalaichelvi, P. & Sundaram, S., 2008. Heat Transfer Studies in a Spiral Plate Heat Exchanger for Water - Palm Oil Two Phase System. Brazilian Journal of Chemical Engineering, 25(3), pp. 483-490.

Ramdharee, S., Muzenda, E. & Belaid, M., 2013. A Review of the Equations of State and their Applicability in Phase Equilibrium Modeling. Johannesburg, South Africa, s.n.

Rotstein, E., Resasco, D. & Stephanopoulos, G., 1982. Studies on the Synthesis of Chemical Reaction Paths- I: reaction Characteristics in the (G,T) Space and a Primitive Synthesis Procedure. Cheimcal Engineering Science, 37(9), pp. 1337-1352.

Roy, S., Karim, A. U. & Dilnowshin, M., 2019. U-Tube Type Shell & Tube Heat Exchanger, Bangladesh: Bangladesh University of Engineering and Technology.

Rui, N., Zhang, F., Sun, K., Liu, Z., Xu, W., Stavitski, E., Senanayake, S. D., Rodreguez, J. A. & Liu, C. J., 2020. Hydrogenation of CO_2 to Methanol on a Auδ+–In_2O_3–x Catalyst. ACS Catalysis, 10(19), pp. 11307-11317.

Sanchez-Bayo, F. & Wyckhuys, K. A., 2019. Worldwide decline of the entomofauna: A review of its drivers. Biological Conservation, Volume 232, pp. 8-27.

Sanmarti, E., Friedler, F. & Puigjaner, L., 1998. Combinatorial technique for short term scheduling of multipurpose batch plants based on schedule-graph representation. Computers & Chemical Engineering, 22(1), pp. S847-S850.

Sanmarti, E., Holczinger, T., Puigjainer, L. & Friedler, F., 2002. Combinatorial Framework for Effective Scheduling of Multipurpose Batch Plants. AIChE Journal, 48(11), pp. 2557-2570.

Santos, A., Barbosa-Povoa, A. & Carvalho, A., 2018. Life cycle assessment in chemical industry - a review. Current Opinion in Chemical Engineering, Volume 26, pp. 139-147.

Schmelz, W. J., Hochman, G. & Miller, K. G., 2020. Total cost of carbon capture and storage implemented at a regional scale: northeastern and midwestern United States. Royal Society: Interface Focus, 10(5).

Schobeiri, M. T., 2017. Introduction, Gas Turbines, Applications, Types. In: Gas Turbine Design, Components and System Design Integration. s.l.:Springer, Cham, pp. 1-30.

Seo, H., Lee, D. -Y., Park, S., Fan, L. T., Shafie, S., Bertok, B. & Friedler, F., 2001. Graph-theoretical identification of pathways for biochemical reactions. Biotechnology Letters, Volume 23, pp. 1551-1557.

Sepiacci, P. & Manca, D., 2015. Economic Assessment of Chemical Plants Supported by Environmental and Social Sustainability. Chemical Engineering Transactions, Volume 43, pp. 2209-2214.

Serth, R. W., 2007. Air-Cooled Heat Exchangers. In: Process Heat Transfer. Texas: Academic Press, pp. 629-680.

Shenoy, U. V., 2010. Targeting and design of energy allocation networks for carbon emission reduction. Chemical Engineering Science, Volume 65, pp. 6155-6168.

Singh, B. R. & Singh, O., 2012. Study of Impacts of Global Warming on Climate Change: Rise in Sea Level and Disaster Frequency. Global Warming - Impacts and Future Perspective, September.

Skogestad, S., 2009. Flash calculations. In: Chemical and Energy Process Engineering. Florida: CRC Press, pp. 64-66.

Smidla, J. & Heckl, I., 2010. S-graph Based Scheduling method for Parallel Architecture. Chemical Engineering Transactions, Volume 21, pp. 937-942.

Smith , R. & Linnhoff, B., 1988. The design of separators in the context of overall processes. Chemical Engineering Research and Design, pp. 195-228.

Smith, J. M., Van Ness, H. C., Abbott, M. M. & Swihart, M. T., 2018. Introduction to Chemical Engineering Thermodynamics. 8th ed. New York: McGraw-Hill Education.

Sorokes, J. M., 2013. Selecting a Centrifugal Compressor. American Institute of Chemical Engineers (AIChE) CEP Magazine, June, pp. 44-51.

Sorsamaki, L. & Nappa, M., 2015. Design and selection of separation processes, Finland: VTT Technical Research Centre of Finland Ltd.

Spreight, J. G., 2020. 4 - Distillation. In: The Refinery of the Future (Second Edition). United States: Gulf Professional Publishing, pp. 125-159.

Sridhar, K. & Bicha, K., 2017. Comparative Analysis of Parallel and Counter Flow Heat Exchangers. International Journal of Scientific Engineering and Technology Research, 6(4), pp. 638-644.

Stauffer, E., Dolan, J. A. & Newman, R., 2008. CHAPTER 4 - Chemistry and Physics of Fire and Liquid Fuels. In: Fire Debris Analysis. s.l.:Academic Press, pp. 85-129.

Stewart, M. I., 2014. Chapter Two - Basic Principles. In: Surface Production Operations (Third Edition). Virginia: Gulf Professional Publishing, pp. 9-37.

Sule, Z., Bertok, B., Friedler, F. & Fan, L. T., 2011. Optimal Design of Supply Chains by P-graph Framework under Uncertainties. Chemical Engineering Transactions, Volume 25, pp. 453-458.

Szlama, A. G., Kalauz, K., Bertok, B. & Heckl, I., 2012. Solving a separation-network synthesis problem by interval global optimization technique. Chemical Engineering Transactions, Volume 29, pp. 1525-1530.

Tan, R. R. & Aviso, K. B., 2016. An extended P-graph approach to process network synthesis for multi-period operations. Computer and Chemical Engineering, Volume 85, pp. 40-42.

Tan, R. R., Aviso, K. B., Klemes, J. J., Lam, H. L., Varbanov, P. S. & Friedler, F., 2018. Towards Generalized Process Networks: Prospective New Research Frontiers for the P-graph Framework. Chemical Engineering Transactions, Volume 70, pp. 92-96.

Tan, R. R., Aviso, K. B. & Foo, D. C., 2017. P-graph and Monte Carlo simulation approach to planning carbon management networks. Computers and Chemical Engineering, Volume 106, pp. 872-882.

Tan, R. R., Aviso, K. B., Heulgas, A. P. & Promentilla, M. A. B., 2014. Fuzzy AHP approach to selection problems in process engineering involving quantitative and qualitative aspects. Process Safety and Environmental Protection, Volume 92, pp. 467-475.

Tang, K., 2016. Design and Analysis of a Newly Installed Plate Heat Exchanger Apparatus for the WPI Unit Operation Laboratory Course, Massachusetts: Worcester Polytechnic Institute.

Towler, G. & Sinnott, R., 2008. Separation Columns (Distillation, Absorption and Extraction). In: Chemical Engineering Design: Principles, Practice and Economics of Plant and Process Design. United States of America: Butterworth-Heinemann (Elsevier), pp. 641-792.

Towler, G. & Sinnott, R., 2012. Chemical Engineering Design: Principles, Practice and Economics of Plant and Process Design. 2nd ed. s.l.:Elsevier.

Tursunov, O., Kustov, L., Kustov, A. & Travyanov, A., 2017. A Brief Review of CO_2 Hydrogenation to Methanol over Cu- And Fe- Based Catalysts, New York: 48th IASTEM International Conference.

Turton, R., Bailie, R. C., Whiting, W. B. & Shaeiwitz, J. A., 2009. Analysis, Synthesis, and Design of Chemical Processes. 3rd ed. Boston : Pearson Education, Inc..

U.S. Department of Energy, 1993. Heat Exchanger Fundamentals. In: DOE Fundamentals Handbook: mechanical Science Volume 1 of 2. Tennessee: s.n., pp. 1-18.

U.S. Department of Energy, 2006. Improving Pumping System Performance: A Sourcebook for Industry SEcond Edition. Washington: U.S. Department of Energy.

Van Amsterdam, M. F., De Haan, A. & Stankiewicz, A., 2018. Factorial Techniques applied in Chemical Plant Cost Estimation: A Comparative Study based on Literature and Cases, Delft, Netherlands: Delft University of Technology.

Van der Ham, L. G. J., Van den Berg, H., Benneker, A., Simmelink, G., Timmer, J. & Van Weerden, S., 2012. Hydrogenation of Carbon Dioxide for Methanol Production. Chemical Engineering Transactions, Volume 29, pp. 181-186.

Van Koningsveld, H., Jansen, J. C. & Van Bekkum, H., 1990. The monoclinic framework structure of zeolite H-ZSM-5. Comparison with the orthorhombic framework of as-synthesized ZSM-5. Zeolites, 10(4), pp. 235-242.

Vance, L., Cabezas, H., Heckl, I., Bertok, B. & Friedler, F., 2013. Synthesis of Sustainability Energy Supply Chain by the P-graph Framework. Industrial and Engineering Chemistry Research, Volume 52, pp. 266-274.

Vance, L., Heckl, I., Bertok, B., Cabezas, H. & Friedler, F., 2015. Designing sustainable energy supply chains by the P-graph method for minimal cost, environmental burden, energy resources input. Journal of Cleaner Production, Volume 94, pp. 144-154.

Vanhove, A., 2015. Improvements on the design of carbon dioxide conversion to methanol process using Aspen Plus ® interface, Lisbon: Instituto Superior Técnico.

Varbanov, P. & Friedler, F., 2008. P-graph methodology for cost-effective reduction of carbon emissions involving fuel cell combined cycles. Applied Thermal Engineering, Volume 28, pp. 2020-2029.

Varbanov, P. S., Friedler, F. & Klemes, J. J., 2017. Process Network Design and Optimisation Using P-graph: The Success, the Challenges and Potential Roadmap. Chemical Engineering Transactions, 61(10.3303/CET1761256), pp. 1549-1554.

Varga, T., Szepesi, G. & Simenfalvi, Z., 2017. Horizontal Scraped Surface Heat Exchanger - Experimental Measurements and Numerical Analysis. An International Journal for Engineering and Information Sciences, 12(1), pp. 107-122.

Varga, V., Heckl, I., Friedler, F. & Fan, L. T., 2010. PNS Solutions: a P-Graph Based Programming Framework for Process Network Synthesis. Chemical Engineering Transactions, Volume 21, pp. 1387-1392.

Viswanathan, M. B., Raman, D. R., Rosentrater, K. A. & Shanks, B. H., 2020. A Technoeconomic Platform for Early-Stage Process Design and Cost Estimation of Joint Fermentative-Catalytic Bioprocessing. MDPI: Processes, 8(2), p. 229.

Voll, P., Jennings, M., Hennen, M., Shah, N. & Bardow, A., 2015. The optimum is not enough: A near-optimal solution paradigm for energy systems synthesis. Energy, Volume 82, pp. 446-456.

Wang, Q. -Z., Chen, J. -M., Tseng, M. -L., Luan, H. -M. & Ali, M. H., 2020. Modelling green multimodal transport route performance with witness simulation software. Journal of Cleaner Production, Volume 248, pp. 1-12.

Wankat, P. C., 2011. Separation Process Engineering: Includes Mass Transfer Analysis (Third Edition). In: Massachusetts: Pearson Education, Inc., pp. 13-78.

Wankat, P. C., 2012. Flash Distillation. In: Separation Process Engineering (Includes Mass Transfer Analysis) Third Edition. United States of America: Pearson Education, Inc..

Wankat, P. C., 2012. Separation Process Engineering: Includes Mass Transfer Analysis (Third Edition). 3rd ed. Massachusetts: Pearson Education, Inc..

Waye, S. K., Lustbader, J., Musselman, M. & King, C., 2014. Air-Cooled Heat Exchanger for High-Temperature Power Electronics. San Diego, California, 2014 IEEE Compound Semiconductor IC Symposium.

Williams, J. B., Walters, T. & Han, D.-H., 2002. Double-Pipe Heat Exchanger, s.l.: s.n.

Woodcock, L. V., 2018. On failures of van der Waals' Equation at the Gas-Liquid Critical Point. International Journal of Thermophysics, 39(120), pp. 1-8.

Yaws, C. L., 1999. Chemical Properties Handbook: Physical, Thermodynamic, Environmental, Transport, Safety, and Health Properties for Organic and Inorganic Chemicals. In: New York, United States of America: McGraw-Hill, pp. 1-30.

Yeomans, H. & Grossmann, I. E., 1999. A systematic modeling framework of superstructure optimization in process synthesis. Computers and Chemical Engineering, Volume 23, pp. 709-731.

You, Z., Deng, W., Zhang, Q. & Wang, Y., 2013. Hydrogenation of carbon dioxide to light olefins over non-supported iron catalyst. Chinese Journal of Catalysis, 34(5), pp. 956-963.

Zare, K. B., Kanchan, D. & Patel, N., 2016. Design of Double Pipe Heat Exchanger. International Journal of Science Technology and Management, 5(12), pp. 161-174.

Zhanghuai, S. & Yuan, K., 2000. Synthesis of light hydrocarbons from carbon dioxide and hydrogen over Fe/ZrO2 or Fe/TiO2 catalyst. Journal of Natural Gas Chemistry, 9(4), pp. 283-290.

Zharov, A. A., Garanov, S. A., Talyzin, M. S. & Kovalchuk, N. A., 2019. Carbon dioxide and dimethyl ether mixture as a refrigerant for air conditioning systems for space ground-based infrastructure. AIP Conference Proceedings, 2171(1).

Zhou, J.-G., Li, L.-L., Tseng, M.-L. & Lin, G.-Q., 2020. Green system reliability assessment method based on life cycle: Resources and economical view. Journal of Cleaner Production, Volume 251, pp. 1-11.

Zhu, M., Ge, Q. & Zhu, X., 2020. Catalytic Reduction of CO_2 to CO via Reverse Water Gas Shift Reaction: Recent Advances in the Design of Active and Selective Supported Metal Catalysts. Transactions of Tianjin University, 28(18), pp. 172-187.

Appendix

Appendix A: Process Unit Operations (Background Information)

Presented in this section is a brief overview of various process unit operations, including heat exchangers, pressure-changing unit operations and separations systems, i.e., flash drums and distillation columns. For further information on any of these unit operations, please refer to Coulson and Richardson's Chemical Engineering textbooks.

A.1. Heat Exchanger Unit Operations

A heat exchanger is a unit operation that is focused on the transfer of thermal energy between two or more substances, comprising of a fluid and a working surface exhibiting different temperatures. It is essential, that a temperature difference exist between these two species, as a means by which to promote the necessary heat transfer for temperature adjustment, with heat transfer being able to occur between any two phases, such as between a solid and a liquid, a gas and a solid and so forth (Edreis & Petrov, 2020). Furthermore, heat exchangers are an integral part of any process system, to allow for the recovery of heat, to maximize energy efficiency (Chaudhari & Adroja, 2014). This section focuses on the categories and types of heat exchangers pertinent to this research.

A.1.1. Heat Exchanger Categories

Heat exchangers are often regarded as being one of the most integral unit operations in a process, essentially providing a mechanism that is able to promote the transfer of energy and achieving the necessary reaction conditions. There are many different types of heat exchangers, with the chosen type being dependent on its use, however, heat exchangers can be divided into ten overall categories as detailed in Table A.1 below.

Table A.1: Various categories of heat exchanger unit operations and their purpose (Edreis & Petrov, 2020)

Heat Exchanger Category	Description
Chiller	These are heat exchangers that are focused on the cooling of a liquid through a refrigeration cycle, requiring the use of a refrigerant, which includes chlorofluorocarbons and hydrochlorofluorocarbons.
Condenser	These heat exchangers are focused on a phase change from vapor to liquid, with the desired substance being in the presence of non-condensing gases.
Cooler	These are heat exchangers that are focused on the reduction in temperature of a liquid or gas stream. Such temperature drops are often accomplished with the use of water as the heat exchanger utility.
Heat Exchanger	These unit operations focus on the transfer of heat between two fluids, allowing for one of the substances to be lowered in temperature, whilst the other is heated. This is often utilized in heat transfer networks, allowing for optimal allocation of energy within the process.
Heater	A heater focuses on increasing the temperature of any liquid or gas, through its contact with a heated surface.
Reboiler	These heat exchangers are used in generating steam. Through the utilization of a heating coil, this unit operation is involved in the phase change of a liquid to a vapor, and is often utilized in distillation processes.
Thermosiphon reboiler	These heat exchangers make use of the pressure within the unit operation as a means by which to promote the natural occurrence of converting a liquid to its vapor, i.e., boiling.
Forced circulation reboiler	The utilization of a pumping unit operation as a means to constantly circulate fluid within the reboiler.
Superheater	This heat exchanger is focused primarily around the heating of a stream beyond its boiling point. Often used in the case of saturate steam, this provides a mechanism, by which to

	generate the utility required for the operation of steam engines, and turbines utilized in the production of electricity.
Evaporator	This unit operation focuses on the phase change from liquid to vapor, focusing on complete or partial evaporation of the stream contents.

Section A.1.2 to Section A.1.11 covers the different types of heat exchanger unit operations considered within this research study.

A.1.2. Scraped Wall Heat Exchanger

Also referred to as scraped surface heat exchangers, these unit operations are utilized for thermal transfers that occur between highly viscous fluids, or even sensitive products that may occur in industries such as the food industry. In such cases, the use of other, more conventional heat exchangers, such as shell and tube, or plate heat exchangers, are ineffective and to a large extent, considered to be impossible. This is due to the viscous nature of the fluids in question (Varga, *et al*., 2017).

With highly viscous fluids sediment builds up, which may render the other heat exchanger types inoperable, thereby reinforcing the need for the scraped surface/wall heat exchanger (Varga, *et al*., 2017).

The design of a scraped surface/wall heat exchanger comprises of blades, required for scraping the heat transfer surface, exposing the untreated fluid and allowing for this layer to be heated. A secondary function of these blades allows for the mixing and agitation of the fluid, preventing the aforementioned silt. A schematic view of this heat exchanger can be seen in Figure A.1 below, based on a two-blade system investigated by Li and Zhou (2017).

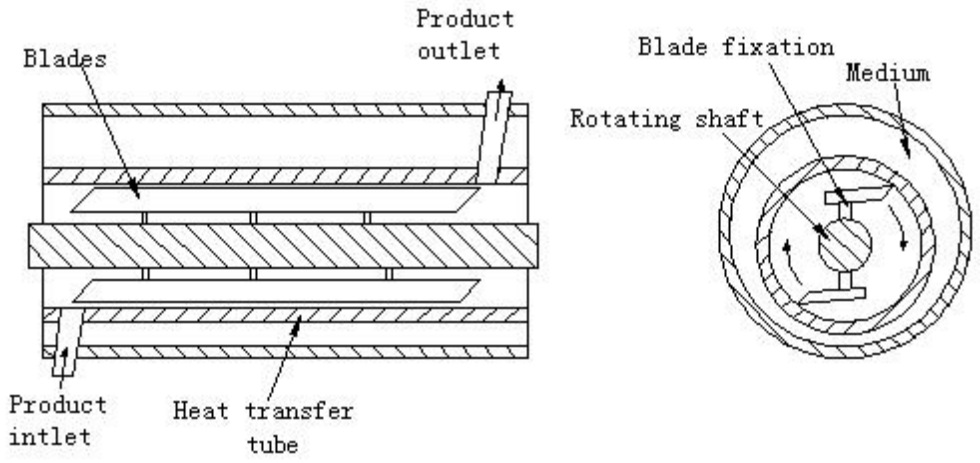

Figure A.1: Schematic representation of a scraped surface/wall heat exchanger containing two blades (Li & Zhou, 2017)

However, this heat exchanger can prove to be quite expensive, in terms of maintenance and mechanical cleaning, as this is a manual process (Varga, *et al.*, 2017). There are two main types of designs associated with a scraped surface heat exchanger, dictated by the rotating blade and the residence time in the heat exchanger, however both have proven to have high capital and operating costs. Furthermore, their designs are often considered to be very specific to the application, and therefore it is essential that they are considered, and designed, on a case-by-case basis (Larowski & Taylor, 1983).

A.1.3. Bayonet Heat Exchangers

The bayonet heat exchanger has a unique feature in that it allows for flow to move backwards within the unit operations, being referred to as a refluent heat exchanger unit operation. The design of a bayonet tube heat exchanger comprises of two concentric tubes, closed off at one end, where the fluid first flows within the inner tube, before being returned via the annular gap (Kabeel & Abdullah, 2016).

The need for these heat exchanges is especially important when the unit operation is required to penetrate a hard-to-reach area, such as below the Earth's surface (geotechnical engineering) and cannot be accessible to a traditional inlet/outlet conventional stream flow (Lock & Minhas, 1997). Other uses of the bayonet heat exchanger include internal circulation of refrigerants required to maintain ground water temperatures. In industrial settings, these unit operations are

typically utilized in suction tank heaters and counter flow heat exchangers within a chemical processing plant (Kabeel & Abdullah, 2016).

Recent research has found that such configurations are optimal in high temperature heat exchangers, as the remaining end of the heat exchanger is given the flexibility of being able to contract and expand freely. This is a key feature of the bayonet heat exchanger (Kayansayan, 1996). An investigation conducted by Kabeel and Abdullah (2016) found that the design of the bayonet tubes is integral in its efficiency, with an internal helical tape structure increasing the heat transfer area, but conversely having an increase in the friction factor. Furthermore, the presence of the helical tape increases the pressure drop over the heat exchanger, which could be advantageous in terms of decreasing the pump power required in the process (Kabeel & Abdullah, 2016). A diagrammatic representation of a bayonet heat exchanger can be seen in Figure A.2.

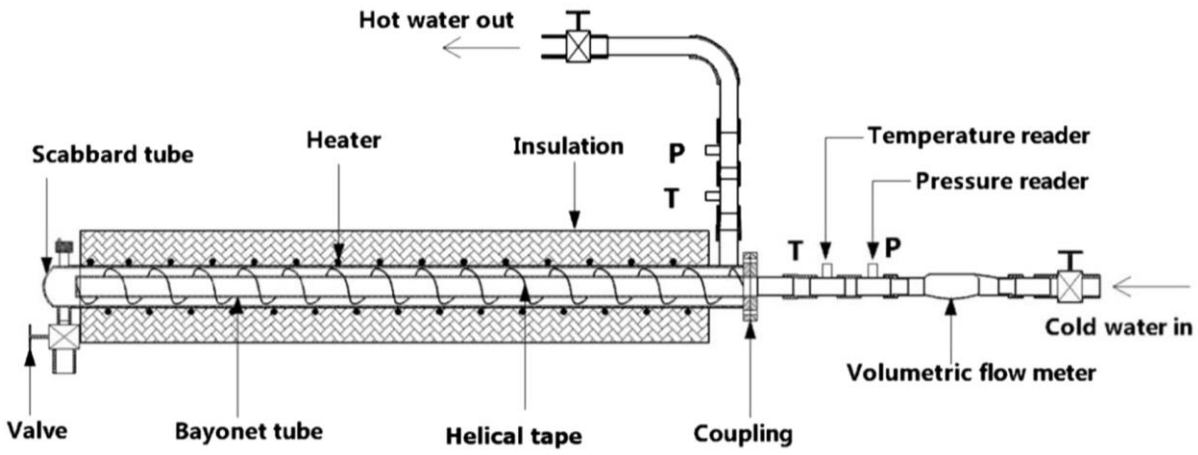

Figure A.2: Diagrammatic cross-section of a bayonet heat exchanger with a helical tape (Kabeel & Abdullah, 2016)

A.1.4. Floating Head Heat Exchangers

Floating head heat exchangers are characterized by the ability to remove tubes within the heat exchanger system, allowing for and promoting ease of cleaning and any replacements that may be necessary during the maintenance process. With a floating head heat exchanger, however, these tubes are stationery sheets fixed in place with a shell flange (Golder & Goud, 2018).

As a result, the opposite side of the sheet has the flexibility of expanding when necessary. Furthermore, the head cover of a floating head heat exchanger is fixed onto the aforementioned

floating sheet, thereby allowing for the entire system to be removed when cleaning. A schematic representation of this heat exchanger can be seen in Figure A.3 (Rabah, 2014).

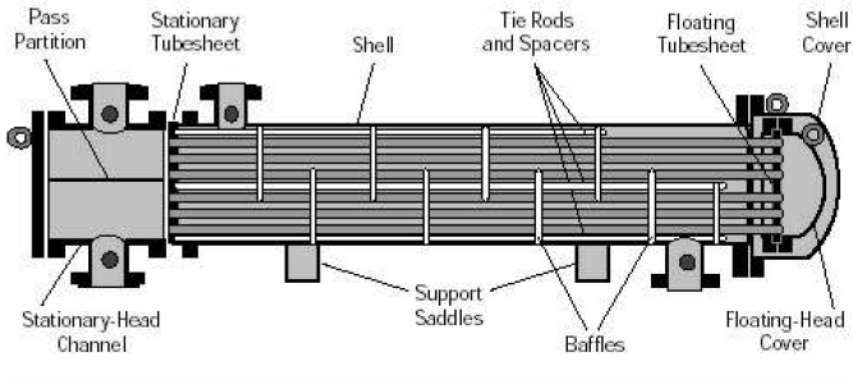

Figure A.3: Diagrammatic representation of a floating head heat exchanger (Rabah, 2014)

The disadvantage of a floating head heat exchanger is that these unit operations are not suitable in large thermal shock applications as the tubes act as a unit in expansions, and therefore are unable to expand independently. Furthermore, the unit operations are deemed to be quite costly (Mukherjee, 1998). despite their limitations in terms of their design pressures and temperatures. These heat exchangers were found to apply to unique and limited ranges of operating conditions (Golder & Goud, 2018).

A.1.5. Fixed Tube Heat Exchanger

Fixed tube heat exchangers are considered to be one of the simplest and cheapest heat exchanger constructions, whereby the tube sheet is welded to the shell, to allow for little to no movement between the shell and the tubes (Golder & Goud, 2018). Furthermore, the tubes that are found within this type of heat exchanger unit operation, are able to be cleaned mechanically, allowing for ease of maintenance. A schematic view of a fixed sheet heat exchanger unit operation can be seen in Figure A.4.

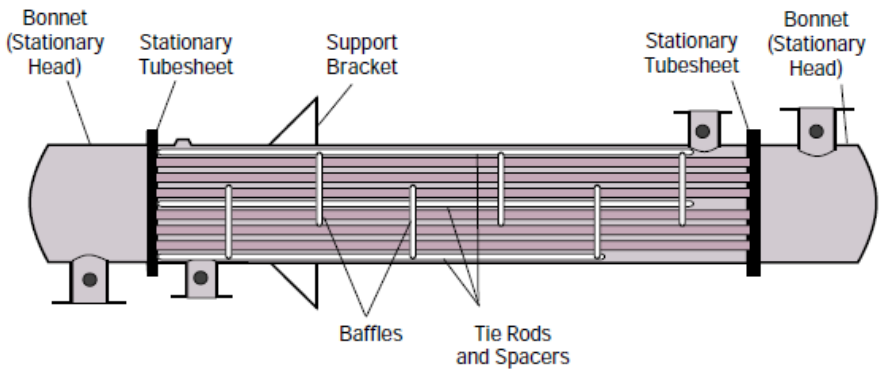

Figure A.4: Diagrammatic representation of a fixed-tube heat exchanger (Mukherjee, 1998)

The disadvantage of such unit operations, however, is that whilst the inner tubes of the unit can be cleaned mechanically, the fixed nature of the system prevents the outer tubes from being cleaned mechanically. As a result, this unit operation is only utilized in situations where only the shell side of the unit operation needs to be cleaned (Mukherjee, 1998), (Golder & Goud, 2018).

Despite the economic benefit realized by the low cost noted by the unit operation, there are concerns in operating this unit operation at large temperature differences, with the heat exchanger being unable to absorb the differential stress under these conditions. One possible solution in addressing this concern is the introduction of an expansion joint to the fixed tube heat exchanger, however, this can be quite costly, outweighing the advantage of the low cost associated with such units (Mukherjee, 1998).

A.1.6. U-Tube Heat Exchanger

The U-tube heat exchanger is similar to the floating tube heat exchanger, in that they are both able to have a removable tube bundle. However, within this heat exchanger unit operation, the tubes are bent into a ‘U’ shape, with the flow going back onto the tube sheet. Tubes are able to freely expand at the U-based end of the tube, however the tubes are unable to do so at the tube sheet (Golder & Goud, 2018). A diagrammatic representation of the U-tube heat exchanger can be seen in Figure A.5 below (Maheshwari & Trivedi, 2016).

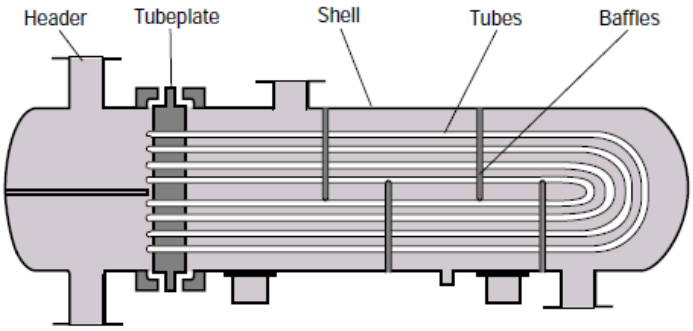

Figure A.5: Diagrammatic representation of the U-Tube heat exchanger (Maheshwari & Trivedi, 2016)

The advantage of such a design, however, is that it allows for the design of the unit operation to be more compact and more efficient, requiring less space due to its bent nature. Another advantage of these heat exchangers lies in their light weight and ease of repairing. Furthermore, these units have been noted to have reduced costs, as they are primarily constructed from copper tubes (Roy, *et al*., 2019).

The heat exchanger tubes do pose a concern in some systems, especially considering the possibility of corrosion within the heat exchanger unit operation, and it is for this reason that many processes consider and implement the use of stainless-steel tubes within these heat exchangers. This may increase the initial capital cost of the unit operation; however, it was also found that this reduces the frequency of maintenance of the unit operation, thereby providing an overall economic benefit to the plant (Roy, *et al*., 2019).

The concern with steel usage within the heat exchanger is that such occurrences lower the possible transferrable heat, reducing the efficiency of the heat exchanger under such conditions. Other disadvantages noted in these types of unit operations were their inability to deal with contaminated matter, as these may contain high levels of suspended particles, hindering the operation of the unit, and resulting in higher maintenance frequencies (Roy, *et al*., 2019).

Furthermore, the ‘U’ shape of the inner tubes can make the unit operation difficult to clean, and therefore it is important that it is utilized in conjunction with fluids that are unlikely to leave remnants or traces behind, in an attempt to maximize the life of the U-tube heat exchanger (Mukherjee, 1998). The orientation of the heat exchanger is especially important when draining the heat exchanger and can prove to be extremely difficult when in a vertical position (Golder & Goud, 2018).

A.1.7. Kettle Reboiler

A kettle reboiler heat exchanger is considered to be the most common form of an evaporator, often utilizing either a floating head or a U-type tube system as detailed in the previous sections, along with a large shell. It is important to note, however, that within a kettle reboiler the shell is much larger than the tubing system, allowing for the space between the two to promote the adequate separation of the liquid droplets from the produced vapour (Jacimovic, *et al.*, 2008). Figure A.6 shows a cross section of the space noted within a kettle reboiler allowing for the separation process, with H_{sep} representing the space between the liquid and vapour, i.e., the separation zone.

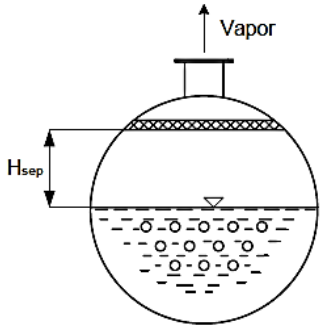

Figure A.6: Cross section of the space between liquid and vapour that exists in kettle reboilers (Jacimovic, et al., 2008)

These types of unit operations are utilized in cases where large heat transfer surfaces are needed, however as a result of the large area they are able to provide, they are also extremely costly. This makes their use specific to high temperature change systems. A kettle reboiler is generally paired with a distillation column, in the configuration shown in Figure A.7 (Heaslip, 2008).

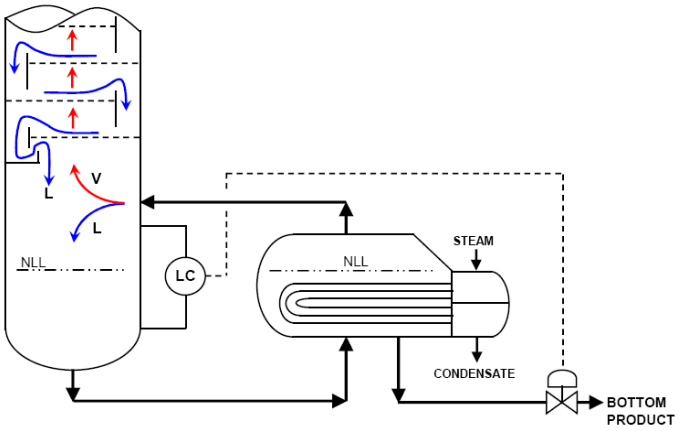

Figure A.7: Pairing of a kettle reboiler with the bottom stream of a distillation column (Heaslip, 2008)

A.1.8. Double Pipe Heat Exchanger

Double pipe heat exchanger systems are common in most processes and are able to perform the basic function of the transfer of heat from a hot fluid to a cold fluid by means of a cylindrical wall. Constructed from cylindrical pipes, these heat exchangers are considered to be inexpensive and easily maintained, and as a result are very attractive for implementation in chemical processes where a temperature change is required (Chaudhari & Adroja, 2014).

The design consists of one pipe, containing the process fluid, with a second fluid flowing in the gap between the outer layer of the pipe and the second pipe, i.e., the two pipes are placed in a concentric tube structure. The advantage of such a design lies in the dual flow configurations possible. In other words, the two fluids can either flow in the same direction, co-current flow, or in opposite direction, counter current flow (Williams, *et al*., 2002).

These heat exchangers are able to achieve high temperature changes and are effective in high pressure systems, due to the fact that they have small diameters (Chaudhari & Adroja, 2014). Figure A.8 shows the flow that is experienced within a double piped heat exchanger, in a co-current flow configuration.

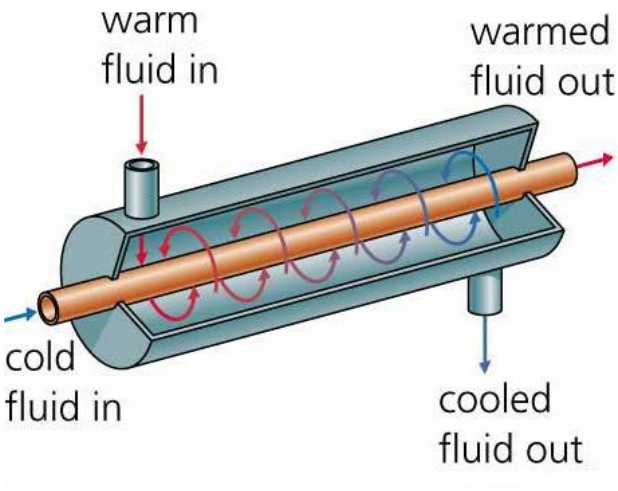

Figure A.8: Diagrammatic representation of the flow in a double-pipe heat exchanger (Zare, et al., 2016)

Heat exchangers with a counter current flow are the more common choice in industry as the heat transfer is much more effective, allowing for greater temperature changes. This is also due to an increased heat transfer surface area over which the fluid is exposed to the heating/cooling utility (Zare, *et al*., 2016). With either configuration, this type of heat exchanger does not have any direct contact between the fluid and the utility (Golder & Goud, 2018).

In some cases, the heat transfer and efficiency of the heat exchanger process can be increased by introducing multiple passes of the stream, thereby increasing the contact time and heat transfer surface. This can be achieved through the recycling of the stream within the heat exchanger, allowing for several passes, or the addition of multiple tubes/pipes to increase the contact time and surface area for smaller flows of the process stream (U.S. Department of Energy, 1993).

A.1.9. Plate Heat Exchanger

Plate heat exchangers are constructed using a number of stainless-steel plates that are separated by means of seals. Due to the fact that these plates are not separated using adhesive mixtures, the plates are close together, resulting in a constricted build within the heat exchanger configuration. Unlike the double piped heat exchanger, where flow configurations can either be co-current or counter-current, plate heat exchangers are only able to operate in with a counter-current flow configuration (Edreis & Petrov, 2020), as shown in Figure A.9.

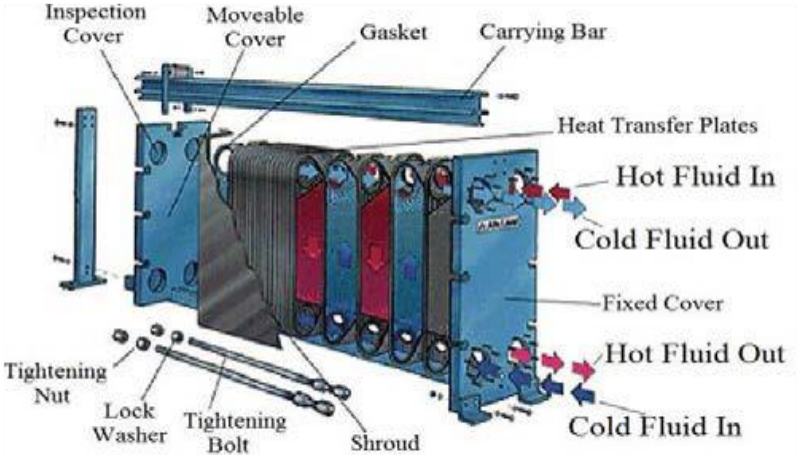

Figure A.9: Diagrammatic representation of a plate heat exchanger (Tang, 2016)

These heat exchangers are commonly utilized in the oil and gas industry, as they have proven to be highly efficient, due to the large heat transfer surface area. In fact, there are studies that report efficiencies as high as 95% with these configurations. The type of plate heat exchanger, and number of associated plates, is in direct proportion to the heating requirements of the process, with an increase in the number of plates resulting in a subsequent increase in heat transfer. This allows for the cost to be controlled by the number of plates within the unit operation (Edreis & Petrov, 2020).

The disadvantage of such unit operations, however, is that it can be difficult to maintain. During the maintenance or repair of plate heat exchangers, the entire unit must be stripped and deconstructed, before performing the repair and reassembling the unit. This can be expensive and time consuming. However, without any cleaning procedure, and subject to the fluid passing through the heat exchanger, such unit operations have been known to give a maximum service life of approximately three years. Therefore, if not cleaned and repaired, this shows the frequency with which these unit operations would need to be replaced (Edreis & Petrov, 2020).

As a result of the corrugated plates within the heat exchanger, the flow becomes turbulent, providing a self-cleaning effect, which is considered advantageous over double pipe heat exchangers. An added advantage of the plate heat exchanger is that it is more compact than double pipe heat exchangers, which allow for a greater capacity to be handled in a smaller space (Tang, 2016).

Plate heat exchangers can also exist within a spiral configuration, where the fluid flows in the centre of the heat exchanger, and the secondary fluid flows on the outside of the plate. The advantage of this configuration is that there is a lower pressure drop across the heat exchanger. Furthermore, the spiral configuration has proven to have fewer dead zones, resulting in minimal accumulation within the unit operation (Edreis & Petrov, 2020).

These designs, however, are the intellectual property of certain companies, resulting in limited manufacturers. Therefore, such configurations are more expensive, and can impact on the feasibility of a process (Edreis & Petrov, 2020).

A.1.10. Air-Cooled Heat Exchangers

Air-cooled heat exchangers are utilized as coolers within a process. As opposed to the utilization of other utilities for heat transfer, this configuration makes use of ambient air, in order to facilitate the heat transfer, and even condense the stream in question (Serth, 2007). However, the limitation of this heat exchanger is that it is unable to cool streams below a temperature that is 20^{o}C above the ambient air temperature (Edreis & Petrov, 2020). Figure A.10 shows the flow of air over the process stream within an air-cooled heat exchanger.

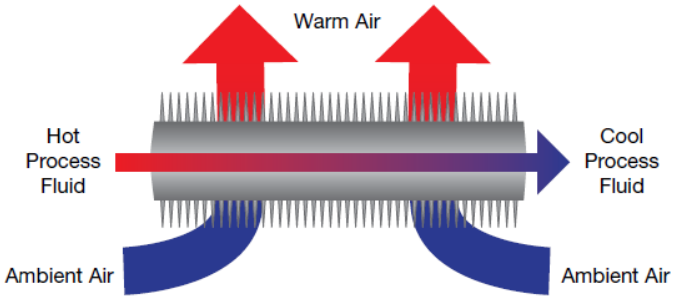

Figure A.10: Diagrammatic representation for the flow of air within an air-cooled heat exchanger (Boes, 2017)

One such system that employs the air-cooled heat exchangers is within the automotive field, where inverters are cooled with ambient air, negating the need for cooling water. The heat from the vehicle, generated through its operation, is expelled to the ambient air (Waye, *et al.*, 2014).

Whilst the advantage of such a heat exchanger is the fact that the utility is much cheaper, i.e., air instead of cooling water, the cost of the unit far outweighs the lowered utility cost. Due to the fact that air has a much lower heat transfer co-efficient, these heat exchangers need to be extremely large, in order to increase its heat transfer area (Edreis & Petrov, 2020).

Furthermore, there are many other considerations that have to be constantly accounted for within an air-cooled heat exchanger, such as the seasonal changes in air conditions and so forth. This would require adjustments to be made to the system, or provisions made when designing the system initially, once again increasing the cost of the system. These seasonal changes may also cause increased frequency in the maintenance of air-cooled heat exchangers (Edreis & Petrov, 2020).

The flow of air within an air-cooled heat exchanger can either be described as a forced draft or an induced draft and is dependent on the positioning of the fan in relation to the process stream flow. A forced draft has the fan situated below the stream flow, causing the air to be forced through the tubes, whereas in an induced flow the fan is situated above the flow, pulling the air through the tubes (Boes, 2017).

A.1.11. Spiral Tube Heat Exchanger

Traditionally, heat exchangers comprise of a flat or straight tubing structure, however it is possible to build a heat exchanger with a spiral coil, referred to as a spiral tube heat exchanger. These coils have a circular pattern and are enclosed within the heat exchanger shell

(Deshpande, 2020). Figure A.11 shows the spiral coils present within these heat exchanger unit operations.

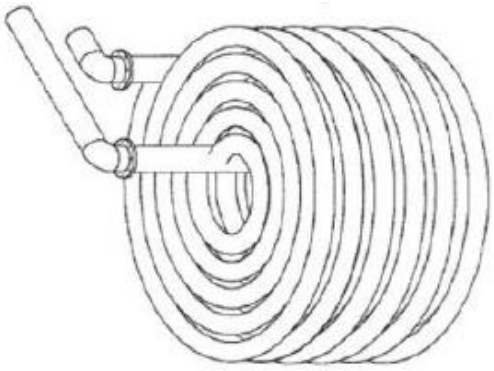

Figure A.11: Diagrammatic representation of the coil within spiral tube heat exchangers (Florez, 2018)

The coils, depicted in Figure A.11, are advantageous to the heat exchanger system as they provide a large heat transfer surface, increasing the efficiency of the unit operation, whilst simultaneously reducing the its associated size (Deshpande, 2020). Other advantages noted in these heat exchangers, include lower fouling rates and ease of maintenance. In fact, these heat exchangers are even able to handle low temperature fluids that are highly viscous (Ramachandran, *et al*., 2008), (Khorshidi & Heidari, 2016).

Overall, the aforementioned advantages of the spiral tube heat exchanger results in a lower operating and capital cost associated with these unit operations, thereby increasing the economic feasibility of the process in which it is utilized (Jassim, 2016).

The disadvantage of this configuration, however, aligns with that reported for the spiral plate heat exchangers. There are a limited number of manufacturers within this field, as the design of such heat exchangers are proprietary. As a result, these unit operations may be difficult to obtain, especially if they are to be designed for each specific process (Bhavsar, *et al*., 2013).

A.2. Pressure-Changing Unit Operations

Compressors and turbines are unit operations that are primarily focused on the change of pressure in a stream, with this change in pressure resulting in energy either being released or absorbed by the process, allowing for the possibility of energy integration. For example, when considering unit operations such as gas turbines, chemical energy that may be present within the stream is converted to mechanical energy, via shaft power. Alternatively, this chemical

energy can be converted to kinetic energy, which is utilized in systems such as aircrafts (Schobeiri, 2017). This section covers the various types of compressors and turbine unit operations, utilized and considered throughout the course of this research, as well as their associated advantages and disadvantages.

A.2.1. Centrifugal Compressor

A centrifugal compressor, also referred to as a radial compressor, is utilized extensively within chemical processes, providing a unit operation focused on the compression of fluids. This compression involves the reduction of the volume of the fluid, which can either be in the form of a gas, liquid, or a gas/liquid mixture (Sorokes, 2013).

However, as mentioned in Section 2.7. Equations of State, a thermodynamic relationship exists between the pressure, temperature and volume of any fluid. As a result, the lowering of the volume of the fluid, during this compression stage, will result in subsequent changes to the temperature and pressure of the fluid, as show in Figure A.12.

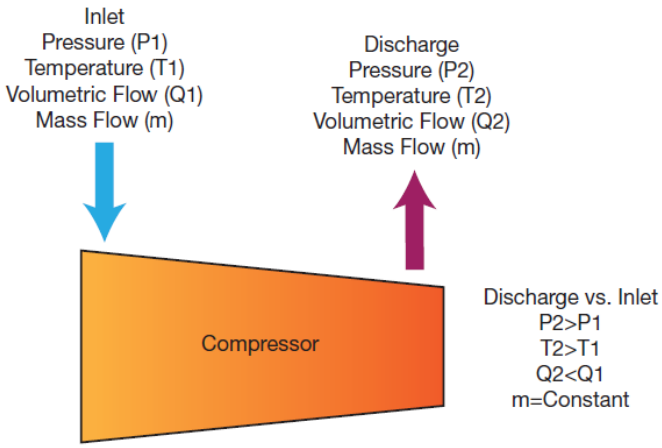

Figure A.12: Relationship that exists between the thermodynamic parameters surrounding a compressor (Sorokes, 2013)

A centrifugal compressor increases the pressure of a gas, by spinning the gas flow at a high speed. This spinning process further elevates the temperature of the gas within the unit operation. The power required to operate the centrifugal compressor is provided by an electric motor. Overall, a centrifugal compressor comprises an impellor, diffuser and a casing, as seen in the diagrammatic representation in Figure A.13 (Bandarkar, *et al.*, 2019).

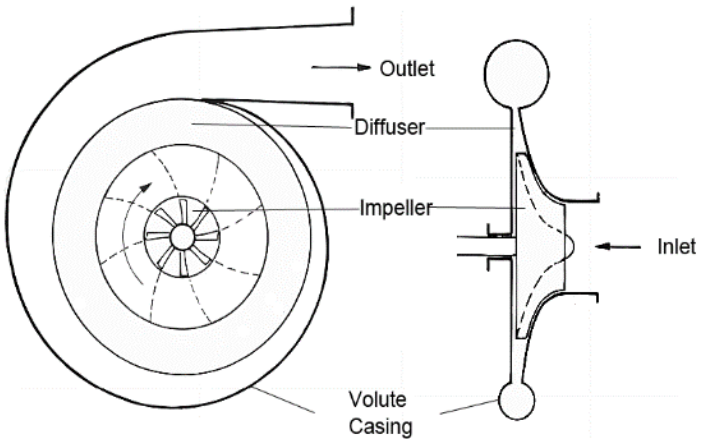

Figure A.13: Diagrammatic representation of a centrifugal compressor (Bandarkar, et al., 2019)

The advantage of a centrifugal compressor is that it has good reliability and is cheap to maintain. These unit operations have a wide range of pressures that they can be used for, thereby increasing the application of these compressors to various types of chemical processes. The disadvantage of these unit operations, however, lies in their unstable nature at low flow rates, coupled with their moderate efficiency. Therefore, these unit operations can often require large amounts of energy for their operation (Gresh, 2018).

A.2.2. Reciprocating Compressor

A reciprocating compressor is referred to as a positive displacement compressor, whose sole focus is on the compression of a gas. This unit operation takes a quantity of gas from the suction line, before compressing and moving the gas to the discharge line. The unit operation comprises of a piston, cylinder, valves, and other components, as shown in the schematic representation in Figure A.14 (Alhelal & Sultan, 2015).

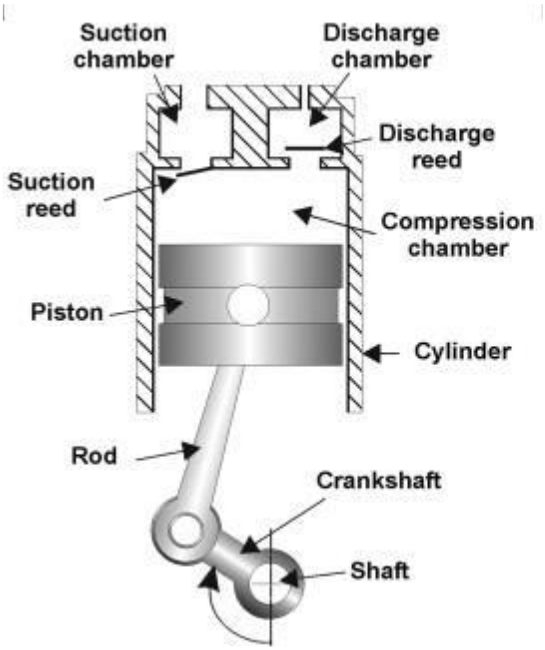

Figure A.14: Diagrammatic representation of a reciprocating compressor and its components (Alhelal & Sultan, 2015)

This compressor system is often utilized within processes because of its high-pressure ratio that it is able to achieve, with a low flow rate. As a result, the reciprocating compressor is commonly utilized in oil refineries and natural gas processing plants (Alhelal & Sultan, 2015).

However, the disadvantage of this compressor system is that it is unable to be self-regulated, as is the case with a centrifugal compressor. Therefore, during the operation of such a compressor, it would continue to displace the gas in the process, until switched off. This would be a good compressor system to make use of should there be an unlimited supply of the associated gas in question, however, this is impractical for a process. In a chemical process, there is a finite, or limited amount of each gas, and therefore these unit operations would have to be accompanied with major control processes (Bloch, 2006).

Another concern in the utilization and operation of a reciprocating compressor lies in its start up. This compressor unit operation is required to be unloaded before started. If the compressor is full, the typical ratio of peak to mean torque power with such unit operations, is 3 to 1, therefore implying that a 100% capacity would need to have a torque power in excess of 300% to operate. This is impractical, with current motors only producing torque power efficiencies between the range of 40% and 60%. Therefore, the start-up procedures for this type of compressor can be a major concern (Bloch, 2006).

A.2.3. Axial Compressor

Axial flow compressors are compressors where the flow enters and leaves the unit operation in an axial direction, i.e., parallel with the axis of rotation. The mechanism of pressure change within an axial compressor, involves the flow being accelerated through the unit operation, before being diffused in order to increase its pressure. The acceleration of the flow is achieved via a rotating airfoil, i.e., blades, whereas the diffusing nature of the unit operation comes from stationary blades that are known as stators (Boyce, 2012). Figure A.15 shows a diagrammatic representation of an axial compressor.

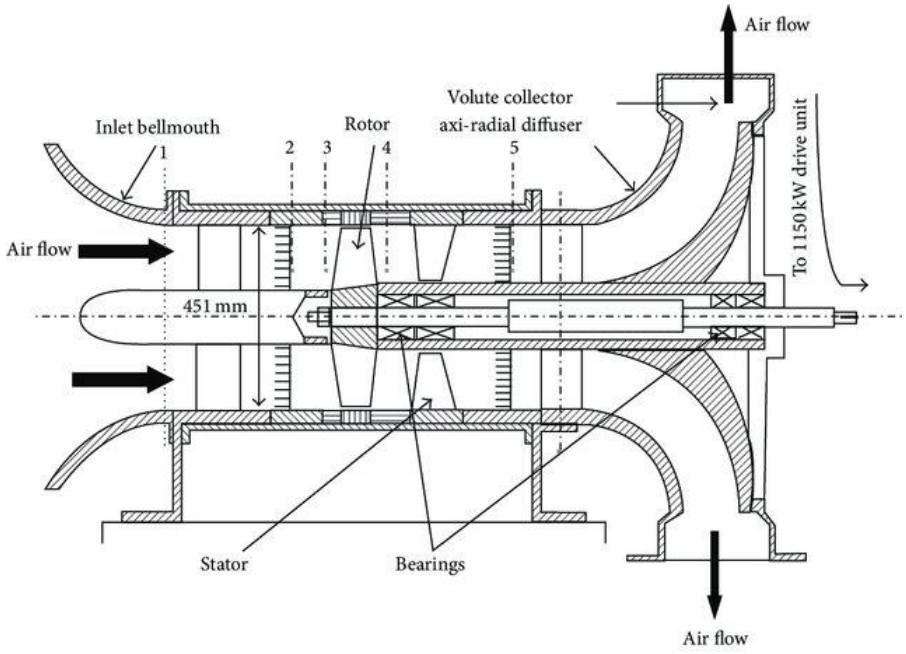

Figure A.15: Diagrammatic representation of an axial compressor unit operation (Alone, et al., 2014)

Axial flow compressors can typically handle a large flowrate moving through the unit operation and can take in flow rates of up to one million cubic meters per hour. These unit operations are most often found in blast furnaces and air separation processes (Bloch, 2006). Typical industrial and aerospace axial compressors have stage efficiencies in excess of 80%, whereas the range of supersonic axial compressors, often used in research-based studies, have a stage efficiency of between 75% and 85% (Boyce, 2012).

The advantage of these unit operations is that whilst they do tend to have a greater capital cost than you would expect from a centrifugal compressor, they are able to provide energy savings that are able to outweigh the additional cost (Brown, 1997).

The disadvantage of an axial flow compressor, however, is that the blading within the unit operation can be fragile and expensive, and therefore effective control processes would be needed to ensure that the blade is not damaged. In such cases where the blade is damaged, the compressor would need to be maintained or even replaced, which is an expensive process (Gresh, 2018).

A.2.4. Rotary Compressor

Much like a reciprocating compressor, a rotary compressor is also classified as a positive displacement compressor, where compression occurs as a result of the rotation within the unit operation. Based on research conducted by Guzda & Szmolke (2015), the use of a piston can replace the crankshaft within a rotary compressor, allowing for a drastic noise reduction in the operation of this compressor. Furthermore, this allows the design of the unit operation to be more compact, as shown in Figure A.16.

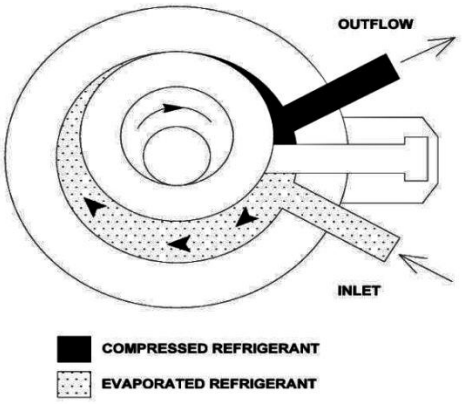

Figure A.16: Diagrammatic representation of a rotary compressor (Guzda & Szmolke, 2015)

The advantage of rotary compressors is that they are able to provide better efficiencies than that noted with a reciprocating compressor, resulting in many processes replacing their existing reciprocating compressors with that of a rotary compressor. In fact, this type of compressor has been reported to be widely utilized throughout small and medium air conditioning units. The disadvantage with these compressor systems, however, is that they are limited in their capacity and as such are mainly utilized in cases where lower flow rates are being utilized (Diniz & Deschamps, 2016).

A.3. Separation Systems (Flash Drums & Distillation Columns)

One of the most crucial steps in any chemical process is the separation of products from the unreacted feed stream, as well as the separation of the product from other products that may be produced during the course of the process. This process is often quite costly, however, imperative in achieving product purities that allow for the desired product to be sold within the existing market (Sorsamaki & Nappa, 2015).

The type of separation process chosen in any given scenario, is dependent on the chemical species involved and the degree of separation required. Some separation systems include membranes, phase separators, distillation columns, adsorption columns and solvent extractions (Sorsamaki & Nappa, 2015). This section focuses specifically on those separation systems utilized throughout the course of this research, namely flash drum/phase separators and distillation columns, providing a brief overview of these unit operations and their associated advantages and disadvantages.

A.3.1. Flash Drums

Flash drums are one of the simplest, inexpensive separation unit operations, which utilize the flash evaporation procedure as the basis for the separation process. During the separation process, a liquid stream is partially vaporized at specific operating conditions (in terms of pressure and temperature). Due the two phases that now exist within the unit operation, the vapor can be removed from the unit as an overhead stream, whereas the liquid can be drained from the bottom of the flash drum. This process, in its entirety, is termed flash distillation (Iggland & Mazzotti, 2015).

A stream that contains two chemical species, that are to be separated via a flash drum unit operation, is referred to as a binary flash mixture, with each stream having its own composition of the chemical species, denoted by x, y and z. A diagrammatic representation of a flash drum unit operation, detailing such, can be seen in Figure A.17 (Iggland & Mazzotti, 2015).

Figure A.17 shows a feed stream (F), with composition z entering a flash drum unit operation at a predefined pressure (P_F) and enthalpy (h_F). This feed stream is then separated into a vapor stream (V) and a liquid stream (L) having its own compositions (y and x) and enthalpy (H_V and

h_L), respectively. This separation occurs at a predefined temperature (T) and pressure (P), with a certain amount of heat energy (Q) being added to the unit, in order to achieve these operating conditions.

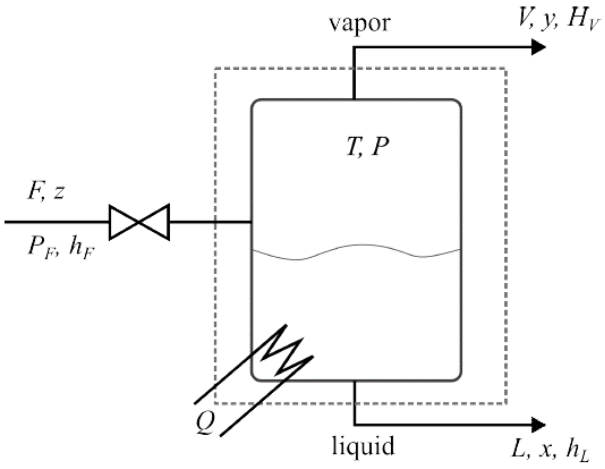

Figure A.17: Diagrammatic representation of a flash drum unit operation (Iggland & Mazzotti, 2015)

The disadvantage of the flash drum system, however, is that it often results in a drastic drop in the pressure of the system, and inefficient separations in multiple specie streams. This is unfavourable in crude oil processing plants, as this may result in the vaporization of hydrocarbons that can have negative safety implications. Therefore, in such instances, multiple phase separators are utilized, as a means to control the levels and pressure of each system, focusing on a single separation in each unit operation (Al-Mhanna, 2018).

Due to the mechanism of this separation system utilizing the equilibrium of the two chemical species, large degrees of separation are unable to be achieved, and as a result this separation is not typically used for final product separation. However, as a means by which to increase the separation efficiency, demisters (Figure A.18) can be added to the unit (Wankat, 2012).

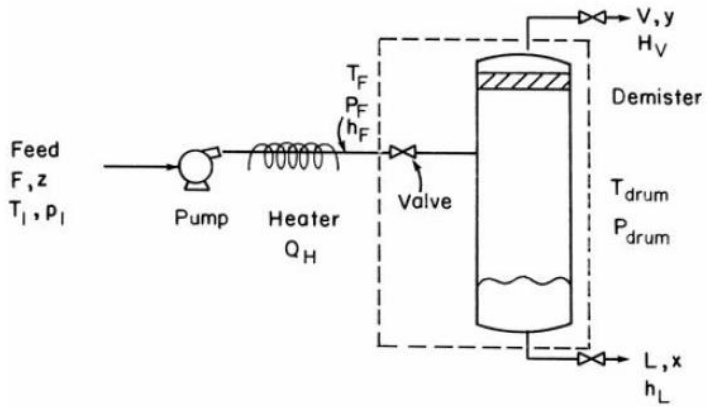

Figure A.18: Flash drum unit operation with a demister for increased separation efficiency (Wankat, 2012)

These demisters are employed to prevent liquid droplets from escaping through the vapor stream overhead, thereby increasing the separation efficiency of the process. These separation vessels can either exist as a vertical or horizontal vessel, with the orientation being dependent on the application and system in question (Wankat, 2012).

A.3.2. Distillation Columns

Distillation columns are separation unit operations that have become increasingly prominent in the oil and gas industry, where the separation is focused on liquid-liquid mixtures. Typically, these mixtures have very similar boiling points, and as such are referred to as azeotropes. As a result of their boiling points being in close proximity, it is difficult to establish a clear phase difference between the two species, necessitating the need for a distillation column (Bamatov & Bamatov, 2020).

A distillation column is comprised of five main components, as follows (Spreight, 2020):

1. The shell of the distillation column – This shell houses the components of the streams, as well as the necessary trays within the column that promote the separation of the liquids in question.
2. The column internals – Within the shell of the distillation column there are either trays, plates or packing required as a means by which to enhance the separation within the vessel. Each tray acts as a vapor-liquid equilibrium stage, within the separation process, further separating the vapor/liquid and allowing for greater product purities to be achieved.
3. A reboiler – The reboiler is a heat exchanger unit operation found at the bottom stream of the distillation column. This heat exchanger serves to reboil some of the liquid (partial vaporization), to be fed back to the distillation column, in an effort to promote the separation process (Kolmetz & Dwijayanti, 2013).
4. A condenser – This heat exchanger focuses primarily on the condensing of the vapor stream leaving the top of the distillation column, with a portion of this condensate being recycled to the distillation column via the reflux stream.
5. The reflux drum – This drum holds the condensate from the condenser, before it is recycled back to the distillation column.

It is essential that all five of these components be present within a distillation column, for effective separation procedures. Figure A.19 shows the configuration of the aforementioned distillation column components.

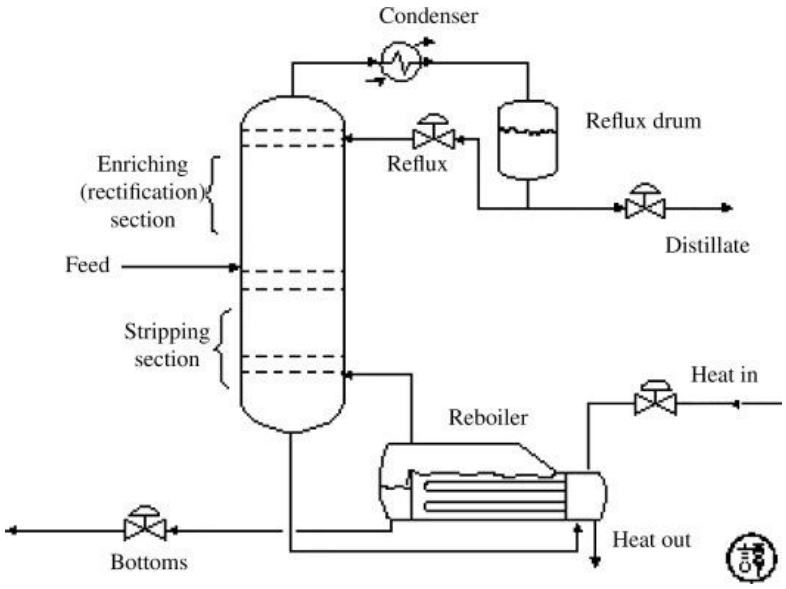

Figure A.19: Diagrammatic representation of the configuration for a distillation column (Spreight, 2020)

During the process of separation, via a distillation column, a single feed stream enters the column, with there being at least two outputs. It is possible that there can be more than two outputs, evident in fractional distillation systems (Bamatov & Bamatov, 2020).

Whilst distillation columns are considered to be the cheaper option when separating a liquid-liquid mixture, there are drawbacks and shortcomings with this unit operation. One of the major concerns with distillation columns, is the conditions under which it operates. There is a large amount of energy required in distillation columns, specifically that which is required and expelled by the reboiler and condenser respectively (Ozkul & Kayabasi, 2018).

Should there be a loss in cooling energy, this may cause the column to suffer overpressure. As a result, pressure-relief valves are essential in maintaining and ensuring safety when operating processes involving distillation columns. A loss in the energy from the reboiler however, will result in under pressure of the distillation column. Therefore, it is essential that energy management and control be of the utmost importance in these systems, in order to mitigate and manage the associated risks (Lees, 2012).

Appendix B: ASSF Tool Overview and User Interface

The information provided in this Appendix aims to provide the reader with an overview of the ASSF tool, dividing the tool into two main sections, i.e., that which is focused on building the RPD, and the subsequent analysis thereof. Additionally, the user interface of the ASSF tool is detailed within this Appendix.

B.1. ASSF Tool Part #1 – Reaction Pathway Database Development

Figure B.1 provides a diagrammatic representation of the first part of the ASSF tool, which is focused on developing the RPD and its potential combinations. This section focuses on the inputs required within this segment of the ASSF tool, its operation thereof, and its respective output, leading to the user's first major decision-making step within the tool's operation.

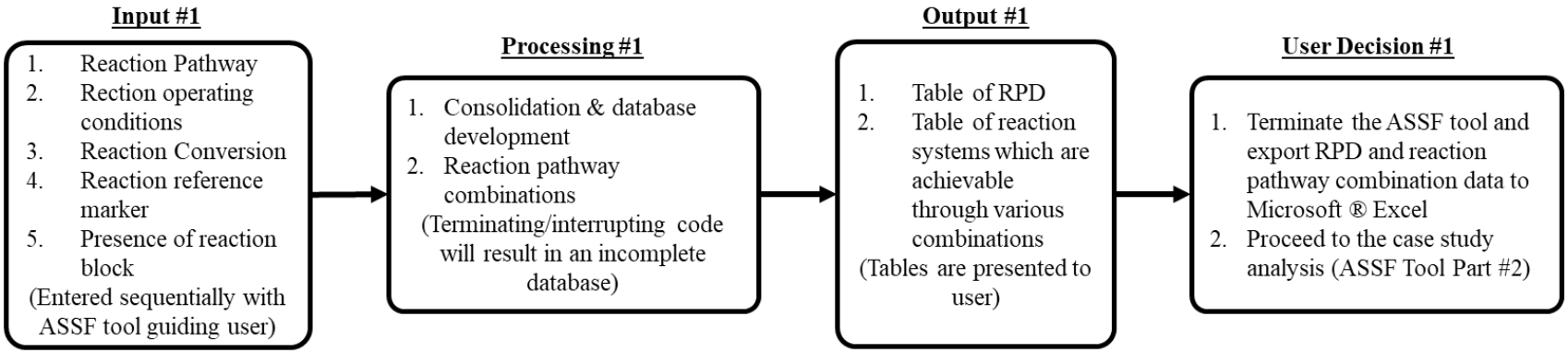

Figure B.1: Input/Output diagram of the ASSF tool Part 1

B.1.1. Input Data Required from User

The first part of the ASSF tool utilizes data that can be grouped together into one broad category, which is deemed as the RPD development input. This input requires five main points of information from the user, namely:

- Reaction pathway/Reaction equation
- Reaction operating conditions (temperature and pressure)
- Reaction conversion
- Reaction reference marker
- Presence/absence of a reaction block

When entering the reaction equations into the ASSF tool, the user must follow a specific syntax. This is explained in more detail in Chapter 3 (Section 3.3). Any deviation from this syntax renders the reaction unreadable by the ASSF tool. As a result, the pathway will not be taken into account when developing the database. Additionally, all chemical equations entered by the user has to be stoichiometrically balanced. Should a chemical reaction not be balanced the user is prompted to revise the reaction pathway accordingly, until the necessary balancing constraints are met.

After successfully meeting these checks relating to the input of a chemical equation, the user is prompted for the reaction's operating conditions. This encompasses the reaction's temperature and pressure which allow for the reaction mechanism to proceed. The default values set within the ASSF tool is for the temperature to be noted in degrees Celsius, and the pressure to be noted in bar. Therefore, it is necessary that all operating conditions entered by the user adheres to the predefined units.

The reaction conversion is entered with respect to the first reactant in the chemical equation. Furthermore, the presence of a reaction block refers to the possibility of multiple chemical reactions occurring simultaneously, either over the presence of a single catalyst or within a single reactor unit operation. As a result, if a reaction is noted as being part of a reaction block, this reactive system remains grouped together throughout the analysis, ensuring that none of the sub-reactions are isolated when determining the combinations which are achievable.

A reference marker is also utilized within the ASSF tool input, in order to allow for the reaction pathways to be cross referenced throughout the tool's code. This allows for users to refer back to the original source document, when presented with the feasible reactive systems in the reduced search space. The reference marker also allows for the tool, and user, to differentiate between pathways that may have the same chemical equation, but different catalysts or operating conditions.

This input is continuously looped within the ASSF tool, allowing the user to add reaction pathways to the ASSF tool, building an RPD. This occurs in a sequential process, with command prompts guiding the user through each of the required inputs. If, however, the user terminates the program whilst inputting a reaction pathway, or its associated conditions, the ASSF tool does generate an error. This is caused by incomplete information within the RPD, necessitating that the user rebuilds the RPD. Therefore, it is imperative that each prompt from the ASSF tool is read, as the user is provide with an option to conclude the RPD.

B.1.2. Operation and Processing of Input Data

Once all reaction pathways have been entered by the user, the ASSF tool consolidates this input, creating a final RPD. The ASSF tool then systematically goes through each of the reaction pathways in the RPD, tabulating any possible combinations that may be achievable, given a CO_2 and H_2 feed stream.

The tabulated list of possible combinations is referred to as the case study data table and contains all reactive systems that are to be designed within the ASSF tool in its subsequent stages. Upon checking a single reaction pathway for potential combinations, the remainder of the reaction pathways in the RPD undergo the same process, thereby ensuring a complete search space is generated. Thus, the ASSF tool is looped to complete this routine check. Further information on the loops, and their operation, is provided in Appendix C, which provides a basic technical overview of various stages within the ASSF tool.

During this processing stage, the user is unable to interact with the ASSF tool. The tool, however, can be terminated at any point, with the possible combinations at that point in the analysis being visible to the user.

B.1.3. Output Provided to User

The output of this section in the ASSF tool, provides the user with two tables within the tool's command window, displaying the RPD developed and the case study table of all possible reaction pathway combinations. The case study table contains all the necessary information relating to each reaction pathway, including reference markers previously inputted by the user. This allows for users to be able to cross reference this table to its original source with ease.

Upon presenting the user with these two tabular outputs, the first major decision-making step is presented to the user. This requires the user to interact directly with the ASSF tool. During this decision-making step, the user has the option to either continue with the analysis of these case studies within the ASSF tool, or to terminate the tool. Should they choose to terminate the tool, possibly to utilize the case study data in other software platforms or applications, the tool exports the tables to a Microsoft ® Excel spreadsheet. Proceeding with the analysis within the

ASSF tool, on the other hand, results in the tool continuing its second segment, prompting the user for additional inputs.

B.2. ASSF Tool Part #2 – Case Study Analysis

Figure B.2 details the input/output diagram that is associated with the second part of the ASSF tool. This section of the ASSF tool is focused on the utilization of the previously computed case study table, designing, and analyzing each reactive system. This analysis is conducted from both an economic and environmental perspective. It is important to note that the diagram presented in Figure B.2 provides an indication as to the inputs that are required from the user and the final window/screen presented to the user after running the ASSF tool in its entirety (Output). All design, costing, analysis, and search space reduction is encompassed within the processing section of Figure B.2, as this is an automated process, requiring no input from the user.

Furthermore, it is important to note that should the user not have the detailed specifications required for the input of the ASSF tool, the default values within the ASSF tool can be utilized. This, however, should only be utilized on preliminary reactive systems. Having more detailed specifications available and inputted into the ASSF tool will result in the analysis being more accurate and relevant to the user system.

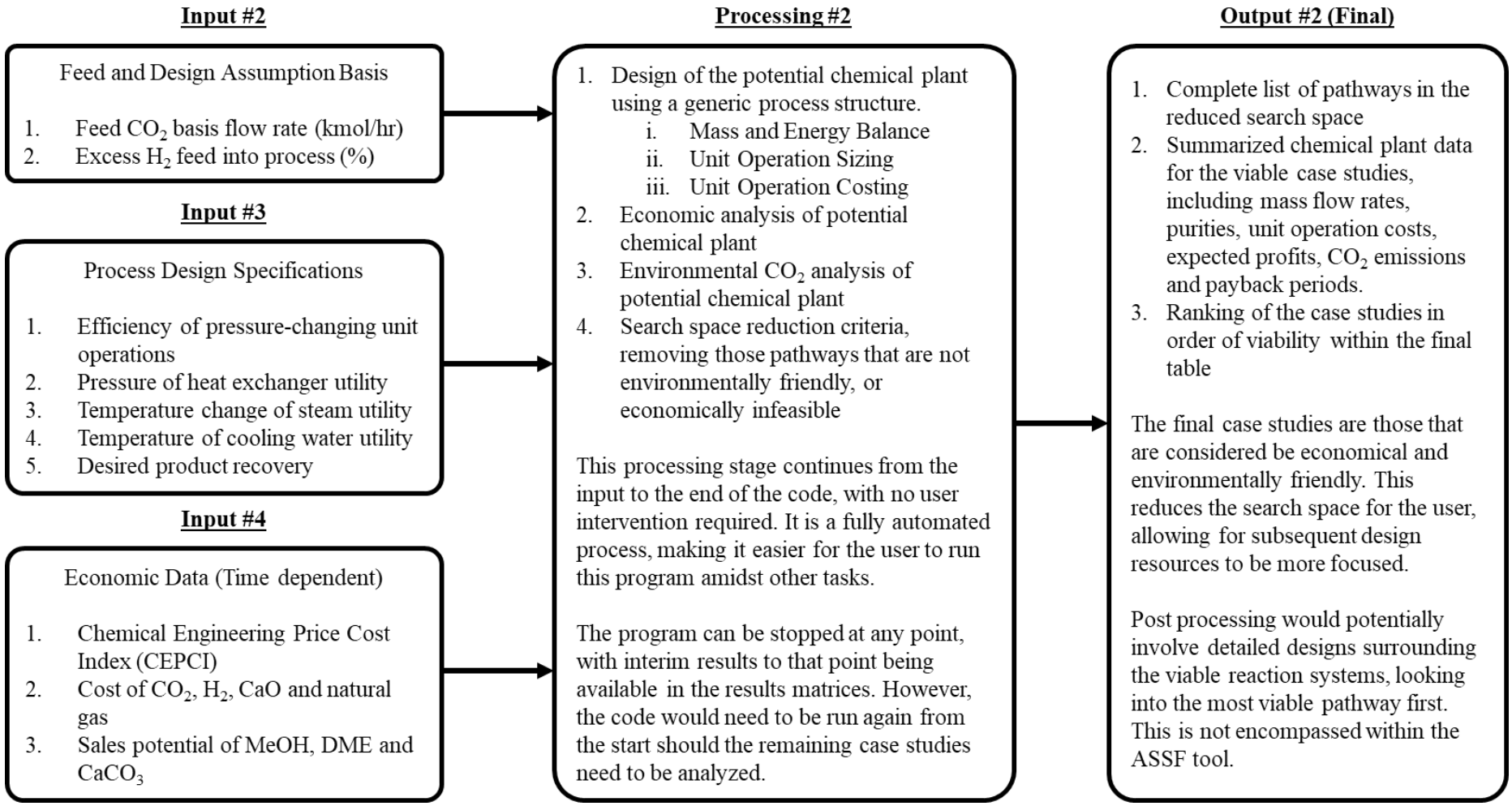

Figure B.2: Input/Output diagram of the ASSF tool Part 2

B.2.1. Input Data Required from User

With the user choosing to continue the analysis of the case study table within this tool, the user is then prompted for more information. These inputs can be sub-divided into three main categories, namely:

- Feed and design basis assumptions
- Process design specifications
- Economic factors

It is important to note that when entering information into the ASSF tool, the user is guided in a sequential process, as described within the first part. Command prompts also help to assist the user as to the units involved with each input. This allows for the potential userbase of the tool to extend beyond those which have engineering knowledge, thereby allowing for a more diverse platform.

The first category deals with the basis on which potential chemical plants are designed and is focused on the inlet feed flow rates. The flow rate that enters the chemical plant is paramount in determining the size of the subsequent unit operations required, as well as the associated potential product that could be produced from the process. The feed and design basis assumptions requires the following inputs from the user:

- Feed CO_2 basis flow rate (kmol/hr)
- Excess H_2 fed into the process (%)

The feed flow rate of CO_2 is chosen by the user, whereas the excess H_2 flow rate is likely to be extracted from the data sources utilized in developing the RPD, hence attesting to the need and use of cross reference markers in the first part of the ASSF tool.

The second input category within this section of the ASSF tool relates to process design specifications. The following data is inputted by the user within this category:

- Efficiency of the pressure changing unit operations (%)
- Pressure of the heat exchanger utility (steam and cooling water) (bar)
- Temperature change of the steam heat exchanger utility (Celsius/Kelvin)
- Temperature change of the cooling water heat exchanger utility (Celsius/Kelvin)
- Desired product recovery (%)

Whilst the user is given the opportunity to input these specifications, allowing for the ASSF tool analysis to be more accurate to the unit operations which they have/are looking to purchase, the ASSF tool currently does not support a range under any of these specifications, requiring that a definitive value be provided within the ASSF code. A sensitivity analysis can be completed through running the ASSF tool multiple times using the same RPD.

The ASSF tool does provide default settings (the assumptions utilized in development of the ASSF tool), allowing users to choose this option should they only require a preliminary analysis, i.e., having no technical requirements. Table B.1 contains the data that is set as the default for the above-mentioned process specifications.

Table B.1: Default values relating to process specifications within the ASSF tool

Process Specification	Value	Units
Pressure-changing unit efficiency (percentage)	74	-
Pressure of heat exchanger steam utility	3	bar
Pressure of heat exchanger cooling water utility	3	bar
Temperature change of steam utility	50	Kelvin
Temperature change of cooling water utility	20	Kelvin
Product recovery (percentage)	99.99	-

A pressure-changing unit efficiency of 74% is an assumed value and was utilized as the basis on which the ASSF tool was developed. This value was chosen, as the efficiency of compressor unit operations typically ranges between 70% and 85%, as dictated by Turbo Machinery International. Therefore, a value within this range was chosen as the default for the ASSF tool.

The final category of inputs needed from the user relates to the economic factors at the time of running this tool. These factors are highly time dependent, with raw material cost and product sales potential, being dependent on the market within the region in which the tool is being utilized, or on the overall global market. As a result, it is necessary that the user input data relevant to the time of utilizing the ASSF tool, allowing for more accurate results.

The following data is required within the economic factor category, with all costs and sales potentials being inputted in dollars per tonnage ($/ton):

- Chemical Engineering Price Cost Index (CEPCI)
- Cost of CO_2

- Cost of H_2
- Cost of natural gas
- Cost of calcium oxide (CaO)
- Sales potential of MeOH
- Sales potential of DME
- Sales potential of calcium carbonate ($CaCO_3$)

The CEPCI value is required to account for inflation when purchasing unit operations, allowing the ASSF tool to calculate an estimate of the relevant unit operation costs at the time of utilizing this tool. Furthermore, it is important to note that all costs associated with the reactant feed should be the cost of a pure feed, i.e., without the presence of any contaminants. The cleaning procedures associated with the reactant feed streams are beyond the scope of this research study.

Once all these data have been inputted into the second part of the ASSF tool, the processing of the data can begin. This processing occurs in conjunction with the previously developed case study data table.

B.2.2. Operating and Processing of Input Data

After entering the second stage of inputs required by the ASSF tool, each reactive system/combination is designed utilizing a preliminary design procedure. This involves designing potential chemical plants associated with each reaction pathway, focusing on the following key points in their design:

- Mass and energy balances
- Unit operation sizing
- Unit operation costing

A brief explanation of the loops in each sub-section of this design process is given in Appendix C, with a more detailed structure of these loops being provided within the explanations of Chapter 3. Section 3.2 contains the process flow diagrams associated with the generic chemical plant structure utilized in the preliminary design procedure.

Upon completing all stages in the design procedure for each reactive system, the data is consolidated into a single table. This table contains all essential information from each case study design, allowing for subsequent analyses from an economic and environmental standpoint.

The economic analysis encompasses the gross profit of the potential chemical plant, and a simplified payback period calculation, whereas the environmental analysis looks at the potential benefit of the chemical plant to atmospheric CO_2 levels. This environmental standpoint compares the amount of CO_2 exiting the chemical process to that which is being taken into the process. It is important to note, however, that the CO_2 exiting the process considers both the unreacted feed, as well as the CO_2 that is being produced due to combustion of methane, with natural gas (primarily composed of methane) being used as the primary source to meet the energy requirements of the process and its associated unit operations Should more CO_2 exit this process than is being taken in at the feed, the overall impact of the process would be emitting CO_2 to the atmosphere, deeming the process environmentally infeasible.

The potential chemical plants which exhibit either economic or environmental infeasibilities, are eliminated from the search space using predefined search space reduction criteria. These search space reduction criteria are explicated in Section 3.14. The final search space of reactive systems is then ranked in order of feasibility, allowing the user to focus their design resources on those reactions with the greatest likelihood of success. The ranking system employed within the ASSF tool utilizes a performance index, finding a draw-off between the environmental and economic benefits of the potential chemical plant. The details of this performance index are explicated in Section 3.14.4.

This processing stage within the ASSF tool is a fully automated process, requiring no intervention by the user. This allows for the ASSF tool to be utilized simultaneously, or in the background, when completing other tasks. This increases the efficiency with which design resources are utilized within the initial design process.

When analyzing multiple reactive systems/case studies, the ASSF tool indicates to the user which case studies have already been analyzed and which is in the process of being analyzed. This provides the user with an indication as to the progress of the tool's operation. The ASSF tool can be terminated at any point during this analysis, with the intermittent results to that point being available to the user. However, should the user wish to continue the analysis, the ASSF tool would need to restart, as the tool does not currently support a pause/resume feature.

B.2.3. Output Provided to User

Upon completion of this processing stage, the user is presented with a completed table of the reaction pathways within the reduced search space. These pathways exhibit both economic and environmental feasibilities. Furthermore, a performance index is utilized to find draw-offs between these criteria, thereby allowing for the case studies to be ranked in order of viability. This is covered extensively in Section 3.14, dealing with the search space reduction criteria.

The user is also presented with a summarized table containing the chemical plant data for those promising case studies, including mass and molar flow rates, unit operation sizing and costing, expected, preliminary gross profits, CO_2 emissions and payback periods. This data can be exported to Microsoft ® Excel should the user opt to do so.

Post processing of these results would potentially involve detailed designs of each reactive system, starting from that which was deemed to be the most viable pathway by the ASSF tool. This detailed design, however, is not encompassed within the scope of the ASSF tool. The primary purpose of this tool is to provide a precursory, rapid, screening tool that allows the user to determine the pathways with the greatest likelihood for success, when presented with a large database.

B.3. ASSF Tool User Interface

Whilst an understanding of the ASSF tool is provided within the overview, as well as the introduction section (Chapter 1), the utilization of this tool becomes clearer when provided with the user interface. As this tool was coded using the MATLAB software platform the ASSF tool makes use of a MATLAB styled interface.

The first screen presented to the user upon running the ASSF tool provides a basic introduction to the use of the ASSF tool, highlighting the range of chemical species accounted for in this tool, as well as the necessary syntax that needs to be followed when inputting stoichiometric reaction equations. This initial screen is presented in Figure B.3.

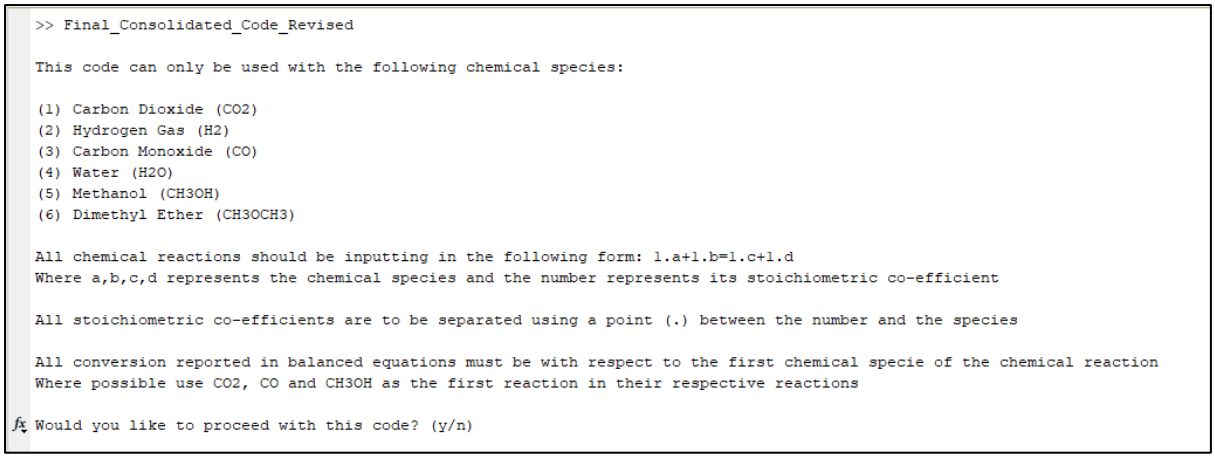

Figure B.3: Introductory screen to the ASSF tool detailing reaction equation syntax and chemical specie limitations

It is imperative that the user understand these limitations of the ASSF code before proceeding to the next stage within this tool, as this will serve as the crux for all information that will be requested at future points in its operation. After agreeing to these conditions, the ASSF tool proceeds directly to the input of the stoichiometric reaction equations necessary to build the RPD, as shown in Figure B.4.

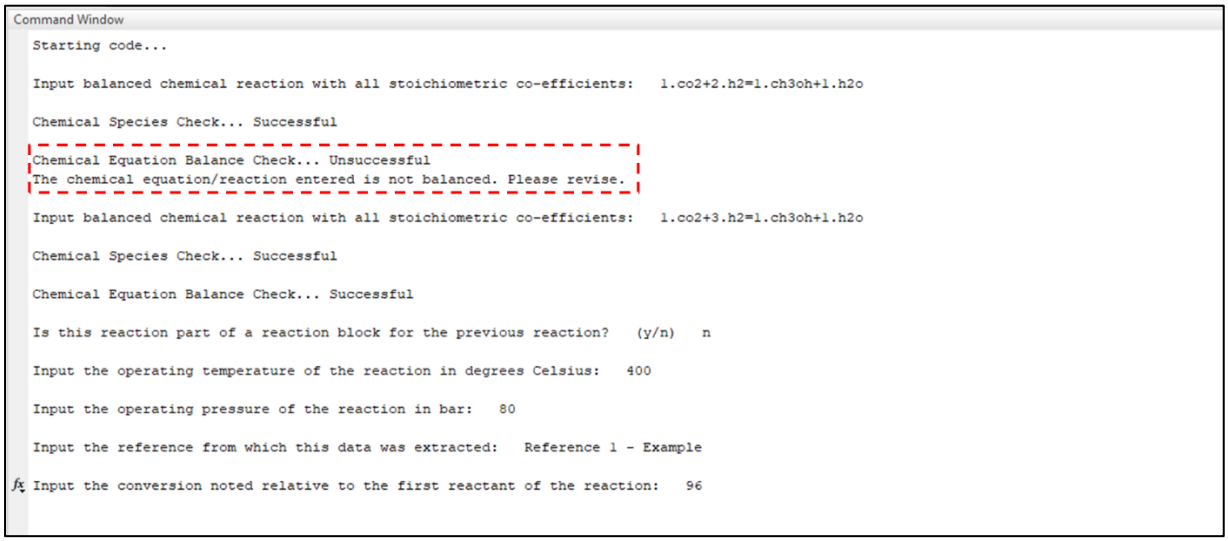

Figure B.4: ASSF tool interface associated with entering reaction equations and their associated operating conditions

As seen in Figure B.4, once a chemical reaction is inputted into the ASSF tool, the chemical species are first checked to ensure that all components of the reactive system are within the bounds of this tool, before then checking if the reaction is balance. Should either of these two checks be unsuccessful, as seen in the highlighted portion of the above screenshot, the user is asked to revise the chemical equation until these two checks are satisfied.

Upon clearing these checks, the user is prompted to enter the necessary reaction conditions associated with that specific chemical reaction, including its operating temperature, operating pressure, conversion, and a reference marker. This reference marker is imperative as it will allow for the final search space to be cross-referenced by the user at a later stage. When all information relevant to a chemical reaction has been inputted, the user is prompted to either compile the RPD or continue to add reaction pathways. Should the user choose to continue to add reaction pathways, the user interface is identical to that which is presented in Figure B.4. However, should the user choose to compile the reaction pathway database the user is presented with the screen shown in Figure B.5.

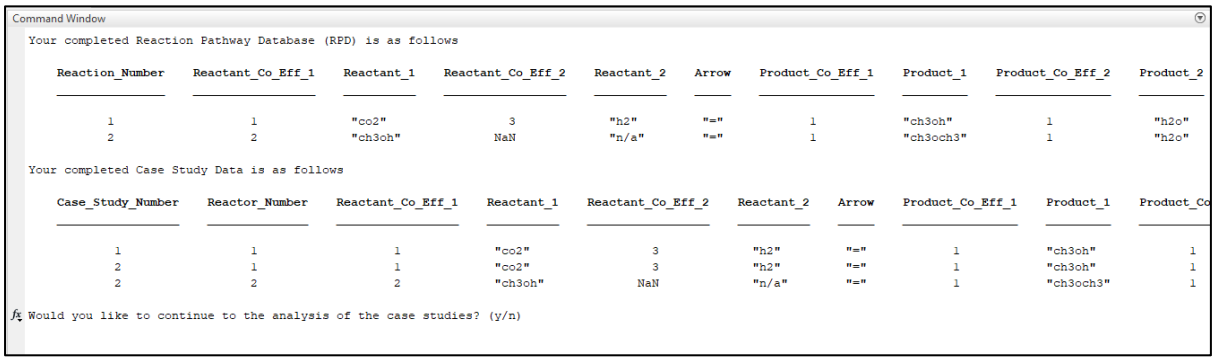

Figure B.5: Intermediary results obtained from the ASSF tool of the final consolidated RPD and the possible reaction pathway combinations

As seen by the above screenshot, compiling the chemical reactions results in the user being presented with a completed RPD, to be utilized in the subsequent analysis procedures, as well as a list of all possible reaction pathway combinations. As mentioned previously, this does not provide novel reactive pathways, but bases these combinations on the likelihood of utilizing the product from one reactive system in a secondary/tertiary reactor system, thereby producing a new product. Each one of these combinations is referred to as a case study.

As seen in the final line of Figure B.5, the user is prompted as to whether they would like to continue through to the analysis of all reaction pathway combinations derived within the ASSF tool. Should the user choose not to proceed to the analysis, the case study table is exported to a Microsoft Excel file for the user to refer to when needed. However, if the user chooses to proceed to the analysis, employing the full capabilities of the ASSF tool, the user is requested for economic data, at the time of running the tool, as well as process design parameters, as shown in Figures B.6 and B.7.

However, should the user not have information relating to the process system, such as the unit operation efficiency, utility information and targeted purity, the ASSF tool does have default values which can be used to provide a preliminary basis on which to conduct the analysis.

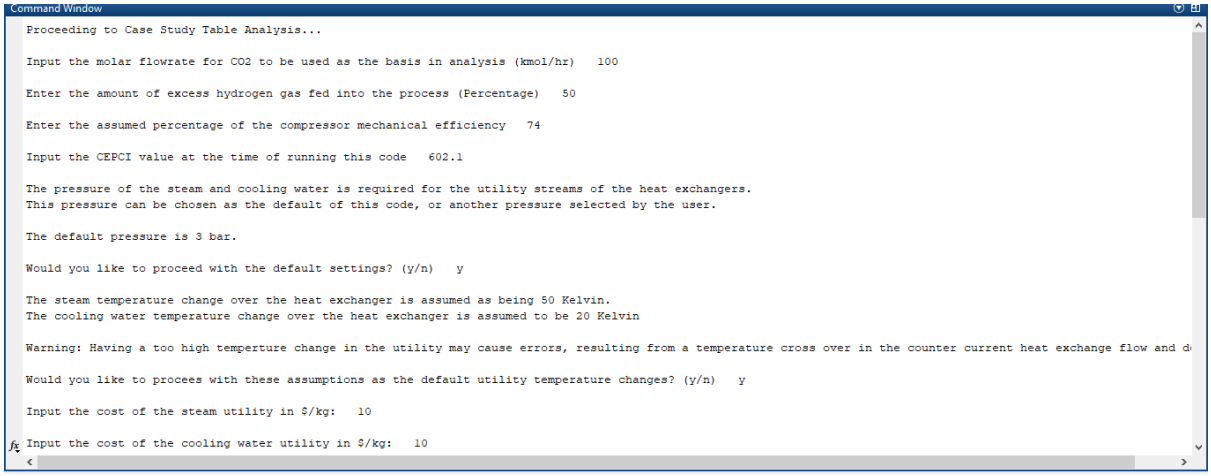

Figure B.6: ASSF tool input screen for the economic and process data required for the analysis of the possible reaction pathway combinations (Part 1)

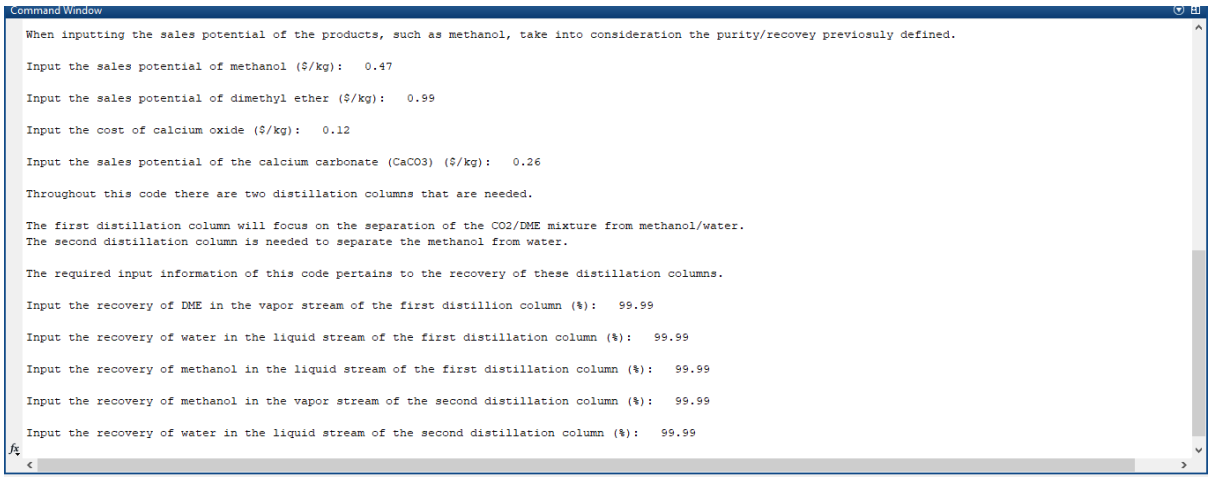

Figure B.7: ASSF tool input screen for the economic and process data required for the analysis of the possible reaction pathway combinations (Part 2)

After inputting all economic and process specific data, the user is given one final chance to review all inputted data, allowing for any incorrect values to be adjusted, before proceeding to the analysis. This review of inputted data is represented as shown in Figure B.8.

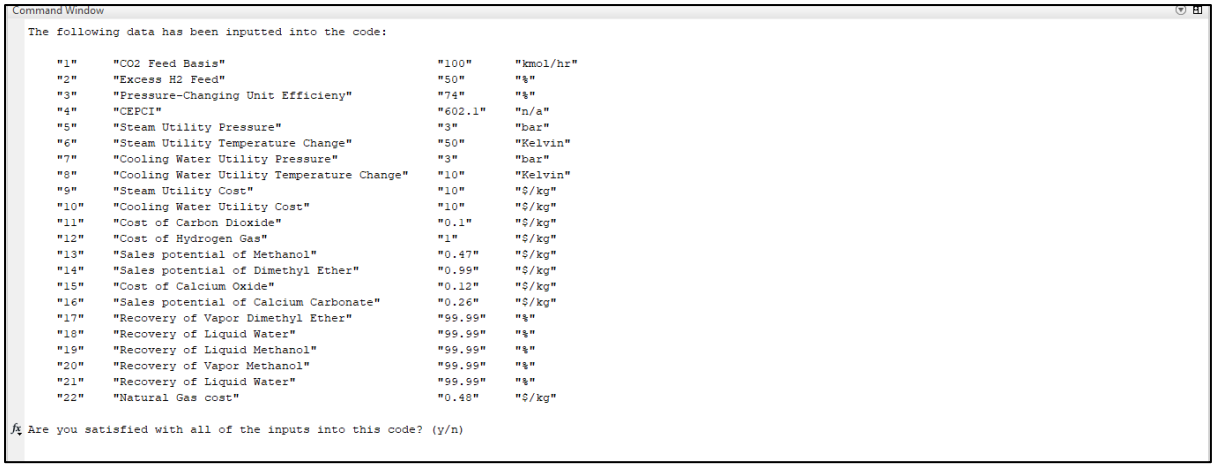

Figure B.8: Final consolidation and review of economic and process data inputted into the ASSF tool

During the analysis of each individual case study, the ASSF tool displays the case study number that is currently undergoing the analysis, thereby allowing the user to also keep track of the tool's progress. This is shown in Figure B.9.

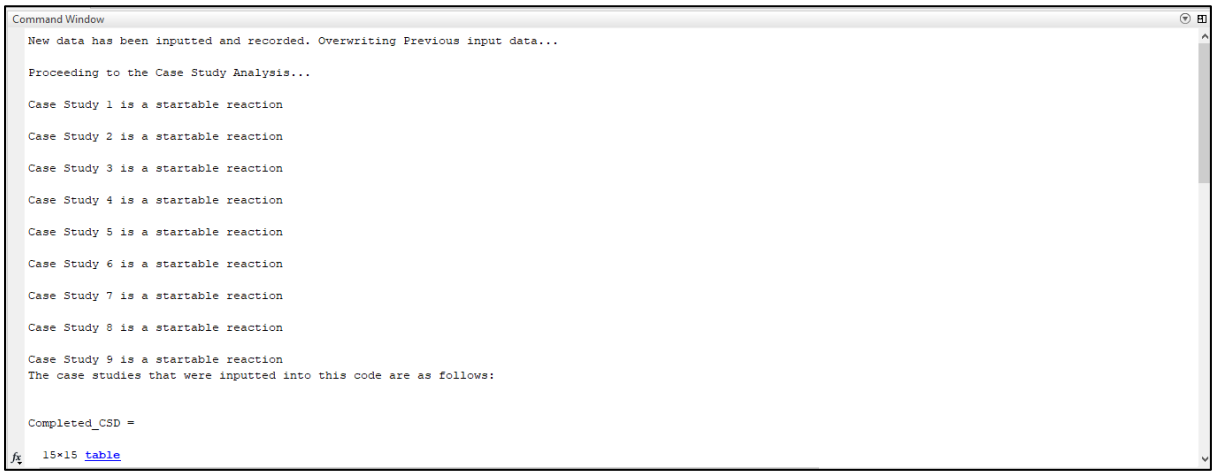

Figure B.9: Screen showing the progress of the ASSF tool using the case study currently being analysed

Finally, the user is presented with a completed case study table of all reactive systems analyzed, along with the promising reaction pathway and its associated process data based on the ASSF tool analysis, as shown in Figures B.10 and B.11.

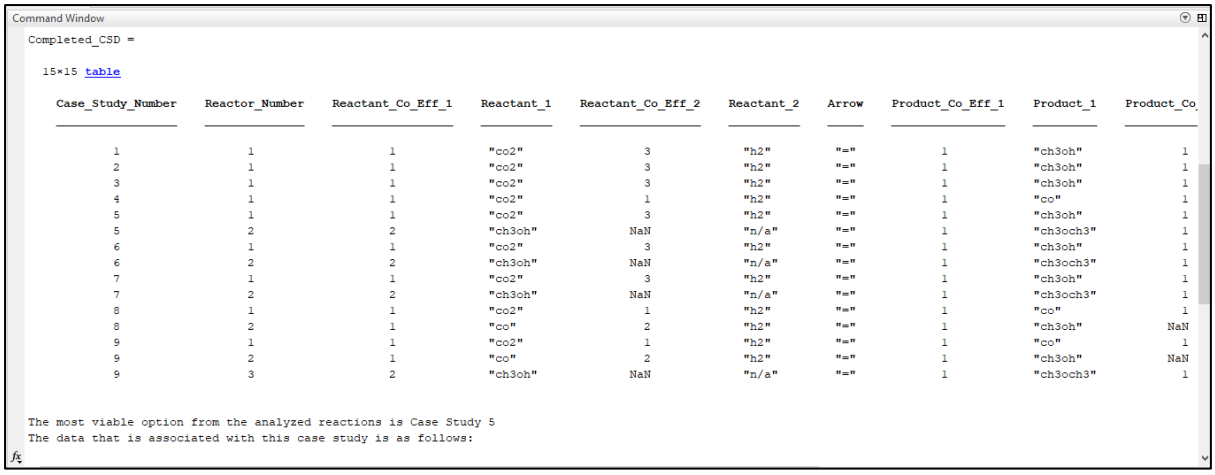

Figure B.10: ASSF tool results screen showing the case studies that were analysed within this tool

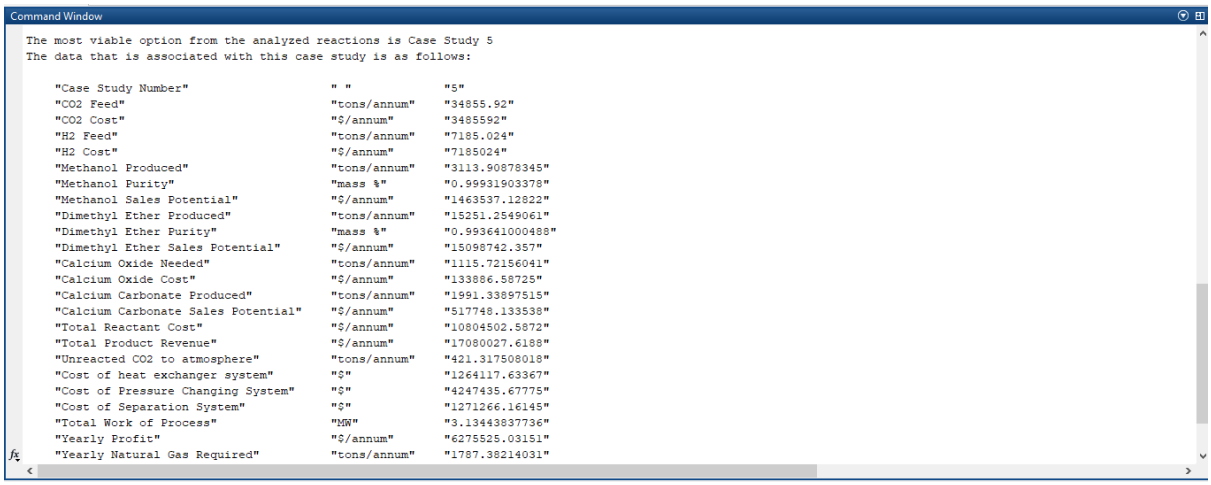

Figure B.11: ASSF tool results screen showing the economic and process data associated with the promising/feasible reactive systems

Using the case study number of the feasible reactive system, together with the case study table and reference markers presented in the results screen of the ASSF tool, the user is able to focus their design resources on the promising reaction pathways, furthering their design in intricate software platforms such as Aspen ® Plus and CHEMCAD. Should the ASSF tool determine more than one reactive system to be promising within the search space, all case studies and their associated data are presented in the final table, with the case studies being ranked in order of expected process feasibility.

Appendix C: Technical Overview of the ASSF Tool

The ASSF tool is comprised of many components, with each component being integral in the tool's operation. This Appendix, provides a basic overview of the technical components within the ASSF tool, focusing on a more detailed structure of the overall code, as well as a basic overview of the loops existing within the code's structure.

C.1. Complete Overview of the ASSF Tool

Figure C.1 provides a diagrammatic representation of the ASSF tool, highlighting the required information, as well as the chronological order by which the ASSF tool operates. The advantage of presenting the ASSF tool using a flow chart representation, is that the loops and sequence of building-blocks, within the development of this code, can be clearly perceived, prior to the detailed explanations provided in Chapter 3.

There are two types of data required by the ASSF tool, namely that which is inputted by the user and the data coded directly into the ASSF tool. As highlighted in Figure C.1, the data required throughout the course of the ASSF tool's operation, included the properties of the chemical species involved and the constants related to the sizing and costing of unit operations. All this data is coded directly into the ASSF tool, allowing for properties and constants to be extracted whenever it is necessary within a stream or unit operation.

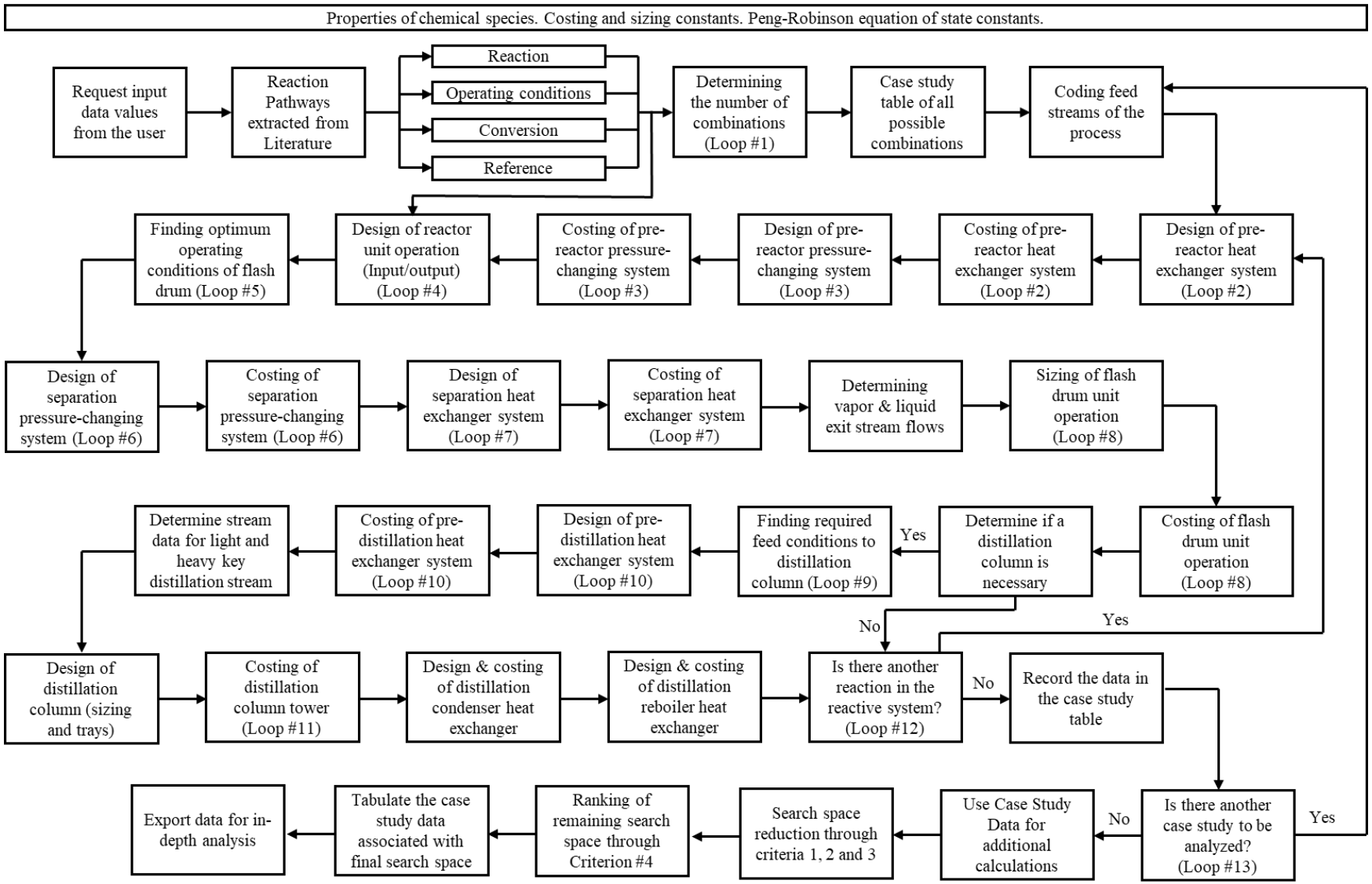

Figure C.1: Flow chart representation of the ASSF tool providing an overview of the code in its entirety

C.2. Input Data Required

The data requested from the user is that which is time/situation dependent, such as economic factors and purity requirements. The following data is required to be inputted by the user when utilizing the ASSF tool:

- CO_2 feed flow rate basis (kmol/hr)
- Percentage excess H_2 feed (%) – By feeding excess H_2 into the reactive system, CO_2 becomes the limiting reagent, aiding in increased CO_2 conversions. This minimizes the amount of unreacted CO_2 exiting the process, thereby providing an environmental benefit.
- Pressure-changing unit operation efficiency (%)
- Chemical Engineering Price Cost Index (CEPCI)
- Pressure of the heat exchanger utility, i.e cooling water or steam (bar)
- Temperature change associated with steam utility (^oC)
- Temperature change associated with cooling water utility (^oC)
- Cost of reactants and utilities (CO_2, H_2, CaO and natural gas) ($/kg)
- Sales potential of products (CH_3OH and DME) ($/kg)
- Distillation column recovery percentage (%)

The ASSF tool initially requests that the user input the reaction pathways and their associated reaction conditions. As shown in Figure C.1, this comprises of the operating conditions for the reaction pathway (temperature and pressure), conversion and a reference marker. The reference marker is essential, as this allows for cross-referencing within the ASSF tool, when developing and analyzing the associated reaction pathway combinations/case studies.

C.3. Development of the Reaction Pathway Database and Associated Combinations

Once all of the required input data has been entered into the ASSF tool, the user is presented with a tabulated output of this data, allowing for the user to verify the inputs accordingly. This occurs through a systematic approach within the ASSF tool, with each reaction being added to the table upon entry. By doing so, the ASSF tool is able overwrite previous individual reaction

pathways that have already been tabulated, reusing variables through each loop. This lowers the number of variables utilized in the ASSF tool, ultimately resulting in the reduction of memory usage and computational time associated with this section of the ASSF tool.

The final, tabulated reaction pathway list, and its associated conditions, is known as the RPD, and is the key component in determining the number of possible reaction pathway combinations. At this point in the ASSF tool, all user data has been inputted, and therefore subsequent stages in the ASSF tool are fully automated.

The first loop within this automated process involves the construction of reaction pathway combinations, ensuring that alternative reaction mechanisms are considered in the production of a single/multiple product(s). Figure C.2 provides a basic flow chart of the first automated loop within the ASSF tool.

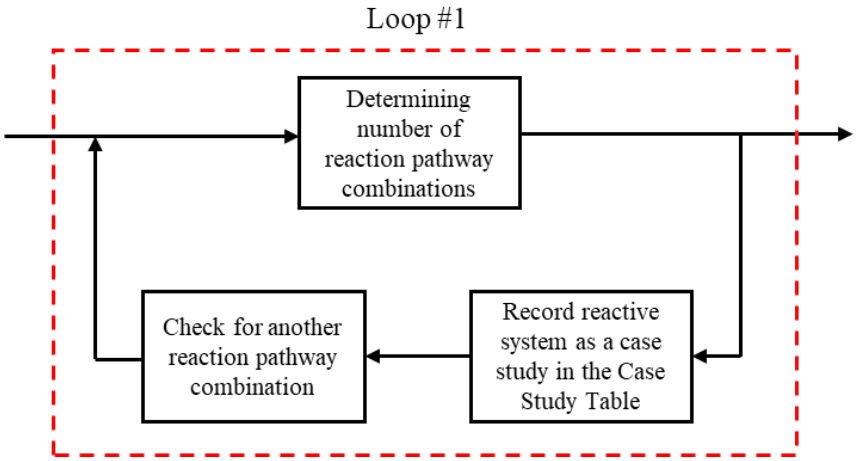

Figure C.2: Basic flow chart of Loop #1 - Determining the number of reaction pathway combinations possible

As per Figure C.2, the ASSF tool systematically goes through each of the reaction pathways within the RPD, tabulating any possible reaction pathway combinations. This case study table contains all the systems that are to be designed and analyzed in subsequent sections of the ASSF tool. Upon checking a single reaction pathway for potential combinations, the remainder of the reaction pathways in the RPD undergo the same process, thereby ensuring a complete search space. This repetitive nature identifies this section of the ASSF tool as its first major automated loop.

After this loop is complete, and all reaction pathways have been analyzed for potential reaction pathway combinations, the case studies are tabulated and presented to the user. The user is requested to either proceed with the analysis or terminate the program and export the associated results.

Should the user choose to not proceed with the analysis of these case studies, the reaction pathway combinations are exported to a Microsoft ® Excel spreadsheet, allowing for the data to be subsequently utilized by the user. Proceeding with the analysis, on the other hand, continues to the automated design and analysis procedure, whereby the search space is reduced through various economic and environmental considerations.

C.4. The Feed Streams

After initiating the analysis of the aforementioned case studies, the feed streams are first coded, detailing the flow rates for CO_2 and H_2 that is to be utilized as a basis for subsequent process design. The is especially important in the design of unit operations and their respective sizes.

It is important to note that this feed stream, whilst not a loop in itself, is part of an overall loop within the ASSF tool, whereby the analysis of each case study begins at this point. Therefore, whilst there still exist case studies to be analyzed within the reaction pathway combination table, the entire automated design code is looped back to these feed streams.

C.5. Pre-Reactor Heat Exchanger System

The feed streams are mixed into a single stream for subsequent pressurizing and heating. The mixed stream passes through a pre-reactor heat exchanger system. The purpose of this system is to bring the feed streams to the desired reaction operating temperature, thereby facilitating the reaction process. This system forms the second major overall loop of the ASSF tool, as represented by the flow chart given in Figure C.3.

As shown by Figure C.3, the main loop within the design of the pre-reactor heat exchanger system is to ensure that the sizing of the heat exchanger (heat transfer area) is within the costing constraints developed by Turton, *et al*. (2009). During this loop, the required heat exchanger is first sized and recorded as a preliminary value. The heat transfer area is then checked against the associated size constraints.

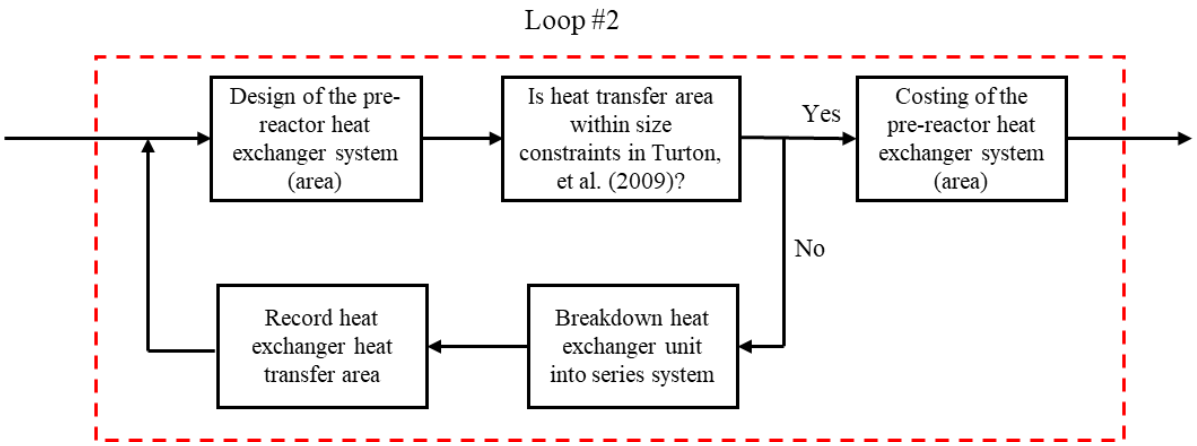

Figure C.3: Basic flow chart of Loop #2 – Design and costing of the pre-reactor heat exchanger system

Should the heat transfer area not abide by the costing constraints, the heat exchanger is divided into multiple unit operations in series, with an incremental temperature increase. This lowers the individual area size of each heat exchanger and is explained in detail within Section 3.7. This loop continues until all heat exchangers lie within the costing constraints, before proceeding to the costing of the heat exchanger system.

C.6. Pressure-Changing Unit Operation System

After adjusting the feed stream temperature to that of the reaction temperature, the focus of the ASSF tool then shifts to meeting the required reaction pressure. This is achieved through the use of a pressure-changing unit operation, whereby an increase in pressure is accomplished through use of a compressor, and a decrease in pressure is accomplished by utilizing a turbine.

This loop, within the ASSF tool, operates in a similar manner to that of the heat exchanger system detailed in Figure C.3, and is represented by means of the flowsheet in Figure C.4. The key differences between these two loops lies in the sizing of the pressure-changing unit operation being represented in terms of its fluid power, typically expressed in kilowatts (kW).

Furthermore, should the fluid power of the unit operation not lie within the costing constraints, the pressure-changing unit operations are broken down into multiple parallel unit operations (Section 3.8). This differs from the series configuration of the heat exchanger system.

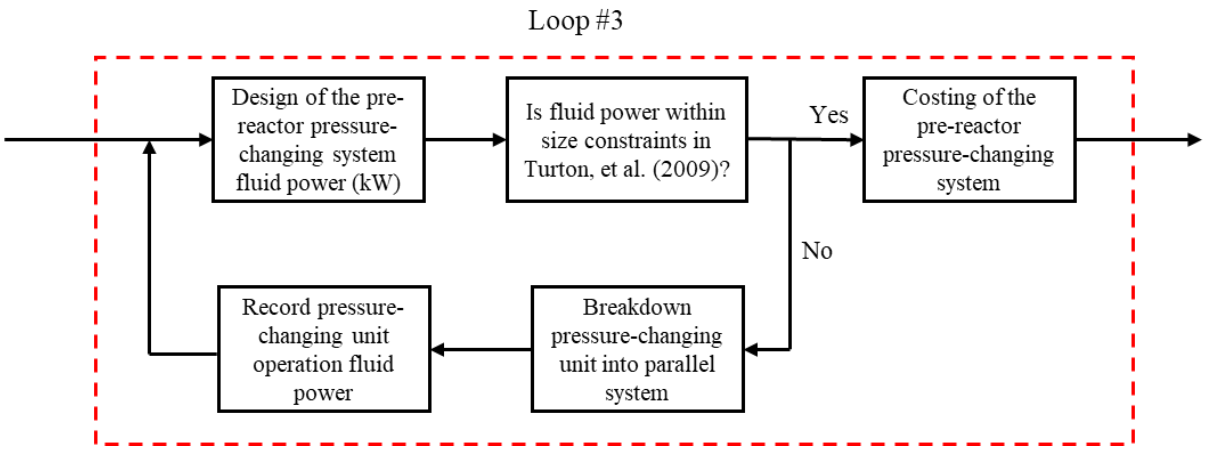

Figure C.4: Basic flow chart of Loop #3 – Design and costing of the pre-reactor pressure-changing system

A parallel pressure-changing unit operation system is chosen, in order to lower the flow rate through each unit operation, thereby reducing the associated fluid power. The ASSF tool was initially coded to develop a series pressure-changing unit operation system. However, due to the constant, large flow rate through all unit operations, this proved to have minimal impact on the fluid power ratings, especially at high operating pressures. Hence the introduction of a parallel unit operation system.

C.7. Reactor Unit Operation

The ASSF tool considers the reactor unit operation in terms of its input and output, not focusing on the intricate design of the reactor unit operation. This is due to the fact that the RPD contains the reaction conversions noted in literature and previous experimentation. The purpose of this is to utilize the ASSF tool as a means to reduce the search space of reaction pathways under consideration, providing the user with the reduced search space to analyse further by means of in-depth reaction kinetics.

The reactor unit operation, however, forms the fourth major loop in the ASSF tool. This loop is represented by means of the flow chart presented in Figure C.5. As shown by Figure C.5, this fourth loop comprises of two sub-loops. The first of these sub-loops determines the presence of a limiting reagent within the reactive system, correcting for this reagent and ensuring that none of the exit flow rates are expressed as negative values within the ASSF tool. Furthermore, this ensures that subsequent reaction conversions, within the reactive system, can also be adjusted.

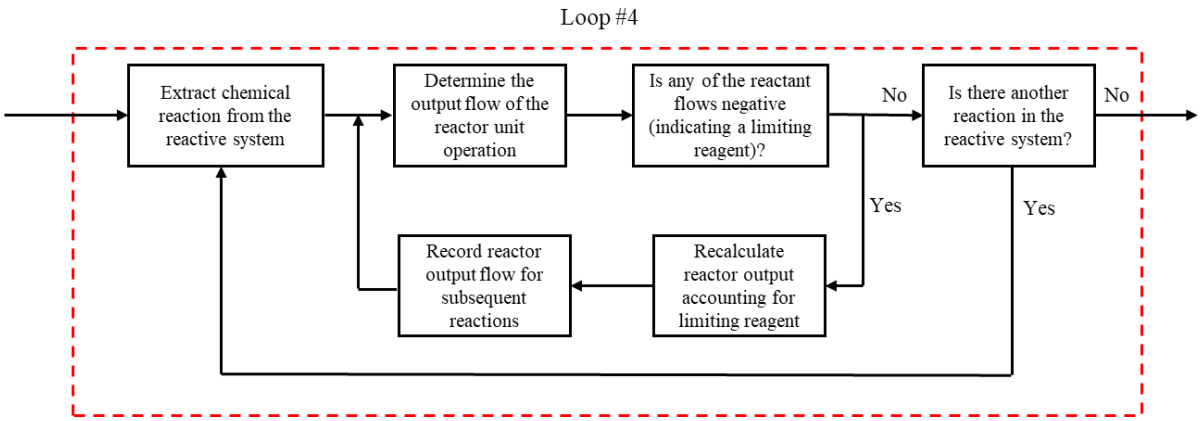

Figure C.5: Basic flow chart of Loop #4 – Input/output flow of the reactor unit operation

After accounting for the possibility of a limiting reagent within the reaction, the second sub-loop within this segment of the ASSF tool, checks to see if there are any other reactions present within the reactive system. The ASSF tool deals with each reaction in a sequential process. Therefore, if there are three reactions occurring in a single reactor unit operation, the ASSF tool first calculates the outputs associated with the first reaction, before using these results as intermediates for the second and third reactions.

C.8. Achieving the Separation Conditions

In order to find the optimum operating conditions required for effective separation, the ASSF tool utilizes an iterative approach. This involves utilizing a basis for the separation pressure and temperature, and iteratively solving for the separation pressure that is able to achieve a CO_2 separation in excess of 95%. Figure C.6 provides a flow sheet representation of the loop utilized in determining the optimum operating conditions for the subsequent separation systems.

As shown in Figure C.6, the assumed pressure and temperature (chosen as ambient conditions) was used in calculating the φ value, denoted within the Rachford-Rice equation (Appendix E). This symbol is denoted as the fraction of the feed that exists within the vapor phase and is utilized in calculating the composition of the vapor and liquid streams exiting the phase separator/flash drum. The first check, however, is to ensure that the value of φ lies between 0 and 1, ensuring that a practical value is achieved from the Rachford-Rice equation. Should this constraint not be met, the pressure is increased incrementally, until the φ value lies within these constraints.

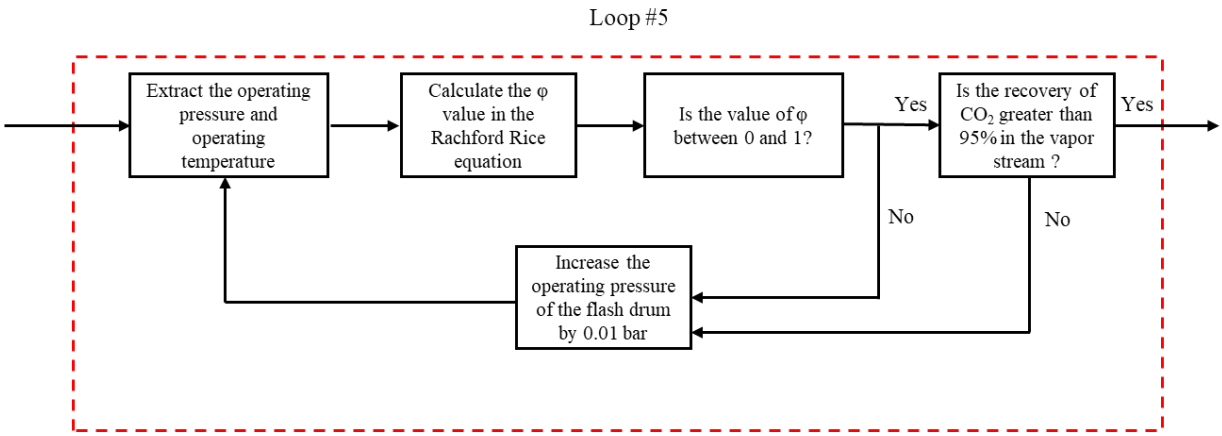

Figure C.6: Basic flow chart of Loop #5 – Determining the operating conditions required for separation

The focus is placed on increasing the pressure of the separation process, rather than temperature, as pressure-changing unit operations are found to be more expensive than heat exchangers. Therefore, in order to reduce the cost of the process, the pressure change for separation, when compared to the reactor's exit stream, should ideally be minimal. Therefore, an increase in pressure, from ambient conditions, lowers the subsequent cost of the pressure-changing unit operation.

The second loop/check determines the optimum operating conditions of the separation system and is dependent on the fraction of CO_2 removed from the product stream. As a basis, this was set to a removal rate of 95%, ensuring minimal impact on the purity of the product stream. Through subsequent tests of the ASSF tool it was found that 100% separation via the flash drum was not possible, as a portion of the CO_2 is dissolved within the liquid product stream. Therefore, should this removal factor of 95% not be met, the pressure is once again increased, beginning the iterative process. These iterations are terminated when both conditions are met, with the final operating conditions at this point being noted as the separation conditions.

Loops 6 and 7 (depicted in Figure C.1), detailing the separation pressure-changing unit operation and heat exchanger systems, were designed and coded in a similar manner to the pre-reactor unit operations. Therefore, the flow charts depicted for Loops 2 and 3 (Figure C.3 and C.4, respectively) still hold true for the design and costing of the unit operations required to meet the separation conditions.

C.9. Flash Drum Unit Operation – Separation System

After designing and costing the unit operations required to meet the separation conditions, the ASSF tool proceeds to the design and costing of the flash drum unit operation, which utilizes vapor-liquid equilibrium to achieve a phase separation. This section of the ASSF tool is the eighth major loop, represented by means of the flow chart provided in Figure C.7.

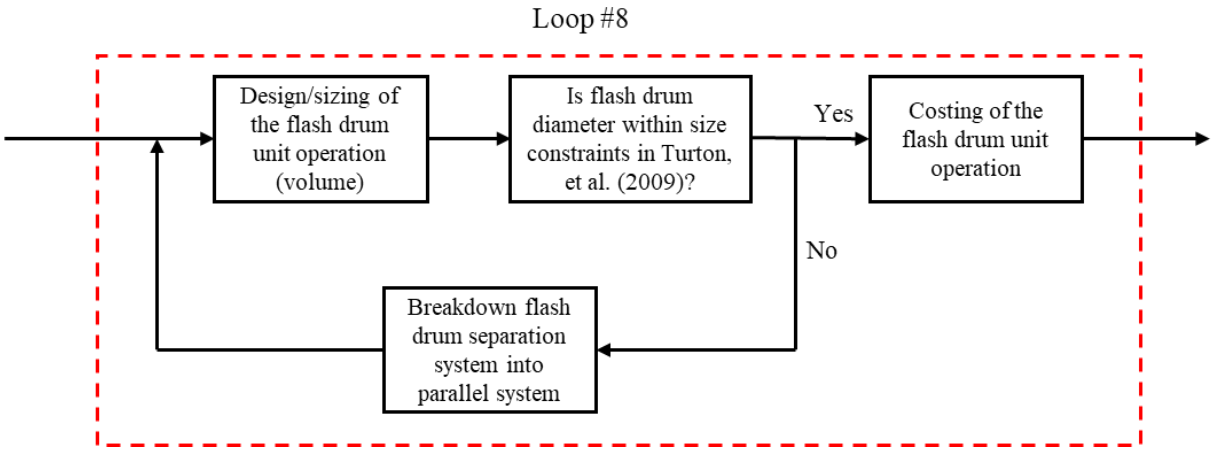

Figure C.7: Basic flow chart of Loop #8 – Design and costing of the flash drum unit operation

Utilizing the φ value calculated in the Rachford-Rice equation, the composition of the vapor and liquid stream exiting the flash drum unit operation is calculated. The temperature and pressure of these streams are recorded as being the same as the operation temperature of the flash drum, with all other subsequent stream data being calculated by means of these known conditions.

As per Figure C.7, the loop within this section of the ASSF tool, ensures that the flash drum size constraints are met, as per the costing equations developed by Turton, *et al*. (2009). Should the flash drum volume lie outside of the range previously defined, the unit operation is broken down into multiple unit operations in a parallel configuration, thereby lowering the flow rate to each unit (Section 3.9). This loop continues until the size constraints are met, before proceeding to the costing of the unit operation.

C.10. Distillation Columns – Separation System

Upon designing and costing the flash drum unit operation, the ASSF tool proceeds to the sizing and costing of the distillation column, should one be required. Therefore, the first focus of the ASSF tool is to determine whether or not a distillation column is necessary within the process. This is determined through two main criteria, namely:

- Checking the presence of a product stream
- Checking the purity of the product stream.

Should a product stream exist, with a purity less than 99 wt%, this would require a distillation column to achieve a product capable of commercialization. It is imperative that high purity be achieved for the associated product, as this is a key factor when competing in the current market.

If a distillation column is deemed necessary, the feed stream to the distillation column is adjusted to create a stream with vapor-liquid equilibrium, defined as the quality of the distillation feed stream. This is accomplished through use of the Rachford-Rice procedure, as detailed in Figure C.6. The difference in this however, is that the temperature is varied to achieve a separable stream, as opposed to varying the operating pressure. This iterative process is the ninth major loop within the ASSF tool.

The tenth major loop within the ASSF tool involves the design and sizing of the heat exchanger system, to achieve these distillation feed stream conditions. This employs a loop similar to that utilized in the pre-reactor heat exchanger system (Loop #2, Figure C.3).

Upon meeting all of these conditions, the distillation column is sized and costed, by means of the eleventh major loop within the ASSF tool. This also employs the size constraints detailed by the relevant costing equations, however, since the distillation column comprises of both a tower and internal trays, both sizing constraints must be adhered to. This loop can be represented by the flow chart provided in Figure C.8.

As shown in Figure C.8, after conducting a preliminary sizing of the distillation column, the size constraints are checked for the tower first, in terms of its volume, and for tray area. Should either of these two constraints not be met, the code is looped back, breaking down the distillation column into multiple distillation columns in a parallel configuration. This reduces the flow rate to each distillation column, thereby reducing their associated size.

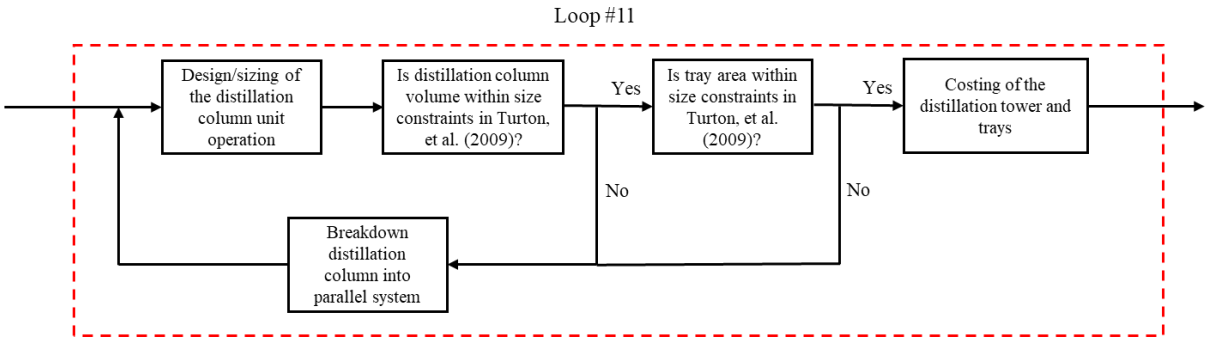

Figure C.8: Basic flow chart of Loop #11 – Design and costing of the distillation column

The final stream exiting the distillation column then contains marketable product/s, and/or a waste stream, depending on the mixture being separated.

C.11. Data Consolidation and Search Space Reduction

When all unit operations are designed and costed, relating to the specific reactor unit operation, a check is made to ensure that there are no other reactors involved within this overall chemical process. Each reactor unit operation follows its own generic flow sheet (Section 3.2), ensuring effective and accurate comparisons between the case studies. Therefore, should an additional reactor be required in the process, the twelfth loop extracts the product stream to be treated as an intermediate, and loops back to the design and costing of the pre-reactor unit operations. This loop continues until all reactors in the reactive system have been accounted for.

The thirteenth loop checks if there are any other case studies to be analysed within the ASSF tool, based on the aforementioned reaction pathway combinations. Should this be the case, the entire code is looped back to the feed streams of the processes, designing and costing the subsequent case studies, or reaction pathway combinations. Loops 12 and 13 are detailed in Figure C.1, which provides an overview of the operating mechanism behind the ASSF tool.

The case study data for all chemical processes designed within the ASSF tool are then tabulated, allowing for subsequent calculations to be conducted. These calculations look at the case studies from an economic and environmental perspective, eliminating those that are infeasible based on predefined criteria.

The final reduced search space is then ranked in order of its viability, whereby a trade-off between economic and environmental benefits is found. This ranking provides the user with an

ordered list of which reactive system should be investigated first, therefore allowing for design resources to be optimally allocated. Furthermore, with the aforementioned search space reduction criteria, all reaction pathways within the reduced search space are deemed to exhibit environmental and economic feasibilities. This ensures that all reactive systems in the final reduced search space have the potential for implementation.

Finally, the reduced search space is presented to the user in the form of a table with subsequent exporting of the results to Microsoft ® Excel being possible from the ASSF tool.

Appendix D: Flowchart Representations of ASSF Tool Segments

This Appendix contains flowchart representations of the code responsible for the various segments within the ASSF tool, allowing for the coding framework and loops to be easily perceived.

D.1. Code Associated with Reaction Pathway Database Development

Figure D.1 provides a diagrammatic representation of the code responsible for the development of the RPD, as detailed in Section 3.3. This section of the ASSF tool is represented by means of a flowchart, allowing for the reader to follow the chronological order by which the tool operates, highlighting possible decision-making stages, and their associated loops.

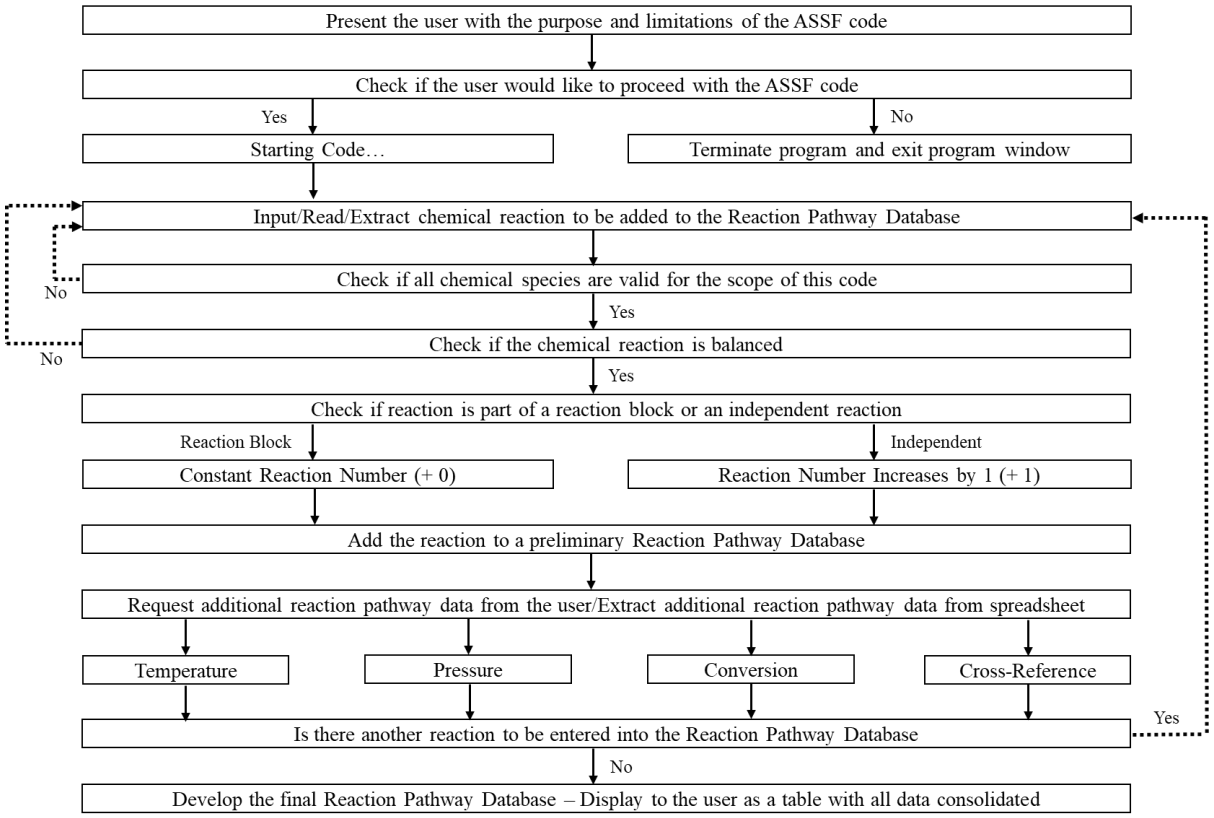

Figure D.1: Flowchart representation of the code associated with the development of the RPD

As shown in Figure D.1, there are three main coding loops that exists within this section of the ASSF tool. The first two loops exist to ensure that the provisionary reaction pathway checks

(Section 3.3.1) are met, in terms of the chemical species involved and the balancing of the chemical reaction. The third loop within this section of the ASSF tool checks if any further chemical reactions need to be added to the database. This is the deciding step on whether the user is prompted for an additional reaction, or if the database is complete.

Upon completion of the RPD, the user is presented with a completed database, allowing the user to check and confirm all recorded data. This is the RPD that forms the foundation of subsequent stages within the ASSF tool, including the reaction pathway combinations and their associated analysis thereof.

D.2. Code Associated with Reaction Pathway Combinations

Figure D.2 provides a diagrammatic representation of the code focused on the development of the associated reaction pathway combinations, utilizing the RPD previously developed.

As per Figure D.2, the input into this section of the code is automatically extracted from the RPD developed, which is highlighted within Section 3.3. This RPD, however, contains detailed information of the reaction pathway, and associated reaction pathway blocks, including operating conditions, conversions and cross-reference markers.

When considering reaction pathway combinations, however, the only required information is the reactants, products, and a cross-referencing marker, as this information will determine whether a product can be utilized as an intermediate, if paired with another reaction within the database. As a result, in order to reduce the memory usage of the ASSF tool, the stoichiometric co-efficients, operating conditions and conversions of all reactions were removed from the RPD matrix, with a separate, undisturbed RPD being stored in the background of the ASSF tool for future use. This reduced RPD can be referred to as the ‘Basic RPD’ (B-RPD).

In order to reduce the computational time of this section within the ASSF tool, reaction blocks are reduced to a single overall reaction. This procedure allows for only a single reaction to then be registered within the B-RPD. By doing so, the search for reaction pathway combinations is limited to the single overall reaction. This ultimately reduces unnecessary computational time, as the ASSF tool does not need to consider each reaction within a reaction block. In any case, all sub-reactions within a reaction block are unable to be split and are therefore grouped together as a single entity.

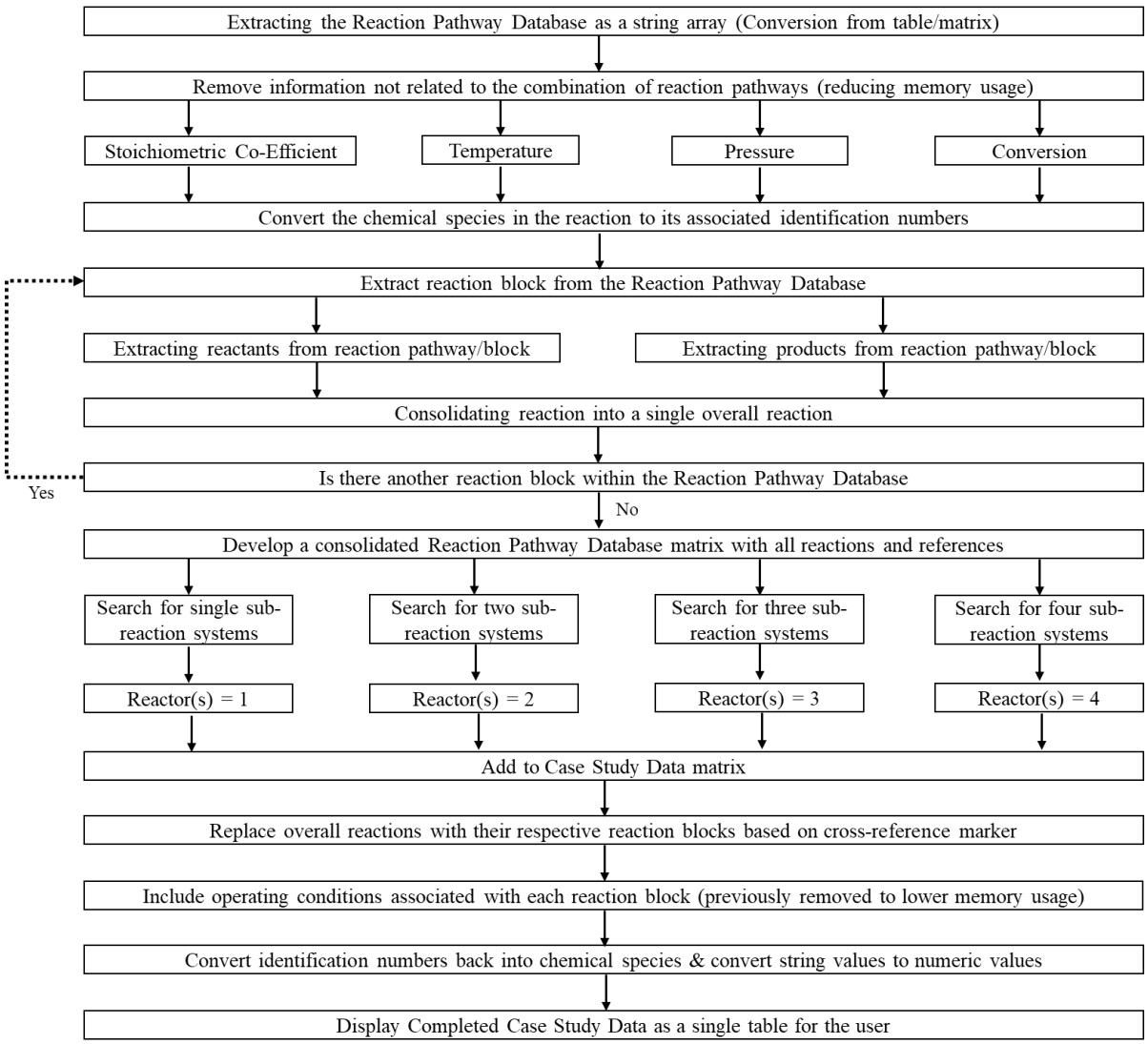

Figure D.2: Flowchart representation of the code associated with determining the reaction pathway combinations possible

When combining reactions, it is important to note that these reactions occur in separate reactor unit operations. As a result, a two sub-reaction system will have two reactor unit operations, each associated with its own generic process, as shown in Figure 3.2 and explained in Section 3.2.

Upon determining the possible reaction pathway combinations, the ASSF tool then compiles the case study data into a single matrix. During this stage, the chemical species identification numbers are replaced with the appropriate chemical formula, promoting readability with the user. Furthermore, the previously excluded operating conditions in the B-RPD, is reintroduced into the case study data providing the user with a table comprising of the complete data set associated with each case study/combination.

D.3. Code Associated with Chemical Species and Stream Vapor Pressure

Figure D.3 provides a diagrammatic representation of the code focused on calculating the vapor pressure of the chemical species present within a stream, as well as the total stream vapor pressure, as detailed in Section 3.6.2.

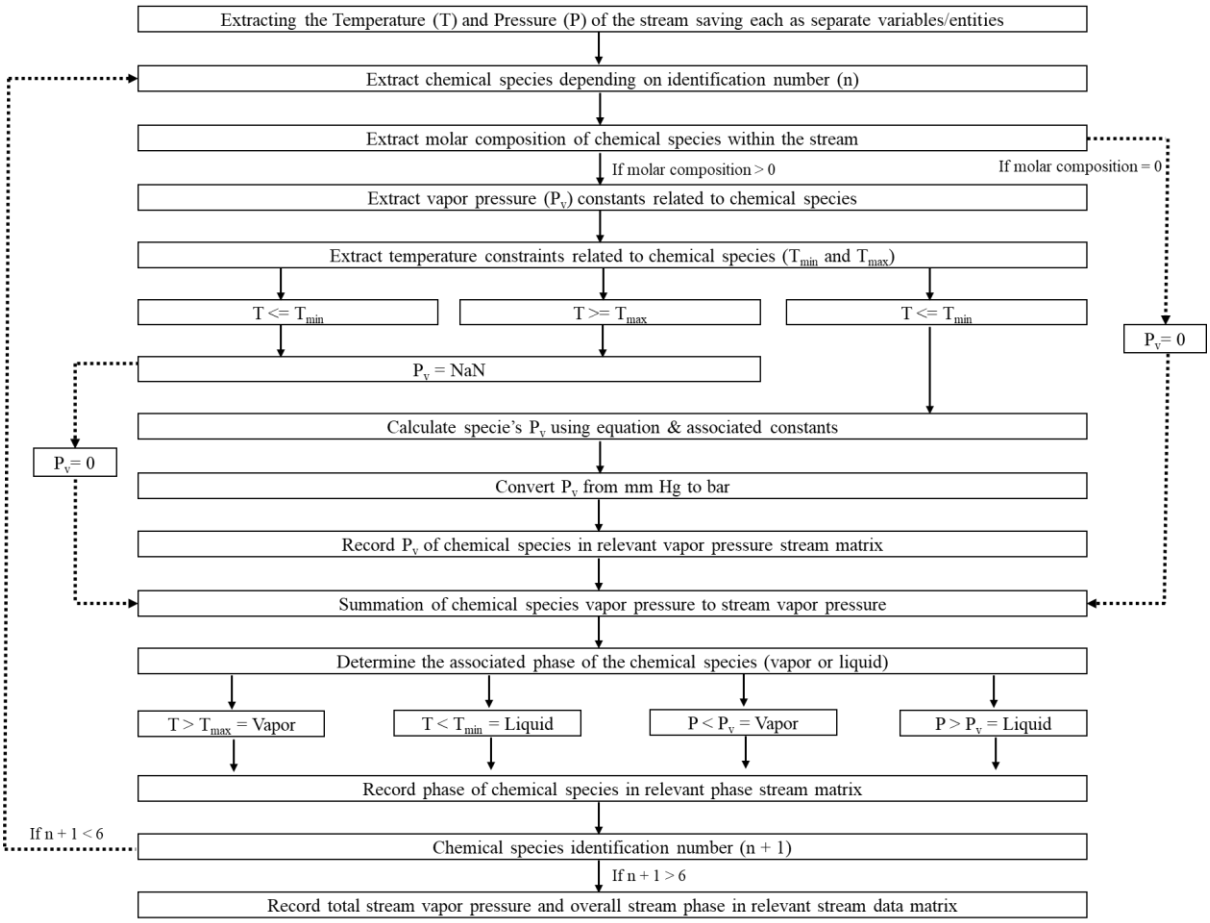

Figure D.3: ASSF tool section associated with the calculation of species and stream vapor pressures

D.4. Code Associated with Chemical Species and Stream Enthalpies

Figure D.4 provides a diagrammatic representation of the code focused on calculating the enthalpy of the chemical species present within a stream, as well as the total stream enthalpy, as detailed in Section 3.6.3.

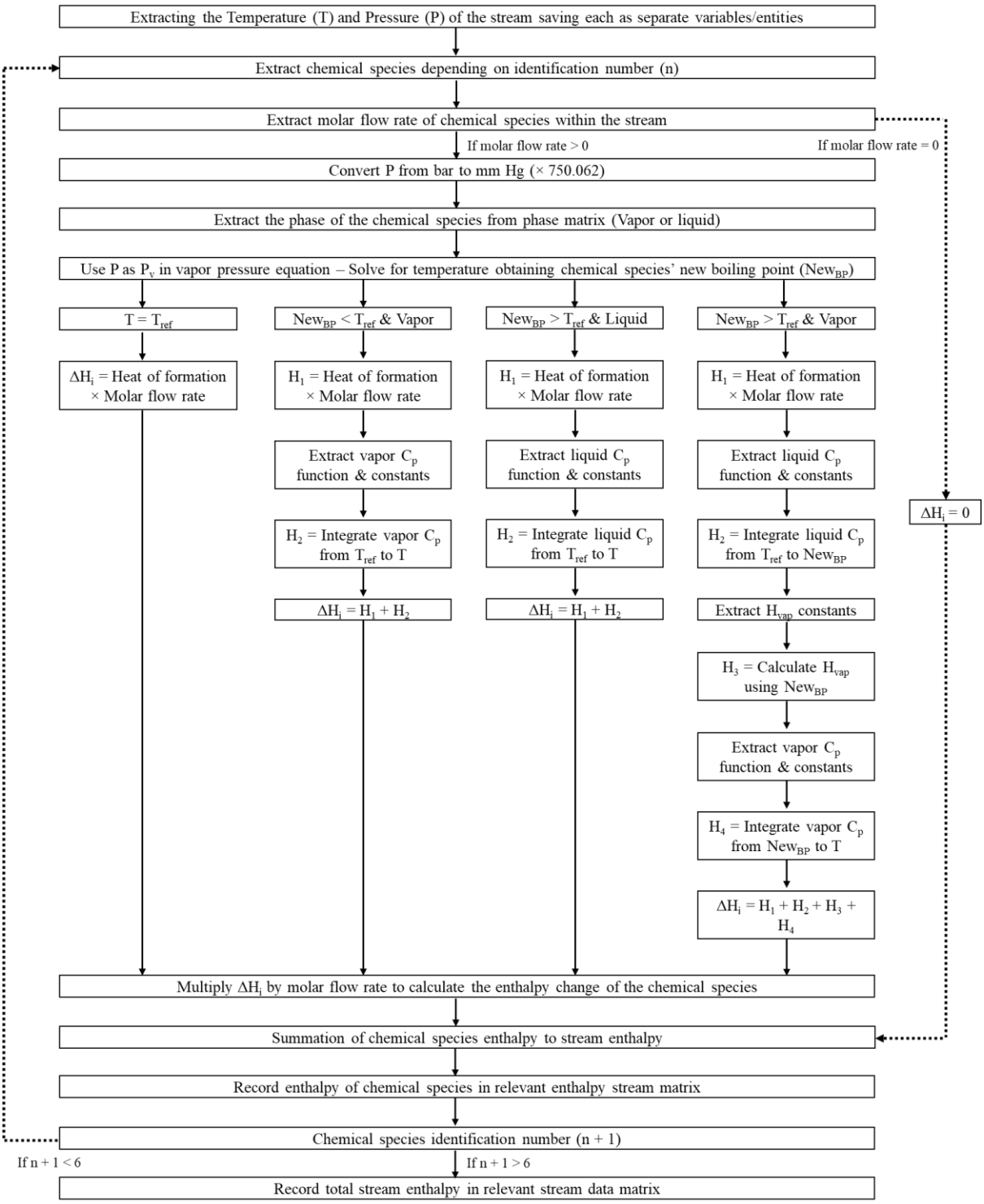

Figure D.4: ASSF tool section associated with the calculation of chemical species and stream enthalpies

D.5. Code Associated with Chemical Species and Stream Volumetric Flow Rate

Figure D.5 provides a diagrammatic representation of the code focused on calculating the volumetric flow rate of the chemical species present within a stream, as well as the total stream volumetric flow rate. This is dependent on the Peng-Robinson EOS, as well as the phase of the chemical species, as detailed in Section 3.6.4.

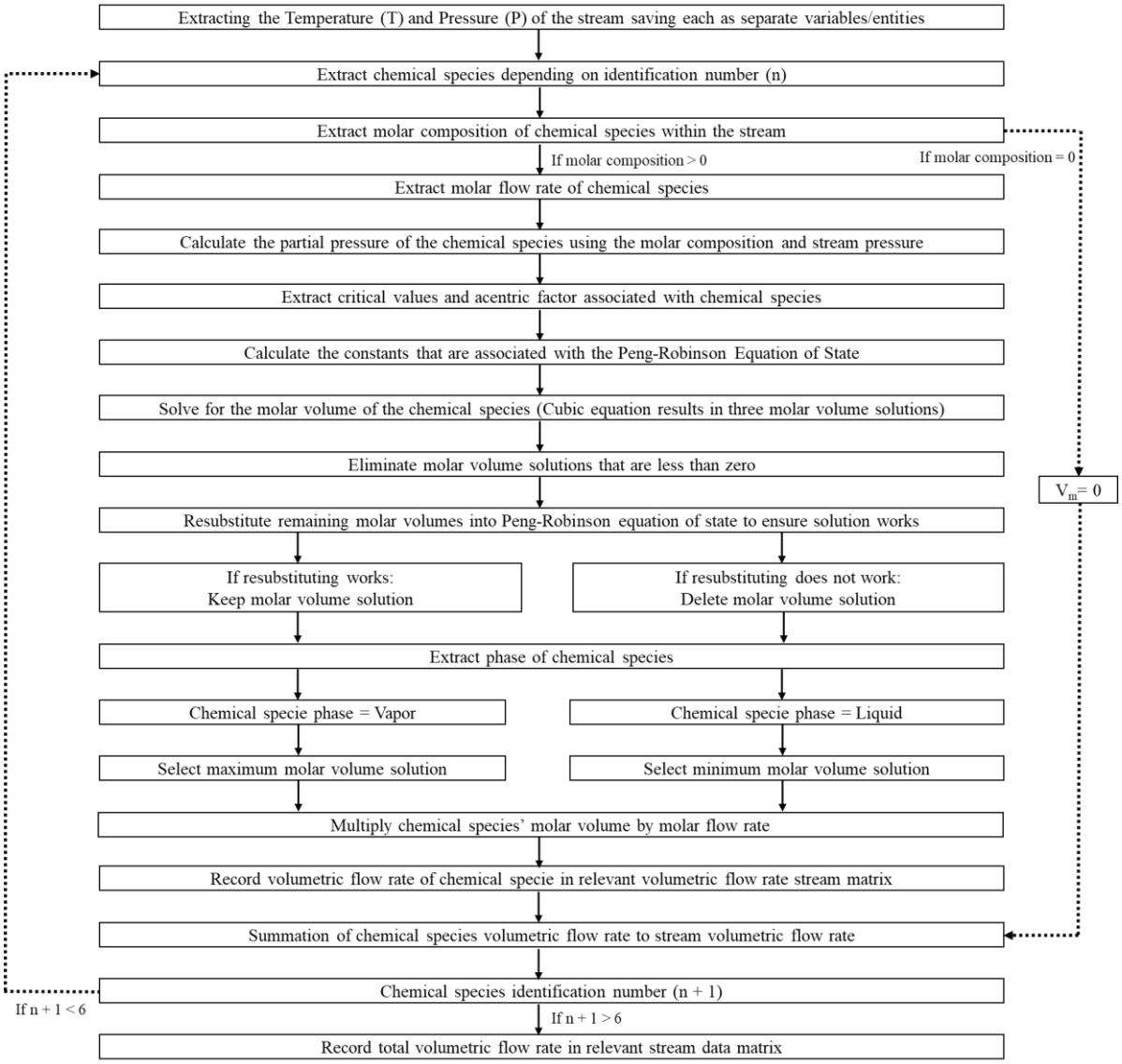

Figure D.5: ASSF tool section associated with the calculation of chemical species and stream volumetric flow rate

D.6. Code Associated with Calculating and Recording Stream Data

Figure D.6 provides a diagrammatic representation of all stream data calculated within the ASSF tool. It is important to note that this code was repeated for each stream within all processes considered and analyzed within the ASSF tool.

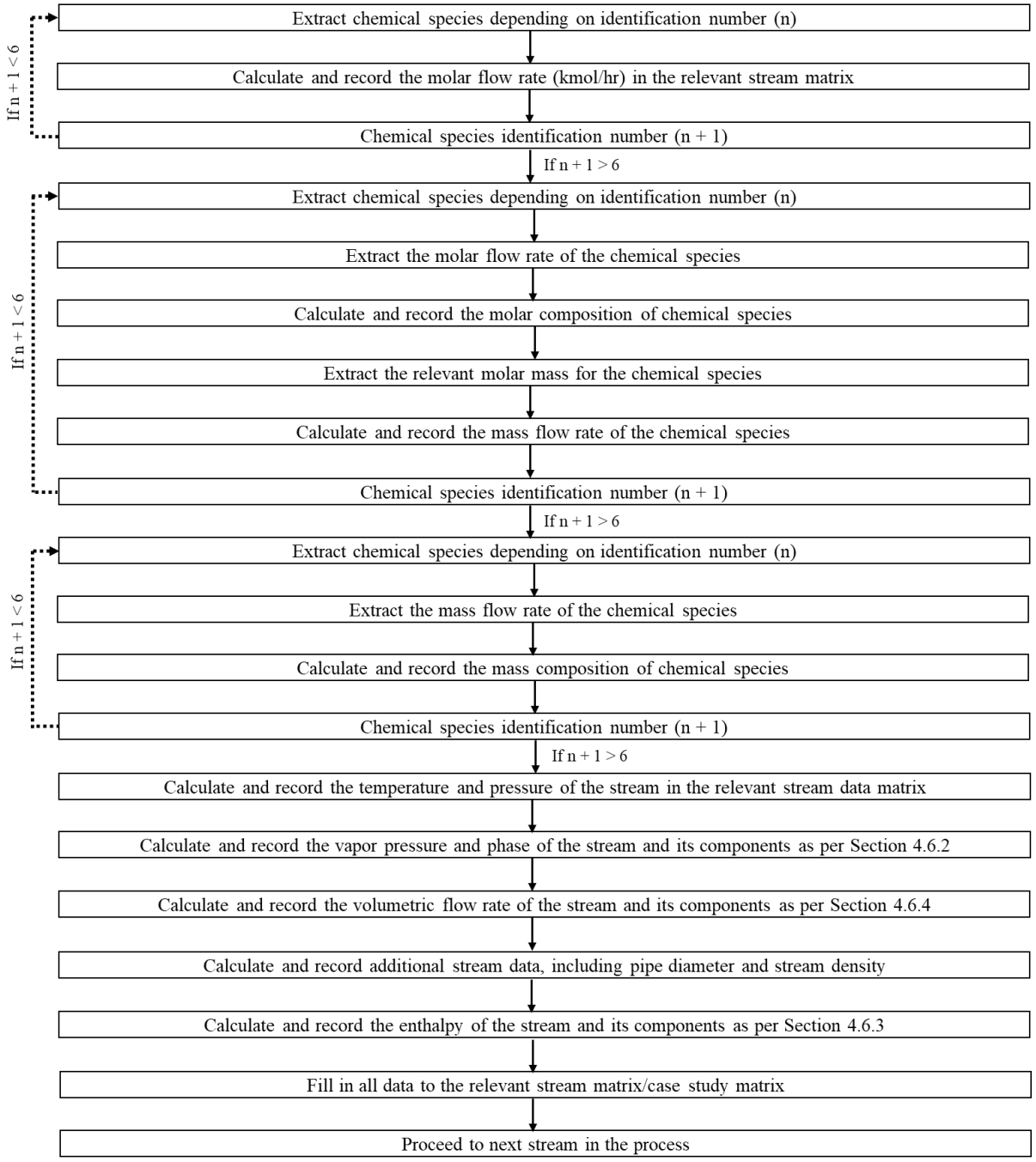

Figure D.6: Diagrammatic representation of the code structure by which stream data is calculated within the ASSF tool

D.7. Code Associated with Sizing and Costing of Heat Exchangers

Figure D.7 provides a diagrammatic representation of the ASSF tool segment focused on the design and costing of the heat exchanger unit operations.

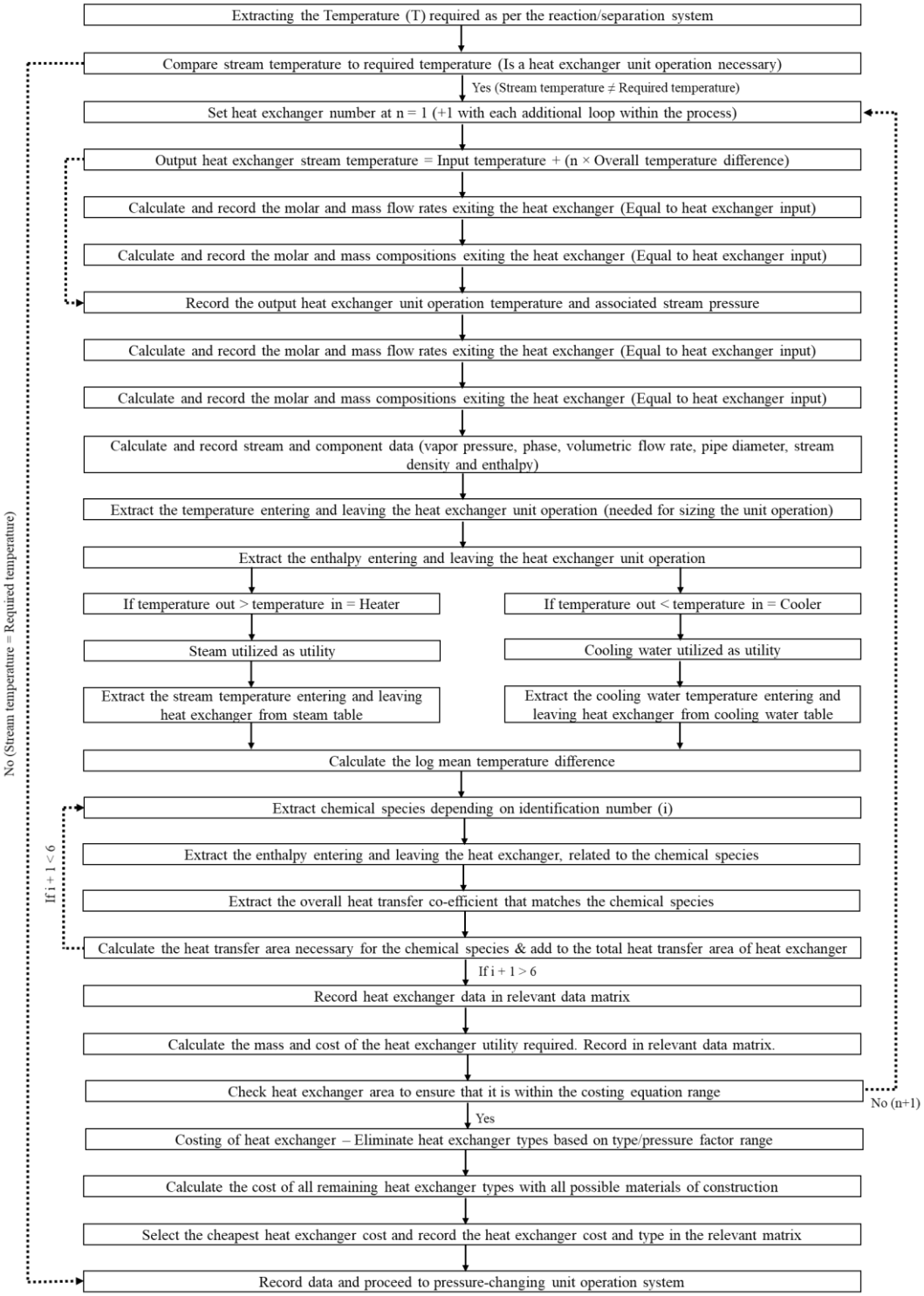

Figure D.7: Diagrammatic representation of the code structure by heat exchangers are designed and costed within the ASSF tool

It is important to note that the main loop within this code is to check if the heat exchanger is within the costing equation size constraints. Should this not be the case, the heat exchanger is broken up into a series of heat exchangers with incremental temperature increases, as detailed in Section 3.7.1.

Furthermore, the costing procedure utilized with all unit operations aims to find the cheapest possible heat exchanger unit operation that is able to perform the necessary function of heating or cooling the appropriate process stream.

D.8. Code Associated with Sizing and Costing of Compressors & Turbines

Figure D.8 provides a diagrammatic representation of the ASSF tool segment that deals with the design and costing of the pressure-changing unit operations in process. As with the heat exchanger unit operation design detailed in Section 3.7, the main loop within this segment of the code, is the check to ensure that the unit operation is within the size constraints detailed within the costing equations. Should the pressure-changing unit operation have a power greater than the upper limit of this constraint, the unit operation is split into multiple parallel unit operations, thereby lowering the flow rate through each unit operation, and consequently the power of each individual unit operation.

Furthermore, the costing procedure employed for this unit operation looked at finding the cheapest possible unit operation that is able to compress or expand the desired stream, aiding in economic feasibility of the designed process.

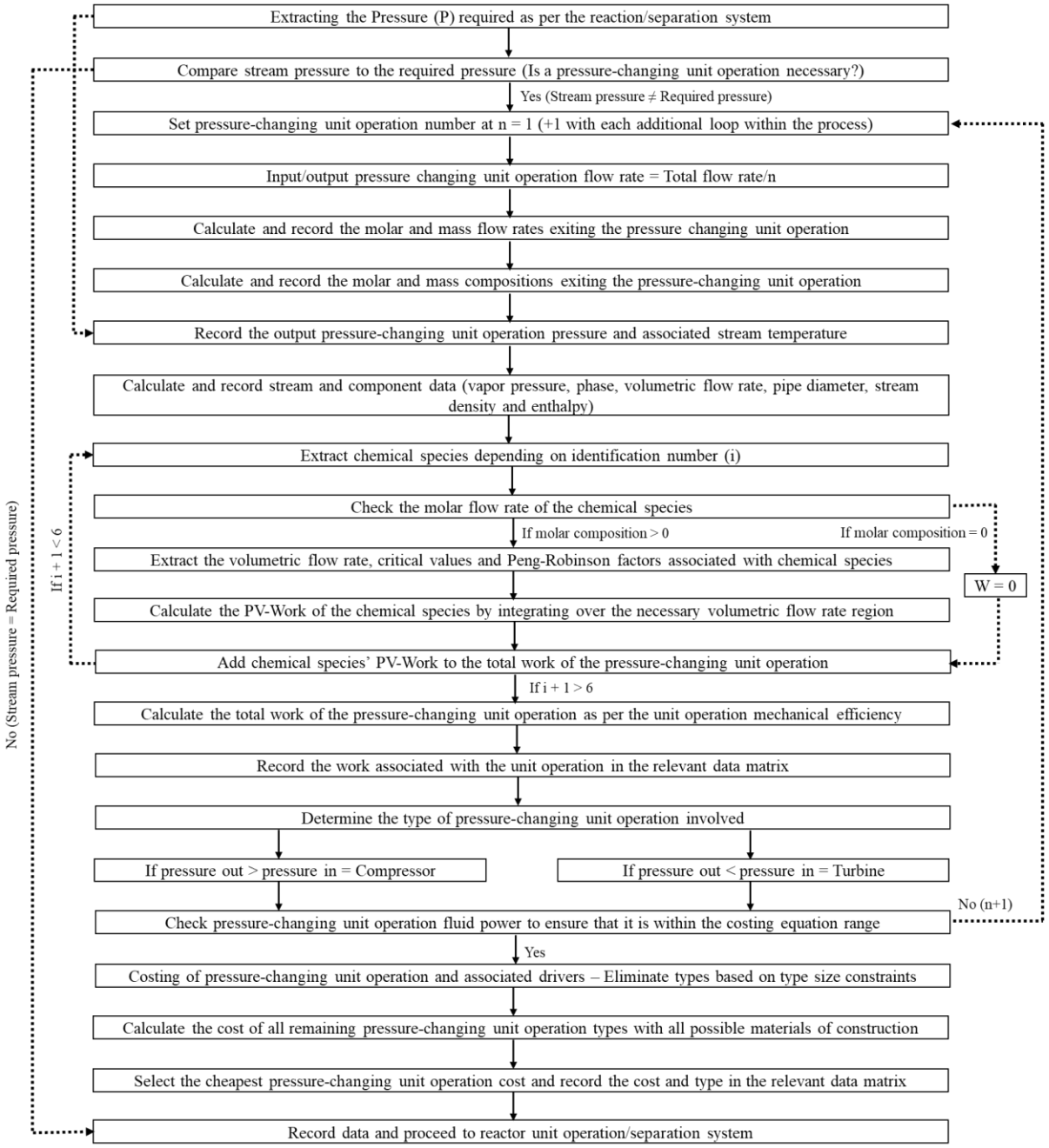

Figure D.8: Diagrammatic representation of the code structure by which pressure-changing unit operations are designed and costed within the ASSF tool

D.9. Code Associated with Sizing and Costing of Flash Drums

The design and costing of flash drum unit operations spanned over four main segments of the ASSF tool, namely:

- Determining the optimum pressure of the flash drum unit operation that is able to achieve a CO_2 vapor recovery rate of 95%.
- Designing and costing the pressure-changing and heat exchanger unit operations necessary in achieving the flash drum operating conditions.
- Determining the vapor and liquid flow rates and compositions leaving the flash drum, as per the Rachford-Rice equation.
- Designing and costing of the flash drum unit operation.

As shown in Figure D.9, there are three main loops within the ASSF tool segment dealing with flash drum unit operations. The first two loops perform iterative calculations to achieve the necessary CO_2 recovery rate, increasing the operating pressure of the flash drum with each iteration. The third loop ensures that the size constraints associated with the costing equations are met, splitting the flash drum into multiple parallel unit operations, if required. This loop follows a similar principle as that which was utilized within the sizing and costing of the pressure-changing unit operations.

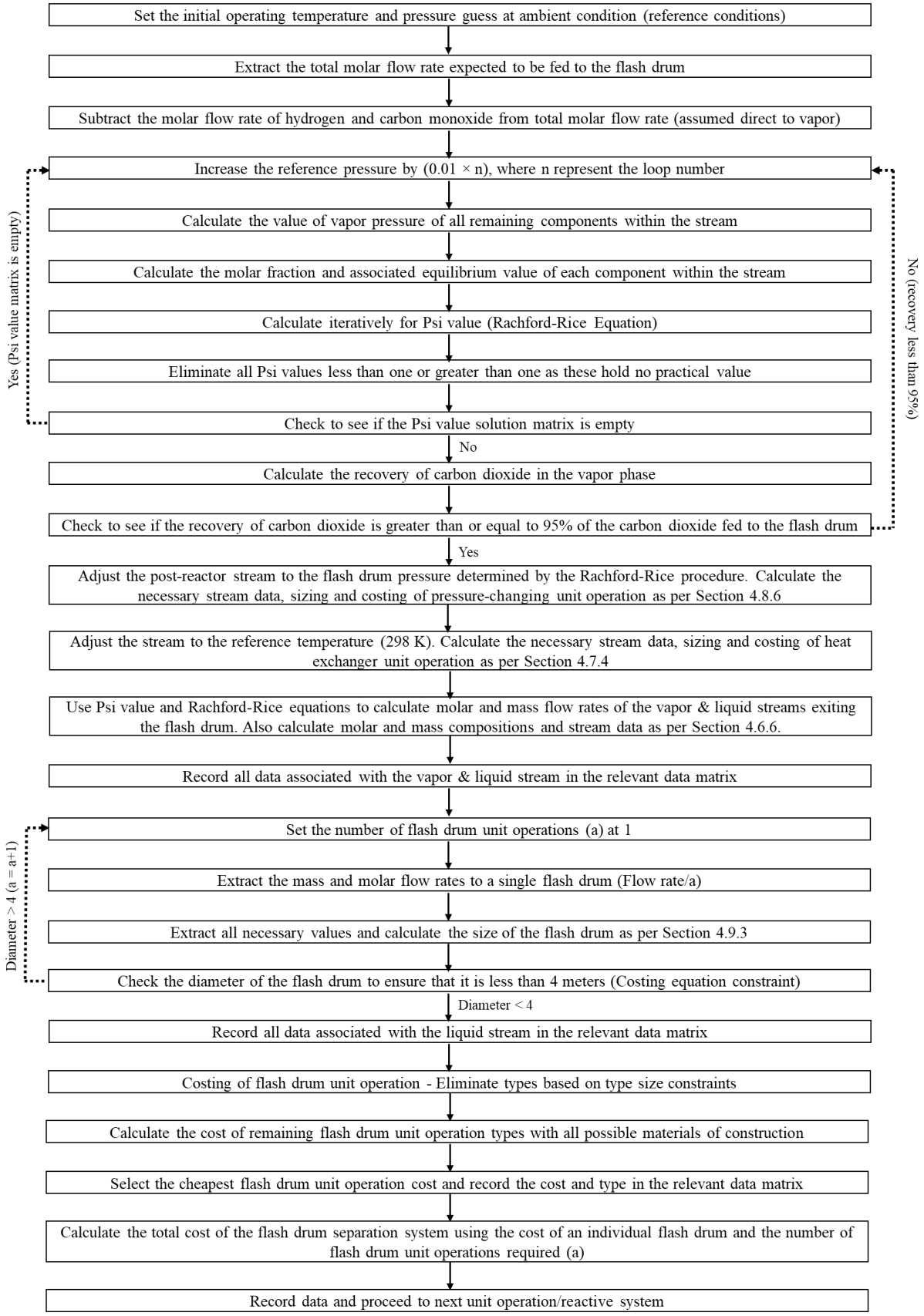

Figure D.9: Diagrammatic representation of the code structure by which flash drum unit operations are designed and costed within the ASSF tool

D.10. Code Associated with Sizing and Costing of Distillation Columns

Figure D.10 provides a flow chart representation of the ASSF tool segment focused on the design and costing of distillation columns.

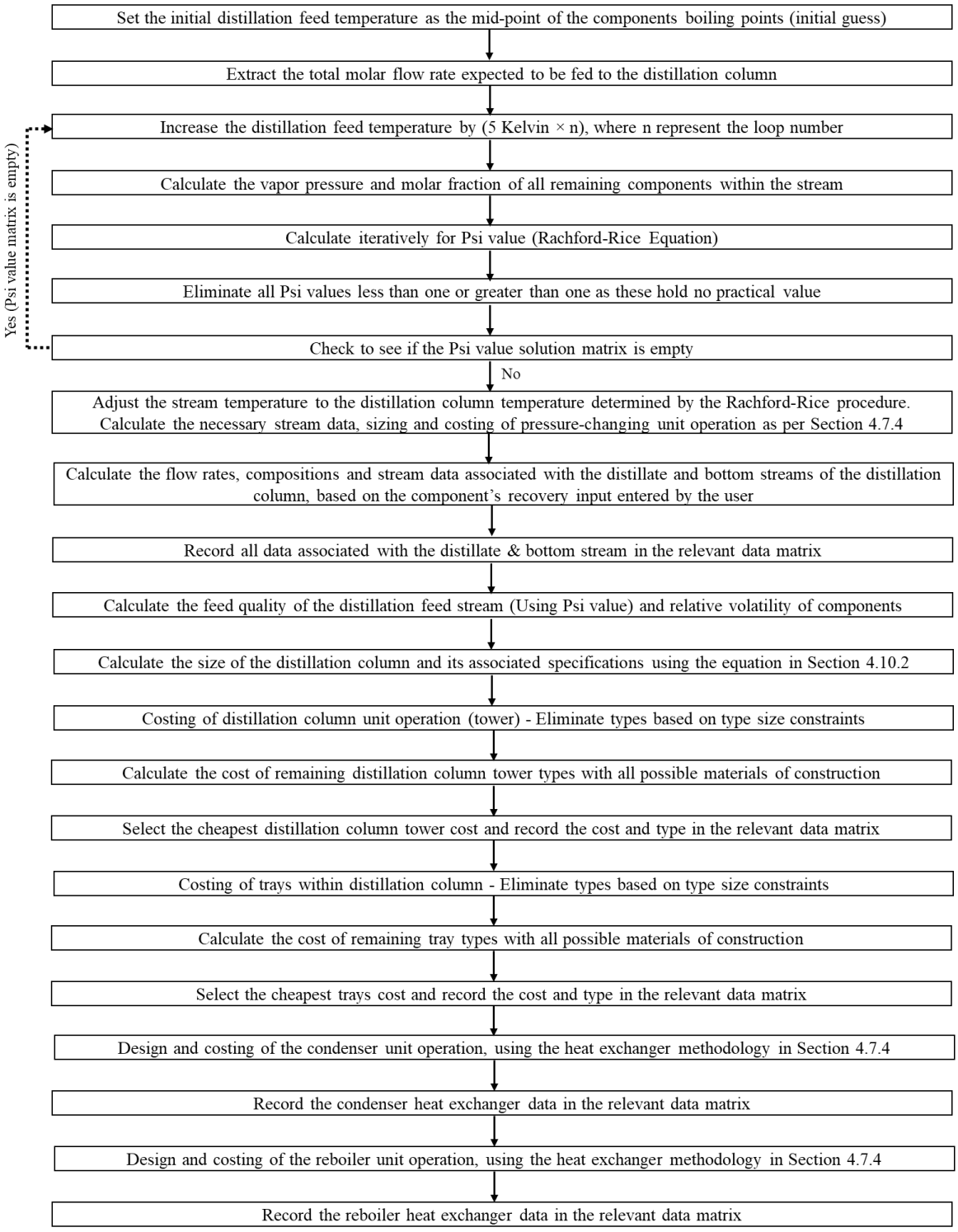

Figure D.10: Diagrammatic representation of the code structure by which distillation columns are designed and costed within the ASSF tool

As can be seen by this diagram, the only loop that exists within this section of the ASSF tool, is the iterative determination of the feed temperature required for the distillation column.

During this loop, the value for φ (denoting the fraction of the feed in the vapor phase) was calculated by constantly changing the temperature of the stream, until a viable fraction ranging between 0 and 1 was found. This value is essential in determining the feed quality of the stream entering the distillation column, required in the subsequent sizing of the distillation column via the Underwood equation.

D.11. Code Associated with Reactor Unit Operations

Figure D.11 provides a diagrammatic representation of the code structure involved with the reactor unit operations, highlighting how multiple simultaneous reactions are handled within the ASSF tool, and the presence of possible limiting reagents.

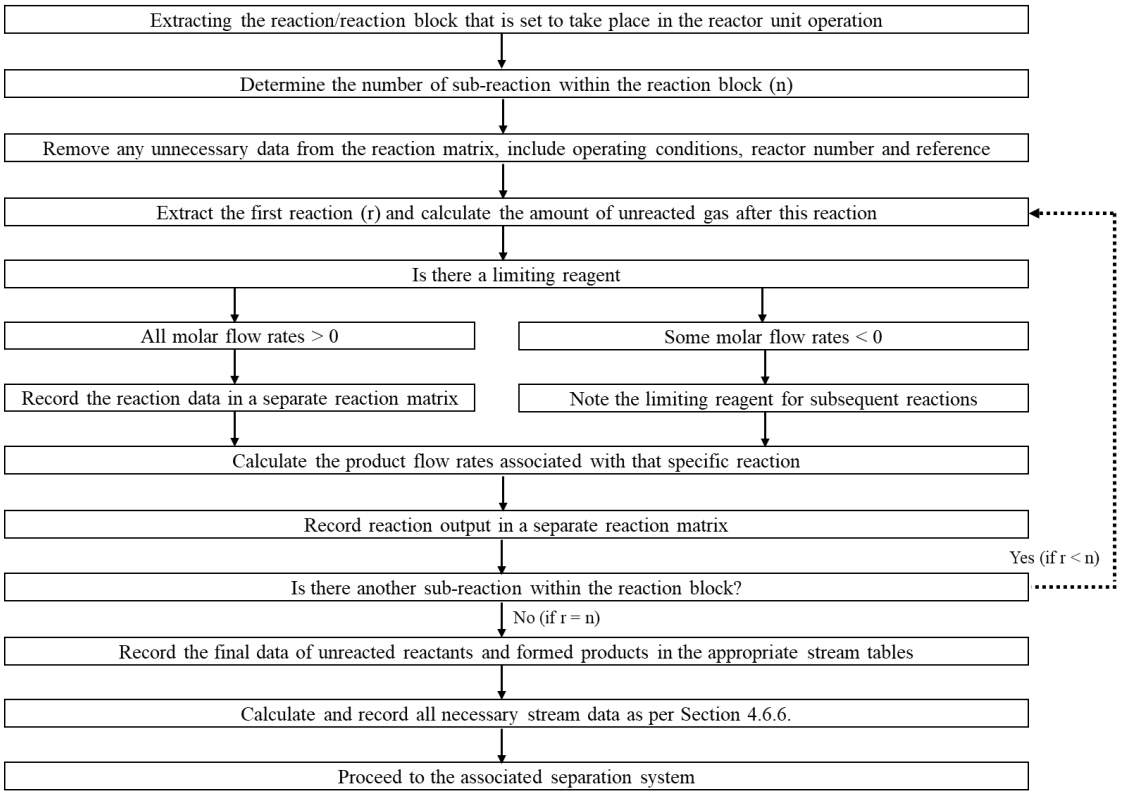

Figure D.11: Diagrammatic representation of the code structure by which reactor unit operations are handled within the ASSF tool

Appendix E: Rachford Rice Methodology

The following equations detail the methodology followed for the Rachford Rice procedure (Skogestad, 2009), utilizing Figure E.1 as a reference for these equations.

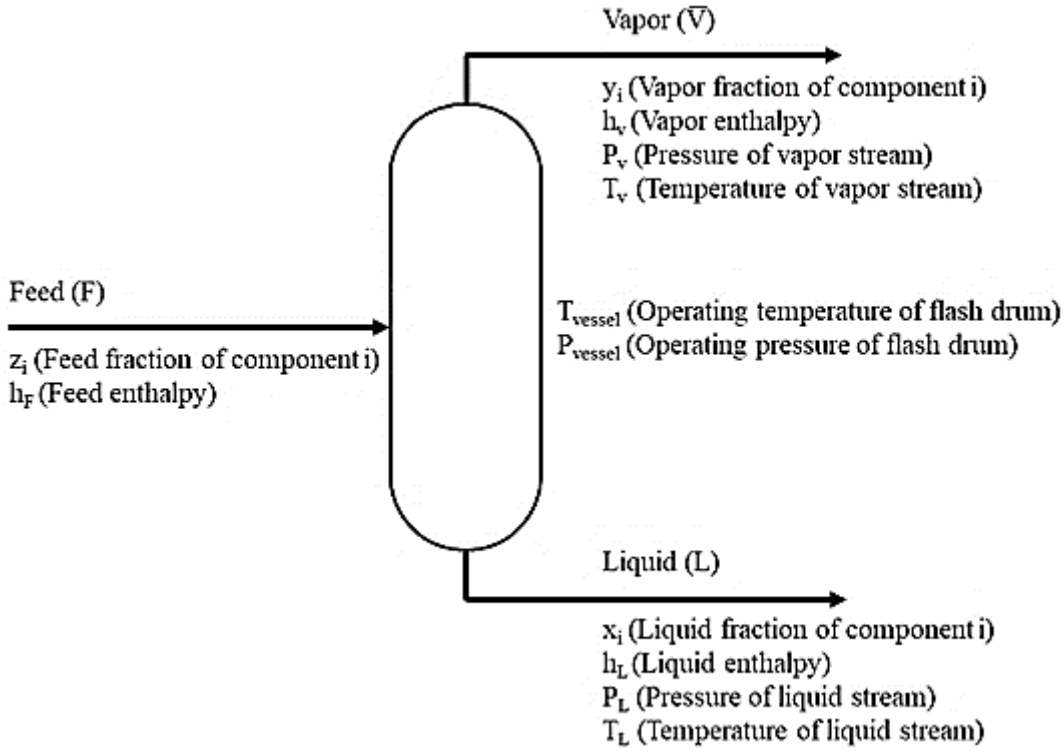

Figure E.1: Schematic representation of a flash drum

An overall balance around the flash drum unit operation, can be represented by means of Equation E.1, whereby the total mass entering the flash drum in the feed stream (F) is equal to the summation of the masses leaving the flash drum in the liquid (L) and vapor ($\overline{V}$) phase.

$$F = L + \overline{V} \qquad \text{(Equation E. 1)}$$

A component mass balance can be conducted around the flash drum unit operation, using the mass composition of a component in the feed stream, liquid stream and vapor stream, denoted by z_i, x_i and y_i, respectively, as per Equation E.2.

$$Fz_i = Lx_i + \overline{V}y_i \qquad \text{(Equation E. 2)}$$

The equilibrium (K_i) value of any chemical species within the stream, is calculated as a ratio of the component's vapor and liquid fractions, as shown in Equation E.3.

$$K_i = \frac{y_i}{x_i} \qquad \text{(Equation E. 3)}$$

When determining the equilibrium separation achievable, the fraction of any component in the liquid or vapor stream is generally not known. As a result, the equilibrium constant is unable to be calculated via Equation E.3. Fortunately, an equilibrium relationship exists between the vessel's operating pressure (P_{vessel}) and the saturation pressure of the components at the predefined process vessel operating temperature ($P_{i\,sat}(T_{vessel})$). This relationship is denoted by Equation E.4, with the saturation pressure of each chemical species being calculated using Equation 3.4.

$$K_i = \frac{P_{i\,sat}(T_{vessel})}{P_{vessel}} \qquad \text{(Equation E. 4)}$$

As a 'quick-check' to ensure the existence of vapor/liquid equilibrium, the K_i value can be analyzed by inspection. Should all component K_i values be greater than one, this indicates a superheated vapor. On the other hand, if all K_i values are less than one, this indicates a subcooled liquid. Therefore, in order for vapor/liquid equilibrium to exist, the K_i values of the chemical species must have some values less than one, and others greater than one.

The fraction of the feed that exists as a vapor can be expressed through the introduction of the term φ, as per Equation E.5.

$$\varphi = \frac{\overline{V}}{F} \qquad \text{(Equation E. 5)}$$

As seen by Equation E.5, a φ value equal to 1 indicates that the entire feed stream exists as a vapor, implying no phase equilibrium. On the other hand, a φ value of 0 indicates that the feed stream is a liquid. In order for there to an equilibrium ratio between the vapor and liquid phases, this value must be between 0 and 1, and was considered to be the first criterion in ensuring that a flash drum can be utilized for separation of a feed stream. Should φ exhibit a saturated vapor or liquid, the ASSF tool automatically and continuously adjusts the operating pressure of the vessel, allowing for equilibrium conditions to be obtained within the flash drum.

Based on Figure E.1, it can be noted that the temperature and pressure of the vapor and liquid stream, will be the same as that of the vessel, thereby leading to Equation E.6 and Equation E.7.

$$P_L = P_v = P_{vessel} \qquad \text{(Equation E. 6)}$$

$$T_L = T_v = T_{vessel} \quad \text{(Equation E. 7)}$$

With y_i and x_i representing the mass fractions of the components within the vapor and liquid stream, respectively, the sum of all the fractions within each stream is equal to one, as denoted by Equation E.8.

$$\sum y_i = \sum x_i = 1 \quad \text{(Equation E. 8)}$$

Equation E.9 details the energy balance around a flash drum unit operation, as per the schematic representation shown in Figure E.1, where Q represents the heat added to/removed from the unit operation.

$$h_F F + Q = h_L L + h_v \overline{V} \quad \text{(Equation E. 9)}$$

When designing the flash drum unit operation, the information known relates to the feed stream, in terms of its associated flow rates, compositions, temperature and pressure, as well as the operating conditions of the flash drum unit operation. Given this information, the Rachford-Rice procedure equations can be derived.

Rearranging Equation E.1:

$$L = F - \overline{V} \quad \text{(Equation E. 10)}$$

Substituting Equation E.10 into Equation E.2, and rearranging accordingly:

$$Fz_i = Fx_i - \overline{V}x_i + \overline{V}y_i \quad \text{(Equation E. 11)}$$

$$y_i = \frac{F}{\overline{V}} z_i + \left(1 - \frac{F}{\overline{V}}\right) x_i \quad \text{(Equation E. 12)}$$

However, substituting Equation E.5 into Equation E.12:

$$y_i = \frac{\varphi - 1}{\varphi} x_i + \frac{1}{\varphi} z_i \quad \text{(Equation E. 13)}$$

Dividing through by x_i, creating an equilibrium term as per Equation E.3.

$$K_i = 1 - \frac{1}{\varphi} + \frac{z_i}{x_i}\frac{1}{\varphi} \quad \text{(Equation E. 14)}$$

Grouping terms together, and rearranging Equation E.14:

$$(1 - K_i)\varphi + \left(\frac{z_i}{x_i} - 1\right) = 0 \quad \text{(Equation E. 15)}$$

$$y_i = \frac{z_i K_i}{1 + \varphi(K_i - 1)} \quad \text{(Equation E. 16)}$$

$$x_i = \frac{z_i}{1 + \varphi(K_i - 1)} \quad \text{(Equation E. 17)}$$

Rearranging Equation E.8, and combining the rearranged equation with Equation E.16 and Equation E.17:

$$\sum y_i - \sum x_i = 0 \quad \text{(Equation E. 18)}$$

$$\sum \frac{z_i K_i}{1 + \varphi(K_i - 1)} - \sum \frac{z_i}{1 + \varphi(K_i - 1)} = 0 \quad \text{(Equation E. 19)}$$

$$\sum \frac{z_i (1 - K_i)}{1 + \varphi(K_i - 1)} = 0 \quad \text{(Equation E. 20)}$$

Equation E.20 is the final Rachford-Rice equation, whereby the values for K_i and z_i for each component within the stream, was used as a means to solve for φ iteratively. Upon solving for the φ value, the respective vapor and liquid flow rates exiting the flash drum was calculated, as well as their compositions. This was the process utilized in determining the separation achievable by the flash drum.

Appendix F: ASSF Tool Data for Application #1

Table F.1, details the ASSF tool data that is associated with the first application, whereby the operating conditions investigated within the work of Gaikwad, *et al*. (2016) was analyzed using the ASSF tool. The data provided in the ASSF tool retains up to 15 decimal points. However, Table F.1 reports all values to two decimal places.

Table F.1: ASSF tool data associated with the investigation conducted by Gaikwad, et al. (2016)

Case Study Number (→)	**Units (↓)**	**1**	**2**	**3**
CO_2 Feed	tons/annum	34,855.92	34,855.92	34,855.92
CO_2 Cost	$/annum	2,091,355.20	2,091,355.20	2,091,355.20
H_2 Feed	tons/annum	4,790.02	4,790.02	4,790.02
H_2 Cost	$/annum	5,987,520.00	5,987,520.00	5,987,520.00
MeOH Produced	tons/annum	10,279.87	19,222.05	20,391.16
MeOH Purity	mass %	92.30	92.46	96.10
MeOH Sales Potential	$/annum	5,139,932.76	9,611,024.03	10,195,580.13
Total Reactant Cost	$/annum	8,078,875.20	8,078,875.20	8,078,875.20
Total Product Revenue	$/annum	5,139,932.76	9,611,024.03	10,195,580.13
Unreacted CO_2 emitted	tons/annum	17,265.34	5,928.70	5,279.25
Cost of Heat Exchangers	$	426,863.16	490,010.01	625,601.13
Cost of Pressure-Changing System	$	10,338,004.07	12,522,769.41	10,517,772.94
Cost of Separation System	$	430,018.07	551,486.74	657,909.53
Total Work of Process	MW	11.34	15.99	13.97
Yearly Profit (before natural gas cost)	$/annum	-2,938,942.44	1,532,148.83	2,116,704.93
Natural Gas Required	tons/annum	n/a	9,116.00	7,966.23
CO_2 released through Natural Gas combustion	tons/annum	n/a	25,012.16	21,857.48
Net CO_2 released	tons/annum	n/a	-3,915.05	-7,719.19
Payback Period	years	n/a	-4.77	-6.91

Case Study Number (→)	Units (↓)	4	5	6
CO_2 Feed	tons/annum	34,855.92	34,855.92	34,855.92
CO_2 Cost	$/annum	2,091,355.20	2,091,355.20	2,091,355.20
H_2 Feed	tons/annum	4,790.02	4,790.02	4,790.02
H_2 Cost	$/annum	5,987,520.00	5,987,520.00	5,987,520.00
MeOH Produced	tons/annum	21,684.63	18,657.29	7,466.21
MeOH Purity	mass %	96.12	92.48	92.21
MeOH Sales Potential	$/annum	10,842,312.60	9,328,644.12	3,733,104.34
Total Reactant Cost	$/annum	8,078,875.20	8,078,875.20	8,078,875.20
Total Product Revenue	$/annum	10,842,312.60	9,328,644.12	3,733,104.34
Unreacted CO_2 emitted	tons/annum	3,696.31	6,907.31	21,175.61
Cost of Heat Exchangers	$	643,483.47	494,498.40	391,014.644
Cost of Pressure-Changing System	$	11,057,324.03	6,756,897.38	5,670,989.52
Cost of Separation System	$	676,391.67	544,275.33	386,842.21
Total Work of Process	MW	12.52	8.66	4.42
Yearly Profit (before natural gas cost)	$/annum	2,763,437.40	1,249,768.92	-4,345,770.86
Natural Gas Required	tons/annum	7,138.09	4,936.71	n/a
CO_2 released through Natural Gas combustion	tons/annum	19,585.24	13,545.17	n/a
Net CO_2 released	tons/annum	-11,574.37	-14,403.44	n/a
Payback Period	years	-18.67	-6.96	n/a

Case Study Number (→)	Units (↓)	7	8	9
CO_2 Feed	tons/annum	34,855.92	34,855.92	34,855.92
CO_2 Cost	$/annum	2,091,355.20	2,091,355.20	2,091,355.20
H_2 Feed	tons/annum	4,790.02	4,790.02	4,790.02
H_2 Cost	$/annum	5,987,520.00	5,987,520.00	5,987,520.00
MeOH Produced	tons/annum	12,247.92	16,360.91	15,281.50
MeOH Purity	mass %	92.38	92.43	92.41
MeOH Sales Potential	$/annum	6,123,959.96	8,180,453.05	7,640,748.35
Total Reactant Cost	$/annum	8,078,875.20	8,078,875.20	8,078,875.20
Total Product Revenue	$/annum	6,123,959.96	8,180,453.05	7,640,748.35
Unreacted CO_2 emitted	tons/annum	15,174.97	9,743.95	11,005.75
Cost of Heat Exchangers	$	442,098.63	472,385.01	468,770.65
Cost of Pressure-Changing System	$	5,511,731.46	6,521,881.14	5,643,469.67
Cost of Separation System	$	457,860.59	514,190.54	499,892.53
Total Work of Process	MW	5.44	6.62	5.58
Yearly Profit (before natural gas cost)	$/annum	-1,954,915.24	101,577.85	-438,126.85
Natural Gas Required	tons/annum	n/a	3,773.90	n/a
CO_2 released through Natural Gas combustion	tons/annum	n/a	10,354.71	n/a
Net CO_2 released	tons/annum	n/a	-14,757.26	n/a
Payback Period	years	n/a	-4.39	n/a

Case Study Number (→)	Units (↓)	10	11	12
CO_2 Feed	tons/annum	34,855.92	34,855.92	34,855.92
CO_2 Cost	$/annum	2,091,355.20	2,091,355.20	2,091,355.20
H_2 Feed	tons/annum	4,790.02	4,790.02	4,790.02
H_2 Cost	$/annum	5,987,520.00	5,987,520.00	5,987,520.00
MeOH Produced	tons/annum	14,451.98	6,050.26	7,137.25
MeOH Purity	mass %	92.42	92.13	92.22
MeOH Sales Potential	$/annum	7,225,991.49	3,025,129.59	3,568,626.58
Total Reactant Cost	$/annum	8,078,875.20	8,078,875.20	8,078,875.20
Total Product Revenue	$/annum	7,225,991.49	3,025,129.59	3,568,626.58
Unreacted CO_2 emitted	tons/annum	12,340.11	22,918.53	21,783.35
Cost of Heat Exchangers	$	466,136.05	373,699.43	390,213.90
Cost of Pressure-Changing System	$	5,226,207.31	4,557,101.69	4,551,908.86
Cost of Separation System	$	488,455.66	364,656.25	381,409.09
Total Work of Process	MW	4.93	2.47	2.54
Yearly Profit (before natural gas cost)	$/annum	-852,883.71	-5,053,745.61	-4,510,248.62
Natural Gas Required	tons/annum	n/a	n/a	n/a
CO_2 released through Natural Gas combustion	tons/annum	n/a	n/a	n/a
Net CO_2 released	tons/annum	n/a	n/a	n/a
Payback Period	years	n/a	n/a	n/a

Case Study Number (→)	Units (↓)	13	14	15
CO_2 Feed	tons/annum	34,855.92	34,855.92	34,855.92
CO_2 Cost	$/annum	2,091,355.20	2,091,355.20	2,091,355.20
H_2 Feed	tons/annum	4,790.02	4,790.02	4,790.02
H_2 Cost	$/annum	5,987,520.00	5,987,520.00	5,987,520.00
MeOH Produced	tons/annum	7,667.81	7,973.17	6,760.87
MeOH Purity	mass %	92.25	92.29	92.12
MeOH Sales Potential	$/annum	3,833,906.12	3,986,587.18	3,380,436.77
Total Reactant Cost	$/annum	8,078,875.20	8,078,875.20	8,078,875.20
Total Product Revenue	$/annum	3,833,906.12	3,986,587.18	3,380,436.77
Unreacted CO_2 emitted	tons/annum	21,093.32	20,958.98	21,678.54
Cost of Heat Exchangers	$	412,275.13	418,059.27	405,903.29
Cost of Pressure-Changing System	$	4,474,901.57	4,492,943.81	4,205,041.58
Cost of Separation System	$	389,868.06	394,157.22	376,408.10
Total Work of Process	MW	2.47	2.30	1.99
Yearly Profit (before natural gas cost)	$/annum	-4,244,969.08	-4,092,288.02	-4,698,438.43
Natural Gas Required	tons/annum	n/a	n/a	n/a
CO_2 released through Natural Gas combustion	tons/annum	n/a	n/a	n/a
Net CO_2 released	tons/annum	n/a	n/a	n/a
Payback Period	years	n/a	n/a	n/a

Case Study Number (→)	Units (↓)	16	17	18
CO_2 Feed	tons/annum	34,855.92	34,855.92	34,855.92
CO_2 Cost	$/annum	2,091,355.20	2,091,355.20	2,091,355.20
H_2 Feed	tons/annum	4,790.02	4,790.02	4,790.02
H_2 Cost	$/annum	5,987,520.00	5,987,520.00	5,987,520.00
MeOH Produced	tons/annum	1,231.06	2,526.73	3,276.55
MeOH Purity	mass %	89.10	91.13	91.39
MeOH Sales Potential	$/annum	615,528.12	1,263,363.95	1,638,277.20
Total Reactant Cost	$/annum	8,078,875.20	8,078,875.20	8,078,875.20
Total Product Revenue	$/annum	615,528.12	1,263,363.95	1,638,277.20
Unreacted CO_2 emitted	tons/annum	27,083.19	26,440.64	25,167.60
Cost of Heat Exchangers	$	240,800.77	341,810.04	366,050.26
Cost of Pressure-Changing System	$	2,952,061.59	2,955,967.92	2,926,472.39
Cost of Separation System	$	293,954.30	320,496.34	321,938.82
Total Work of Process	MW	1.17	1.22	1.20
Yearly Profit (before natural gas cost)	$/annum	-7,463,347.08	-6,815,511.25	-6,440,598.00
Natural Gas Required	tons/annum	n/a	n/a	n/a
CO_2 released through Natural Gas combustion	tons/annum	n/a	n/a	n/a
Net CO_2 released	tons/annum	n/a	n/a	n/a
Payback Period	years	n/a	n/a	n/a

Case Study Number (→)	Units (↓)	19	20	21
CO_2 Feed	tons/annum	34,855.92	34,855.92	34,855.92
CO_2 Cost	$/annum	2,091,355.20	2,091,355.20	2,091,355.20
H_2 Feed	tons/annum	4,790.02	4,790.02	4,790.02
H_2 Cost	$/annum	5,987,520.00	5,987,520.00	5,987,520.00
MeOH Produced	tons/annum	3,494.06	1,096.92	903.16
MeOH Purity	mass %	91.44	87.26	88.96
MeOH Sales Potential	$/annum	1,747,027.63	548,461.22	451,582.31
Total Reactant Cost	$/annum	8,078,875.20	8,078,875.20	8,078,875.20
Total Product Revenue	$/annum	1,747,027.63	548,461.22	451,582.31
Unreacted CO_2 emitted	tons/annum	24,848.96	25,074.17	28,719.66
Cost of Heat Exchangers	$	373,684.96	321,608.63	231,728.51
Cost of Pressure-Changing System	$	2,864,349.54	2,787,120.40	2,298,571.48
Cost of Separation System	$	325,337.67	294,561.35	283,122.87
Total Work of Process	MW	1.12	0.95	0.61
Yearly Profit (before natural gas cost)	$/annum	-6,331,847.57	-7,530,413.98	-7,627,292.89
Natural Gas Required	tons/annum	n/a	n/a	n/a
CO_2 released through Natural Gas combustion	tons/annum	n/a	n/a	n/a
Net CO_2 released	tons/annum	n/a	n/a	n/a
Payback Period	years	n/a	n/a	n/a

Case Study Number (→)	Units (↓)	22	23	24
CO_2 Feed	tons/annum	34,855.92	34,855.92	34,855.92
CO_2 Cost	$/annum	2,091,355.20	2,091,355.20	2,091,355.20
H_2 Feed	tons/annum	4,790.02	4,790.02	4,790.02
H_2 Cost	$/annum	5,987,520.00	5,987,520.00	5,987,520.00
MeOH Produced	tons/annum	1,429.28	926.16	621.24
MeOH Purity	mass %	89.89	88.02	84.31
MeOH Sales Potential	$/annum	714,638.35	463,078.08	310,619.56
Total Reactant Cost	$/annum	8,078,875.20	8,078,875.20	8,078,875.20
Total Product Revenue	$/annum	714,638.35	463,078.08	310,619.56
Unreacted CO_2 emitted	tons/annum	27,420.34	27,386.37	27,321.32
Cost of Heat Exchangers	$	343,501.33	275,226.57	419,101.02
Cost of Pressure-Changing System	$	2,314,176.68	2,331,804.91	2,311,449.67
Cost of Separation System	$	297,919.80	287,034.97	288,895.76
Total Work of Process	MW	0.64	0.61	0.57
Yearly Profit (before natural gas cost)	$/annum	-7,364,236.85	-7,615,797.12	-7,768,255.64
Natural Gas Required	tons/annum	n/a	n/a	n/a
CO_2 released through Natural Gas combustion	tons/annum	n/a	n/a	n/a
Net CO_2 released	tons/annum	n/a	n/a	n/a
Payback Period	years	n/a	n/a	n/a

Case Study Number (→)	Units (↓)	25
CO_2 Feed	tons/annum	34,855.92
CO_2 Cost	$/annum	2,091,355.20
H_2 Feed	tons/annum	4,790.02
H_2 Cost	$/annum	5,987,520.00
MeOH Produced	tons/annum	479.06
MeOH Purity	mass %	81.61
MeOH Sales Potential	$/annum	239,528.32
Total Reactant Cost	$/annum	8,078,875.20
Total Product Revenue	$/annum	239,528.32
Unreacted CO_2 emitted	tons/annum	27,624.48
Cost of Heat Exchangers	$	402,477.54
Cost of Pressure-Changing System	$	2,264,499.25
Cost of Separation System	$	289,264.21
Total Work of Process	MW	0.50
Yearly Profit (before natural gas cost)	$/annum	-7,839,346.88
Natural Gas Required	tons/annum	n/a
CO_2 released through Natural Gas combustion	tons/annum	n/a
Net CO_2 released	tons/annum	n/a
Payback Period	years	n/a

Appendix G: ASSF Tool Data for Application #2

Table G.1 contains the ASSF tool data associated with its second application, i.e., the production of MeOH via CO_2 hydrogenation at low pressures. As with the first application, the ASSF tool retains all data to 15 decimal points, with only two decimal points being used in these tables to report the associated values.

Table G.1: ASSF tool data associated with the investigation conducted by Leonzio, et al. (2019)

Case Study Number (→)	**Units (↓)**	**1**	**2**	**3**
CO_2 Feed	tons/annum	34,855.92	34,855.92	34,855.92
CO_2 Cost	$/annum	2,091,355.20	2,091,355.20	2,091,355.20
H_2 Feed	tons/annum	4,790.02	4,790.02	4,790.02
H_2 Cost	$/annum	5,987,520.00	5,987,520.00	5,987,520.00
MeOH Produced	tons/annum	2,375.38	1,090.15	386.07
MeOH Purity	mass %	92.16	91.85	91.09
MeOH Sales Potential	$/annum	1,187,689.46	545,076.02	193,037.35
Total Reactant Cost	$/annum	8,078,875.20	8,078,875.20	8,078,875.20
Total Product Revenue	$/annum	1,187,689.46	545,076.02	193,037.35
Unreacted CO_2 emitted	tons/annum	30,122.71	31,970.81	33,075.42
Cost of Heat Exchangers	$	273,449.24	238,371.74	223,677.18
Cost of Pressure-Changing System	$	1,416,645.22	1,525,546.08	1,581,902.01
Cost of Separation System	$	281,903.17	245,246.75	261,483.63
Total Work of Process	MW	0.29	0.24	0.22
Yearly Profit (before natural gas cost)	$/annum	-6,891,185.74	-7,533,799.18	-7,885,837.85

Case Study Number (→)	Units (↓)	4	5	6
CO_2 Feed	tons/annum	34,855.92	34,855.92	34,855.92
CO_2 Cost	$/annum	2,091,355.20	2,091,355.20	2,091,355.20
H_2 Feed	tons/annum	4,790.02	4,790.02	4,790.02
H_2 Cost	$/annum	5,987,520.00	5,987,520.00	5,987,520.00
MeOH Produced	tons/annum	0.00	0.00	4,474.42
MeOH Purity	mass %	0.00	0.00	92.34
MeOH Sales Potential	$/annum	0.00	0.00	2,237,209.22
Total Reactant Cost	$/annum	8,078,875.20	8,078,875.20	8,078,875.20
Total Product Revenue	$/annum	0.00	0.00	2,237,209.22
Unreacted CO_2 emitted	tons/annum	33,804.71	34,158.65	27,165.39
Cost of Heat Exchangers	$	170,534.90	174,461.35	327,479.67
Cost of Pressure-Changing System	$	1,639,889.41	1,626,368.24	1,662,825.40
Cost of Separation System	$	96,831.92	89,147.97	322,295.36
Total Work of Process	MW	0.18	0.19	0.48
Yearly Profit (before natural gas cost)	$/annum	-8,078,875.20	-8,078,875.20	-5,841,665.98

Case Study Number (→)	Units (↓)	7	8	9
CO_2 Feed	tons/annum	34,855.92	34,855.92	34,855.92
CO_2 Cost	$/annum	2,091,355.20	2,091,355.20	2,091,355.20
H_2 Feed	tons/annum	4,790.02	4,790.02	4,790.02
H_2 Cost	$/annum	5,987,520.00	5,987,520.00	5,987,520.00
MeOH Produced	tons/annum	2,894.66	1,595.94	844.76
MeOH Purity	mass %	92.24	92.04	91.69
MeOH Sales Potential	$/annum	1,447,328.63	797,970.94	422,381.78
Total Reactant Cost	$/annum	8,078,875.20	8,078,875.20	8,078,875.20
Total Product Revenue	$/annum	1,447,328.63	797,970.94	422,381.78
Unreacted CO_2 emitted	tons/annum	29,384.37	31,232.37	32,339.58
Cost of Heat Exchangers	$	301,012.04	261,663.47	245,148.79
Cost of Pressure-Changing System	$	1,823,294.46	1,871,835.61	1,903,270.98
Cost of Separation System	$	294,358.55	260,921.74	265,161.08
Total Work of Process	MW	0.39	0.37	0.35
Yearly Profit (before natural gas cost)	$/annum	-6,631,546.57	-7,280,904.26	-7,656,493.42

Case Study Number (→)	Units (↓)	10	11	12
CO_2 Feed	tons/annum	34,855.92	34,855.92	34,855.92
CO_2 Cost	$/annum	2,091,355.20	2,091,355.20	2,091,355.20
H_2 Feed	tons/annum	4,790.02	4,790.02	4,790.02
H_2 Cost	$/annum	5,987,520.00	5,987,520.00	5,987,520.00
MeOH Produced	tons/annum	0.00	6,325.94	4,474.42
MeOH Purity	mass %	0.00	92.40	92.34
MeOH Sales Potential	$/annum	0.00	3,162,967.69	2,237,209.22
Total Reactant Cost	$/annum	8,078,875.20	8,078,875.20	8,078,875.20
Total Product Revenue	$/annum	0.00	3,162,967.69	2,237,209.22
Unreacted CO_2 emitted	tons/annum	33,804.71	24,576.18	27,165.39
Cost of Heat Exchangers	$	174,303.10	357,760.03	333,937.59
Cost of Pressure-Changing System	$	1,954,374.57	1,810,928.05	2,043,820.28
Cost of Separation System	$	96,831.92	354,938.81	322,295.36
Total Work of Process	MW	0.26	0.68	0.53
Yearly Profit (before natural gas cost)	$/annum	-8,078,875.20	-4,915,907.51	-5,841,665.98

Case Study Number (→)	Units (↓)	13	14	15
CO_2 Feed	tons/annum	34,855.92	34,855.92	34,855.92
CO_2 Cost	$/annum	2,091,355.20	2,091,355.20	2,091,355.20
H_2 Feed	tons/annum	4,790.02	4,790.02	4,790.02
H_2 Cost	$/annum	5,987,520.00	5,987,520.00	5,987,520.00
MeOH Produced	tons/annum	2,894.66	1,595.94	844.76
MeOH Purity	mass %	92.24	92.04	91.69
MeOH Sales Potential	$/annum	1,447,328.63	797,970.94	422,381.78
Total Reactant Cost	$/annum	8,078,875.20	8,078,875.20	8,078,875.20
Total Product Revenue	$/annum	1,447,328.63	797,970.94	422,381.78
Unreacted CO_2 emitted	tons/annum	29,384.37	31,232.37	32,339.58
Cost of Heat Exchangers	$	307,417.14	267,954.32	248,867.00
Cost of Pressure-Changing System	$	2,096,224.06	2,124,879.70	2,130,358.61
Cost of Separation System	$	294,358.55	260,921.74	265,161.08
Total Work of Process	MW	0.51	0.48	0.43
Yearly Profit (before natural gas cost)	$/annum	-6,631,546.57	-7,280,904.26	-7,656,493.42

Case Study Number (→)	Units (↓)	16	17	18
CO_2 Feed	tons/annum	34,855.92	34,855.92	34,855.92
CO_2 Cost	$/annum	2,091,355.20	2,091,355.20	2,091,355.20
H_2 Feed	tons/annum	4,790.02	4,790.02	4,790.02
H_2 Cost	$/annum	5,987,520.00	5,987,520.00	5,987,520.00
MeOH Produced	tons/annum	7,917.73	5,799.46	4,213.33
MeOH Purity	mass %	92.41	92.36	92.31
MeOH Sales Potential	$/annum	3,958,867.38	2,899,729.71	2,106,667.04
Total Reactant Cost	$/annum	8,078,875.20	8,078,875.20	8,078,875.20
Total Product Revenue	$/annum	3,958,867.38	2,899,729.71	2,106,667.04
Unreacted CO_2 emitted	tons/annum	22,354.96	25,313.95	27,533.87
Cost of Heat Exchangers	$	382,117.29	354,227.81	334,882.95
Cost of Pressure-Changing System	$	1,893,986.85	2,219,387.87	2,277,680.42
Cost of Separation System	$	381,642.33	345,536.00	317,409.90
Total Work of Process	MW	0.90	0.67	0.65
Yearly Profit (before natural gas cost)	$/annum	-4,120,007.82	-5,179,145.49	-5,972,208.16

Case Study Number (→)	Units (↓)	19	20	21
CO_2 Feed	tons/annum	34,855.92	34,855.92	34,855.92
CO_2 Cost	$/annum	2,091,355.20	2,091,355.20	2,091,355.20
H_2 Feed	tons/annum	4,790.02	4,790.02	4,790.02
H_2 Cost	$/annum	5,987,520.00	5,987,520.00	5,987,520.00
MeOH Produced	tons/annum	2,634.16	1,341.70	8,979.37
MeOH Purity	mass %	92.21	91.95	92.41
MeOH Sales Potential	$/annum	1,317,078.74	670,848.52	4,489,685.79
Total Reactant Cost	$/annum	8,078,875.20	8,078,875.20	8,078,875.20
Total Product Revenue	$/annum	1,317,078.74	670,848.52	4,489,685.79
Unreacted CO_2 emitted	tons/annum	29,753.68	31,601.60	20,873.98
Cost of Heat Exchangers	$	303,464.83	263,007.49	398,089.00
Cost of Pressure-Changing System	$	2,305,860.68	2,305,826.15	1,946,771.12
Cost of Separation System	$	288,539.38	253,259.76	398,847.42
Total Work of Process	MW	0.61	0.54	1.12
Yearly Profit (before natural gas cost)	$/annum	-6,761,796.46	-7,408,026.68	-3,589,189.41

Case Study Number (→)	Units (↓)	22	23	24
CO_2 Feed	tons/annum	34,855.92	34,855.92	34,855.92
CO_2 Cost	$/annum	2,091,355.20	2,091,355.20	2,091,355.20
H_2 Feed	tons/annum	4,790.02	4,790.02	4,790.02
H_2 Cost	$/annum	5,987,520.00	5,987,520.00	5,987,520.00
MeOH Produced	tons/annum	7,121.32	5,269.48	3,683.44
MeOH Purity	mass %	92.41	92.35	92.30
MeOH Sales Potential	$/annum	3,560,660.03	2,634,738.82	1,841,720.66
Total Reactant Cost	$/annum	8,078,875.20	8,078,875.20	8,078,875.20
Total Product Revenue	$/annum	3,560,660.03	2,634,738.82	1,841,720.66
Unreacted CO_2 emitted	tons/annum	23,465.93	26,054.43	28,274.84
Cost of Heat Exchangers	$	375,963.60	351,963.25	332,775.44
Cost of Pressure-Changing System	$	2,361,579.72	2,432,693.22	2,461,008.20
Cost of Separation System	$	368,459.79	336,290.60	308,107.85
Total Work of Process	MW	0.83	0.79	0.74
Yearly Profit (before natural gas cost)	$/annum	-4,518,215.17	-5,444,136.38	-6,237,154.54

Case Study Number (→)	Units (↓)	25
CO_2 Feed	tons/annum	34,855.92
CO_2 Cost	$/annum	2,091,355.20
H_2 Feed	tons/annum	4,790.02
H_2 Cost	$/annum	5,987,520.00
MeOH Produced	tons/annum	2,113.97
MeOH Purity	mass %	92.13
MeOH Sales Potential	$/annum	1,056,984.98
Total Reactant Cost	$/annum	8,078,875.20
Total Product Revenue	$/annum	1,056,984.98
Unreacted CO_2 emitted	tons/annum	30,492.78
Cost of Heat Exchangers	$	289,967.00
Cost of Pressure-Changing System	$	2,454,914.60
Cost of Separation System	$	275,187.22
Total Work of Process	MW	0.66
Yearly Profit (before natural gas cost)	$/annum	-7,021,890.22

Appendix H: ASSF Tool Data for Application #3

Table H.1 details the ASSF tool data associated with the analysis of the small RPD developed within the third application of the ASSF tool. All values reported within these tables are given to two decimal places, whereas the ASSF tool is able to maintain up to 15 decimal points, thereby increasing the accuracy of the subsequent calculations.

Table H.1: ASSF tool data associated with the sample RPD developed in Application #3

Case Study Number (→)	**Units (↓)**	**1**	**2**	**3**
CO_2 Feed	tons/annum	34,855.92	34,855.92	34,855.92
CO_2 Cost	$/annum	3,485,592.00	3,485,592.00	3,485,592.00
H_2 Feed	tons/annum	7,185.02	7,185.02	7,185.02
H_2 Cost	$/annum	7,185,024.00	7,185,024.00	7,185,024.00
MeOH Produced	tons/annum	24,332.28	1,595.94	4,396.04
MeOH Purity	mass %	96.15	92.04	92.33
MeOH Sales Potential	$/annum	11,436,170.93	750,092.68	2,066,138.58
DME Produced	tons/annum	0.00	0.00	0.00
DME Purity	mass %	0.00	0.00	0.00
DME Sales Potential	$/annum	0.00	0.00	0.00
CaO Needed	tons/annum	0.00	0.00	0.00
CaO Cost	$/annum	0.00	0.00	0.00
$CaCO_3$ Produced	tons/annum	0.00	0.00	0.00
$CaCO_3$ Sales Potential	$/annum	0.00	0.00	0.00
Total Reactant Cost	$/annum	10,670,616.00	10,670,616.00	10,670,616.00
Total Product Revenue	$/annum	11,436,170.93	750,092.68	2,066,138.58
Unreacted CO_2 emitted	tons/annum	421.32	31,232.37	27,275.94
Cost of Heat Exchangers	$	845,787.34	318,804.29	386,646.30
Cost of Pressure-Changing System	$	2,683,679.94	2,049,014.49	1,990,284.82
Cost of Separation System	$	714,593.25	256,350.21	316,726.75
Yearly Profit (before natural gas cost)	$/annum	765,554.93	-9,920,523.32	-8,604,477.42

Case Study Number (→)	Units (↓)	4	5	6
CO_2 Feed	tons/annum	34,855.92	34,855.92	34,855.92
CO_2 Cost	$/annum	3,485,592.00	3,485,592.00	3,485,592.00
H_2 Feed	tons/annum	2,395.01	7,185.02	7,185.02
H_2 Cost	$/annum	2,395,008.00	7,185,024.00	7,185,024.00
MeOH Produced	tons/annum	0.00	3,113.91	204.24
MeOH Purity	mass %	0.00	99.93	99.93
MeOH Sales Potential	$/annum	0.00	1,463,537.13	95,992.66
DME Produced	tons/annum	0.00	15,251.25	1,000.32
DME Purity	mass %	0.00	99.36	98.64
DME Sales Potential	$/annum	0.00	15,098,742.36	990,318.90
CaO Needed	tons/annum	0.00	1,115.72	158.21
CaO Cost	$/annum	0.00	133,886.59	18,985.03
$CaCO_3$ Produced	tons/annum	0.00	1,991.34	282.37
$CaCO_3$ Sales Potential	$/annum	0.00	517,748.13	73,416.34
Total Reactant Cost	$/annum	5,880,600.00	10,804,502.59	10,689,601.03
Total Product Revenue	$/annum	0.00	17,080,027.62	1,159,727.90
Unreacted CO_2 emitted	tons/annum	14,259.89	421.32	31,232.37
Cost of Heat Exchangers	$	118,944.54	1,264,117.63	401,440.32
Cost of Pressure-Changing System	$	272,207.17	4,247,435.68	2,567,120.66
Cost of Separation System	$	107,162.87	1,271,266.16	595,015.10
Yearly Profit (before natural gas cost)	$/annum	-5,880,600.00	6,275,525.03	-9,529,873.13

Case Study Number (→)	Units (↓)	7	8	9
CO_2 Feed	tons/annum	34,855.92	34,855.92	34,855.92
CO_2 Cost	$/annum	3,485,592.00	3,485,592.00	3,485,592.00
H_2 Feed	tons/annum	7,185.02	2,395.01	2,395.01
H_2 Cost	$/annum	7,185,024.00	2,395,008.00	2,395,008.00
MeOH Produced	tons/annum	562.58	0.00	0.00
MeOH Purity	mass %	99.93	0.00	0.00
MeOH Sales Potential	$/annum	264,412.85	0.00	0.00
DME Produced	tons/annum	2,755.40	0.00	0.00
DME Purity	mass %	98.69	0.00	0.00
DME Sales Potential	$/annum	2,727,844.34	0.00	0.00
CaO Needed	tons/annum	418.35	0.00	0.00
CaO Cost	$/annum	50,202.24	0.00	0.00
$CaCO_3$ Produced	tons/annum	746.67	0.00	0.00
$CaCO_3$ Sales Potential	$/annum	194,135.33	0.00	0.00
Total Reactant Cost	$/annum	10,720,818.24	5,880,600.00	5,880,600.00
Total Product Revenue	$/annum	3,186,392.52	0.00	0.00
Unreacted CO_2 emitted	tons/annum	27,275.94	14,259.13	14,259.13
Cost of Heat Exchangers	$	499,890.14	207,306.39	249,154.63
Cost of Pressure-Changing System	$	2,636,769.36	1,238,319.83	1,945,136.14
Cost of Separation System	$	651,557.50	217,306.32	217,306.32
Yearly Profit (before natural gas cost)	$/annum	-7,534,425.72	-5,880,600.00	-5,880,600.00

Appendix I: Reaction Pathway Combinations for Application #4

Table I.1 details all possible reaction pathway combinations determined through use of the ASSF tool, in conjunction with the 22 reaction RPD developed by Jugmohan, *et al*. (2020) (Table 5.10). The case study numbers that are presented within these tables, are referenced within the thesis, when analyzing and reducing the search space. Case study numbers containing 2/3 reactions, indicate that the RPD inputted allows for the possibility of utilizing certain products as intermediates in the overall chemical process, thereby expanding the process boundaries to incorporate a second and third reactor unit operation, respectively. The reference provided in the final column acts as a reference marker, allowing for the case study and reaction pathway combinations to be cross referenced when utilized in the ASSF tool. Table I.1 represents the temperature (T) in degrees Celsius, the pressure (P) in bar, and the conversion (X) as a percentage in relation to the first reactant of the associated chemical reaction equation.

Table I.1: Case studies derived and analysed when using the ASSF tool (Application #4)

Case Study No.	Reactor No.	Reaction	T	P	X	Reference
1	1	$CO_2 + 3H_2 \leftrightarrow CH_3OH + H_2O$	240	20	11.6	(Fan & Wu, 2016)
2	1	$CO_2 + 3H_2 \leftrightarrow CH_3OH + H_2O$	280	442	85.5	(Gaikwad, *et al*., 2016)
3	1	$CO_2 + 3H_2 \leftrightarrow CH_3OH + H_2O$	200.85	40	61.54	(Cabrera, *et al*., 1998)
4	1	$CO_2 + 3H_2 \leftrightarrow CH_3OH + H_2O$	260	330	93.58	(Vanhove, 2015)
5	1	$CO_2 + 3H_2 \leftrightarrow CH_3OH + H_2O$	240	80	96	(Bellotti, *et al*., 2017)
6	1	$CO_2 + 3H_2 \leftrightarrow CH_3OH + H_2O$	220	18.9	17.20	(Gnanamani, *et al*., 2015)
7	1	$CO_2 + 3H_2 \leftrightarrow CH_3OH + H_2O$	250	20	5	(Van der Ham, *et al*., 2012)
8	1	$CO_2 + 3H_2 \leftrightarrow CH_3OH + H_2O$	220	80	18	(CHEMIK, 2014)
9	1	$CO_2 + H_2 \leftrightarrow CO + H_2O$	340	20	2.77	(You, *et al*., 2013)
10	1	$CO_2 + H_2 \leftrightarrow CO + H_2O$	260	442	4.5	(Gaikwad, *et al*., 2016)

Case Study No.	Reactor No.	Reaction	T	P	X	Reference
11	1	$CO_2 + H_2 \leftrightarrow CO + H_2O$	200	40	34.38	(Cabrera, *et al*., 1998)
12	1	$CO_2 + H_2 \leftrightarrow CO + H_2O$	260	330	13.5	(Vanhove, 2015)
13	1	$CO_2 + H_2 \leftrightarrow CO + H_2O$	350	15	9.42	(Zhanghuai & Yuan, 2000)
14	1	$CO_2 + H_2 \leftrightarrow CO + H_2O$	350	15	4.79	(Zhanghuai & Yuan, 2000)
15	1	$CO_2 + H_2 \leftrightarrow CO + H_2O$	250	50	2.70	(Van der Ham, *et al*., 2012)
16	1	$CO_2 + H_2 \leftrightarrow CO + H_2O$	260	20	0.75	(Van der Ham, *et al*., 2012)
17	1	$CO_2 + H_2 \leftrightarrow CO + H_2O$	90	70	15.13	(Chan, *et al*., 2018)
18	1	$CO_2 + H_2 \leftrightarrow CO + H_2O$	200	80	5.76	(CHEMIK, 2014)
19	1	$CO_2 + 3H_2 \leftrightarrow CH_3OH + H_2O$	240	20	11.6	(Fan & Wu, 2016)
	2	$2CH_3OH \leftrightarrow CH_3OCH_3 + H_2O$	400	25	86.76	(Matzen & Demirel, 2016)
20	1	$CO_2 + 3H_2 \leftrightarrow CH_3OH + H_2O$	280	442	85.5	(Gaikwad, *et al*., 2016)
	2	$2CH_3OH \leftrightarrow CH_3OCH_3 + H_2O$	400	25	86.76	(Matzen & Demirel, 2016)
21	1	$CO_2 + 3H_2 \leftrightarrow CH_3OH + H_2O$	200.85	40	61.54	(Cabrera, *et al*., 1998)
	2	$2CH_3OH \leftrightarrow CH_3OCH_3 + H_2O$	400	25	86.76	(Matzen & Demirel, 2016)
22	1	$CO_2 + 3H_2 \leftrightarrow CH_3OH + H_2O$	260	330	93.58	(Vanhove, 2015)
	2	$2CH_3OH \leftrightarrow CH_3OCH_3 + H_2O$	400	25	86.76	(Matzen & Demirel, 2016)
23	1	$CO_2 + 3H_2 \leftrightarrow CH_3OH + H_2O$	240	80	96	(Bellotti, *et al*., 2017)
	2	$2CH_3OH \leftrightarrow CH_3OCH_3 + H_2O$	400	25	86.76	(Matzen & Demirel, 2016)
24	1	$CO_2 + 3H_2 \leftrightarrow CH_3OH + H_2O$	220	18.9	17.20	(Gnanamani, *et al*., 2015)
	2	$2CH_3OH \leftrightarrow CH_3OCH_3 + H_2O$	400	25	86.76	(Matzen & Demirel, 2016)

Case Study No.	Reactor No.	Reaction	T	P	X	Reference
25	1	$CO_2 + 3H_2 \leftrightarrow CH_3OH + H_2O$	250	20	5	(Van der Ham, *et al*., 2012)
	2	$2CH_3OH \leftrightarrow CH_3OCH_3 + H_2O$	400	25	86.76	(Matzen & Demirel, 2016)
26	1	$CO_2 + 3H_2 \leftrightarrow CH_3OH + H_2O$	220	80	18	(CHEMIK, 2014)
	2	$2CH_3OH \leftrightarrow CH_3OCH_3 + H_2O$	400	25	86.76	(Matzen & Demirel, 2016)
27	1	$CO_2 + H_2 \leftrightarrow CO + H_2O$	340	20	2.77	(You, *et al*., 2013)
	2	$CO + 2H_2 \leftrightarrow CH_3OH$	280	442	1.67	(Gaikwad, *et al*., 2016)
28	1	$CO_2 + H_2 \leftrightarrow CO + H_2O$	340	20	2.77	(You, *et al*., 2013)
	2	$CO + 2H_2 \leftrightarrow CH_3OH$	260	330	90.53	(Vanhove, 2015)
29	1	$CO_2 + H_2 \leftrightarrow CO + H_2O$	340	20	2.77	(You, *et al*., 2013)
	2	$CO + 2H_2 \leftrightarrow CH_3OH$	250	20	7.04	(Van der Ham, *et al*., 2012)
30	1	$CO_2 + H_2 \leftrightarrow CO + H_2O$	260	442	4.5	(Gaikwad, *et al*., 2016)
	2	$CO + 2H_2 \leftrightarrow CH_3OH$	280	442	1.67	(Gaikwad, *et al*., 2016)
31	1	$CO_2 + H_2 \leftrightarrow CO + H_2O$	260	442	4.5	(Gaikwad, *et al*., 2016)
	2	$CO + 2H_2 \leftrightarrow CH_3OH$	260	330	90.53	(Vanhove, 2015)
32	1	$CO_2 + H_2 \leftrightarrow CO + H_2O$	260	442	4.5	(Gaikwad, *et al*., 2016)
	2	$CO + 2H_2 \leftrightarrow CH_3OH$	250	20	7.04	(Van der Ham, *et al*., 2012)
33	1	$CO_2 + H_2 \leftrightarrow CO + H_2O$	200	40	34.38	(Cabrera, *et al*., 1998)
	2	$CO + 2H_2 \leftrightarrow CH_3OH$	280	442	1.67	(Gaikwad, *et al*., 2016)

Case Study No.	Reactor No.	Reaction	T	P	X	Reference
34	1	$CO_2 + H_2 \leftrightarrow CO + H_2O$	200	40	34.38	(Cabrera, *et al*., 1998)
	2	$CO + 2H_2 \leftrightarrow CH_3OH$	260	330	90.53	(Vanhove, 2015)
35	1	$CO_2 + H_2 \leftrightarrow CO + H_2O$	200	40	34.38	(Cabrera, *et al*., 1998)
	2	$CO + 2H_2 \leftrightarrow CH_3OH$	250	20	7.04	(Van der Ham, *et al*., 2012)
36	1	$CO_2 + H_2 \leftrightarrow CO + H_2O$	260	330	13.5	(Vanhove, 2015)
	2	$CO + 2H_2 \leftrightarrow CH_3OH$	280	442	1.67	(Gaikwad, *et al*., 2016)
37	1	$CO_2 + H_2 \leftrightarrow CO + H_2O$	260	330	13.5	(Vanhove, 2015)
	2	$CO + 2H_2 \leftrightarrow CH_3OH$	260	330	90.53	(Vanhove, 2015)
38	1	$CO_2 + H_2 \leftrightarrow CO + H_2O$	260	330	13.5	(Vanhove, 2015)
	2	$CO + 2H_2 \leftrightarrow CH_3OH$	250	20	7.04	(Van der Ham, *et al*., 2012)
39	1	$CO_2 + H_2 \leftrightarrow CO + H_2O$	350	15	9.42	(Zhanghuai & Yuan, 2000)
	2	$CO + 2H_2 \leftrightarrow CH_3OH$	280	442	1.67	(Gaikwad, *et al*., 2016)
40	1	$CO_2 + H_2 \leftrightarrow CO + H_2O$	350	15	9.42	(Zhanghuai & Yuan, 2000)
	2	$CO + 2H_2 \leftrightarrow CH_3OH$	260	330	90.53	(Vanhove, 2015)
41	1	$CO_2 + H_2 \leftrightarrow CO + H_2O$	350	15	9.42	(Zhanghuai & Yuan, 2000)
	2	$CO + 2H_2 \leftrightarrow CH_3OH$	250	20	7.04	(Van der Ham, *et al*., 2012)
42	1	$CO_2 + H_2 \leftrightarrow CO + H_2O$	350	15	4.79	(Zhanghuai & Yuan, 2000)
	2	$CO + 2H_2 \leftrightarrow CH_3OH$	280	442	1.67	(Gaikwad, *et al*., 2016)

Case Study No.	Reactor No.	Reaction	T	P	X	Reference
43	1	$CO_2 + H_2 \leftrightarrow CO + H_2O$	350	15	4.79	(Zhanghuai & Yuan, 2000)
	2	$CO + 2H_2 \leftrightarrow CH_3OH$	260	330	90.53	(Vanhove, 2015)
44	1	$CO_2 + H_2 \leftrightarrow CO + H_2O$	350	15	4.79	(Zhanghuai & Yuan, 2000)
	2	$CO + 2H_2 \leftrightarrow CH_3OH$	250	20	7.04	(Van der Ham, *et al*., 2012)
45	1	$CO_2 + H_2 \leftrightarrow CO + H_2O$	250	50	2.70	(Van der Ham, *et al*., 2012)
	2	$CO + 2H_2 \leftrightarrow CH_3OH$	280	442	1.67	(Gaikwad, *et al*., 2016)
46	1	$CO_2 + H_2 \leftrightarrow CO + H_2O$	250	50	2.70	(Van der Ham, *et al*., 2012)
	2	$CO + 2H_2 \leftrightarrow CH_3OH$	260	330	90.53	(Vanhove, 2015)
47	1	$CO_2 + H_2 \leftrightarrow CO + H_2O$	250	50	2.70	(Van der Ham, *et al*., 2012)
	2	$CO + 2H_2 \leftrightarrow CH_3OH$	250	20	7.04	(Van der Ham, *et al*., 2012)
48	1	$CO_2 + H_2 \leftrightarrow CO + H_2O$	260	20	0.75	(Van der Ham, *et al*., 2012)
	2	$CO + 2H_2 \leftrightarrow CH_3OH$	280	442	1.67	(Gaikwad, *et al*., 2016)
49	1	$CO_2 + H_2 \leftrightarrow CO + H_2O$	260	20	0.75	(Van der Ham, *et al*., 2012)
	2	$CO + 2H_2 \leftrightarrow CH_3OH$	260	330	90.53	(Vanhove, 2015)
50	1	$CO_2 + H_2 \leftrightarrow CO + H_2O$	260	20	0.75	(Van der Ham, *et al*., 2012)
	2	$CO + 2H_2 \leftrightarrow CH_3OH$	250	20	7.04	(Van der Ham, *et al*., 2012)
51	1	$CO_2 + H_2 \leftrightarrow CO + H_2O$	90	70	15.13	(Chan, *et al*., 2018)
	2	$CO + 2H_2 \leftrightarrow CH_3OH$	280	442	1.67	(Gaikwad, *et al*., 2016)

Case Study No.	Reactor No.	Reaction	T	P	X	Reference
52	1	$CO_2 + H_2 \leftrightarrow CO + H_2O$	90	70	15.13	(Chan, *et al*., 2018)
	2	$CO + 2H_2 \leftrightarrow CH_3OH$	260	330	90.53	(Vanhove, 2015)
53	1	$CO_2 + H_2 \leftrightarrow CO + H_2O$	90	70	15.13	(Chan, *et al*., 2018)
	2	$CO + 2H_2 \leftrightarrow CH_3OH$	250	20	7.04	(Van der Ham, *et al*., 2012)
54	1	$CO_2 + H_2 \leftrightarrow CO + H_2O$	200	80	5.76	(CHEMIK, 2014)
	2	$CO + 2H_2 \leftrightarrow CH_3OH$	280	442	1.67	(Gaikwad, *et al*., 2016)
55	1	$CO_2 + H_2 \leftrightarrow CO + H_2O$	200	80	5.76	(CHEMIK, 2014)
	2	$CO + 2H_2 \leftrightarrow CH_3OH$	260	330	90.53	(Vanhove, 2015)
56	1	$CO_2 + H_2 \leftrightarrow CO + H_2O$	200	80	5.76	(CHEMIK, 2014)
	2	$CO + 2H_2 \leftrightarrow CH_3OH$	250	20	7.04	(Van der Ham, *et al*., 2012)
57	1	$CO_2 + H_2 \leftrightarrow CO + H_2O$	340	20	2.774	(You, *et al*., 2013)
	2	$CO + 2H_2 \leftrightarrow CH_3OH$	280	442	1.67	(Gaikwad, *et al*., 2016)
	3	$2CH_3OH \leftrightarrow CH_3OCH_3 + H_2O$	400	25	86.76	(Matzen & Demirel, 2016)
58	1	$CO_2 + H_2 \leftrightarrow CO + H_2O$	340	20	2.77	(You, *et al*., 2013)
	2	$CO + 2H_2 \leftrightarrow CH_3OH$	260	330	90.53	(Vanhove, 2015)
	3	$2CH_3OH \leftrightarrow CH_3OCH_3 + H_2O$	400	25	86.76	(Matzen & Demirel, 2016)
59	1	$CO_2 + H_2 \leftrightarrow CO + H_2O$	340	20	2.77	(You, *et al*., 2013)
	2	$CO + 2H_2 \leftrightarrow CH_3OH$	250	20	7.04	(Van der Ham, *et al*., 2012)
	3	$2CH_3OH \leftrightarrow CH_3OCH_3 + H_2O$	400	25	86.76	(Matzen & Demirel, 2016)

Case Study No.	Reactor No.	Reaction	T	P	X	Reference
60	1	$CO_2 + H_2 \leftrightarrow CO + H_2O$	260	442	4.5	(Gaikwad, *et al*., 2016)
	2	$CO + 2H_2 \leftrightarrow CH_3OH$	280	442	1.67	(Gaikwad, *et al*., 2016)
	3	$2CH_3OH \leftrightarrow CH_3OCH_3 + H_2O$	400	25	86.76	(Matzen & Demirel, 2016)
61	1	$CO_2 + H_2 \leftrightarrow CO + H_2O$	260	442	4.5	(Gaikwad, *et al*., 2016)
	2	$CO + 2H_2 \leftrightarrow CH_3OH$	260	330	90.53	(Vanhove, 2015)
	3	$2CH_3OH \leftrightarrow CH_3OCH_3 + H_2O$	400	25	86.76	(Matzen & Demirel, 2016)
62	1	$CO_2 + H_2 \leftrightarrow CO + H_2O$	260	442	4.5	(Gaikwad, *et al*., 2016)
	2	$CO + 2H_2 \leftrightarrow CH_3OH$	250	20	7.04	(Van der Ham, *et al*., 2012)
	3	$2CH_3OH \leftrightarrow CH_3OCH_3 + H_2O$	400	25	86.76	(Matzen & Demirel, 2016)
63	1	$CO_2 + H_2 \leftrightarrow CO + H_2O$	200	40	34.38	(Cabrera, *et al*., 1998)
	2	$CO + 2H_2 \leftrightarrow CH_3OH$	280	442	1.67	(Gaikwad, *et al*., 2016)
	3	$2CH_3OH \leftrightarrow CH_3OCH_3 + H_2O$	400	25	86.76	(Matzen & Demirel, 2016)
64	1	$CO_2 + H_2 \leftrightarrow CO + H_2O$	200	40	34.38	(Cabrera, *et al*., 1998)
	2	$CO + 2H_2 \leftrightarrow CH_3OH$	260	330	90.53	(Vanhove, 2015)
	3	$2CH_3OH \leftrightarrow CH_3OCH_3 + H_2O$	400	25	86.76	(Matzen & Demirel, 2016)
65	1	$CO_2 + H_2 \leftrightarrow CO + H_2O$	200	40	34.38	(Cabrera, *et al*., 1998)
	2	$CO + 2H_2 \leftrightarrow CH_3OH$	250	20	7.04	(Van der Ham, *et al*., 2012)
	3	$2CH_3OH \leftrightarrow CH_3OCH_3 + H_2O$	400	25	86.76	(Matzen & Demirel, 2016)

Case Study No.	Reactor No.	Reaction	T	P	X	Reference
66	1	$CO_2 + H_2 \leftrightarrow CO + H_2O$	260	330	13.5	(Vanhove, 2015)
	2	$CO + 2H_2 \leftrightarrow CH_3OH$	280	442	1.67	(Gaikwad, *et al*., 2016)
	3	$2CH_3OH \leftrightarrow CH_3OCH_3 + H_2O$	400	25	86.76	(Matzen & Demirel, 2016)
67	1	$CO_2 + H_2 \leftrightarrow CO + H_2O$	260	330	13.5	(Vanhove, 2015)
	2	$CO + 2H_2 \leftrightarrow CH_3OH$	260	330	90.53	(Vanhove, 2015)
	3	$2CH_3OH \leftrightarrow CH_3OCH_3 + H_2O$	400	25	86.76	(Matzen & Demirel, 2016)
68	1	$CO_2 + H_2 \leftrightarrow CO + H_2O$	260	330	13.5	(Vanhove, 2015)
	2	$CO + 2H_2 \leftrightarrow CH_3OH$	250	20	7.04	(Van der Ham, *et al*., 2012)
	3	$2CH_3OH \leftrightarrow CH_3OCH_3 + H_2O$	400	25	86.76	(Matzen & Demirel, 2016)
69	1	$CO_2 + H_2 \leftrightarrow CO + H_2O$	350	15	9.42	(Zhanghuai & Yuan, 2000)
	2	$CO + 2H_2 \leftrightarrow CH_3OH$	280	442	1.67	(Gaikwad, *et al*., 2016)
	3	$2CH_3OH \leftrightarrow CH_3OCH_3 + H_2O$	400	25	86.76	(Matzen & Demirel, 2016)
70	1	$CO_2 + H_2 \leftrightarrow CO + H_2O$	350	15	9.42	(Zhanghuai & Yuan, 2000)
	2	$CO + 2H_2 \leftrightarrow CH_3OH$	260	330	90.53	(Vanhove, 2015)
	3	$2CH_3OH \leftrightarrow CH_3OCH_3 + H_2O$	400	25	86.76	(Matzen & Demirel, 2016)
71	1	$CO_2 + H_2 \leftrightarrow CO + H_2O$	350	15	9.42	(Zhanghuai & Yuan, 2000)
	2	$CO + 2H_2 \leftrightarrow CH_3OH$	250	20	7.04	(Van der Ham, *et al*., 2012)
	3	$2CH_3OH \leftrightarrow CH_3OCH_3 + H_2O$	400	25	86.76	(Matzen & Demirel, 2016)

Case Study No.	Reactor No.	Reaction	T	P	X	Reference
72	1	$CO_2 + H_2 \leftrightarrow CO + H_2O$	350	15	4.79	(Zhanghuai & Yuan, 2000)
	2	$CO + 2H_2 \leftrightarrow CH_3OH$	280	442	1.67	(Gaikwad, *et al*., 2016)
	3	$2CH_3OH \leftrightarrow CH_3OCH_3 + H_2O$	400	25	86.76	(Matzen & Demirel, 2016)
73	1	$CO_2 + H_2 \leftrightarrow CO + H_2O$	350	15	4.79	(Zhanghuai & Yuan, 2000)
	2	$CO + 2H_2 \leftrightarrow CH_3OH$	260	330	90.53	(Vanhove, 2015)
	3	$2CH_3OH \leftrightarrow CH_3OCH_3 + H_2O$	400	25	86.76	(Matzen & Demirel, 2016)
74	1	$CO_2 + H_2 \leftrightarrow CO + H_2O$	350	15	4.79	(Zhanghuai & Yuan, 2000)
	2	$CO + 2H_2 \leftrightarrow CH_3OH$	250	20	7.04	(Van der Ham, *et al*., 2012)
	3	$2CH_3OH \leftrightarrow CH_3OCH_3 + H_2O$	400	25	86.76	(Matzen & Demirel, 2016)
75	1	$CO_2 + H_2 \leftrightarrow CO + H_2O$	250	50	2.70	(Van der Ham, *et al*., 2012)
	2	$CO + 2H_2 \leftrightarrow CH_3OH$	280	442	1.67	(Gaikwad, *et al*., 2016)
	3	$2CH_3OH \leftrightarrow CH_3OCH_3 + H_2O$	400	25	86.76	(Matzen & Demirel, 2016)
76	1	$CO_2 + H_2 \leftrightarrow CO + H_2O$	250	50	2.70	(Van der Ham, *et al*., 2012)
	2	$CO + 2H_2 \leftrightarrow CH_3OH$	260	330	90.53	(Vanhove, 2015)
	3	$2CH_3OH \leftrightarrow CH_3OCH_3 + H_2O$	400	25	86.76	(Matzen & Demirel, 2016)
77	1	$CO_2 + H_2 \leftrightarrow CO + H_2O$	250	50	2.70	(Van der Ham, *et al*., 2012)
	2	$CO + 2H_2 \leftrightarrow CH_3OH$	250	20	7.04	(Van der Ham, *et al*., 2012)
	3	$2CH_3OH \leftrightarrow CH_3OCH_3 + H_2O$	400	25	86.76	(Matzen & Demirel, 2016)

Case Study No.	Reactor No.	Reaction	T	P	X	Reference
78	1	$CO_2 + H_2 \leftrightarrow CO + H_2O$	260	20	0.75	(Van der Ham, *et al*., 2012)
	2	$CO + 2H_2 \leftrightarrow CH_3OH$	280	442	1.67	(Gaikwad, *et al*., 2016)
	3	$2CH_3OH \leftrightarrow CH_3OCH_3 + H_2O$	400	25	86.76	(Matzen & Demirel, 2016)
79	1	$CO_2 + H_2 \leftrightarrow CO + H_2O$	260	20	0.75	(Van der Ham, *et al*., 2012)
	2	$CO + 2H_2 \leftrightarrow CH_3OH$	260	330	90.53	(Vanhove, 2015)
	3	$2CH_3OH \leftrightarrow CH_3OCH_3 + H_2O$	400	25	86.76	(Matzen & Demirel, 2016)
80	1	$CO_2 + H_2 \leftrightarrow CO + H_2O$	260	20	0.75	(Van der Ham, *et al*., 2012)
	2	$CO + 2H_2 \leftrightarrow CH_3OH$	250	20	7.04	(Van der Ham, *et al*., 2012)
	3	$2CH_3OH \leftrightarrow CH_3OCH_3 + H_2O$	400	25	86.76	(Matzen & Demirel, 2016)
81	1	$CO_2 + H_2 \leftrightarrow CO + H_2O$	90	70	15.13	(Chan, *et al*., 2018)
	2	$CO + 2H_2 \leftrightarrow CH_3OH$	280	442	1.67	(Gaikwad, *et al*., 2016)
	3	$2CH_3OH \leftrightarrow CH_3OCH_3 + H_2O$	400	25	86.76	(Matzen & Demirel, 2016)
82	1	$CO_2 + H_2 \leftrightarrow CO + H_2O$	90	70	15.13	(Chan, *et al*., 2018)
	2	$CO + 2H_2 \leftrightarrow CH_3OH$	260	330	90.53	(Vanhove, 2015)
	3	$2CH_3OH \leftrightarrow CH_3OCH_3 + H_2O$	400	25	86.76	(Matzen & Demirel, 2016)
83	1	$CO_2 + H_2 \leftrightarrow CO + H_2O$	90	70	15.13	(Chan, *et al*., 2018)
	2	$CO + 2H_2 \leftrightarrow CH_3OH$	250	20	7.04	(Van der Ham, *et al*., 2012)
	3	$2CH_3OH \leftrightarrow CH_3OCH_3 + H_2O$	400	25	86.76	(Matzen & Demirel, 2016)

Case Study No.	Reactor No.	Reaction	T	P	X	Reference
84	1	$CO_2 + H_2 \leftrightarrow CO + H_2O$	200	80	5.76	(CHEMIK, 2014)
	2	$CO + 2H_2 \leftrightarrow CH_3OH$	280	442	1.67	(Gaikwad, *et al*., 2016)
	3	$2CH_3OH \leftrightarrow CH_3OCH_3 + H_2O$	400	25	86.76	(Matzen & Demirel, 2016)
85	1	$CO_2 + H_2 \leftrightarrow CO + H_2O$	200	80	5.76	(CHEMIK, 2014)
	2	$CO + 2H_2 \leftrightarrow CH_3OH$	260	330	90.53	(Vanhove, 2015)
	3	$2CH_3OH \leftrightarrow CH_3OCH_3 + H_2O$	400	25	86.76	(Matzen & Demirel, 2016)
86	1	$CO_2 + H_2 \leftrightarrow CO + H_2O$	200	80	5.76	(CHEMIK, 2014)
	2	$CO + 2H_2 \leftrightarrow CH_3OH$	250	20	7.04	(Van der Ham, *et al*., 2012)
	3	$2CH_3OH \leftrightarrow CH_3OCH_3 + H_2O$	400	25	86.76	(Matzen & Demirel, 2016)

Appendix J: ASSF Tool Data for Application #4

Table J.1 details the ASSF tool results associated with the RPD developed by Jugmohan, *et al*. (2020) and the reaction pathway combinations provided in Appendix I. All values reported within this table is given to two decimal places, and NG is used to denote the natural gas utility which is required to meet the energy requirements of the necessary unit operations.

Table J.1: ASSF tool data associated with the RPD developed by Jugmohan, et al. (2020)

Case Study Number (→)	**1**	**2**	**3**
CO_2 Feed Flow (tons/annum)	34,855.92	34,855.92	34,855.92
H_2 Feed Flow (tons/annum)	4,790.02	4,790.02	4,790.02
CaO Needed (tons/annum)	0.00	0.00	0.00
CaO Cost ($/annum)	0.00	0.00	0.00
MeOH Produced (tons/annum)	2,009.20	21,423.47	15,225.95
MeOH Purity (mass %)	92.12	96.13	92.47
MeOH Sales Potential ($/annum)	1,004,601.40	1,071,1736.18	7,612,977.21
DME Produced (tons/annum)	0.00	0.00	0.00
DME Purity (mass %)	0.00	0.00	0.00
DME Sales Potential ($/annum)	0.00	0.00	0.00
$CaCO_3$ Produced (tons/annum)	0.00	0.00	0.00
$CaCO_3$ Sales Potential ($/annum)	0.00	0.00	0.00
Total Reactant Cost ($/annum)	8,078,875.20	8,078,875.20	8,078,875.20
Total Product Revenue ($/annum)	1,004,601.40	10,711,736.18	7,612,977.21
Total Unit Operation Cost ($)	2,256,259.25	12,310,152.95	2,753,693.76
Unreacted CO_2 to Atmosphere (before NG) (tons/annum)	30,640.91	4,193.19	12,166.67
Yearly Profit (before NG) ($/annum)	-7,074,273.80	2,632,860.98	-465,897.99

Case Study Number (→)	4	5	6
CO_2 Feed Flow (tons/annum)	34,855.92	34,855.92	34,855.92
H_2 Feed Flow (tons/annum)	4,790.02	4,790.02	4,790.02
CaO Needed (tons/annum)	0.00	0.00	0.00
CaO Cost ($/annum)	0.00	0.00	0.00
MeOH Produced (tons/annum)	23,662.92	24,332.28	3,476.60
MeOH Purity (mass %)	96.15	96.15	92.26
MeOH Sales Potential ($/annum)	11,831,458.13	12,166,139.29	1,738,302.49
DME Produced (tons/annum)	0.00	0.00	0.00
DME Purity (mass %)	0.00	0.00	0.00
DME Sales Potential ($/annum)	0.00	0.00	0.00
$CaCO_3$ Produced (tons/annum)	0.00	0.00	0.00
$CaCO_3$ Sales Potential ($/annum)	0.00	0.00	0.00
Total Reactant Cost ($/annum)	8,078,875.20	8,078,875.20	8,078,875.20
Total Product Revenue ($/annum)	11,831,458.13	12,166,139.29	1,738,302.49
Total Unit Operation Cost ($)	11,977,003.39	4,265,942.11	2,252,626.12
Unreacted CO_2 to Atmosphere (before NG) (tons/annum)	1,289.00	421.32	28,568.65
Yearly Profit (before NG) ($/annum)	3,752,582.93	4,087,264.09	-6,340,572.71

Case Study Number (→)	7	8	9
CO_2 Feed Flow (tons/annum)	34,855.92	34,855.92	34,855.92
H_2 Feed Flow (tons/annum)	4,790.02	4,790.02	1,596.67
CaO Needed (tons/annum)	0.00	0.00	0.00
CaO Cost ($/annum)	0.00	0.00	0.00
MeOH Produced (tons/annum)	386.07	3,683.44	0.00
MeOH Purity (mass %)	91.09	92.30	0.00%
MeOH Sales Potential ($/annum)	193,037.35	1,841,720.66	0.00
DME Produced (tons/annum)	0.00	0.00	0.00
DME Purity (mass %)	0.00	0.00	0.00
DME Sales Potential ($/annum)	0.00	0.00	0.00
$CaCO_3$ Produced (tons/annum)	0.00	0.00	0.00
$CaCO_3$ Sales Potential ($/annum)	0.00	0.00	0.00
Total Reactant Cost ($/annum)	8,078,875.20	8,078,875.20	4,087,195.20
Total Product Revenue ($/annum)	193,037.35	1,841,720.66	0.00
Total Unit Operation Cost ($)	2,320,279.56	3,398,682.91	182,286.56
Unreacted CO_2 to Atmosphere (before NG) (tons/annum)	33,075.42	28,274.84	0.00
Yearly Profit (before NG) ($/annum)	-7,885,837.85	-6,237,154.54	-4,087,195.20

Case Study Number (→)	10	11	12
CO_2 Feed Flow (tons/annum)	34,855.92	34,855.92	34,855.92
H_2 Feed Flow (tons/annum)	1,596.67	1,596.67	1,596.67
CaO Needed (tons/annum)	0.00	0.00	0.00
CaO Cost ($/annum)	0.00	0.00	0.00
MeOH Produced (tons/annum)	0.00	0.00	0.00
MeOH Purity (mass %)	0.00	0.00	0.00
MeOH Sales Potential ($/annum)	0.00	0.00	0.00
DME Produced (tons/annum)	0.00	0.00	0.00
DME Purity (mass %)	0.00	0.00	0.00
DME Sales Potential ($/annum)	0.00	0.00	0.00
$CaCO_3$ Produced (tons/annum)	0.00	0.00	0.00
$CaCO_3$ Sales Potential ($/annum)	0.00	0.00	0.00
Total Reactant Cost ($/annum)	4,087,195.20	4,087,195.20	4,087,195.20
Total Product Revenue ($/annum)	0.00	0.00	0.00
Total Unit Operation Cost ($)	596,382.88	1,844,693.74	114,858.49
Unreacted CO_2 to Atmosphere (before NG) (tons/annum)	0.00	22698.19	0.00
Yearly Profit (before NG) ($/annum)	-4,087,195.20	-4,087,195.20	-4,087,195.20

Case Study Number (→)	13	14	15
CO_2 Feed Flow (tons/annum)	34,855.92	34,855.92	34,855.92
H_2 Feed Flow (tons/annum)	1,596.67	1,596.67	1,596.67
CaO Needed (tons/annum)	0.00	0.00	0.00
CaO Cost ($/annum)	0.00	0.00	0.00
MeOH Produced (tons/annum)	0.00	0.00	0.00
MeOH Purity (mass %)	0.00	0.00	0.00
MeOH Sales Potential ($/annum)	0.00	0.00	0.00
DME Produced (tons/annum)	0.00	0.00	0.00
DME Purity (mass %)	0.00	0.00	0.00
DME Sales Potential ($/annum)	0.00	0.00	0.00
$CaCO_3$ Produced (tons/annum)	0.00	0.00	0.00
$CaCO_3$ Sales Potential ($/annum)	0.00	0.00	0.00
Total Reactant Cost ($/annum)	4,087,195.20	4,087,195.20	4,087,195.20
Total Product Revenue ($/annum)	0.00	0.00	0.00
Total Unit Operation Cost ($)	230,993.43	230,993.43	1,001,385.90
Unreacted CO_2 to Atmosphere (before NG) (tons/annum)	0.00	0.00	0.00
Yearly Profit (before NG) ($/annum)	-4,087,195.20	-4,087,195.20	-4,087,195.20

Case Study Number (→)	16	17	18
CO_2 Feed Flow (tons/annum)	34,855.92	34,855.92	34,855.92
H_2 Feed Flow (tons/annum)	1,596.67	1,596.67	1,596.67
CaO Needed (tons/annum)	0.00	0.00	0.00
CaO Cost ($/annum)	0.00	0.00	0.00
MeOH Produced (tons/annum)	0.00	0.00	0.00
MeOH Purity (mass %)	0.00	0.00	0.00
MeOH Sales Potential ($/annum)	0.00	0.00	0.00
DME Produced (tons/annum)	0.00	0.00	0.00
DME Purity (mass %)	0.00	0.00	0.00
DME Sales Potential ($/annum)	0.00	0.00	0.00
$CaCO_3$ Produced (tons/annum)	0.00	0.00	0.00
$CaCO_3$ Sales Potential ($/annum)	0.00	0.00	0.00
Total Reactant Cost ($/annum)	4,087,195.20	4,087,195.20	4,087,195.20
Total Product Revenue ($/annum)	0.00	0.00	0.00
Total Unit Operation Cost ($)	825,003.16	1,217,792.19	1,284,143.42
Unreacted CO_2 to Atmosphere (before NG) (tons/annum)	0.00	0.00	0.00
Yearly Profit (before NG) ($/annum)	-4,087,195.20	-4,087,195.20	-4,087,195.20

Case Study Number (→)	19	20	21
CO_2 Feed Flow (tons/annum)	34,855.92	34,855.92	34,855.92
H_2 Feed Flow (tons/annum)	4,790.02	4,790.02	4,790.02
CaO Needed (tons/annum)	196.92	987.28	1,420.76
CaO Cost ($/annum)	23,630.83	118,473.11	170,491.58
MeOH Produced (tons/annum)	265.88	2,835.04	2,014.90
MeOH Purity (mass %)	99.93	99.93	99.93
MeOH Sales Potential ($/annum)	132,942.45	1,417,521.85	1,007,452.14
DME Produced (tons/annum)	1,253.05	13,360.90	9,495.77
DME Purity (mass %)	98.65	99.36	98.71
DME Sales Potential ($/annum)	1,240,523.09	13,227,291.92	9,400,817.04
$CaCO_3$ Produced (tons/annum)	351.47	1,762.09	2,535.78
$CaCO_3$ Sales Potential ($/annum)	91,381.96	458,143.20	659,302.03
Total Reactant Cost ($/annum)	8,102,506.03	8,197,348.31	8,249,366.78
Total Product Revenue ($/annum)	1,464,847.50	15,102,956.98	11,067,571.20
Total Unit Operation Cost ($)	3,248,284.28	14,735,491.82	4,763,009.04
Unreacted CO_2 to Atmosphere (before NG) (tons/annum)	30,640.91	4,193.19	12,166.67
Yearly Profit (before NG) ($/annum)	-6,637,658.53	6,905,608.67	2,818,204.42

Case Study Number (→)	22	23	24
CO_2 Feed Flow (tons/annum)	34,855.92	34,855.92	34,855.92
H_2 Feed Flow (tons/annum)	4,790.02	4,790.02	4,790.02
CaO Needed (tons/annum)	1,086.17	1,115.72	334.12
CaO Cost ($/annum)	130,340.43	133,886.59	40,094.25
MeOH Produced (tons/annum)	3,131.40	3,219.98	460.07
MeOH Purity (mass %)	99.93	99.93	99.93
MeOH Sales Potential ($/annum)	1,565,698.61	1,609,988.15	230,035.70
DME Produced (tons/annum)	14,757.55	15,175.00	2,168.21
DME Purity (mass %)	99.36	99.36	98.67
DME Sales Potential ($/annum)	14,609,970.59	15,023,248.65	2,146,527.33
$CaCO_3$ Produced (tons/annum)	1,938.60	1,991.34	596.33
$CaCO_3$ Sales Potential ($/annum)	504,034.92	517,748.13	155,047.07
Total Reactant Cost ($/annum)	8,209,215.63	8,212,761.79	8,118,969.45
Total Product Revenue ($/annum)	16,679,704.12	17,150,984.93	2,531,610.11
Total Unit Operation Cost ($)	14,517,900.92	6,839,630.70	3,270,848.20
Unreacted CO_2 to Atmosphere (before NG) (tons/annum)	1,289.00	421.32	28,568.65
Yearly Profit (before NG) ($/annum)	8,470,488.49	8,938,223.14	-5,587,359.34

Case Study Number (→)	25	26	27
CO_2 Feed Flow (tons/annum)	34,855.92	34,855.92	34,855.92
H_2 Feed Flow (tons/annum)	4,790.02	4,790.02	1,596.67
CaO Needed (tons/annum)	43.23	352.08	0.00
CaO Cost ($/annum)	5,188.08	42,249.42	0.00
MeOH Produced (tons/annum)	0.00	487.44	0.00
MeOH Purity (mass %)	0.00	99.93	0.00
MeOH Sales Potential ($/annum)	0.00	243721.39	0.00
DME Produced (tons/annum)	240.78	2297.20	0.00
DME Purity (mass %)	98.46	98.68	0.00
DME Sales Potential ($/annum)	238,370.45	2,274,232.33	0.00
$CaCO_3$ Produced (tons/annum)	77.16	628.39	0.00
$CaCO_3$ Sales Potential ($/annum)	20,062.63	163,381.27	0.00
Total Reactant Cost ($/annum)	8,084,063.28	8,121,124.62	4,087,195.20
Total Product Revenue ($/annum)	258,433.08	2,681,335.00	0.00
Total Unit Operation Cost ($)	2,703,106.48	4,435,336.76	1,740,370.40
Unreacted CO_2 to Atmosphere (before NG) (tons/annum)	33,075.42	28,274.84	33,888.98
Yearly Profit (before NG) ($/annum)	-7,825,630.20	-5,439,789.62	-4,087,195.20

Case Study Number (→)	28	29	30
CO_2 Feed Flow (tons/annum)	34,855.92	34,855.92	34,855.92
H_2 Feed Flow (tons/annum)	1,596.67	1,596.67	1,596.67
CaO Needed (tons/annum)	0.00	0.00	0.00
CaO Cost ($/annum)	0.00	0.00	0.00
MeOH Produced (tons/annum)	0.00	0.00	0.00
MeOH Purity (mass %)	0.00	0.00	0.00
MeOH Sales Potential ($/annum)	0.00	0.00	0.00
DME Produced (tons/annum)	0.00	0.00	0.00
DME Purity (mass %)	0.00	0.00	0.00
DME Sales Potential ($/annum)	0.00	0.00	0.00
$CaCO_3$ Produced (tons/annum)	0.00	0.00	0.00
$CaCO_3$ Sales Potential ($/annum)	0.00	0.00	0.00
Total Reactant Cost ($/annum)	4,087,195.20	4,087,195.20	4,087,195.20
Total Product Revenue ($/annum)	0.00	0.00	0.00
Total Unit Operation Cost ($)	2,032,876.74	1,038,671.95	1,527,891.84
Unreacted CO_2 to Atmosphere (before NG) (tons/annum)	33,888.06	33,888.99	33,279.17
Yearly Profit (before NG) ($/annum)	-4,087,195.20	-4,087,195.20	-4,087,195.20

Case Study Number (→)	31	32	33
CO_2 Feed Flow (tons/annum)	34,855.92	34,855.92	34,855.92
H_2 Feed Flow (tons/annum)	1,596.67	1,596.67	1,596.67
CaO Needed (tons/annum)	0.00	0.00	0.00
CaO Cost ($/annum)	0.00	0.00	0.00
MeOH Produced (tons/annum)	0.00	0.00	0.00
MeOH Purity (mass %)	0.00	0.00	0.00
MeOH Sales Potential ($/annum)	0.00	0.00	0.00
DME Produced (tons/annum)	0.00	0.00	0.00
DME Purity (mass %)	0.00	0.00	0.00
DME Sales Potential ($/annum)	0.00	0.00	0.00
$CaCO_3$ Produced (tons/annum)	0.00	0.00	0.00
$CaCO_3$ Sales Potential ($/annum)	0.00	0.00	0.00
Total Reactant Cost ($/annum)	4,087,195.20	4,087,195.20	4,087,195.20
Total Product Revenue ($/annum)	0.00	0.00	0.00
Total Unit Operation Cost ($)	1,856,362.03	2,112,829.89	5,243,538.00
Unreacted CO_2 to Atmosphere (before NG) (tons/annum)	33,263.20	33,278.87	22,697.66
Yearly Profit (before NG) ($/annum)	-4,087,195.20	-4,087,195.20	-4,087,195.20

Case Study Number (→)	34	35	36
CO_2 Feed Flow (tons/annum)	34,855.92	34,855.92	34,855.92
H_2 Feed Flow (tons/annum)	1,596.67	1,596.67	1,596.67
CaO Needed (tons/annum)	0.00	0.00	0.00
CaO Cost ($/annum)	0.00	0.00	0.00
MeOH Produced (tons/annum)	7,059.14	0.00	0.00
MeOH Purity (mass %)	93.53	0.00	0.00
MeOH Sales Potential ($/annum)	3,529,571.26	0.00	0.00
DME Produced (tons/annum)	0.00	0.00	0.00
DME Purity (mass %)	0.00	0.00	0.00
DME Sales Potential ($/annum)	0.00	0.00	0.00
$CaCO_3$ Produced (tons/annum)	0.00	0.00	0.00
$CaCO_3$ Sales Potential ($/annum)	0.00	0.00	0.00
Total Reactant Cost ($/annum)	4,087,195.20	4,087,195.20	4,087,195.20
Total Product Revenue ($/annum)	3,529,571.26	0.00	0.00
Total Unit Operation Cost ($)	4,690,433.09	3,244,152.93	1,156,112.07
Unreacted CO_2 to Atmosphere (before NG) (tons/annum)	22,210.28	22,691.10	30,091.09
Yearly Profit (before NG) ($/annum)	-557,623.94	-4,087,195.20	-4,087,195.20

Case Study Number (→)	37	38	39
CO_2 Feed Flow (tons/annum)	34,855.92	34,855.92	34,855.92
H_2 Feed Flow (tons/annum)	1,596.67	1,596.67	1,596.67
CaO Needed (tons/annum)	0.00	0.00	0.00
CaO Cost ($/annum)	0.00	0.00	0.00
MeOH Produced (tons/annum)	2,203.07	0.00	0.00
MeOH Purity (mass %)	92.00	0.00	0.00
MeOH Sales Potential ($/annum)	1,101,535.82	0.00	0.00
DME Produced (tons/annum)	0.00	0.00	0.00
DME Purity (mass %)	0.00	0.00	0.00
DME Sales Potential ($/annum)	0.00	0.00	0.00
$CaCO_3$ Produced (tons/annum)	0.00	0.00	0.00
$CaCO_3$ Sales Potential ($/annum)	0.00	0.00	0.00
Total Reactant Cost ($/annum)	4,087,195.20	4,087,195.20	4,087,195.20
Total Product Revenue ($/annum)	1,101,535.82	0.00	0.00
Total Unit Operation Cost ($)	1,319,900.16	1,555,973.91	1,892,884.55
Unreacted CO_2 to Atmosphere (before NG) (tons/annum)	29,958.86	30,089.23	31,535.32
Yearly Profit (before NG) ($/annum)	-2,985,659.38	-4,087,195.20	-4,087,195.20

Case Study Number (→)	40	41	42
CO_2 Feed Flow (tons/annum)	34,855.92	34,855.92	34,855.92
H_2 Feed Flow (tons/annum)	1,596.67	1,596.67	1,596.67
CaO Needed (tons/annum)	0.00	0.00	0.00
CaO Cost ($/annum)	0.00	0.00	0.00
MeOH Produced (tons/annum)	1,250.03	0.00	0.00
MeOH Purity (mass %)	91.77	0.00	0.00
MeOH Sales Potential ($/annum)	625,015.36	0.00	0.00
DME Produced (tons/annum)	0.00	0.00	0.00
DME Purity (mass %)	0.00	0.00	0.00
DME Sales Potential ($/annum)	0.00	0.00	0.00
$CaCO_3$ Produced (tons/annum)	0.00	0.00	0.00
$CaCO_3$ Sales Potential ($/annum)	0.00	0.00	0.00
Total Reactant Cost ($/annum)	4,087,195.20	4,087,195.20	4,087,195.20
Total Product Revenue ($/annum)	625,015.36	0.00	0.00
Total Unit Operation Cost ($)	2,239,622.31	1,190,893.08	1,873,392.77
Unreacted CO_2 to Atmosphere (before NG) (tons/annum)	31,459.40	31,534.27	33,175.00
Yearly Profit (before NG) ($/annum)	-3,462,179.84	-4,087,195.20	-4,087,195.20

Case Study Number (→)	43	44	45
CO_2 Feed Flow (tons/annum)	34,855.92	34,855.92	34,855.92
H_2 Feed Flow (tons/annum)	1,596.67	1,596.67	1,596.67
CaO Needed (tons/annum)	0.00	0.00	0.00
CaO Cost ($/annum)	0.00	0.00	0.00
MeOH Produced (tons/annum)	274.41	0.00	0.00
MeOH Purity (mass %)	90.53	0.00	0.00
MeOH Sales Potential ($/annum)	1372,05.68	0.00	0.00
DME Produced (tons/annum)	0.00	0.00	0.00
DME Purity (mass %)	0.00	0.00	0.00
DME Sales Potential ($/annum)	0.00	0.00	0.00
$CaCO_3$ Produced (tons/annum)	0.00	0.00	0.00
$CaCO_3$ Sales Potential ($/annum)	0.00	0.00	0.00
Total Reactant Cost ($/annum)	4,087,195.20	4,087,195.20	4,087,195.20
Total Product Revenue ($/annum)	137,205.68	0.00	0.00
Total Unit Operation Cost ($)	2,314,586.11	1,215,580.11	2,338,766.39
Unreacted CO_2 to Atmosphere (before NG) (tons/annum)	33,156.22	33,174.66	33,913.89
Yearly Profit (before NG) ($/annum)	-3,949,989.52	-4,087,195.20	-4,087,195.20

Case Study Number (→)	46	47	48
CO_2 Feed Flow (tons/annum)	34,855.92	34,855.92	34,855.92
H_2 Feed Flow (tons/annum)	1,596.67	1,596.67	1,596.67
CaO Needed (tons/annum)	0.00	0.00	0.00
CaO Cost ($/annum)	0.00	0.00	0.00
MeOH Produced (tons/annum)	0.00	0.00	0.00
MeOH Purity (mass %)	0.00	0.00	0.00
MeOH Sales Potential ($/annum)	0.00	0.00	0.00
DME Produced (tons/annum)	0.00	0.00	0.00
DME Purity (mass %)	0.00	0.00	0.00
DME Sales Potential ($/annum)	0.00	0.00	0.00
$CaCO_3$ Produced (tons/annum)	0.00	0.00	0.00
$CaCO_3$ Sales Potential ($/annum)	0.00	0.00	0.00
Total Reactant Cost ($/annum)	4,087,195.20	4,087,195.20	4,087,195.20
Total Product Revenue ($/annum)	0.00	0.00	0.00
Total Unit Operation Cost ($)	2,650,946.47	2,119,922.33	2,107,791.01
Unreacted CO_2 to Atmosphere (before NG) (tons/annum)	33,913.70	33,913.89	34,594.48
Yearly Profit (before NG) ($/annum)	-4,087,195.20	-4,087,195.20	-4,087,195.20

Case Study Number (→)	49	50	51
CO_2 Feed Flow (tons/annum)	34,855.92	34,855.92	34,855.92
H_2 Feed Flow (tons/annum)	1,596.67	1,596.67	1,596.67
CaO Needed (tons/annum)	0.00	0.00	0.00
CaO Cost ($/annum)	0.00	0.00	0.00
MeOH Produced (tons/annum)	0.00	0.00	0.00
MeOH Purity (mass %)	0.00	0.00	0.00
MeOH Sales Potential ($/annum)	0.00	0.00	0.00
DME Produced (tons/annum)	0.00	0.00	0.00
DME Purity (mass %)	0.00	0.00	0.00
DME Sales Potential ($/annum)	0.00	0.00	0.00
$CaCO_3$ Produced (tons/annum)	0.00	0.00	0.00
$CaCO_3$ Sales Potential ($/annum)	0.00	0.00	0.00
Total Reactant Cost ($/annum)	4,087,195.20	4,087,195.20	4,087,195.20
Total Product Revenue ($/annum)	0.00	0.00	0.00
Total Unit Operation Cost ($)	2,462,359.69	1,402,249.29	2,632,368.59
Unreacted CO_2 to Atmosphere (before NG) (tons/annum)	34,594.45	34,594.50	29,513.67
Yearly Profit (before NG) ($/annum)	-4,087,195.20	-4,087,195.20	-4,087,195.20

Case Study Number (→)	52	53	54
CO_2 Feed Flow (tons/annum)	34,855.92	34,855.92	34,855.92
H_2 Feed Flow (tons/annum)	1,596.67	1,596.67	1,596.67
CaO Needed (tons/annum)	0.00	0.00	0.00
CaO Cost ($/annum)	0.00	0.00	0.00
MeOH Produced (tons/annum)	2,587.53	0.00	0.00
MeOH Purity (mass %)	92.06	0.00	0.00
MeOH Sales Potential ($/annum)	1,293,766.19	0.00	0.00
DME Produced (tons/annum)	0.00	0.00	0.00
DME Purity (mass %)	0.00	0.00	0.00
DME Sales Potential ($/annum)	0.00	0.00	0.00
$CaCO_3$ Produced (tons/annum)	0.00	0.00	0.00
$CaCO_3$ Sales Potential ($/annum)	0.00	0.00	0.00
Total Reactant Cost ($/annum)	4,087,195.20	4,087,195.20	4,087,195.20
Total Product Revenue ($/annum)	1,293,766.19	0.00	0.00
Total Unit Operation Cost ($)	2,913,853.61	2,393,671.36	2,545,412.76
Unreacted CO_2 to Atmosphere (before NG) (tons/annum)	29,359.31	29,511.46	32,832.86
Yearly Profit (before NG) ($/annum)	-2,793,429.01	-4,087,195.20	-4,087,195.20

Case Study Number (→)	55	56	57
CO_2 Feed Flow (tons/annum)	34,855.92	34,855.92	34,855.92
H_2 Feed Flow (tons/annum)	1,596.67	1,596.67	1,596.67
CaO Needed (tons/annum)	0.00	0.00	38,863.15
CaO Cost ($/annum)	0.00	0.00	4,663,577.79
MeOH Produced (tons/annum)	457.20	0.00	0.00
MeOH Purity (mass %)	91.00	0.00	0.00
MeOH Sales Potential ($/annum)	228,600.23	0.00	0.00
DME Produced (tons/annum)	0.00	0.00	7.33
DME Purity (mass %)	0.00	0.00	0.22
DME Sales Potential ($/annum)	0.00	0.00	7,258.53
$CaCO_3$ Produced (tons/annum)	0.00	0.00	69,362.92
$CaCO_3$ Sales Potential ($/annum)	0.00	0.00	18,034,358.38
Total Reactant Cost ($/annum)	4,087,195.20	4,087,195.20	8,750,772.99
Total Product Revenue ($/annum)	228,600.23	0.00	18,041,616.91
Total Unit Operation Cost ($)	3,021,973.55	2,530,716.58	3,693,059.53
Unreacted CO_2 to Atmosphere (before NG) (tons/annum)	32,803.09	32,832.40	12,298.10
Yearly Profit (before NG) ($/annum)	-3,858,594.97	-4,087,195.20	9,290,843.92

Case Study Number (→)	58	59	60
CO_2 Feed Flow (tons/annum)	34,855.92	34,855.92	34,855.92
H_2 Feed Flow (tons/annum)	1,596.67	1,596.67	1,596.67
CaO Needed (tons/annum)	38,863.15	38,863.15	38,173.23
CaO Cost ($/annum)	4,663,577.79	4,663,577.79	4,580,787.84
MeOH Produced (tons/annum)	0.00	0.00	0.00
MeOH Purity (mass %)	0.00	0.00	0.00
MeOH Sales Potential ($/annum)	0.00	0.00	0.00
DME Produced (tons/annum)	397.46	30.91	11.89
DME Purity (mass %)	10.50	0.90	0.36
DME Sales Potential ($/annum)	393,481.98	30,598.84	11,774.84
$CaCO_3$ Produced (tons/annum)	69,362.92	69,362.92	68,131.55
$CaCO_3$ Sales Potential ($/annum)	18,034,358.38	18,034,358.38	17,714,204.28
Total Reactant Cost ($/annum)	8,750,772.99	8,750,772.99	8,667,983.04
Total Product Revenue ($/annum)	18,427,840.36	18,064,957.22	17,725,979.11
Total Unit Operation Cost ($)	4,044,562.33	2,996,865.76	3,414,348.66
Unreacted CO_2 to Atmosphere (before NG) (tons/annum)	12,328.49	12,353.48	12,134.82
Yearly Profit (before NG) ($/annum)	9,677,067.37	9,314,184.23	9,057,996.07

Case Study Number (→)	61	62	63
CO_2 Feed Flow (tons/annum)	34,855.92	34,855.92	34,855.92
H_2 Feed Flow (tons/annum)	1,596.67	1,596.67	1,596.67
CaO Needed (tons/annum)	38,173.23	38,173.23	26,029.76
CaO Cost ($/annum)	4,580,787.84	4,580,787.84	3,123,571.19
MeOH Produced (tons/annum)	0.00	0.00	0.00
MeOH Purity (mass %)	0.00	0.00	0.00
MeOH Sales Potential ($/annum)	0.00	0.00	0.00
DME Produced (tons/annum)	644.76	50.14	90.86
DME Purity (mass %)	16.23	1.48	3.85
DME Sales Potential ($/annum)	638,308.91	49,637.63	89,946.66
$CaCO_3$ Produced (tons/annum)	68,131.55	68,131.55	46,457.90
$CaCO_3$ Sales Potential ($/annum)	17,714,204.28	17,714,204.28	12,079,052.79
Total Reactant Cost ($/annum)	8,667,983.04	8,667,983.04	7,210,766.39
Total Product Revenue ($/annum)	18,352,513.19	17,763,841.91	12,168,999.45
Total Unit Operation Cost ($)	3,756,897.81	4,010,728.68	6,259,834.55
Unreacted CO_2 to Atmosphere (before NG) (tons/annum)	12,139.26	12,099.16	8,277.41
Yearly Profit (before NG) ($/annum)	9,684,530.14	9,095,858.86	4,958,233.06

Case Study Number (→)	64	65	66
CO_2 Feed Flow (tons/annum)	34,855.92	34,855.92	34,855.92
H_2 Feed Flow (tons/annum)	1,596.67	1,596.67	1,596.67
CaO Needed (tons/annum)	559.52	26,029.76	34,575.75
CaO Cost ($/annum)	67,142.94	3,123,571.19	4,149,090.56
MeOH Produced (tons/annum)	934.16	0.00	0.00
MeOH Purity (mass %)	99.93	0.00	0.00
MeOH Sales Potential ($/annum)	467,080.62	0.00	0.00
DME Produced (tons/annum)	4,402.48	383.01	35.68
DME Purity (mass %)	98.90	14.44	1.17
DME Sales Potential ($/annum)	4,358,459.60	379,176.35	35,324.51
$CaCO_3$ Produced (tons/annum)	998.64	46,457.90	61,710.78
$CaCO_3$ Sales Potential ($/annum)	259,646.12	12,079,052.79	16,044,802.83
Total Reactant Cost ($/annum)	4,154,338.14	7,210,766.39	8,236,285.76
Total Product Revenue ($/annum)	5,085,186.35	12,458,229.14	16,080,127.34
Total Unit Operation Cost ($)	5,914,365.18	4,198,845.38	2,592,966.55
Unreacted CO_2 to Atmosphere (before NG) (tons/annum)	22,210.28	8,267.12	10,986.70
Yearly Profit (before NG) ($/annum)	930,848.21	5,247,462.74	7,843,841.57

Case Study Number (→)	67	68	69
CO_2 Feed Flow (tons/annum)	34,855.92	34,855.92	34,855.92
H_2 Feed Flow (tons/annum)	1,596.67	1,596.67	1,596.67
CaO Needed (tons/annum)	219.62	34,575.75	36,205.41
CaO Cost ($/annum)	26,354.01	4,149,090.56	4,344,649.43
MeOH Produced (tons/annum)	291.54	0.00	0.00
MeOH Purity (mass %)	99.93	0.00	0.00
MeOH Sales Potential ($/annum)	145,770.12	0.00	0.00
DME Produced (tons/annum)	1,373.96	150.42	24.91
DME Purity (mass %)	98.62	4.75	0.78
DME Sales Potential ($/annum)	1,360,221.68	148,912.89	24,656.51
$CaCO_3$ Produced (tons/annum)	391.97	61,710.78	64,619.39
$CaCO_3$ Sales Potential ($/annum)	101,912.66	16,044,802.83	16,801,041.68
Total Reactant Cost ($/annum)	4,113,549.21	8,236,285.76	8,431,844.63
Total Product Revenue ($/annum)	1,607,904.46	16,193,715.72	16,825,698.19
Total Unit Operation Cost ($)	2,337,137.70	3,008,378.10	3,737,127.11
Unreacted CO_2 to Atmosphere (before NG) (tons/annum)	29,958.86	11,001.85	11,498.09
Yearly Profit (before NG) ($/annum)	-2,505,644.75	7,957,429.96	8,393,853.56

Case Study Number (→)	70	71	72
CO_2 Feed Flow (tons/annum)	34,855.92	34,855.92	34,855.92
H_2 Feed Flow (tons/annum)	1,596.67	1,596.67	1,596.67
CaO Needed (tons/annum)	128.49	36,205.41	38,055.67
CaO Cost ($/annum)	15,419.33	4,344,649.43	4,566,680.94
MeOH Produced (tons/annum)	0.00	0.00	0.00
MeOH Purity (mass %)	0.00	0.0	0.00
MeOH Sales Potential ($/annum)	0.00	0.00	0.00
DME Produced (tons/annum)	779.59	104.99	12.67
DME Purity (mass %)	98.58	3.22	0.38
DME Sales Potential ($/annum)	771,794.64	103,941.20	12,544.39
$CaCO_3$ Produced (tons/annum)	229.34	64,619.39	67,921.74
$CaCO_3$ Sales Potential ($/annum)	59,627.54	16,801,041.68	17,659,651.95
Total Reactant Cost ($/annum)	4,102,614.53	8,431,844.63	8,653,876.14
Total Product Revenue ($/annum)	831,422.19	16,904,982.88	17,672,196.34
Total Unit Operation Cost ($)	2,685,164.85	2,792,819.64	3,737,913.95
Unreacted CO_2 to Atmosphere (before NG) (tons/annum)	31,459.40	11,507.68	12,065.21
Yearly Profit (before NG) ($/annum)	-3,271,192.34	8,473,138.25	9,018,320.20

Case Study Number (→)	73	74	75
CO_2 Feed Flow (tons/annum)	34,855.92	34,855.92	34,855.92
H_2 Feed Flow (tons/annum)	1,596.67	1,596.67	1,596.67
CaO Needed (tons/annum)	32.88	38,055.67	38,891.73
CaO Cost ($/annum)	3,945.94	4,566,680.94	4,667,007.39
MeOH Produced (tons/annum)	0.00	0.00	0.00
MeOH Purity (mass %)	0.00	0.00	0.00
MeOH Sales Potential ($/annum)	0.00	0.00	0.00
DME Produced (tons/annum)	171.14	53.42	7.14
DME Purity (mass %)	98.35	1.58	0.21
DME Sales Potential ($/annum)	169,427.21	52,881.73	7,071.44
$CaCO_3$ Produced (tons/annum)	58.69	67,921.74	69,413.93
$CaCO_3$ Sales Potential ($/annum)	15,259.19	17,659,651.95	18,047,620.85
Total Reactant Cost ($/annum)	4,091,141.14	8,653,876.14	8,754,202.59
Total Product Revenue ($/annum)	184,686.40	17,712,533.67	18,054,692.29
Total Unit Operation Cost ($)	2,619,007.29	3,084,695.50	4,292,726.38
Unreacted CO_2 to Atmosphere (before NG) (tons/annum)	33,156.22	12,069.38	12,316.46
Yearly Profit (before NG) ($/annum)	-3,906,454.74	9,058,657.54	9,300,489.70

Case Study Number (→)	76	77	78
CO_2 Feed Flow (tons/annum)	34,855.92	34,855.92	34,855.92
H_2 Feed Flow (tons/annum)	1,596.67	1,596.67	1,596.67
CaO Needed (tons/annum)	38,891.73	38,891.73	39,672.18
CaO Cost ($/annum)	4,667,007.39	4,667,007.39	4,760,661.71
MeOH Produced (tons/annum)	0.00	0.00	0.00
MeOH Purity (mass %)	0.00	0.00	0.00
MeOH Sales Potential ($/annum)	0.00	0.00	0.00
DME Produced (tons/annum)	387.21	30.11	1.98
DME Purity (mass %)	10.25	0.88	0.06
DME Sales Potential ($/annum)	383,339.96	29,810.16	1,962.47
$CaCO_3$ Produced (tons/annum)	69,413.93	69,413.93	70,806.88
$CaCO_3$ Sales Potential ($/annum)	18,047,620.85	18,047,620.85	18,409,788.22
Total Reactant Cost ($/annum)	8,754,202.59	8,754,202.59	8,847,856.91
Total Product Revenue ($/annum)	18,430,960.81	18,077,431.00	18,411,750.69
Total Unit Operation Cost ($)	4,676,633.04	4,098,658.30	3,833,165.27
Unreacted CO_2 to Atmosphere (before NG) (tons/annum)	12,341.36	12,319.12	12,458.27
Yearly Profit (before NG) ($/annum)	9,676,758.22	9,323,228.42	9,563,893.78

Case Study Number (→)	79	80	81
CO_2 Feed Flow (tons/annum)	34,855.92	34,855.92	34,855.92
H_2 Feed Flow (tons/annum)	1,596.67	1,596.67	1,596.67
CaO Needed (tons/annum)	39,672.18	39,672.18	33,924.21
CaO Cost ($/annum)	4,760,661.71	4,760,661.71	4,070,905.39
MeOH Produced (tons/annum)	0.00	0.00	0.00
MeOH Purity (mass %)	0.00	0.00	0.00
MeOH Sales Potential ($/annum)	0.00	0.00	0.00
DME Produced (tons/annum)	107.46	8.36	39.99
DME Purity (mass %)	3.01	0.24	1.33
DME Sales Potential ($/annum)	106,384.82	8,272.94	39,589.61
$CaCO_3$ Produced (tons/annum)	70,806.88	70,806.88	60,547.91
$CaCO_3$ Sales Potential ($/annum)	18,409,788.22	18,409,788.22	15,742,455.68
Total Reactant Cost ($/annum)	8,847,856.91	8,847,856.91	8,158,100.59
Total Product Revenue ($/annum)	18,516,173.03	18,418,061.15	15,782,045.29
Total Unit Operation Cost ($)	4,571,040.81	3,138,820.09	4,040,570.50
Unreacted CO_2 to Atmosphere (before NG) (tons/annum)	12,546.59	12,528.16	10,789.46
Yearly Profit (before NG) ($/annum)	9,668,316.12	9,570,204.24	7,623,944.70

Case Study Number (→)	82	83	84
CO_2 Feed Flow (tons/annum)	34,855.92	34,855.92	34,855.92
H_2 Feed Flow (tons/annum)	1,596.67	1,596.67	1,596.67
CaO Needed (tons/annum)	255.63	33,924.21	37,669.59
CaO Cost ($/annum)	30,675.91	4,070,905.39	4,520,350.22
MeOH Produced (tons/annum)	342.42	0.00	0.00
MeOH Purity (mass %)	99.93	0.00	0.00
MeOH Sales Potential ($/annum)	171,208.65	0.00	0.00
DME Produced (tons/annum)	1,613.73	168.58	15.22
DME Purity (mass %)	98.64	5.39	0.46
DME Sales Potential ($/annum)	1,597,595.65	166,892.75	15,071.79
$CaCO_3$ Produced (tons/annum)	456.25	60,547.91	67,232.65
$CaCO_3$ Sales Potential ($/annum)	118,625.75	15,742,455.68	17,480,488.08
Total Reactant Cost ($/annum)	4,117,871.11	8,158,100.59	8,607,545.42
Total Product Revenue ($/annum)	1,887,430.04	15,909,348.42	17,495,559.86
Total Unit Operation Cost ($)	3,653,469.23	3,816,687.65	4,358,424.26
Unreacted CO_2 to Atmosphere (before NG) (tons/annum)	29,359.31	10,788.53	11,967.75
Yearly Profit (before NG) ($/annum)	-2,230,441.07	7,751,247.84	8,888,014.44

Case Study Number (→)	85	86
CO_2 Feed Flow (tons/annum)	34,855.92	34,855.92
H_2 Feed Flow (tons/annum)	1,596.67	1,596.67
CaO Needed (tons/annum)	51.76	37,669.59
CaO Cost ($/annum)	6,210.71	4,520,350.22
MeOH Produced (tons/annum)	0.00	0.00
MeOH Purity (mass %)	0.00	0.00
MeOH Sales Potential ($/annum)	0.00	0.00
DME Produced (tons/annum)	285.14	64.18
DME Purity (mass %)	98.44	1.92
DME Sales Potential ($/annum)	282,284.95	63,536.17
$CaCO_3$ Produced (tons/annum)	92.37	67232.65
$CaCO_3$ Sales Potential ($/annum)	24,017.23	17,480,488.08
Total Reactant Cost ($/annum)	4,093,405.91	8,607,545.42
Total Product Revenue ($/annum)	306,302.18	17,544,024.24
Total Unit Operation Cost ($)	3,504,884.63	4,356,314.71
Unreacted CO_2 to Atmosphere (before NG) (tons/annum)	32,803.09	11,977.27
Yearly Profit (before NG) ($/annum)	-3,787,103.73	8,936,478.82